The role of starch in the day/night re-programming of stomata in plants with Crassulacean Acid Metabolism

Natalia Hurtado Castano

Doctor of Philosophy

School of Natural and Environmental Sciences

February 2020

Declaration

This thesis is submitted to Newcastle University for the degree of Doctor of Philosophy. The research detailed within was performed between the years 2015-2019 and it was supervised by Professor Anne Borland and Professor Jeremy Barnes. I certify that none of the material offered in this thesis has been previously submitted by me for a degree or any other qualification at this or any other university.

Natalia Hurtado C.

Natalia Hurtado Castano

Abstract

Crassulacean acid metabolism (CAM) is a specialised type of photosynthesis characterised by the unique inverted stomatal rhythm, which increases water use efficiency (WUE) and enhances the potential for sustainable biomass production in warmer and drier conditions. Starch turnover in the mesophyll of CAM species supports nocturnal CO_2 assimilation and CAM activity. In C_3 plants, starch metabolism has been reported to play an important role in determining stomatal behaviour; in this case, guard cell starch degradation is triggered by blue light, producing osmolytes that promotes stomatal opening. Based on the importance of starch and the little knowledge regarding CAM stomatal behaviour, this study tested the hypothesis that starch metabolism has been re-programmed in CAM plants to enable nocturnal stomatal opening, by using biochemical and genetic characterisation of wild type and RNAi lines with curtailed starch metabolism in the constitutive CAM species *Kalanchoë fedtschenkoi*.

Measurements of guard cell starch content over 24 hours in wild type plants of *K. fedtschenkoi* indicated a day/night shift in starch turnover compared to C_3, evidenced by an increment over the first hours of the day and a diminution at the beginning of the night. The characterisation of the RNAi lines confirmed that curtailed starch metabolism affected nocturnal CO_2 fixation, besides the phosphorolytic starch degradation has a pivotal role for driving nocturnal CAM activity evidenced, in the same way, in both mesophyll and epidermis proteome datasets. Furthermore, higher levels of soluble sugars in the epidermis of the RNAi lines appeared to curtail completely stomatal closure during the day, indicating that guard cell starch biosynthesis is an important sink for carbohydrates, ensuring day-time stomatal closure.

Finally, this thesis constituted an approach for the understanding of starch metabolism in CAM stomata and together with further studies lead to the potential engineering of CAM into C_3 to enhance WUE.

Acknowledgments

I want to express my deeply gratitude to my supervisor Professor Anne Borland for her support, guidance and encouragement during this entire thesis. I really enjoyed all our discussions trying to understand the mysteries of CAM stomata. I also want to thank to my second supervisor Professor Jeremy Barnes for his support, guidance and for having always a funny story to share during our meetings. Besides my supervisors, I am very grateful with Helen Martin, the most patience laboratory technician I have ever met, for her time, immense help and explanations.

My sincere thanks to Dr Vasilios Andriotis for his help and guidance with the proteins native PAGE and for his valuable advises during the postdoc application process. I also want to thank to the School of Natural and Environmental Sciences for the opportunity of working as a demonstrator, it was a great experience and a personal challenge teaching in an international environment. Thanks to Dr Alex Laude and Dr Rolando Berlinguer-Palmini in the Bio-Imaging Unit at Medical School for the valuable help in the conduction of the fluorescence microscopy. Also, thanks to Dr Simon Kometa at NUIT for his assistance with statistical analysis. I want to thank to all the members of Plant and Microbial Research Group for sharing every week their interesting projects and contributing with important discussions about our research, as well as for the nice conversations during our coffee breaks and the delicious cooking off competitions, making this time very enjoyable.

I am very grateful with Dr James Hartwell, Dr Susanna Boxall, Dr Louisa Dever and Nina Pugh at University of Liverpool for providing the RNA sequence datasets, and for giving me the opportunity of joining their research group for training in Real time-qPCR. I want to thank to Sabrina Fluetsch at University of Zurich for performing the staining and confocal microscopy of the epidermal samples, the resulting data were a valuable resource for this thesis. Also my deepest gratitude with Dr Paul Abraham in Oak Ridge National Laboratory (USA) for conducting the proteomics experiment and providing the data.

I want to thank to all the people I have met during the last four years and made life enjoyable in Newcastle. First, to all my Latin American friends, who made me feel at home and enriched our culture with all the diverse food, talks, trips and great moments we spent together. I want to thank specially to Alidi Kusuma, Joshua Loh and Jui Chanapan for being the best support during this process, for their valuable friendship, for sharing their amazing culture, for all the delicious meals we shared together and for encouraged me to finish this

thesis. Also, I am very grateful with all the people I worked with in Geneius – Synlab for their time, help and for making all the hard work enjoyable with nice conversations

Finally, I want to thank to the most important people, who made this thesis possible, my parents Luz Stella and Manuel, my sister Sofia and my beautiful niece Julieta, for their love and support through the distance, for being part of this process and encourage me to continue following my dreams.

This thesis was funded by the Government of Colombia through the Administrative Department of Science, Technology and Innovation – Colciencias and the Newton-Caldas fund partnership.

Table of Contents

List of Figures

List of Tables

List of Equations

Abbreviations

ABA	Abscisic acid
ABCB	ATP-binding cassette transporter
ADP	Adenosine diphosphate
ADP-forming	α-1,4-glucan- synthase
AGPase	ADP Glucose pyrophosphorylase
ALMT	Aluminium-activated malate transporters
AMY	α-amylase
ANOVA	Analysis of variance
APS	Ammonium persulfate
ATP	Adenosine triphosphate
BAM	β-amylase
BCA	β-carbonic anhydrase
BES	Branching enzyme
Bicine	N, N-Bis (2-hydroxyethyl) glycine
BLUS1	Blue light signalling 1
BSA	Bovine serum albumin
C_3	C_3 carbon fixation pathway as the sole mechanism to fix CO_2 by Rubisco
C_4	C_4 carbon fixation pathway as the sole mechanism to fix CO_2 by PEP and Rubisco
CA	Carbonic anhydrase
$CaCl_2$	Calcium chloride
CAM	Crassulacean acid metabolism
cDNA	Complementary DNA
Ci	Internal CO_2 concentration
CO_2	Carbon dioxide
Ct	Threshold cycle
cTPs	Chloroplastic transit peptides
DBE	Debranching enzyme
DHAP	Dihydroxyacetone phosphate
DNA	Deoxyribonucleic acid
DPE	Disproportionating enzyme
DSP	Phosphoglucan phosphatase amyloplastic
DTT	Dithiothreitol

EDTA	Ethylenediaminetetraacetic acid
EGTA	Egtazic acid
FPKM	Fragments per kilobase of exon model per million reads map
Fru6P	Fructose 6-phosphate
GBSS	Granule-bound starch synthase
Glc1P	Glucose 1-phosphate
Glc6P	Glucose 6-phosphate
G6PDH	Glucose 6-phosphate dehydrogenase
GLCT	Glucose transporter
Glu	Glutamic acid
$\mathbf{g_m}$	Mesophyll conductance
$\mathbf{g_{max}}$	Maximum theoretical stomatal conductance
GPT	Glucose 6-phosphate transporter
$\mathbf{g_s}$	Stomatal conductance
GWD	Glucan water dikinase
HCl	Hydrochloric acid
$\mathbf{HCO3^-}$	Bicarbonate
HEPES	4-(2-hydroxyethyl)-1-piperazineethanesulfonic acid
HPIC	High pressure ion chromatography
HT1	High leaf temperature 1
HXK	Hexokinase
IAS	Lower internal air space
INV	Invertase
ISA	Isoamylase
KI	Potassium iodide
LDA	Limit dextrinase
LSD	Less significant difference
LSF	Like starch excess four
MDH	Malate dehydrogenase
MEX	Maltose exporter
MgCl2	Magnesium chloride
mTPs	Mitochondrial targeting peptides
MTT	Thiazolyl Blue Tetrazolium Bromide
NAD	Nicotinamide adenine dinucleotide

NAD-MDH	Nicotinamide dinucleotide malate dehydrogenase
NAD-ME	NAD-malic enzyme
NADP	Nicotinamide adenine dinucleotide phosphate
NADP-ME	NADP-dependent malic enzyme
NaOH	Sodium hydroxide
NRT1.1/CL1	Nitrate transporter 1
NTC	No template controls
OST1	Open stomata 1
PAGE	Polyacrylamide gel electrophoresis
PC	Pyruvate carboxylase
PCR	Polymerase chain reaction
PEG	Polyethylene glycol
PEP	Phosphoenolpyruvate
PEPC	Phosphoenolpyruvate carboxylase
PEPCK	PEP carboxykinase
PFK	Phosphofructokinase
PGA	3-phosphoglyceric acid
PGI	Phosphoglucose isomerase
PGM	Phosphoglucomutase
PHOT	Phototropin
PHS	α-glucan phosphorylase
Pi	Inorganic phosphate
PK	Pyruvate kinase
PLS	Partial least square
PMA	Plasma membrane ATPase
PMS	Phenazine methosulfate
PMSF	Phenylmethylsulfony fluoride
PPCK	Phosphoenolpyruvate carboxylase kinase
PPDK	Pyruvate phosphate dikinase
PPFD	Photosynthetic photon flux density
PPi	Inorganic pyrophosphate
PU	Pullulanase
PWD - GWD3	Phosphoglucan water dikinase
RC	Reliability class

RCF	Relative centrifugal force
RNA	Ribonucleic acid
RNAi	RNA interference
RT-qPCR	Real time quantitative PCR
Rubisco	Ribulose-1,5-bisphosphate carboxylase/oxygenase
SDS-PAGE	Sodium dodecyl sulphate polyacrylamide gel electrophoresis
SEX4	Starch excess 4
SLAC	Slow anion channel-associated
SBPase	Sedoheptulose-1-7 bisphosphatase
SPP	Sucrose phosphatase
SPs	Secretory peptides
SS	Starch synthase
STP	Sugar transporter protein
SUC	Sucrose transporters
SUSY	Sucrose synthase
TCA	Tricarboxylic acid
TEDI	Thioesterase/thiol ester dehydrase-isomerase
TEMED	Tetramethylethylenediamine
Thr	Threonine
TKT	Transketolase
Tm	Primer melting temperature
TP	Triose phosphate
TPT	Triose phosphate translocator
Tris	Trisaminomethane
UDPG	Uridine diphosphate glucose
VPD	Vapour-pressure deficit
WT	Wild type
WUE	Water Use Efficiency
WUEi	Instantaneous Water Use Efficiency

Chapter 1. General introduction

1.1. Crassulacean acid metabolism

Crassulacean acid metabolism (CAM) is a specialised type of photosynthesis found in about 7% (at least 343 genera across 36 families) of higher plants worldwide, that evolved independently many times in response to selective pressures forced by water limitation. CAM leads to an altered mode of photosynthesis that improves water use efficiency (WUE) of plants in arid and semi-arid habitats. Comparing with species that perform C_3 and C_4 photosynthesis, WUE in CAM is 6-fold and 3-fold higher, respectively, thanks to the unique inverted stomatal rhythm (the pores on the leaves open at night and close during the day) that allows the conservation of water (Borland *et al.*, 2009).

Carbon processing in CAM consists of four phases (Figure 1. 1). Phase I occurs throughout the night, where stomata are open to allow the entrance of atmospheric CO_2 which is captured as bicarbonate (HCO_3^-) and assimilated via the cytosolic enzyme phosphoenolpyruvate carboxylase (PEPC). During this period, PEPC catalyses the conversion of HCO_3^- and PEP (phosphoenolpyruvate) to oxaloacetate which is converted to malic acid via nicotinamide dinucleotide malate dehydrogenase (NAD-MDH) and is subsequently accumulated in the vacuole. During early dawn (phase II), stomata remain open for the continuing uptake of atmospheric CO_2, which together with that released from early malate decarboxylation, is re-fixed in the Calvin cycle via Rubisco. During phase III (most of the day), stomata are closed and net uptake of CO_2 from the atmosphere does not occur. Previously stored malic acid exits the vacuole and is decarboxylated by NAD (P)-malic enzyme (NAD-ME, NADP-ME) or PEP carboxykinase (PEPCK), depending on the species, to supply CO_2 for re-fixation via Rubisco and processing via the Calvin cycle. Pyruvate, a three-carbon compound, is released by malate decarboxylation and is converted to PEP by pyruvate phosphate dikinase (PPDK), to sustain starch synthesis via gluconeogenesis. Finally, Phase IV occurs at the end of the light period where internal CO_2 concentration decreases as result of a depletion of accumulated malic acid, leading to the opening of stomata and uptake of atmospheric CO_2 (Borland *et al.*, 2014).

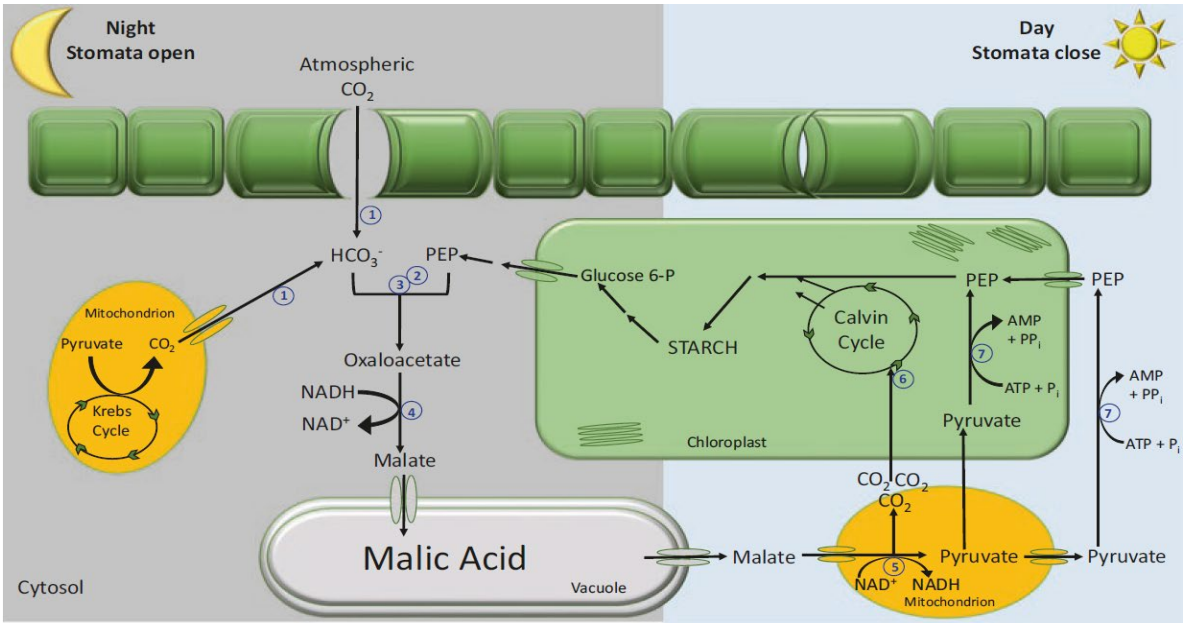

Figure 1. 1. Biochemical reactions occurring in mesophyll cells of CAM plants during night/day cycle. At night, atmospheric CO_2 is taken up through open stomata and assimilated in form of malate, which is accumulated in the vacuole as malic acid. During the day, malate exits the vacuole and is decarboxylated by the mitochondrial NAD-ME, behind closed stomata. CO_2 produced is re-fixed in the chloroplast via Rubisco and the Calvin cycle and pyruvate is converted to PEP, synthesising starch. The main enzymes are numbered: (1) Carbonic anhydrase - CA, (2) Phosphoenolpyruvate carboxylase - PEPC, (3) Phosphoenolpyruvate carboxylase kinase - PPCK, (4) NAD malate dehydrogenase NAD-MDH, (5) Either Malic enzyme NAD-ME or Phosphoenolpyruvate carboxykinase PEPCK, (6) Rubisco, (7) Pyruvate phosphate dikinase – PPDK (Borland *et al.*, 2018).

1.2. Crassulacean acid metabolism for sustainable agriculture in a warmer drier world

For the next 30 years, it is predicted that the world population will reach 9 billion inhabitants, increasing the necessity of expanding available cropland area to produce about 50% more food. A key constraint to achieve this purpose is the accelerated climate change that is expected to generate extreme weathers as high temperatures and drier regions that will affect rainfall patterns worldwide, threaten agriculture sustainability and thus food security (Borland *et al.*, 2015). One potential solution to decrease water use in agriculture and improve water use efficiency (WUE) is the introduction of the metabolic cycles of crassulacean acid metabolism (CAM) into C_3 plants. This approach would allow the cultivation of these species in current arid environments unsuitable for sustainable production, taking into account that CAM plants use up to 80% less water to produce similar amounts of biomass compared with C_3 and C_4 species (Liu *et al.*, 2018). Additionally, CAM can inhabit water-limited environments such as semi-arid deserts or seasonally dry forests. This is possible because CAM plants maximise water use efficiency (WUE) by shifting all or part of the atmospheric

CO_2 uptake to the night-time, when evapotranspiration rates are reduced compared with the daytime (Borland *et al.*, 2014; Cushman *et al.*, 2015). This potential of CAM in resilient agriculture is evidenced in the production of *Ananas comosus*, *Agave sisalana*, *Agave tequilana*, *Opuntia ficus-indica* and *Aloe vera* (Davis *et al.*, 2019). The higher productivity of these crops in arid and semi-arid habitats constitute an extensive market value and evidence their potential for sustainable production of biomass in a warmer and drier world. In addition, CAM crops avoid competition for existing land resources because they can grow on marginal or degraded land with poor soil conditions, where precipitation is insufficient to support traditional C_3 or C_4 crops (Yang *et al.*, 2015).

CAM bioengineering into C_3 plants is feasible considering that CAM is a mechanism that can concentrate carbon in a single cell, so it does not require differentiated mesophyll and bundle sheath cell types as is the case for C_4 photosynthesis (Borland *et al.*, 2014). Besides, the convergent evolution of CAM from C_3 implies that all the proteins required for CAM are homologous to those in species performing C_3 photosynthesis. This is also evidenced by the induction of CAM in facultative species under drought or salt stress showing compatibilities in signalling cascades between CAM and C_3 (Yang *et al.*, 2015).

One of the most challenging aspects of engineering CAM traits into C_3 plants is the control module for nocturnal stomatal opening and closure during the daytime. Different studies have attributed the greater water use efficiency of CAM plants and their success in arid habits to the inverted daily stomatal rhythm, which consist of stomatal opening during the night and closure during the day. It is currently not known if stomatal control for CAM is mainly due to signalling processes that originate in the mesophyll or if the guard cells *per se* show altered metabolism in CAM versus C_3. Most of the current experimental data and information about stomatal guard cell signalling is generated in C_3 plants, where the importance of starch in the diurnal opening of stomata has recently been highlighted (Santelia and Lawson, 2016). The role of starch in stomatal regulation in CAM plants is the focus of this thesis. Investigating how starch turnover is integrated with stomatal signalling pathways in the response to external stimuli such as light, as well as internal factors like CO_2 concentration (C_i) and metabolite turnover will help to understand the mechanisms responsible for stomatal opening/closure in CAM plants (Lee, 2010).

To design core CAM modules that could be engineered into C_3 species requires the establishment of model systems to study CAM evolution, carboxylation and decarboxylation pathways, and inverted stomatal behaviour. Such CAM models will provide the molecular information that could ultimately lead to future crop improvement to enhance water use

efficiency under arid ecosystems (Yang *et al.*, 2015). For this purpose, the development of a stable transformation system has made *Kalanchoë fedtschenkoi* a biological model for understanding important features of CAM, such as circadian control of phosphoenolpyruvate carboxylase (PEPC), nocturnal CO_2 fixation and diurnal malic acid decarboxylation (Dever *et al.*, 2015; Hartwell *et al.*, 2016).

Kalanchoë transformation is based on a double stranded RNA (hairpin RNA) approach (Hartwell *et al.*, 2016). A short fragment of the gene to be silenced is amplified and cloned into a pENTR/D Gateway-compatible entry vector and recombined into the intron-containing hairpin RNAi binary vector which is subsequently introduced into *Agrobacterium tumefaciens* (Karimi *et al.*, 2002). The *Agrobacterium*-mediated transformation of *K. fedtschenkoi* triggers a post-transcriptional silencing of the gene of interest allowing the further study of its function. This approach has allowed the silencing of CAM decarboxylation enzymes NAD-malic enzyme (NAD-ME) and pyruvate orthophosphate dikinase (PPDK) evidencing that NAD-ME is the main enzyme implicated in the diurnal decarboxylation of malate in the mitochondria of mesophyll cells of this species and its silencing completely supresses nocturnal CO_2 fixation (Dever *et al.*, 2015). Additionally, Boxall *et al.* (2017) using RNAi lines of *K. fedtschenkoi* with reduced expression of phosphoenolpyruvate carboxylase kinase (PPCK), identified that this protein allows nocturnal CO_2 fixation by the phosphorylation/activation of phosphoenolpyruvate carboxylase (PEPC). PPCK activates nocturnal carboxylation by reducing PEPC sensitivity to feedback inhibition by malate and is regulated at the level of transcription and is under circadian control (Boxall *et al.* (2017).

In addition to the development of RNAi lines, the sequencing of the *Kalanchoë fedtschenkoi* genome enables the identification of changes in the expression of genes that are important for CAM and its convergent evolution from C_3 species. The diploid genome (2n=34) of *K. fedtschenkoi*, estimated as ~260Mb in size is composed of 30,964 annotated protein-coding genes (Yang *et al.*, 2017). A comparison between the CAM genomes of *K. fedtschenkoi and Ananas comosus* with the C_3 genome of *Arabidopsis thaliana* revealed a widespread diel rescheduling of genes involved in nocturnal CO_2 fixation, circadian rhythm, carbohydrate metabolism, stomatal movement and heat stress response, indicating convergent evolution in diel reprogramming of gene transcription in eudicot and monocot CAM lineages (Yang *et al.*, 2017).

Taking into account the importance of the inverted stomatal behaviour for the conservative water properties of plants with CAM, this general introduction will describe the key components of CAM, the convergent evolution from C_3 plants and will focus on stomatal

guard cell metabolism and the importance of starch in CAM and stomatal behaviour. Having set the scene and provided this framework, this general introduction will conclude stating the core hypotheses to be tested in this thesis.

1.3. Evolution of crassulacean acid metabolism

Convergent evolution of crassulacean acid metabolism from C_3 ancestors occurred multiple times across 400 genera and 36 families of vascular plants, colonising terrestrial, epiphytic and aquatic environments. Higher representation of CAM species are found in the families Cactaceae, Euphorbiaceae, Crassulaceae, Bromeliaceae, Orchidaceae, and Asparagaceae (Heyduk *et al.*, 2016). Most of the CAM terrestrial habitats are characterised by water-constraints and poor nutrient conditions, while in the aquatic environments CO_2 availability is limited due to a lower diffusion rate of the gas in water compared to air and competition with aquatic plants performing C_3 photosynthesis (Borland *et al.*, 2018). The evolution of anatomical characteristics such as succulence, large cells and large vacuoles enhances water storage, nocturnal accumulation of malate and thus the availability of carbon for re-fixation by Rubisco during the day (Heyduk *et al.*, 2016). Similarly, lower internal air space (IAS) reduces mesophyll conductance (g_m) minimizing CO_2 efflux and enhancing its recapture during the day and at night (Niechayev *et al.*, 2019).

Strict temporal control of nocturnal carbon assimilation and diurnal decarboxylation seems to be crucial for C_3 to CAM evolution. According to Bräutigam *et al.* (2017), atmospheric CO_2 assimilation, synthesis of organic acids and their subsequent breakdown for CO_2 fixation also occurs in C_3 plants, but the greater influx of atmospheric CO_2 and the ability to be fixed nocturnally increases in CAM. Orthologous genes for phosphoenolpyruvate carboxylase (PEPC), carbonic anhydrase (CA), phosphoenolpyruvate carboxylase kinase (PPCK), phosphoenolpyruvate carboxykinase (PEPCK), NAD-malic enzyme (NAD-ME) and NAD malate dehydrogenase (NAD-MDH) are found in both C_3 and C_4 species. However, opposite patterns of diel expression of many CAM-genes have been identified in the CAM orchid *Phalaenopsis equestris* which suggest that differences in the diel regulation of expression of genes implicated in CO_2 fixation was critical during CAM evolution (Zhang *et al.*, 2016). The circadian clock seems to be a key regulator of CAM, and in the CAM species pineapple cis-regulatory elements (CCA1 binding site, Evening element, G-box element and TCP15 binding motif) activate diel expression patterns of genes necessary for CAM nocturnal carbon assimilation (Wai *et al.*, 2017). For instance, in the case of β-carbonic anhydrase, the circadian-related cis-acting element CCA1-binding site is not present in C_3 and C_4 species,

suggesting specific circadian regulatory pathways for gene expression between CAM and non-CAM photosynthesis (Ming *et al.*, 2015).

The multiple independent emergences from C_3 have led to a wide range of CAM phenotypes, that in some cases depend on the environmental factors, evidencing the high diversity between and within species (Cushman, 2001). An ontogenetic change from C_3 to CAM occurs in constitutive (obligate) species, found mainly in the Cactaceae and Crassulaceae families. In this case, the youngest leaves present a C_3-like metabolism, while the CAM cycle is always present in mature photosynthetic tissues, evidenced by increased nocturnal CO_2 fixation with leaf maturity (Winter *et al.*, 2008). Facultative CAM plants are characterised by metabolic shifts from C_3 to CAM triggered mainly by the environmental conditions. Research on facultative species has been focused on the CAM halophyte *Mesembryanthemum crystallinum* or ice plant, which under well-watered conditions performs C_3 photosynthesis but CAM is induced in response to water deficit and higher salinity (Häusler *et al.*, 2000). Induction of CAM has been reported in the C_4 species *Portulaca umbraticola*, where in well-watered conditions CAM was absent but under drought stress CO_2 capture changed gradually from the light period to the dark. However the nocturnal CO_2 fixation under stress was less than the non-stress CO_2 fixation during the day, indicating that *Portulaca umbraticola* shows weak CAM (Winter, 2019). In C_3-CAM intermediates, the C_3 pathway maximises plant growth and development under well-watered conditions, and according to the scarcity of water a progressive change to CAM is evidenced to ensure integrity of photosynthesis and plant survival (Cushman, 2001).

Kalanchoë fedtschenkoi (Family Crassulaceae, Order Saxifragales), the species selected for this study, is a constitutive CAM species. The genus *Kalanchoë* is composed for about 125 species, taxonomically grouped in three sections by anatomical traits and their capacity to perform CAM: Kitchingia (I), Bryophyllum (II) and Eukalanchoe (III). Kitchingia is characterised by Madagascan non-succulent plants that perform C_3 metabolism most of their life but have the ability to switch to CAM mode when the climate conditions are unfavourable (Gehrig *et al.*, 2001). The Bryophyllum section, where *K. fedtschenkoi* belongs, also includes species from Madagascar, but in this case, they are constitutive CAM plants, with complete CAM activity in their older leaves that decreases in the youngest ones. Finally, the Eukalanchoe section includes thick-leaved succulent species that perform CAM in their entirety despite the climate conditions and are located in the arid South Western region of Madagascar and Eastern Africa (Hartwell *et al.*, 2016).

1.4. Stomatal regulation

Together with the alternative pathway of carbon assimilation, an inverted stomatal behaviour evolved from C_3 to CAM, characterised by stomatal opening during the night period and closing during the day. Stomata are small pores found in the epidermal layers of the leaves, responsible for gas exchange and surrounded by two guard cells, which control the stomatal aperture and closure by the response to diverse stimuli, either internal or external, which include the circadian clock, light intensity, internal CO_2 concentration, humidity and temperature (Bertolino *et al.*, 2019).

The inverted stomatal behaviour of CAM is also accompanied by anatomical traits that influence the magnitude of stomatal conductance (mmol H_2O $m^{-2}s^{-1}$), net CO_2 assimilation (μmol $m^{-2}s^{-1}$), and water use efficiency (Hetherington and Woodward, 2003). Barrera Zambrano *et al.* (2014) performed an anatomical characterisation of different species of the genus *Clusia*, identifying that CAM-performing species (*C. alata*, *C. hilariana* and *C. rosea*) presented lower stomatal densities and larger stomatal pore area compared to those of C_3 (*C. multiflora*, *C. tocuchensis* and *C. grandiflora*) and CAM-C_3 intermediate (*C. minor*, *C. lanceolate* and *C. aripoensis)* species, suggesting that larger stomata in lower densities enhance water use efficiency. The Barrera Zambrano *et al.* (2014) study supports the proposed negative correlation between stomatal density and size, where plants with lower stomatal densities show a greater mean stomatal size, whereas smaller stomata are found in a high density (Lawson and Blatt, 2014). Doheny-Adams *et al.* (2012) suggested that species with lower stomatal density and larger size reduce evapotranspiration rates, resulting in higher water conservation properties, especially in plants exposed to drought.

Diversity in stomatal location has also been reported in different species of vascular plants. Stomata can be located in the lower epidermis of the leaves (hypostomatic), in the upper (hyperstomatic) or in both (amphistomatic) (Wilmer and Fricker, 1996). Amphistomaty is considered an evolutionary adaptation to increase the maximum leaf CO_2 conductance by the reduction of its diffusion pathway to the mesophyll, which is advantageous considering the leaf thickness (Mott *et al.*, 1982). CAM species of Cactaceae such as *Agave* and *Opuntia* and of Crassulaceae such as *Kalanchoë fedtschenkoi*, present amphistomatic and thick leaves which are associated with constitutive CAM activity (Moreira *et al.*, 2012; Monja-Mio *et al.*, 2015). On the other hand, hypostomatic leaves have been reported in species of the genus *Clusia* as *C. pratensis* (facultative CAM) *C. minor* (C_3/CAM intermediate) and *C. tocuchensis* (constitutive C_3), and are considered as an adaptive trait to avoid water loss as a compensation of the lack of succulence, particularly in non-constitutive CAM species (de Faria *et al.*, 2012).

1.4.1. Signalling in stomatal guard cells

Guard cells are involved in the aperture and closure of the pore by the response to diverse stimuli, including circadian clock, hormones, light intensity, changes in atmospheric and internal CO_2 concentration, soil moisture content, humidity, temperature and biotic stress (Hubbard *et al.*, 2007). For example, stomatal conductance increases under lower atmospheric CO_2 concentrations in order to maintain the required levels for mesophyll carbon assimilation, while under higher concentration the conductance decreases with no affectation on the assimilation (Araújo *et al.*, 2011). Likewise, is it well understood that under water limiting conditions the hormone Abscisic acid (ABA) activates S-type anion channels, promoting stomatal closure and the reduction of water loss (Acharya *et al.*, 2013).

Osmolytes have also synergistic effect on stomatal movement by regulating turgor pressure in guard cells. After light activates stomatal opening and exit of protons (H^+), potassium channels allow the influx of K^+ (and counter ions as chloride, nitrate, and sulphate) to guard cells. Potassium is responsible for early morning opening of stomata, but is replaced later in the diel period by sucrose, which is responsible for maintaining guard cell turgor pressure from midday onwards (Talbott and Zeiger, 1996; Lawson *et al.*, 2014). Malate also acts as a counter ion for K^+. According to Lawson *et al.* (2014) increases in PEPC activity, in combination with increased NADP- or NAD-dependent malate dehydrogenase activity result in the accumulation of malate in the guard cells and stomatal opening (Figure 1. 2). Likewise, increased expression of the transporter ABCB14 is related with malate influx into the guard cells, which increases the osmotic pressure and contributes to stomatal opening (Lee *et al.*, 2008).

In C_3 plants is well understood how these stimuli are affecting stomatal regulation, while in CAM plants the most accepted factor driving the unique inverted stomatal behaviour is the diel change in the internal CO_2 concentration (C_i) which occurs as a consequence of the synthesis and degradation of malate (Males and Griffiths, 2017). Thus, lower C_i during the night period triggers stomatal opening and CO_2 assimilation to form malate, while a higher CO_2 concentration during phase III (day-time) from the decarboxylation of the malate accumulated overnight is thought to cause day-time stomatal closure (Males and Griffiths, 2017). Likewise, differences in blue light response between C_3 and CAM have been evidenced by transcriptomic analysis. In *Agave americana* a similar 24 h expression pattern of the blue light receptor *phototropin 1* (*phot1*) was found compared to *Arabidopsis*, while opposite temporal patterns in the expression of genes responsible for the opening of stomata in *Arabidopsis*, such as *open stomata 1/SNF-related protein kinase* (*ost1)* and *high leaf*

temperature 1 (*ht1*) were found in *Agave americana* (Abraham *et al.*, 2016). Transcriptomic analysis in the CAM species *Ananas comosus* and *Kalanchoë fedtschenkoi* showed a temporal shift, from dawn to dusk, in the expression of the blue light receptor *phototropin 2 (phot2)* compared to *Arabidopsis*, suggesting a possible contribution of PHOT2 in the opening of stomata at dusk and during the night (Yang *et al.*, 2017).

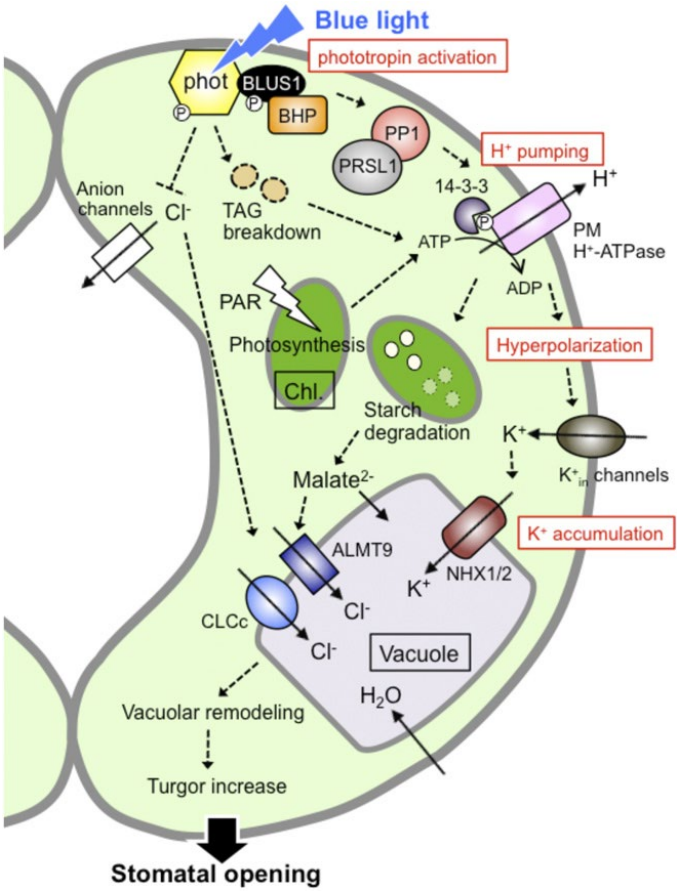

Figure 1. 2. Signalling pathway in response to blue light in stomata guard cells of *Arabidopsis thaliana*. Positive and negative regulators are represented by arrows and a T-bar, respectively (Inoue and Kinoshita, 2017).

1.4.2. Starch turnover influences guard cells metabolism

In C_3 plants, several studies have indicated the requirement of starch for stomatal regulation, evidenced by reduced stomatal opening under blue light of starch deficient lines of *A. thaliana* lacking the enzyme phosphoglucomutase (PGM) (Lasceve *et al.*, 1997). Recent reports in *A. thaliana* identified that starch in the guard cells follows an inverted turnover pattern compared to mesophyll, being degraded during the light period (Santelia and Lunn, 2017). During this process, blue light activates photoreceptors located in the guard cell plasma

membrane and induces H^+ pumping outside the cell through the H^+-ATPase. This reaction produces a negative electric potential inside the guard cell that leads to the uptake of water and K^+, which is the main osmolyte during the first hours of the day. Horrer *et al.* (2016) identified that the main enzymes responsible for starch degradation in *Arabidopsis* guard cells are β-amylase 1 (BAM1) and α-amylase 3 (AMY3), which are activated by blue light through the signalling components phototropins 1 and 2 (PHOT1/PHOT2) and blue light signalling 1 (BLUS1). This reaction generates maltose, which is converted to malate and sucrose, becoming the main counter ions of K^+, promoting the influx of water and an increase in stomatal turgor pressure, allowing the opening of stomata (Santelia and Lawson, 2016). On the other side, synthesis of starch in guard cells is less studied, but has been associated with stomatal closure, serving as a sink for carbon skeletons produced during malate degradation. In this case, sucrose and malate are exported to the guard cell cytosol and are converted into triose phosphate (TP) by gluconeogenesis, which is subsequently imported to the chloroplast via the triose phosphate translocator (TPT). Inside the chloroplast, TPT enters the Calvin cycle to provide substrates, reducing power and energy for the activation of ADP glucose pyrophosphorylase (AGPase) and synthesis of starch (Figure 1. 3), (Daloso *et al.*, 2017).

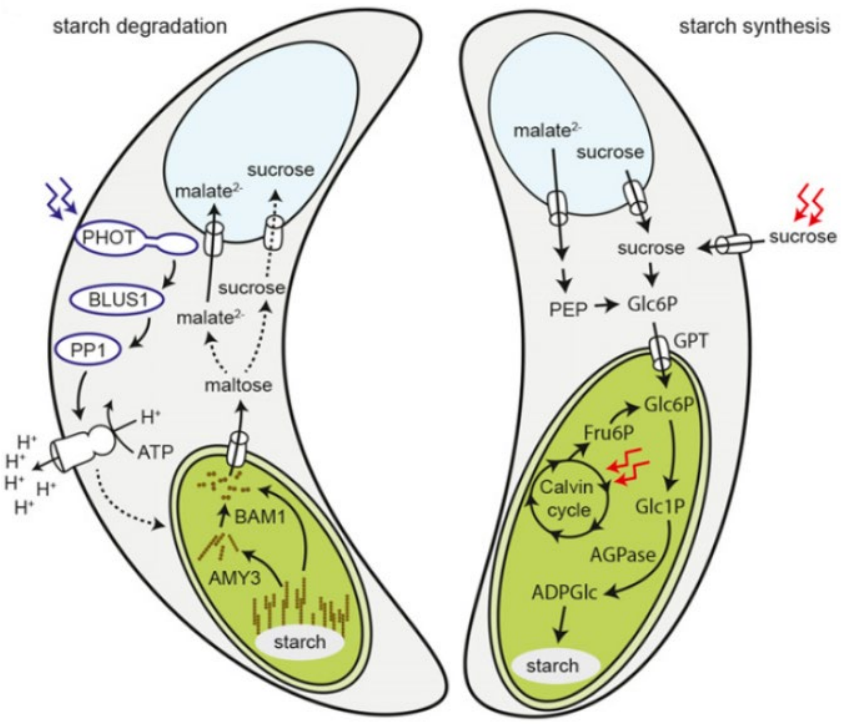

Figure 1. 3. Starch turnover in guard cells of C_3 plants. Blue light activates the H^+-ATPase proton pump that leads to the starch degradation via BAM1 and AMY3 producing malate and sucrose, which enter to the vacuole increasing the turgor pressure and allowing the opening of stomata (Santelia and Lawson, 2016).

1.5. Starch turnover in mesophyll

Starch is the main storage carbohydrate in higher plants, produced by carbon fixation as a product of diurnal photosynthesis. Depending on the species, nocturnal degradation of starch sustains CAM activity by providing phosphoenolpyruvate (PEP) for carboxylation via PEPC during the dark period. The diurnal decarboxylation of malate produces CO_2 that is re-fixed by Rubisco, producing hexose phosphates that are substrates for the day-time synthesis of starch (Borland *et al.*, 2016).

Starch granules are insoluble semi-crystalline packing of glucans composed of polymers of glucose linked in α-1, 4 and α-1, 6 organisation that form amylose and amylopectin molecules, respectively (Xu *et al.*, 2017). Transitory starch is located in the plastids of photosynthetic tissue and is mobilised during day/night cycles to support metabolism and plant growth (Zeeman *et al.*, 2010). In non-photosynthetic organs like roots, tubers, stems and seeds, starch is synthesised for long-term storage within amyloplasts, serving as a source of energy in different growth process such as seed germination, as well as a source of feedstock for industrial applications (Streb and Zeeman, 2012).

1.5.1. Synthesis of starch

In leaves, starch is synthesised during the day period and is considered the final product of a metabolic pathway linked to the Calvin cycle (Figure 1. 4). In this case, the enzyme phosphoglucoisomerase (PGI) catalyses the synthesis of glucose 6-phosphate (Glc6P) from fructose 6-phosphate (Fru6P). Subsequently, Glc6P is converted to glucose 1-phosphate (Glc1P) by the enzyme phosphoglucomutase (PGM) and subsequently transformed into ADP glucose and inorganic pyrophosphate (PPi) by the enzyme ADP glucose pyrophosphorylase (AGPase) in an irreversible step (Stitt and Zeeman, 2012). AGPase is formed by two small catalytic and two large regulatory subunits and is activated allosterically by 3-phosphoglycerate and inhibited by P_i, ensuring that ADP glucose and starch are synthesised under enough substrates availability (Pfister and Zeeman, 2016).

From ADP glucose, the starch granule is formed by a series of reactions. First, starch granule-bound starch synthase (GBSS) synthesises amylose, adding glucose units and elongating individual glucan chains. This process is followed by the addition of glucose from ADP glucose to an existing amylopectin chain by the formation of new α-1, 4 glucosidic linkages. Four soluble isoforms of starch synthases (SSI – SSIV) are involved in this step, but the contribution of each one depends on the tissue and the species. In *Arabidopsis* leaves, SSI

is the more active isoform due to its solubility, followed by SSIII and SSII, while SSIV is implicated in the control of the granule morphology (Pfister and Zeeman, 2016). The branching of amylopectin chains is catalysed by branching enzymes (BEs), by the transfer of α-1, 4-glucan chains to the C3 position of a glycosyl residue of another chain (Bahaji *et al.*, 2014). Finally, debranching enzymes (DBEs) determine the amylopectin structure by cleavage of branch points. Two types of DBEs are involved in this process, both isoamylase (ISA) and pullulanase or limit-dextrinase (PUL or LDA) debranch directly the α-1, 6-glucosidic linkage to synthesise amylopectin but differ in the substrate binding, where PUL or LDA are specific to substrates with short branches as β-limit dextrins and pullulan. Regarding ISA, three isoforms have been identified, but only ISA1 and ISA3 are catalytically active in the formation of amylopectin, while ISA2 forms and heteromeric complex with ISA1 acting as a regulator of activity and stability (Stitt and Zeeman, 2012).

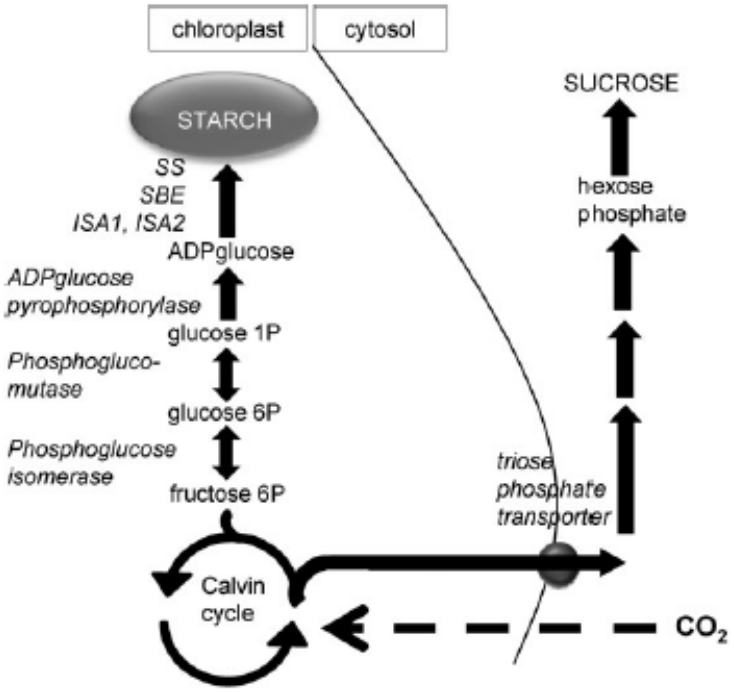

Figure 1. 4. Pathway of starch synthesis in the chloroplast and the export of its products to produce sucrose in the cytosol. Fructose 6-P is produced by the Calvin cycle and is the precursor of starch synthesis with the action of different enzymes (Smith, 2012).

1.5.2. Degradation of starch

Transitory starch is degraded during the night period by the action of enzymes with different functions that catalyse the disruption of insoluble semi-crystalline packing of glucans throughout a network of reactions (Figure 1. 5), (Stitt and Zeeman, 2012). Two

pathways that are capable of starch degradation are present in leaves, the hydrolytic route that produces maltose and glucose by the main action of β-amylases (BAM) and disproportionating enzymes (DPE1) respectively, and the phosphorolytic route that produces glucose 1-phosphate (Glc1P) by the action of the α-glucan phosphorylase 1 (PHS1) (Weise *et al.*, 2006).

In both cases, starch is initially phosphorylated in order to disrupt the crystalline structure of amylopectin and to expose the granule to the following degradation. The enzymes α-glucan water dikinase (GWD1) and phosphoglucan water dikinase (PWD or GWD3) catalyse the phosphorylation of C6 and C3 glycosyl residues, respectively to initiate the glucan hydrolysis and prevent the recrystallization of the granule (Silver *et al.*, 2014). To complete the glucan hydrolysis, the subsequent removal of the phosphate groups by phosphoglucan phosphatases, SEX4 (starch excess4) and LSF2 (like starch excess Four-2) allow the access of debranching enzymes (isoamylase 3 – ISA3 and limit dextrinase – LDA) and β-amylases (BAM) to continue the degradation, releasing long malto-oligosaccharides and maltose, respectively (Li *et al.*, 2017; Santelia and Lunn, 2017). In a parallel reaction, α-amylases (AMY) attack the α-1, 4 linkage of the starch granule releasing branched oligosaccharides that are then degraded by PHS1 to form Glc1P or by ISA3 and LD3 to form long malto-oligosaccharides that are following degraded by BAM and DPE1 (Streb and Zeeman, 2012).

In C_3 plants, BAM and DPE are responsible for the hydrolytic synthesis of maltose and glucose, respectively, which are exported to the cytosol, via MEX1 (maltose exporter 1) and GLCT (glucose transporter) and converted to sucrose to sustain plant growth and development. In contrast, the phosphorolytic synthesis of Glucose 1-phosphate by PHS1 supplies carbon for internal chloroplast metabolism through the oxidative branch of the pentose phosphate pathway and it is suggested that its main role is to control reactive oxygen intermediates under stress conditions (Weise *et al.*, 2006). Nine genes encoding β-amylases have been identified in *Arabidopsis thaliana*, grouped into four BAM subfamilies by amino acids similarities, catalytic activity and cellular location. Subfamily I includes the plastidic BAM5 and BAM6, subfamily II contains BAM1 and BAM3, subfamily III contains the proposed non-catalytic BAM4 and BAM9, and finally, BAM2, and the nuclear BAM7 and BAM8 belong to subfamily IV (Fulton *et al.*, 2008). From these subfamilies, BAM1 and BAM3 are located in the chloroplast and are the main isoforms responsible for starch degradation. Analysis reported that BAM3 catalyses nocturnal degradation in the mesophyll, while BAM1 triggers diurnal starch degradation in the stomatal guard cells (Valerio *et al.*, 2011). Interestingly, BAM4 and BAM9 have the lowest amino acid similarity compared with

the other isoforms, evidenced by substitutions in both catalytic glutamic acid residues (Glu-186 and Glu-380) and the deletion of five amino acids in the flexible loop, responsible for substrate binding (Fulton *et al.*, 2008). The role of BAM4 and BAM9 in starch degradation is not clear and different explanations are proposed. Fulton *et al.* (2008) suggested that BAM4 is a catalytically inactive enzyme and has a regulatory function by its interaction with other proteins to enable starch breakdown, likewise, Hou *et al.* (2017) indicated in potato that BAM9 might form a protein complex with BAM1 to facilitate starch degradation. On the other hand, Li *et al.* (2009) proposed that BAM3 and GWD are not dependant on BAM4 for starch degradation, but this latter facilitates the breakdown apparently by the binding to the starch granule.

In contrast to C_3, CAM plants are thought to use the phosphorolytic pathway to degrade starch (Borland *et al.*, 2016). In this case, PHS1 is responsible for the cleavage of α-1, 4-glucosidic bonds releasing inorganic phosphate (P_i) and glucose 1-phosphate (Glc1P), which is subsequently converted to glucose 6-phosphate (Glc6P) to be exported to the cytosol through the glucose 6-phosphate translocator (GPT1) (Zeeman *et al.*, 2004b). The phosphorolytic production of Glc6P in CAM plants coordinates the nocturnal supply and demand of phosphoenolpyruvate (PEP), being a substrate in its synthesis and activating PEPC allosterically to allow nocturnal CO_2 assimilation (Borland *et al.*, 2016). The hydrolytic production of glucose in CAM has been reported by Häusler *et al.* (2000) in the facultative CAM species *M. crystallinum*. In this case, the plastid glucose transporter (*glct*) showed increased expression under the induction of CAM, indicating that glucose is required for sucrose synthesis or could be also a substrate for PEP formation, (Borland *et al.*, 2016). Differences in the initial granule phosphorylation are also reported between C_3 and CAM. Studies in *Arabidopsis thaliana amy3* deficient lines indicate that GWD1 and PWD are the main enzymes responsible for the initial granule phosphorylation whilst α-amylases do not have a prominent function in this process (Yu *et al.*, 2005). In contrast, the facultative CAM species *Mesembryanthemum crystallinum* revealed an increase transcript abundance of AMY during CAM induction, proposing that its main function is to increase the degradation rate or enable PHS1 to access branched oligosaccharides to be further degraded (Cushman *et al.*, 2008b).

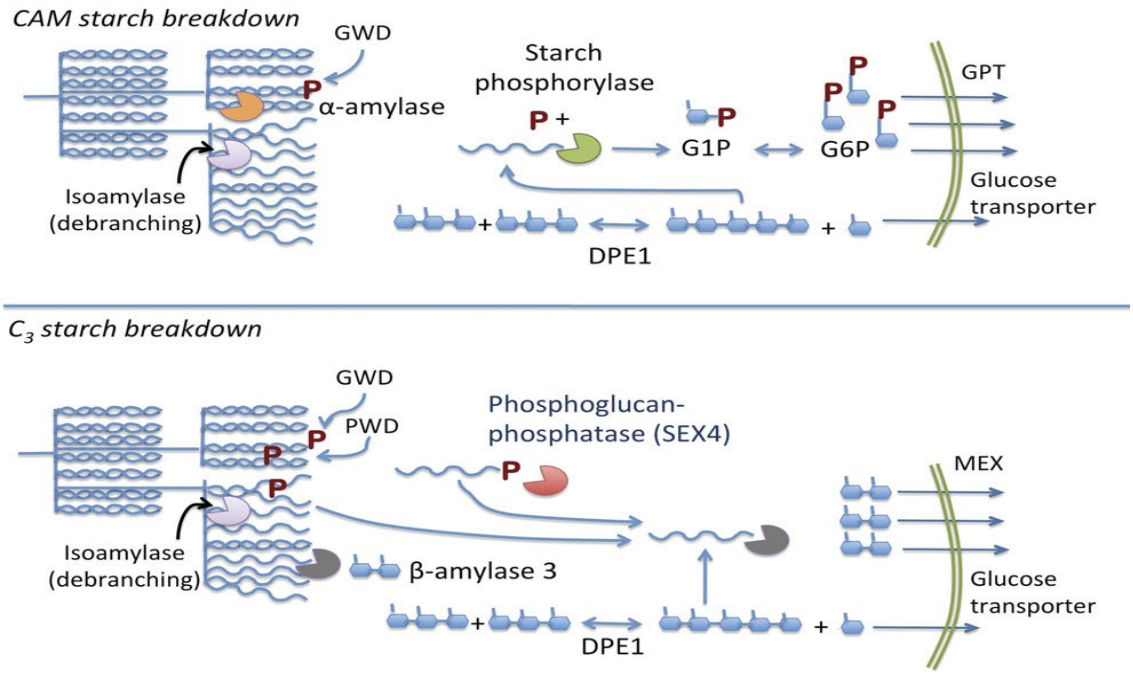

Figure 1. 5. Proposed starch degradation in mesophyll of CAM and C_3 species. In CAM, the phosphorolytic degradation of starch is catalysed by PHS1, releasing Glc6P to the cytosol via GPT1. In C_3 plants, the hydrolytic degradation of starch by BAM3 produces maltose that is finally exported to the cytosol. In both pathways, linear glucans are metabolised by DPE1, which produces glucose, exported by GLCT, however the maltose metabolism in CAM plants needs to be elucidated (Weise *et al.*, 2011).

1.6. Aims and Hypothesis

The greater water use efficiency of CAM plants and their success in arid habits can be attributed to the inverted daily stomatal rhythm. Nevertheless, most of the current experimental data and information about stomatal guard cell signalling is generated in C_3 plants. Recent studies have highlighted the importance of guard cell starch metabolism for stomatal regulation in C_3 species. Based on this background, I will test the hypothesis that starch metabolism has been re-programmed in CAM plants to enable stomatal opening at night. Ultimately, this research will help to predict the minimum set of genetic interventions required to engineer CAM into C_3 crops as a means of increasing their water use efficiency based on stomatal behaviour. For that purpose, the following sub-hypotheses will be addressed in this thesis:

Hypothesis 1: The inverted stomatal rhythm in CAM plants is reflected by differential expression of genes implicated in starch metabolism between guard cell-enriched epidermis and mesophyll.

Hypothesis 2: Starch is important for providing substrates for nocturnal CAM activity and osmolytes for stomatal opening.

Hypothesis 3: The differential abundance of key metabolic proteins between mesophyll and guard cell-enriched epidermis provide evidence for functional independence of both tissues.

Hypothesis 4: CAM stomata are insensitive to light and their opening is regulated by factors other than starch degradation, such as the response to a low internal carbon concentration and organic acids accumulation.

Chapter 2. Materials and Methods

2.1. Plant Material

Kalanchoë fedtschenkoi, the selected species for this study presents constitutive CAM phenotype. Three different RNAi lines of *K. fedtschenkoi* were generated and provided by Dr James Hartwell at University of Liverpool. These lines show reduced expression of genes encoding phosphoglucomutase 1 (*pgm1a*), plastidic α-glucan phosphorylase 1 (*phs1*) and β-amylase 9 (*bam9*), respectively.

The RNAi lines, *rPGM1a*, *rPHS1* and *rBAM9,* together with wild type (WT) plants grown in a growth chamber with a 12-h photoperiod and a day/night temperature of 25°C/19°C. For plants propagation, 10 leaves of each line were placed on a tray containing a 3:1 mixture of John Innes No. 2 compost and perlite, to allow the growth of new plantlets on the leaf margin. After 8 weeks, the plantlets were transferred to plastic pots of 127 mm of diameter containing John Innes No. 2 compost and perlite (3:1 proportion). Three biological replicates of each line were placed in each pot to have a total amount of 18 replicates (Figure 2. 1).

For biochemical assays, leaf pair 6 (where pair 1 are youngest leaves growing at the apical zone of the plant) of 12 weeks old plants was selected due to previous sampling optimisation (Appendix A). Epidermal tissue and ground mesophyll were harvested separately on a 24 hour day/night cycle, using three biological replicates for each time point. For sampling purposes, the leaf was blended to allow the separation of the mesophyll from the epidermis, which was following peeled of, maintaining the lower and the upper epidermal surfaces separated to be analysed independently. Immediately the samples were snap frozen in liquid nitrogen and stored at -80°C until their evaluation.

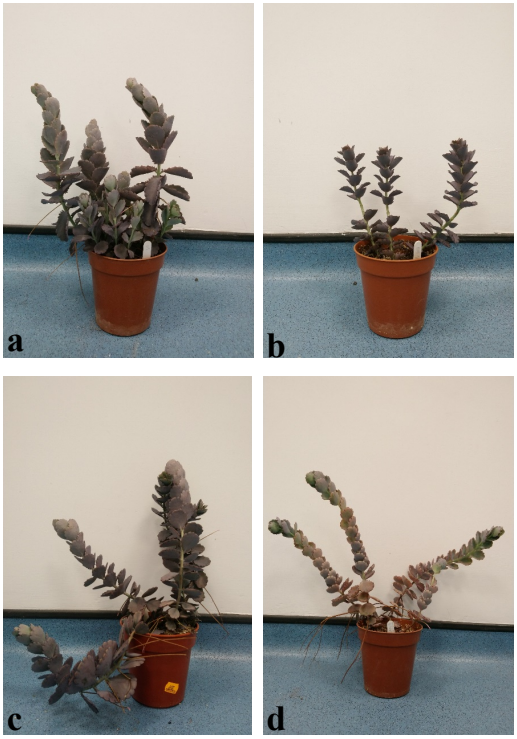

Figure 2. 1. Plants of *Kalanchoë fedtschenkoi* selected to perform this research. Three biological replicates of 12 old weeks were used in biochemical, anatomical, gas exchange analysis and gene expression assays. Wild type (a) and RNAi lines *rPGM1a* (b), *rPHS1* (c) and *rBAM9* (d) were selected to evaluate the re-programming of starch metabolism in CAM stomata. Plant growth conditions were set at 400 µmol CO_2 mol^{-1} air, 25°C/19°C (day/night) and a diurnal photosynthetic photon flux density – PPFD - of 250 µmol $m^{-2}s^{-1}$ at plant height.

2.2. Determination of starch in mesophyll and stomatal guard cells

For quantifying starch content in mesophyll, about 500 mg of frozen leaf tissue was ground in liquid nitrogen. Exactly 1.5 ml of 80% methanol was added and incubated at 60°C for 40 minutes. After that, a centrifugation at 16,060 RCF for 10 minutes was performed, transferring the supernatant to a new tube for soluble sugars and malate analysis. The pellet remaining from the methanol extraction was washed twice with 500 µl of distilled water in order to eliminate remaining soluble sugars, after that the pellet was incubated for one hour at 90°C in 1.5 ml of acetate buffer pH 4.5 to allow starch to gelatinise. The samples were left at room temperature to cool down and then incubated for 24 h at 45ºC with 300 µl of enzyme amyloglucosidase (300 units – Sigma catalogue number A-7255, prepared in acetate buffer pH 4.5) to degrade the starch. Subsequently, this extract was centrifuged at 16,060 RCF for 10 minutes, and the resulting supernatant was collected for the colorimetric phenol/sulphuric acid test (Dubois *et al.*, 1956). First, to 100 µl of digested extract, 400 µl of H_2O, 500 µl of 5% phenol and 2.5 ml of concentrated sulphuric acid were added. The solution was mixed and left to cool for 15 minutes. Finally, the absorbance was measured at 483 nm and compared

with glucose standards of known concentration (0, 25, 50, 100 and 150 µg ml^{-1}). Blanks were prepared by substituting the digested extract for a mix of enzyme and acetate buffer. The glucose equivalents from starch degradation were calculated as follows:

$$Glc\ equivalent = \frac{\left(\left(\frac{A}{G}/180\right) \times DF\right)}{fwt}$$

Equation 2. 1. Calculation of glucose equivalents from starch degradation in leaf mesophyll. A is absorbance, G is gradient of line calculated from calibration curve, DF is dilution factor (volume of sample divided by total volume of enzyme suspension in acetate buffer) and fwt is the fresh weight of tissue.

To determine starch content in guard cells, lower and upper epidermal peels were collected. The peels were stored in a fixative solution (50% v/v methanol, 10% v/v acetic acid) to stop any reaction occurring in the guard cells. Next, the peels were washed with distilled water for 10 minutes, transferred to microscope slides to be stained with Lugol's iodine solution for 3 minutes (6 mM iodine, 43 mM KI, and 0.2 N HCl), followed by a final wash with distilled water to avoid excess of stain in the tissue. Finally, the stained peels were observed by light microscopy using the 40 X stage lens, recording 20 stomata per surface per time point and determining the area of the starch granules with ImageJ software (Appendix B gives more details of these measurements), (Schneider *et al.*, 2012).

2.3. Soluble sugar content in mesophyll and guard cell-enriched epidermis

The supernatant obtained from the methanol extraction was used to determine the soluble sugars content in the leaf mesophyll and guard cell-enriched epidermis. The quantification was conducted by HPIC -High Pressure Ion Chromatography- technique (Thermo Scientific™ Dionex™). First, the methanol extracts of sugars were dried overnight to complete dryness. Then 500 µl of nanopure water was added and mixed thoroughly by vortex. The extracts were desalted, passing 200 µl of the sample throughout ion exchange columns of DOWEX AG50W X4 – 200 and AMBERLITE IRA – 67 and washed with 2.5 ml of nanopure water, collecting this eluent to perform the quantification of sugars. Each sample was evaluated in duplicate (i.e. 2 technical replicates per sample) and the amount of sugars (µmol g^{-1} fwt) was calculated based on 10 ppm standards of trehalose, glucose, fructose, sucrose, maltose and sedoheptulose.

2.4. Quantification of malate in mesophyll and guard cell-enriched epidermis

Malate content was determined by its oxidation, mediated by the enzyme malate dehydrogenase (MDH) to form oxaloacetate, reducing NAD to NADH, based on the method developed by Hohorst (1970). A calibration curve, with known malate concentrations (0, 25, 50, 100, 150, 200 nmoles ml^{-1}) was used to determine the concentration of the samples. First, the methanol extracts that were resuspended in nanopure water for the previous soluble sugars assay were completely dried overnight. Exactly 500 ml of 200 mM bicine buffer, pH 7.8 was added and mixed using vortex. To perform the quantification of malate, in a cuvette 20 µl of the sample, 500 µl of Buffer/NAD (1M glycine, 2.5M hydrazine sulphate, 146.12M EDTA, 17.13M NAD) and 480 µl of nanopure water were added. The starting absorbance at 340 nm was measured and after 2 minutes 10 µl of the MDH enzyme (96 U ml^{-1} - Sigma catalogue number M2634-10KU) was added. The samples were incubated for one hour at 37ºC and after this time, the absorbance was recorded for a second time. The control was prepared by substituting the extract for water.

The malate content (µmol g^{-1} fwt) was calculated as follows:

$$Malate = \frac{\left(\left(\frac{\Delta A}{G}\right) \times DF\right) \Big/ \left((C \times fwt)/D\right)}{1000}$$

Equation 2. 2. Calculation of malate content in leaf mesophyll and guard cell-enriched epidermis. ΔA is the difference in the absorbance before and after incubation with the enzyme, G is the gradient of line calculated from the calibration curve. DF is the dilution factor (volume of methanol used for the extraction divided by total volume of sample used for this assay). fwt is the fresh weight of the tissue, C is the volume before been dried out and D is the volume of Bicine buffer added.

2.5. Gas exchange analysis

Net CO_2 uptake (µmol CO_2 m^{-2} s^{-1}) stomatal conductance (mol H_2O m^{-2} s^{-1}) and transpiration (mmol H_2O m^{-2} s^{-1}) were determined by gas exchange analysis. Three biological replicates of each genotype were evaluated during a 24 h day/night cycle, using the LI-6400XT Portable Photosynthesis System (LI-COR® Biosciences).

A fully expanded leaf was clamped into the leaf chamber fluorometer, supplied with a LED light source and a temperature sensor. Ambient CO_2 concentration was set at 400 µmol

CO_2 mol^{-1} air, the light and temperature were set to track the conditions established in the growth chamber where the assay was conducted (25°C/19°C and a diurnal photosynthetic photon flux density – PPFD - of 250 µmol $m^{-2}s^{-1}$ at plant height). The relative humidity was maintained between 50 and 60% to avoid any condensation that could potentially damage the machine. The data were recorded every 15 minutes and were plotted against time.

Integrated instantaneous water use efficiency (WUE) was measured by calculating the area under the curves of net CO_2 uptake and leaf transpiration at three different times: during the night period, during the light period and over 24 h. The data are presented as the average of three biological replicates for each genotype.

2.6. Protein isolation and quantification

For protein isolation, whole leaves were harvested at the end of the light period. The extraction was performed on 500 mg of powered tissue of wild type and RNAi lines *rPGM1a, rPHS1* and *rBAM9*. Wild type *Arabidopsis thaliana* L. race Columbia was used as control for the native polyacrylamide gels (Native PAGE). The tissue was ground in a 1:3 ratio of ice-cold extraction buffer composed by 300 mM HEPES pH 7.4, 20 mM $MgCl_2$, 10 mM EGTA, 10 mM EDTA, 2 mM DTT, 4 mM Benzamidine, 1 M Phenylmethylsulfony fluoride (PMSF), 1% v/v Triton X-100 and 2% w/v PEG 20000. Subsequently, samples were centrifuged at 16,060 RCF for 10 minutes at 4°C. The supernatant was transferred to a new tube in order to quantify the proteins using Bradford assay. First, a calibration curve with known Bovine Serum Albumin (BSA) concentrations (0, 0.25, 0.50, 1, 1.5 mg ml^{-1}) was prepared to determine the concentration of the samples. Exactly 100 µl of protein extract was added to 3 ml of Bradford reagent (Sigma-Aldrich), then vortexed for 30 seconds, incubated for 5-10 minutes at room temperature and measured at an absorbance of 595 nm. The absorbance was compared with the BSA standards to determine the protein concentration. Blanks were prepared by substituting the extract with water. The proteins obtained were diluted in 1:5 of native gel loading dye (60% v/v glycerol, 0.125% w/v Bromophenol blue, 100mM Tris-HCl pH6.8) in order to obtain a final concentration of 50 µg that was loaded onto the Native polyacrylamide gels.

2.7. Identification of protein isoforms using Native polyacrylamide gels

Native or non-denaturing polyacrylamide gels (Native PAGE) allow determining the proteins in their native state, as well as identifying the different isoforms that constitute the protein. In contrast to SDS-PAGE, protein separation in Native PAGE depends on protein size, shape and charge, given by the amino acid composition and post-translational modifications (Arndt *et al.*, 2012).

Because proteins in native gels usually retain their activity, this can be determined using different substrates. In this case, to study the effect of the silencing incurred via RNAi, amylopectin (0.1% w/v), and oyster glycogen (1% w/v) were used to determine the activity of enzymes related to starch degradation (α and β amylases, debranching enzymes and starch phosphorylases). Likewise, 1% w/v of starch was used to determine the activity of the enzyme phosphoglucomutase (PGM) involved in starch synthesis.

Discontinuous Native PAGE was performed in a Mini-PROTEAN Tetra Cell system (Bio-Rad Laboratories, Inc.). Resolving gels contained 7.5% w/v acrylamide, 375 mM Tris-HCl pH 8.8, 10% w/v APS and 1% TEMED, together with the corresponding substrate. The stacking gel consisted of 3.75% w/v acrylamide, 62.5 mM Tris-HCl pH 6.8, 10% w/v APS and 1% TEMED. The gels ran at 150V in 1 X running buffer (8.1 M Tris-base and 20 M glycine).

For α and β amylases as well as debranching enzymes, amylopectin gels ran for 2.5 h and then were incubated at 37°C for two hours in 100 mM Tris pH7, 1 mM MgCl2, 1 mM $CaCl_2$ and 1 mM DTT. Gels were then stained for 30 seconds with Lugol's solution (6 mM iodine, 43 mM KI, and 0.2 N HCl) and rinsed with water. For the Native PAGE of α-glucan phosphorylases, glycogen gels ran for 3 h and were incubated for two hours at 37°C in 100 mM sodium citrate pH7, 20 mM glucose 1 phosphate (Glc1P). Gels were stained for 30 seconds with Lugol's solution (6 mM iodine, 43 mM KI, and 0.2 N HCl) and rinsed with water.

For Native PAGE of PGM isoforms, the gels ran for 9 h before incubation with 100 mM Tris pH 7.0, 10 mM $MgCl_2$, 0.2 5mM NADP, 7 mM Glc1P, 1 mM MTT, 10mg ml^{-1} PMS and 1U ul^{-1} G6PDH, at 37°C for 4 hours. Finally, the gel was fixed for 5 minutes with 10% acetic acid and rinsed with water.

2.8. RNA isolation and cDNA synthesis

RNA extraction was conducted using 200 mg of frozen powdered tissue. Mesophyll and epidermal tissue were collected independently as mentioned in Section 2.1, however in this case, the epidermal tissue of both surfaces was harvested together to ensure a higher amount of tissue required for this assay. Qiagen RNAeasy Plant mini kit was used following the manufacturer's instructions, with the addition of PEG 20,000 (50 mg ml^{-1}) to the RLC Buffer to avoid interference of the leaves acidity with the isolation. The RNA obtained was eluted in 30 µl of RNAse-free water and its concentration (ng μl^{-1}) was quantified by Nanodrop™ spectrophotometer system. The synthesis of cDNA from the total RNA obtained was performed following the instructions of Qiagen Quantitec Reverse transcription kit and diluted in Elution Buffer 1:4 for RT-qPCR analysis.

2.9. Transcript abundance of genes using Real Time q-PCR

Real time quantitative PCR (RT-qPCR) is the most sensitive and specific technique to determine the expression of genes over different times or conditions. It is expressed as a relative quantification which is the measure of the relative change of the mRNA levels expression against an endogenous control (reference gene) and against a non-treated control which in this case was a cDNA calibrator made from a combination of wild type RNAs from *K. fedtschenkoi* samples taken every 4 hours (Pfaffl, 2006).

Table 2. 1 shows the genes evaluated in wild type and RNAi lines, comparing the transcript abundance between dawn and dusk in both leaf mesophyll and guard cell-enriched epidermis. Primers were designed using Primer 3 module of Geneious software, version 11.0. 3 (Kearse *et al.*, 2012). To determine the efficiency of the primers designed, a standard curve was performed using a ten-fold serial dilution of the cDNA calibrator (12.5, 1.25, 0.125, 0.00125 and 0.00125 ng μl^{-1}). Three technical replicates of each dilution were assayed using the QuantiNova SYBR Green PCR Kit on a Rotor-Gene Q instrument (Qiagen) with the program: 95˚C for 2 min, 40 cycles of 95˚C for 5 s, 60˚C for 10 s and 72˚C for 10 s. To conclude that the PCR reaction was optimal, the coefficient of determination (R^2) should be ≥98% and the efficiency between 0.9 and 1.10 (Pfaffl, 2006).

For each gene of interest, three biological and two technical replicates were evaluated using the same conditions and program of amplification used for the primers optimisation (95°C for 2 min, 40 cycles of 95°C for 5 s, 60°C for 10 s, and 72°C for 10 s). To determine

the relative quantity, the $2^{-\Delta\Delta Ct}$ method (Livak and Schmittgen, 2001) was performed, normalising the data against the cDNA calibrator and the *K. fedtschenkoi* thioesterase/thiol ester dehydrase-isomerase (TEDI) superfamily protein (Phytozome Kaladp0068s0118.1) as reported by Boxall *et al.* (2017). In addition, no template controls (NTC) were added to confirm the absence of contamination.

2.10. Statistical analysis

In order to determine the significant differences between wild type and RNAi lines in all the biochemical measurements over time, an analysis of variance (ANOVA) and LSD (less significant difference) *post hoc* test were performed. The data obtained from gas exchange experiments were analysed by the non-parametric Mann Whitney test, based on its non-normality and the non-homogeneity determined with Shapiro-Wilk and Levene tests, respectively. All the statistical analyses were done using SPSS software (IBM Corp. Released 2016. IBM SPSS Statistics for Windows, Version 24.0. Armonk, NY: IBM Corp).

Table 2. 1. Genes evaluated by RT-qPCR on wild type and RNAi lines of *Kalanchoë fedtschenkoi*. The totality of the primers designed has a Tm of 60°C, and both forward and reverse sequences are presented.

Gene name	Annotation	Forward Primer (5' – 3')	Reverse Primer (5' – 3')
abcb14	ATP-binding cassette transporter	AGCTGTCTTGTTCTCCACCAC	ATGGCCGCCATCACTATCTC
bam9	β-amylase 9	AAAGGTCCATCCCAGGCAAG	TTACAACACAGCAGGCAGGG
bam1	β-amylase 1	TGCTTTGCCTCGCTATGATG	TTTCTCTCGCTTCCCCACTG
bam3	β-amylase 3	CCAGCATGCAAACTGTTCTCC	TCCCCAGCAAGTTCTGTTCC
amy3	α-amylase 3	AGCCTCCAGCCATCATAACC	TGATCACTCACAGGCCTTCG
sbpase	Sedoheptulose-1-7 Bisphosphatase	TACACTGGCGGAATGGTTCC	TGTTGGGGACGTCACATTTG
stp1	Sugar transporter 1	TCATCCACAAAGCTTCACACAAC	GGTAAAGGCGGAAAAGCTTCG
pgm	Phosphoglucomutase	ACAGGAAGAGAGAAGCCCAC	TCACCATGCAAAACTGGCAC
susy1	Sucrose synthase 1	TTCATGCCAATTTACAGCGG	TGAAATCAGTGTGGTTCATGGC
susy3	Sucrose synthase 3	TGTTCCCCTTTCCGCTGATG	GCTCTTCCAAAACCAGAAGACC
phs1	α-glucan phosphorylase 1	AATTCTCTGGGCTCCTTCGC	ACTCGACGCAACTGAGTCTG
glct	Glucose transporter	GAGTGGGCTTCTACTTCGGG	CATACCGAGGGAGGCAAGTC
dpe1	Disproportionating enzyme	ACATCCTCGGTGATTACGCC	GGAAGATGGAAGGCTGGACC
mex1	Maltose exporter 1	TATCCATGAGCCGCAGTGTC	GGCAGCAACAACCGGTTTAG
tpt	Triose phosphate transporter	TGTTTCAGTTTCGCTGCTGC	CGCCATCATCACCAACACAC
gtp1	Glucose 6-phosphate transporter 1	GTACCAGGTGCCAGTGGTAG	CAACACGCTGCACTTACGTC
gtp2	Glucose 6-phosphate transporter 2	GTCTGGTAGAGGTCACAAGCC	CGGGTAGGCTCACAGTGAAC
tedi	Thioesterase/thiol ester dehydrase isomerase	TGTTGTTCCTGCCACAGAAG	TAGAGGGTGAAGGTCCCAGA

Chapter 3. Identification of genes related to starch and sugar metabolism and a potential role in CAM stomatal regulation

3.1. Introduction

The opening of stomata can be summarised as an increase in size and turgor pressure of guard cells by the accumulation of osmotically active substances. This results in a swelling and shape rearrangement, overcoming the back pressure of the subsidiary cells and creating a pore between guard cells (Lawson and Morison, 2004). Plants with crassulacean acid metabolism are characterised by an inverted stomatal rhythm compared with C_3 and C_4 plants, which consists of nocturnal opening and closure during the day, improving water use efficiency that may be three and six times higher than plants with C_4 and C_3 photosynthesis, respectively (Borland *et al.*, 2009). The movement of stomata, as a response to internal and external factors, is regulated by changes in guard cell turgor pressure by the action of osmolytes. In C_3 plants, the activation of guard cell membrane H^+-ATPase mediated by blue light triggers an intracellular negative electrical potential and the efflux of protons (H^+). Following this proton pumping, different membrane channels allow the influx of K^+ and counter ions such as chloride, nitrate, and malate, as well as sucrose to guard cells, resulting in the increase of turgor pressure and stomatal opening (Santelia and Lawson, 2016).

Recent evidence from C_3 plants has shown that starch turnover in guard cells follows an opposite pattern compared to the mesophyll. Starch degradation in mesophyll occurs during the night period to sustain plant metabolism and growth. In C_3 plants, the hydrolytic enzymes β-amylases (especially BAM3), α-amylases and disproportionating enzymes (DPE) mediate starch degradation, producing mainly maltose and lower quantities of glucose, while in CAM plants, starch degradation occurs primarily by the phosphorolytic pathway, catalysed by the enzyme α-glucan phosphorylase (PHS) producing glucose1-phosphate (Glc1P); (Neuhaus and Schulte, 1996).

In contrast to what occurs in mesophyll, starch degradation in C_3 guard cells is catalysed by the enzymes β-amylase 1 (BAM1) and α-amylase 3 (AMY3) that are activated by blue light during the first hours of the day to trigger stomatal opening by the accumulation of osmolytes as malate and sucrose (Streb and Zeeman, 2012; Santelia and Lunn, 2017). Based on the importance of BAM and AMY enzymes in the starch degradation process in guard cells, Horrer *et al.* (2016) using the double mutant *amy3bam1* in *Arabidopsis thaliana*,

demonstrated that the lack of starch degradation in guard cells during the light period curtailed stomatal opening. This affected, in the same way, mesophyll photosynthesis, by a decrease of CO_2 assimilation rate, and plant growth. Likewise, the absence of starch also affects stomatal behaviour in plants, as reported by Lasceve *et al.* (1997) who studied the stomatal response of *A. thaliana* starch deficient mutants lacking the enzyme phosphoglucomutase (PGM) responsible for the interconversion of glucose 6-phosphate into glucose 1-phosphate. Their findings showed a reduction in stomatal opening under blue light, compared with wild type, caused by the deficiency in malate synthesis from starch, which cannot supply the osmolytes required as counter ions for potassium during diurnal stomatal opening.

As the metabolic pathways of starch degradation are located in the chloroplasts, different transporters are required to export the obtained products to the cytosol. Maltose exporter (MEX) and glucose transporter (GLCT) are responsible for the export of maltose and glucose, respectively. Likewise, glucose 6-phosphate transporters 1 and 2 (GPT1 and GPT2) and triose phosphate translocator (TPT) export phosphorylated organic compounds as glucose 6-phosphate (Glc6P) and triose phosphate (TP), respectively (Streb and Zeeman, 2012). Differential expressions of these transporters are observed in the facultative CAM species *Mesembryanthemum crystallinum* induced by water deficit and salinity stress. During C_3 mode, the expression of MEX is predominant while the transcript abundances of GPT1 and GPT2 are negligible. The opposite occurs when CAM is induced; in this case, GPT becomes the major chloroplast transporter during the night-time and TPT in the light period (Häusler *et al.*, 2000; Kore-Eda *et al.*, 2013).

Sucrose, a starch degradation product, is one of the main regulators of stomatal behaviour. According to Lawson *et al.* (2014), in C_3 plants potassium is responsible for early morning opening of stomata, but is replaced later in the diel period by sucrose, which becomes the major osmolyte responsible for maintaining cell turgor pressure from midday onwards. Consequently, stomatal closing at the end of the day is correlated with a decline in the amount of guard cells sucrose and therefore a loss of turgor pressure (Lee, 2010). In CAM plants, some studies have shown that potassium uptake by guard cells is correlated with stomatal opening in *Kalanchoë and Crassula* and that sucrose may also play a major role in guard cell osmoregulation, thus supporting the original theory of starch–sugar involvement, similar to C_3 and C_4 plants (Lee, 2010). In addition to the osmotic role, an energetic function of sucrose has been proposed in recent years. Antunes *et al.* (2011) suggested that sucrose breakdown mediated by sucrose synthase 3 (SUSY3) generates organic acids for ATP production,

required for the opening of stomata, and is involved in the synthesis of malate, that acts as an osmolyte during this process. In the same way, the overexpression of s*usy3* in *Nicotiana tabacum* increases stomatal aperture and conductance, net photosynthetic rate and plant growth (Daloso *et al.*, 2016b).

It has also been suggested that malic acid could be the main osmolyte for the increase of guard cell turgor pressure in CAM plants and the contributions of K^+ and sugar might be inefficient, which could be correlated with the nocturnal CO_2 fixation in form of malate and its possible transport to guard cells to support stomatal opening (Lee, 2010). Similarly, soluble sugars produced by nocturnal starch degradation in mesophyll can be subsequently transported into guard cells to act as osmolytes or be involved in the synthesis of sucrose. This hypothesis is in line with Santelia and Lawson (2016), who propose that sucrose and malate can be synthesised directly in the guard cells or be imported from the apoplast, thus connecting mesophyll and guard cells metabolism.

One of the key questions in stomatal biology and predominantly in CAM research is the understanding of the interconnection between mesophyll metabolism and stomatal responses, as well as the implication of starch in the regulation of CAM stomata. The quantification of starch in stomatal guard cells and the interrogation of RNA sequence databases derived from mesophyll and guard cell-enriched epidermis, and from C_3 and CAM performing leaves of *K. fedtschenkoi* provide an insight and the tools for the development of RNAi lines and the characterisation of genes involved in stomatal behaviour. This will allow elucidating if CAM-specific stomatal properties are exclusively from guard cells or from signals that emanate from the leaf mesophyll. The following hypotheses are proposed within this chapter:

Hypothesis 1: The differential expression of genes related with starch metabolism between guard cell-enriched epidermis and mesophyll determines the inverted stomatal rhythm in CAM plants.

Hypothesis 2: Differentially expressed genes in *K. fedtschenkoi* leaves performing C_3 and CAM photosynthesis influences the inverted stomatal rhythm in CAM plants.

Hypothesis 3: Temporal changes in the expression of genes involved in starch and sugars metabolism underpin the inverted stomatal rhythm in CAM plants.

3.2. Materials and Methods

Starch content in guard cells was quantified in both young (leaf pair 2) and mature leaves (leaf pair 6) of wild type plants. Lower and upper epidermal peels were separately collected and stored in a fixative solution (50% v/v methanol, 10% v/v acetic acid). Epidermis from young leaves were sampled at 8:00, 9:30, 20:00 and 21:30, taking into account that lights came on at 8:30 and turned off at 20:30. The staining and quantification of starch followed the protocol detailed in Section 2.2 (Chapter 2). For mature leaves, the sampling was performed over a 24 h day/night cycle at 9:00, 12:00, 16:00, 20:00, 00:00, 4:00, 6:00 and 8:00. The staining and quantification of starch were performed by Flütsch *et al.* (2018), using the fluorophore propidium iodide and confocal laser scanning microscopy.

Two RNA sequence databases for *Kalanchoë fedtschenkoi*, developed by Dr James Hartwell at University of Liverpool, were selected to determine the expression of genes implicated in stomatal regulation. The first database includes 22,941 transcripts and compares expression in the mesophyll and in guard cell-enriched epidermis of wild type plants during a 24 h day/night cycle. The second dataset compares the expression over 24 hours of 28,525 transcripts in youngest leaves (leaf pair 1) of *K. fedtschenkoi* performing C_3 photosynthesis, against mature leaves (leaf pair 6) that are obligate CAM. Both datasets are presented in FPKM (fragments per kilo base of exon model per million reads map), which is a normalised estimation of gene expression.

Based on the evidence in C_3 plants about the importance of starch metabolism in stomatal opening, genes implicated in starch synthesis and degradation, soluble sugar metabolism and ion transport were queried from the *K. fedtschenkoi* RNA sequence datasets. These literature and bioinformatics approaches were used to identify potential RNAi lines of *K. fedtschenkoi* as well as genes that merited further investigation in both RNAi and wild type lines using Real time qPCR. Genes of specific interest were those with differential expression patterns between mesophyll and guard cell-enriched epidermis and between C_3 and CAM leaves of *K. fedtschenkoi*. Because both datasets are annotated based on their homology with *Arabidopsis*, the transcript sequences were aligned using BLAST against *K. fedtschenkoi* (DOE-JGI, http://phytozome.jgi.doe.gov/) published genome in order to confirm the annotation of the genes selected.

3.3. Results

The content of starch in guard cells (granule area in μm^2) of the youngest leaves (pair 2) followed a significant ($p \leq 0.05$) degradation during the first 30 minutes of light, showing a C_3-like metabolism which was in contrast to that observed in the mature leaves (Figure 3.1). The starch content in mature leaves (pair 6) increased slightly during the day, with a slight diminution at the beginning of the night period and a further increment during the middle of the night (Figure 3.2 and Figure 3.3). This suggests a possible re-programming of starch degradation pathways in the guard cells of constitutive CAM plants that allow their inverted stomatal rhythm.

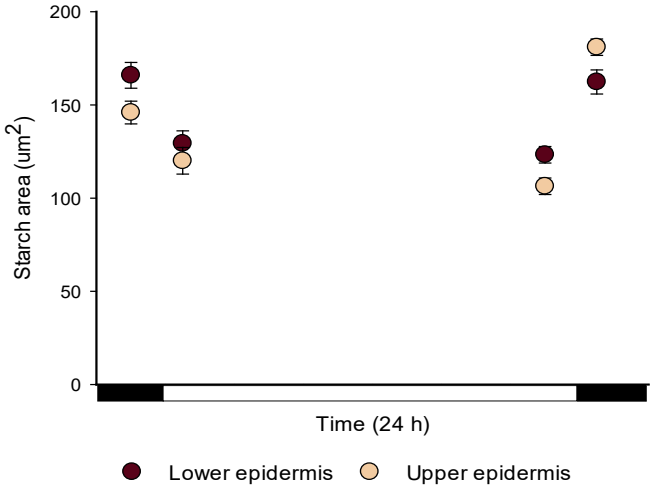

Figure 3. 1. Starch granule area (μm^2) in lower (brown) and upper (beige) epidermal surfaces of guard cells in wild type plants of *K. fedtschenkoi*; during the beginning of both, day and night period (black bar indicates dark time). Leaf pair 2 was used for this analysis and the error bars indicate the standard error of 60 replicates (three biological replicates with 20 views per replicate). Plant growth conditions were set at 400 µmol CO_2 mol^{-1} air, 25°C/19°C (day/night) and a diurnal photosynthetic photon flux density – PPFD - of 250 µmol $m^{-2}s^{-1}$ at plant height.

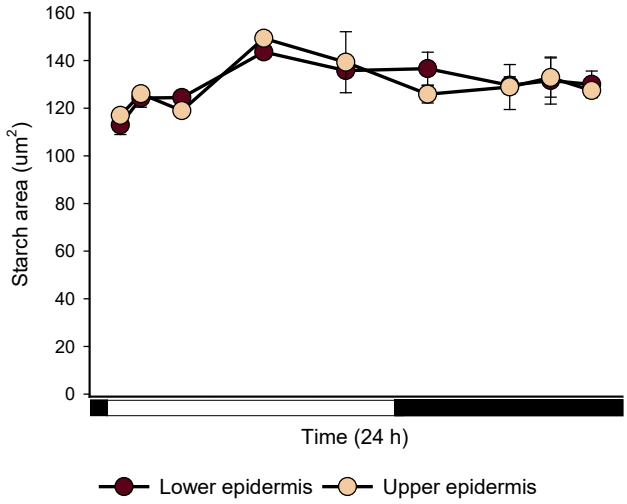

Figure 3. 2. Starch granule area (μm^2) in lower (brown) and upper (beige) epidermal surfaces of guard cells in wild type plants of *K. fedtschenkoi* over 24 h day/night cycle (black bar indicates night period). Leaf pair 6 was used for this analysis and the error bars indicate the standard error of 60 replicates (three biological replicates with 20 views per replicate). Plant growth conditions were set at 400 µmol CO_2 mol^{-1} air, 25°C/19°C (day/night) and a diurnal photosynthetic photon flux density – PPFD - of 250 µmol $m^{-2}s^{-1}$ at plant height.

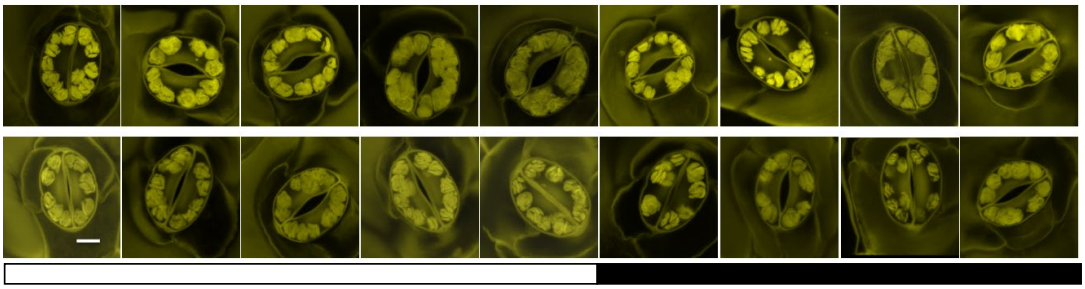

Figure 3. 3. Starch deposits in stomatal guard cells (a – upper epidermal surface, b – lower epidermal surface) of wild type plants of *K. fedtschenkoi* over 24 hours day/night cycle (black bar indicates night period). The tissue corresponds to epidermal peels of leaf pair 6. The staining was conducted by Flütsch *et al.* (2018) using the fluorophore propidium iodide and the images were taken by confocal laser scanning microscopy. The scale bar represents 10 µm. Plant growth conditions were set at 400 µmol CO_2 mol^{-1} air, 25°C/19°C (day/night) and a diurnal photosynthetic photon flux density – PPFD - of 250 µmol $m^{-2}s^{-1}$ at plant height.

The observed starch degradation in the guard cells of C_3 performing leaves during the first hours of the day, together with the diurnal increase on starch content and the nocturnal degradation in the guard cells of CAM performing leaves, led to the interrogation of the RNA sequence databases of *K. fedtschenkoi*, which compare the abundance of transcripts in C_3 and CAM leaves, as well as in the mesophyll and guard cell-enriched epidermis of mature leaves. From these transcripts, 57 genes implicated in the regulation of stomatal movement were

selected and grouped in five categories: anion transporters, starch synthesis, starch degradation, sugar transporters and sugar metabolism (Table 3. 1).

Differences in the expression between mesophyll and guard cell-enriched epidermis and between C_3 and CAM leaves were observed in most of the genes selected for this investigation. The malate transporter *ATP-binding cassette transporter* (*abcb14)*, which is implicated in the import of malate from mesophyll to guard cell, was highly expressed in the guard cell-enriched epidermis and differentially expressed between C_3 and CAM performing leaves depending of the time period with a nocturnal abundance on C_3 leaves. Similarly, a higher abundance was observed in the guard cell-enriched epidermis for the sugar transporter 1 (*stp1)*, which is involve in the hexoses import to the guard cells (Figure 3. 6 and Figure 3. 9). Studying the expression of these two genes could be an important initial point to identify the connection between mesophyll and guard cells metabolism. In comparing the transcript abundances of the genes implicated in starch degradation (α-glucan phosphorylase - *phs1;* β-amylases 1, 2 3 and 9 - *bam1*, *bam2*, *bam3* and *bam9;* α-amylase 3 - *amy3;* disproportionating enzyme 1 - *dpe1*), *phs1* was the most abundant, predominantly expressed in mesophyll and with a higher expression in CAM leaves. On the other hand, *bam2* and *bam9* were most highly expressed in guard cell-enriched epidermis compared to mesophyll, the latter more abundant and higher expressed at the beginning of the night period in CAM performing leaves (Figure 3. 5 and Figure 3. 8).

The expression of the genes implicated in transport of starch degradation products across the chloroplast membrane differed between C_3 and CAM leaves. In this case, triose phosphate translocator (*tpt)* was higher in CAM leaves, while glucose transporter (*glct)* and maltose exporter 1 (*mex1*) were more abundant in C_3 leaves. On the other hand, the glucose 6-phosphate transporters 1 and 2 (*gpt1* and *gpt2*) were also highly expressed in CAM performing leaves, which suggest the importance of Glc6P in starch turnover in CAM plants. Finally, differential expression between mesophyll and guard cell-enriched epidermis was observed for both sucrose synthases 1 and 3 (*susy1* and *susy3*), reflecting that sugars can also be metabolised independently in both mesophyll and guard cells. Likewise, their abundance was higher in CAM performing leaves (Figure 3. 4 and Figure 3. 7). Finally, based on the RNA-sequence expression between mesophyll and guard cell-enriched epidermis and between C_3 and CAM leaves of *K. fedtschenkoi*, Figure 3. 10 and Figure 3. 11 summarise the transcript abundance of the genes selected, representing the highest expression site of each gene over the 24 h.

The efficiency and quality of the reactions for each pair of primers designed were calculated creating a standard curve with different concentrations of the cDNA calibrator explained in Section 2.10 (Chapter 2). Table 3. 2 summarises the Tm for each primer and the parameters calculated. The integrity of the data and the accuracy of the dilutions were measured by a coefficient of determination (R^2) higher of 0.98 and a efficiency between 0.9 and 1.10 (Pfaffl, 2006). In the case of the primers designed for both *pgm* and *abcb14* the efficiency was slightly higher of 1.10, however, the melting curves obtained were accurate to maintain the same conditions for the genetic evaluation.

Finally, the reference gene reliability was determined by the threshold cycle values (C_t) of the control gene *K. fedtschenkoi* thioesterase/thiol ester dehydrase-isomerase (*tedi*), which was used to normalise the expression of the genes of interest. In this case, the expression of the reference gene is constitutive and does not differ among the genotypes, tissues and time points, ensuring that the assay is stable and the variations observed are products of the endogenous variations in every gene of interest that was evaluated (Figure 3. 12).

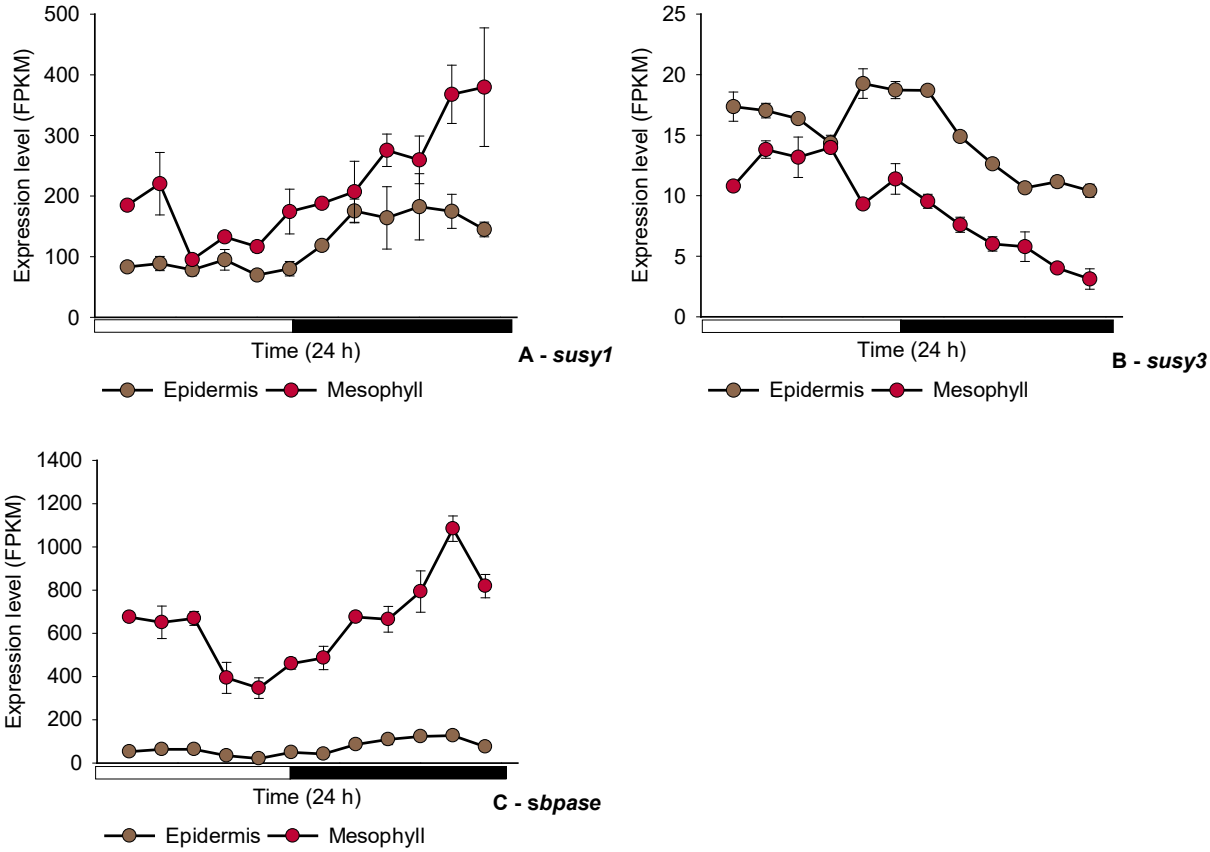

Figure 3. 4. Expression level in the mesophyll (red) and guard cell-enriched epidermis (brown) of genes implicated in sugars metabolism. The data is presented in FPKM (fragments per kilobase of exon model per million reads map) and the expression corresponds to a 24 hour day/night cycle (black bar indicates night period). (A) *susy1*; (B) *susy3*; (C) *sbpase*.

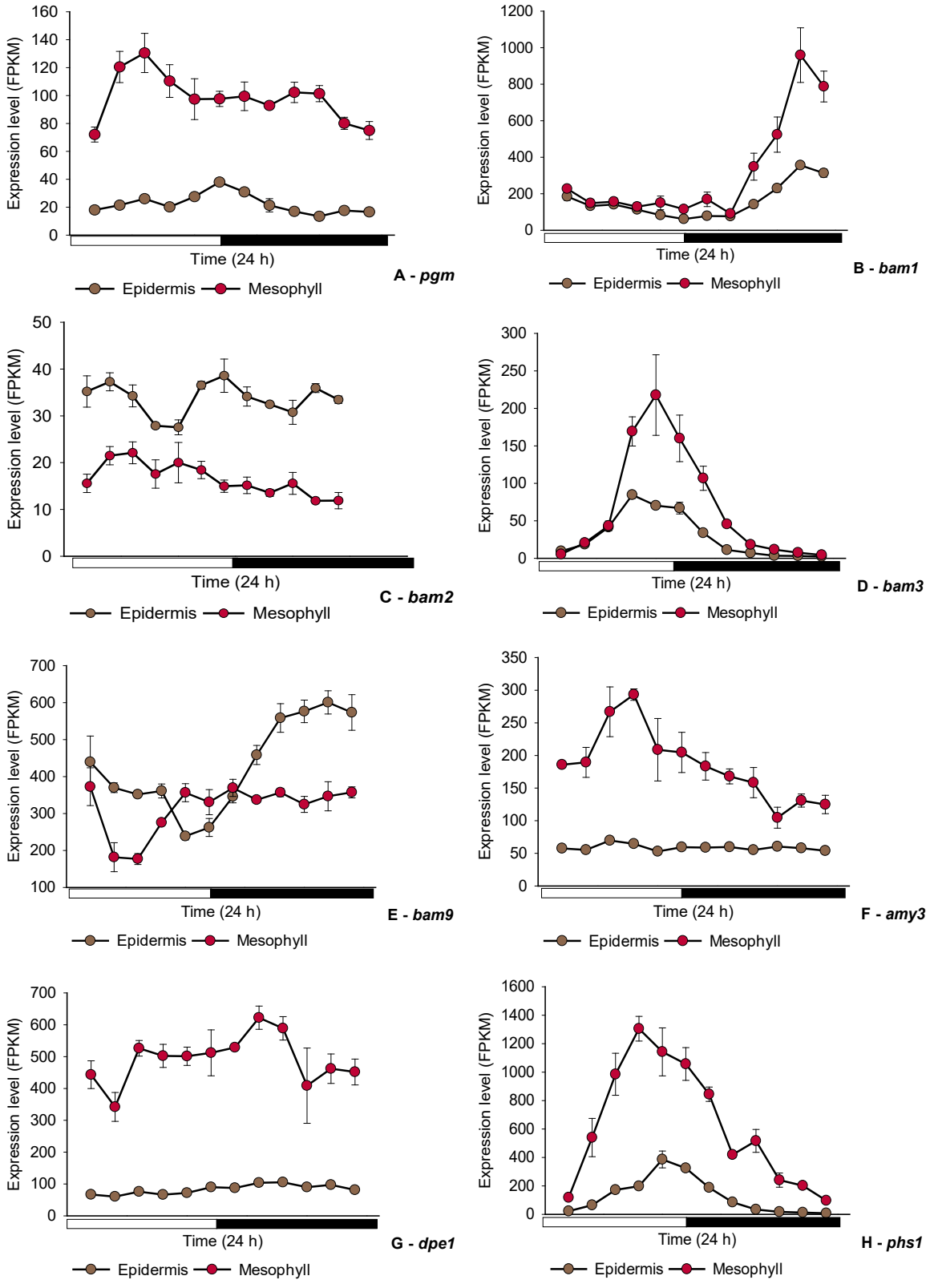

Figure 3. 5. Expression level in the mesophyll (red) and guard cell-enriched epidermis (brown) of genes implicated in starch metabolism. The data is presented in FPKM (fragments per kilobase of exon model per million reads map) and the expression corresponds to a 24 hour day/night cycle (black bar indicates night period). (A) *pgm*; (B) *bam1*; (C) *bam2*; (D) *bam3*; (E) *bam9;* (F) *amy3*; (G) *dpe1*; (H) *phs1*

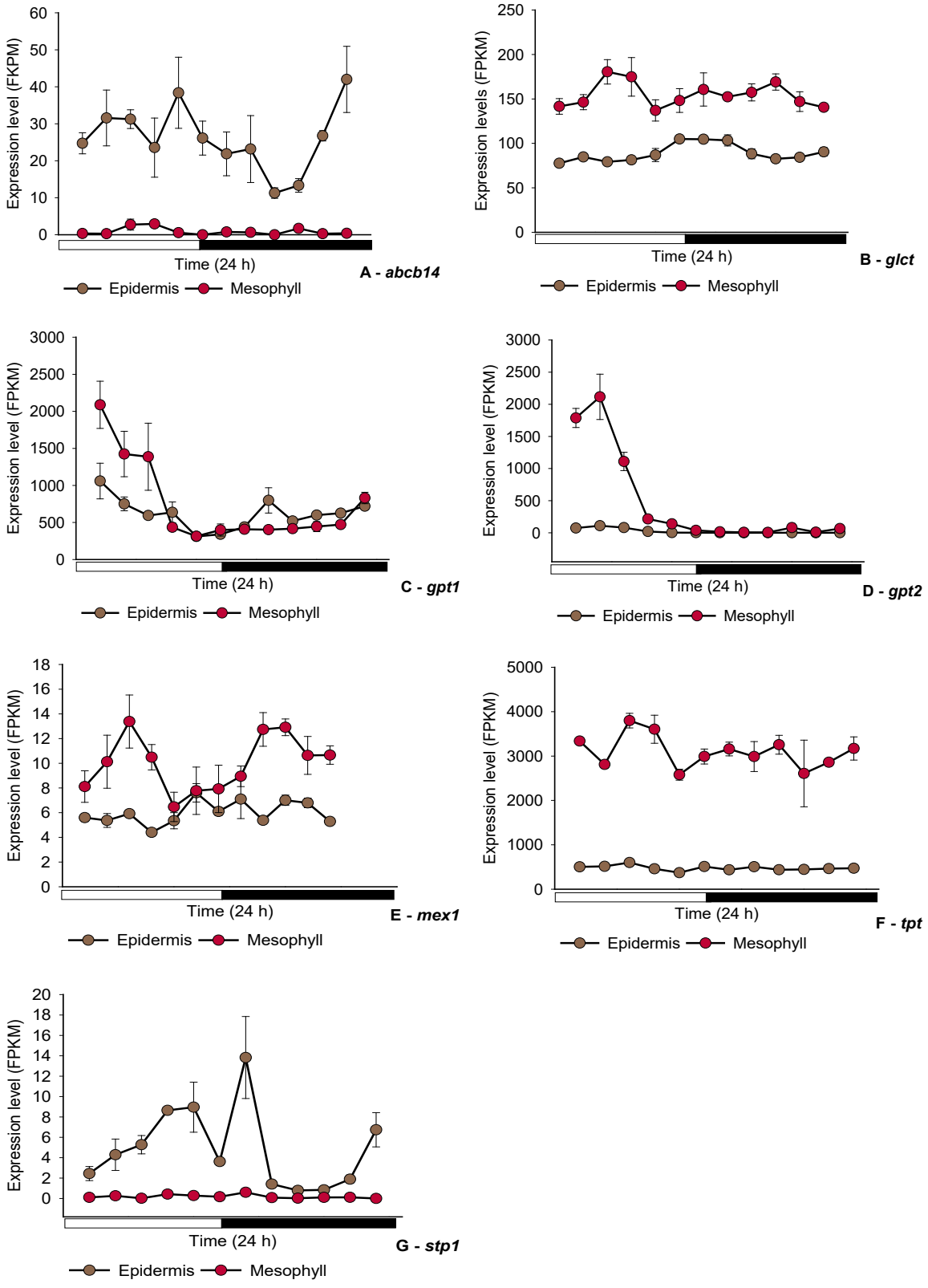

Figure 3. 6. Expression level in the mesophyll (red) and guard cell-enriched epidermis (brown) of genes implicated in malate and sugars transport. The data is presented in FPKM (fragments per kilobase of exon model per million reads map) and the expression corresponds to a 24 hour day/night cycle (black bar indicates night period). (A) *abcb14*; (B) *glct*; (C) *gpt1*; (D) *gpt2;* (E) *mex1*; (F) *tpt*; (G) *stp1*

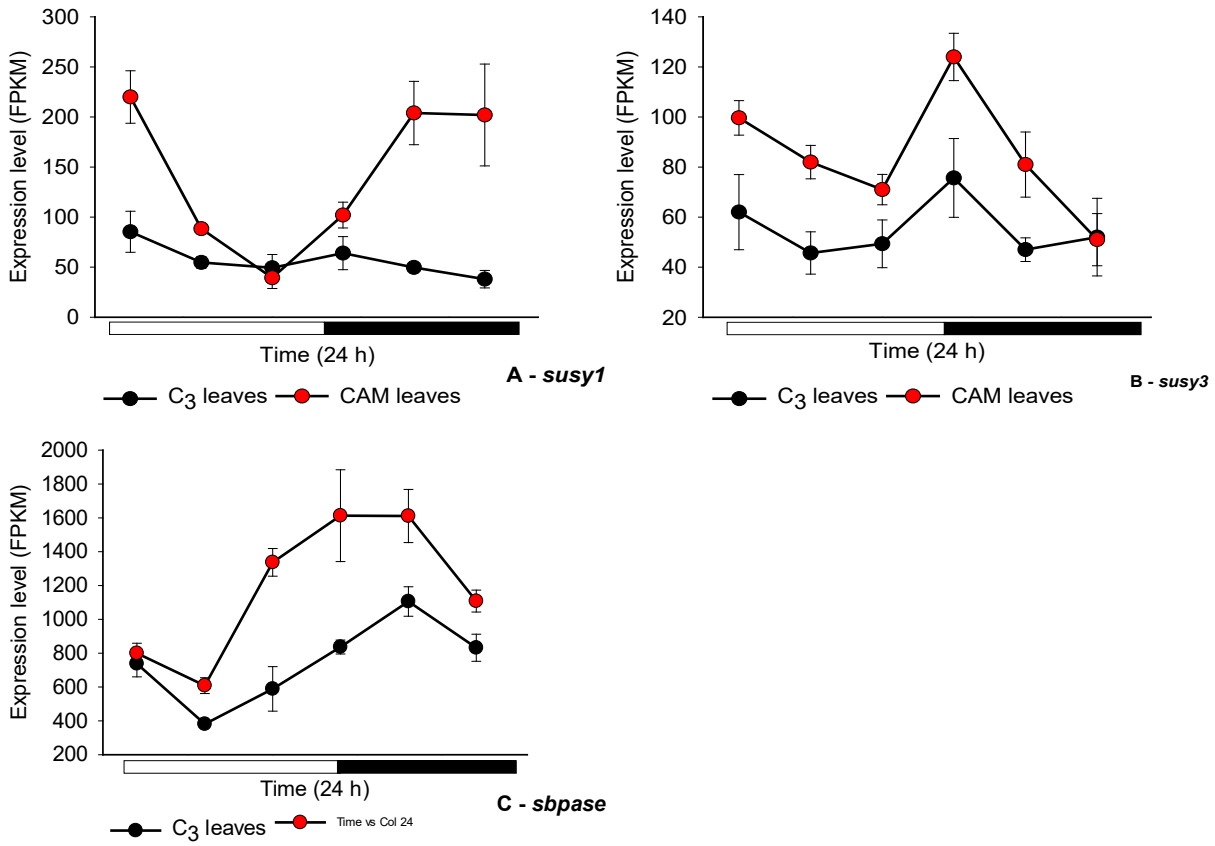

Figure 3. 7. Expression level in C_3 (black) and CAM (red) performing leaves of genes implicated in sugars metabolism. The data is presented in FPKM (fragments per kilobase of exon model per million reads map) and the expression corresponds to a 24 hour day/night cycle (black bar indicates night period). (A) *susy1*; (B) *susy3*; (C) *sbpase*.

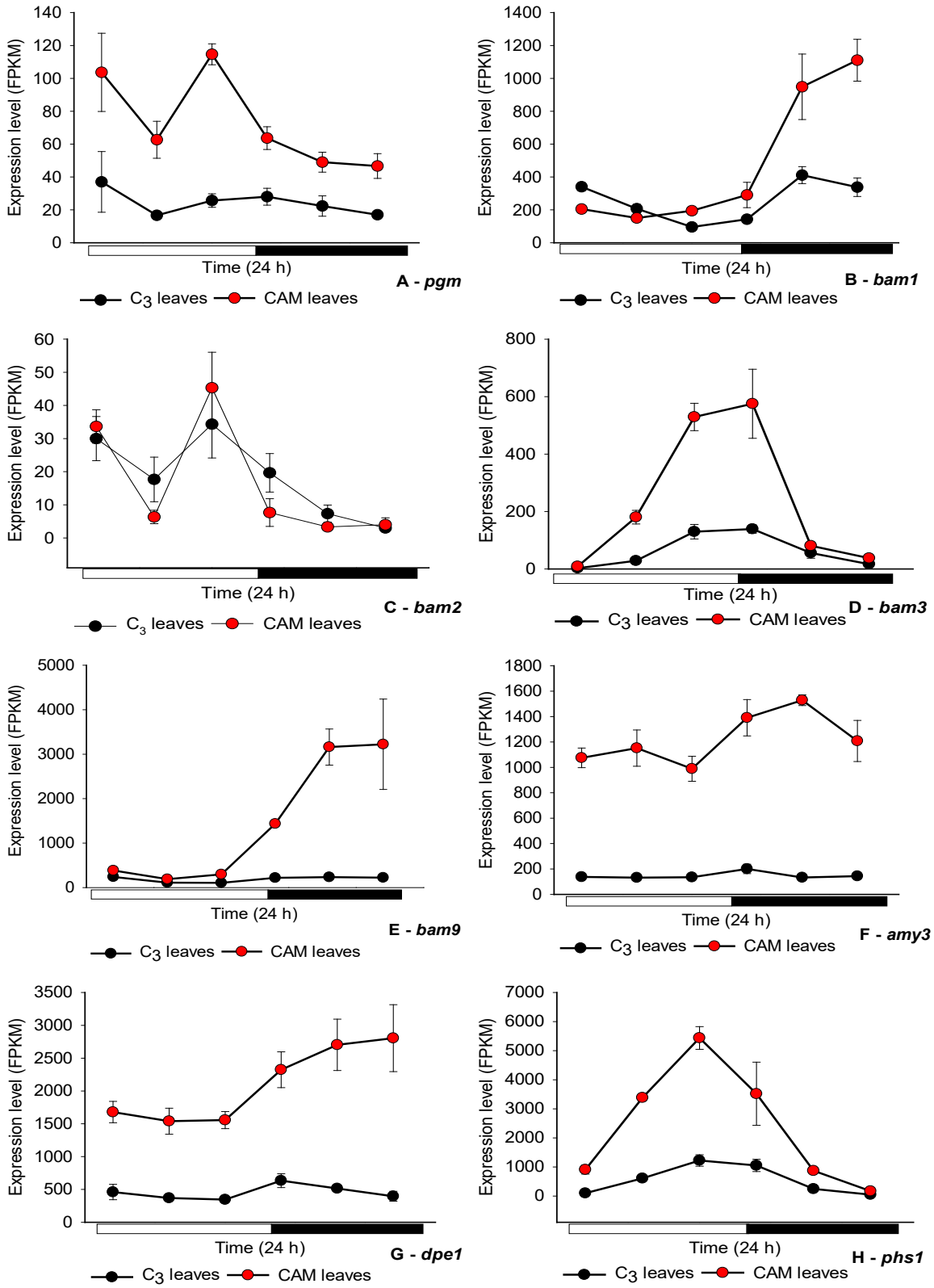

Figure 3. 8. Expression level in C_3 (black) and CAM (red) performing leaves of genes implicated in starch metabolism. The data is presented in FPKM (fragments per kilobase of exon model per million reads map) and the expression corresponds to a 24 hour day/night cycle (black bar indicates night period). (A) *pgm*; (B) *bam1*; (C) *bam2*; (D) *bam3*; (E) *bam9;* (F) *amy3*; (G) *dpe1*; (H) *phs1.*

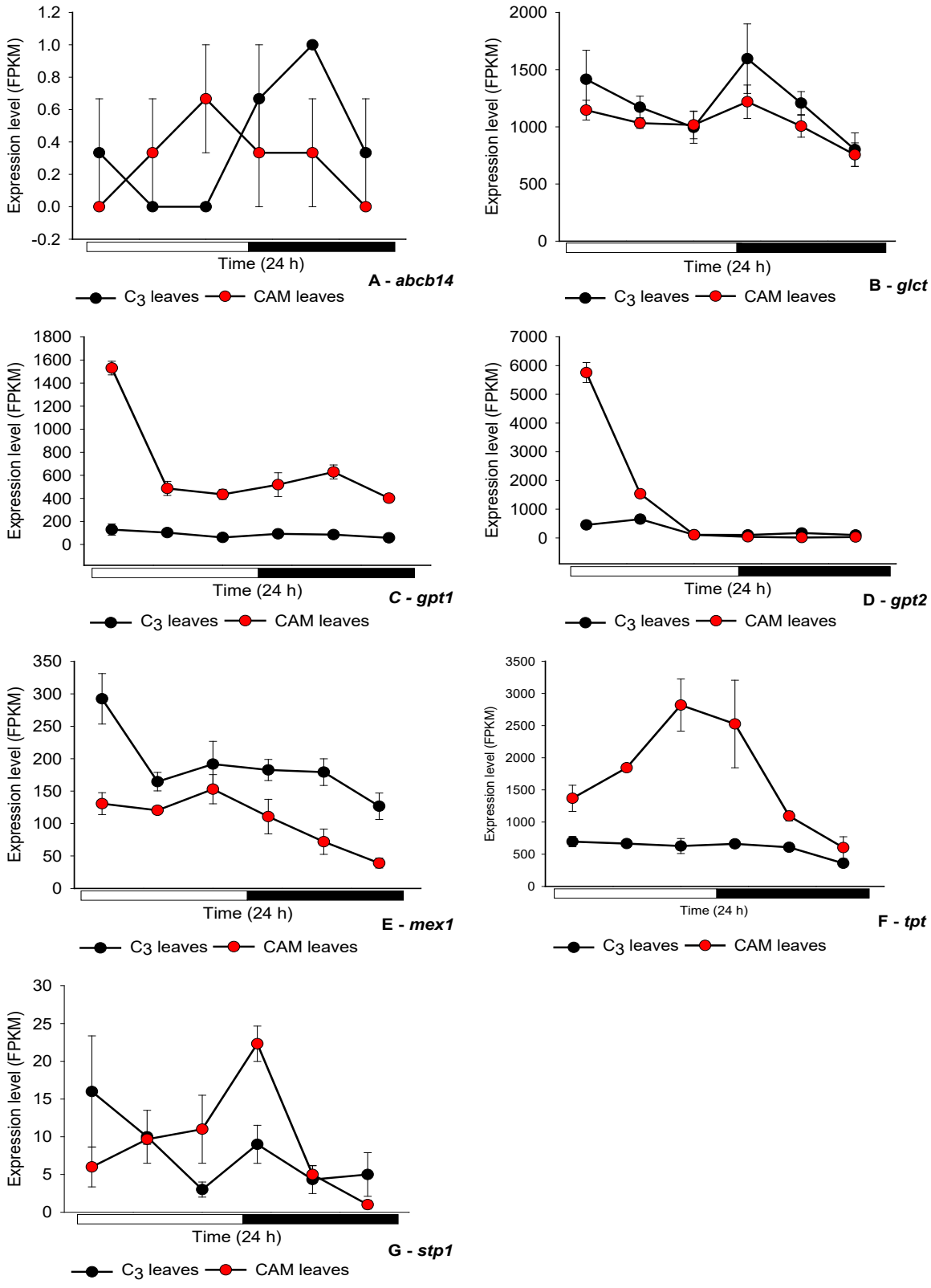

Figure 3. 9. Expression level in C_3 (black) and CAM (red) performing leaves of genes implicated in malate and sugars transport. The data is presented in FPKM (fragments per kilobase of exon model per million reads map) and the expression corresponds to a 24 hour day/night cycle (black bar indicates night period). (A) *abcb14*; (B) *glct*; (C) *gpt1*; (D) *gpt2;* (E) *mex1*; (F) *tpt*; (G) *stp1*

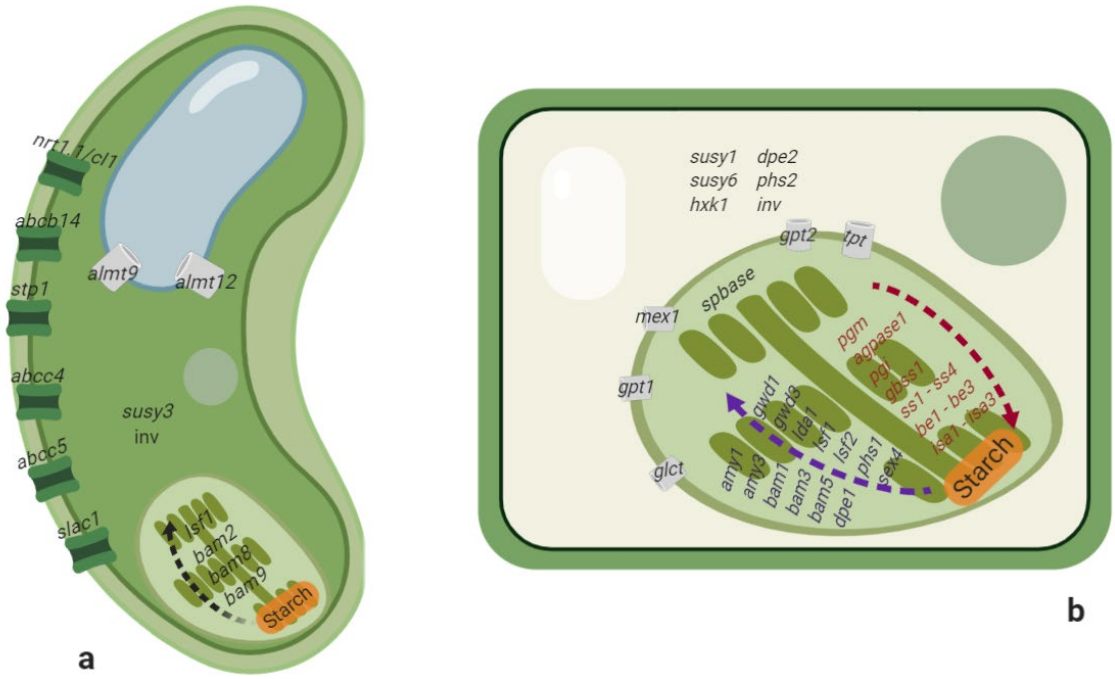

Figure 3. 10. Reported expression of genes in both guard cell-enriched epidermis (a) and mesophyll (b) of *Kalanchoë fedtschenkoi* based on the interrogation of the RNA-sequence database. The overall 24 h expression is presented and represents the highest expression site of each gene.

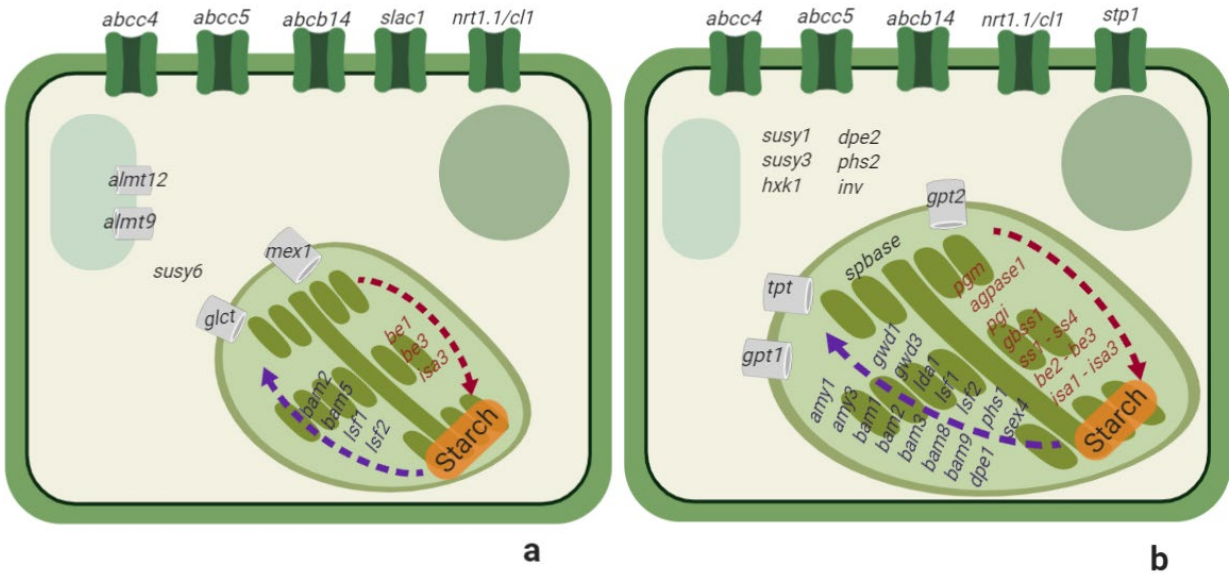

Figure 3. 11. Reported expression of genes in C_3 (a) and CAM (b) performing leaves of *Kalanchoë fedtschenkoi* based on the interrogation of the RNA-sequence database. The overall 24 h expression is presented and represents the highest expression site of each gene.

Table 3. 1. Genes interrogated in both RNA-sequence databases derived from mesophyll and guard cell-enriched epidermis, and from C_3 and CAM performing leaves of *K. fedtschenkoi*. Annotation, gene ID based on the genome published on Phytozome and *Arabidopsis thaliana* orthologues, the reported expression in C_3 plants and the expression in *K. fedtschenkoi* based on both RNAseq dataset are provided.

Category	Gene	*A. thaliana* gene code	*K. fedtschenkoi* gene code	Reported expression site in C_3 plants	RNAseq-based expression site in *K. fedtschenkoi*	RNAseq-based expression C3/CAM in *K. fedtschenkoi*
Anion transporters	Aluminium-activated malate transporter 6 *(almt6)*	AT2G17470	Kaladp0050s0298.1	Guard cells	No match	No match
	Aluminium-activated malate transporter 9 (*almt9*)	AT3G18440	Kaladp0048s0850.1	Mesophyll / Guard cells	Epidermis	C_3
	Aluminium-activated malate transporter 12 (*almt12*)	AT4G17970	Kaladp0091s0013.1	Guard cells	Epidermis	C_3
	ATP-binding cassette C4 (*abcc4*)	AT2G47800	Kaladp0024s0629.1	Guard cells	Epidermis	C_3/CAM
	ATP-binding cassette C5 (*abcc5*)	AT1G04120	Kaladp0058s0229.1	Guard cells	Epidermis	C_3/CAM
	ATP-binding cassette transporter (*abcb14*)	AT1G28010	Kaladp0095s0673.1	Guard cells	Epidermis	C_3/CAM
	Slow Anion Channel-Associated 1 (*slac1*)	AT1G12480	Kaladp0050s0214.1	Guard cells	Epidermis	C_3
	Nitrate transporter 1 (*nrt1.1/cl1*)	AT1G12110	Kaladp1295s0006.1	Guard cells	Epidermis	C_3/CAM
Starch degradation	α-amylase 1 (*amy*1)	AT4G25000	Kaladp0018s0080.1	Mesophyll	Mesophyll	CAM
	α-amylase 2 (*amy2*)	AT1G76130	Kaladp0053s0131.1	Mesophyll	No match	No match
	α-amylase 3 (*amy3*)	AT1G69830	Kaladp0014s0003.1	Mesophyll / Guard cells	Mesophyll	CAM
	β-amylase 1 (*bam1*)	AT3G23920	Kaladp0067s0309.1	Guard cells	Mesophyll	CAM
	β-amylase 2 (*bam2*)	AT4G00490	Kaladp1295s0027.1	Mesophyll	Epidermis	C_3/CAM
	β-amylase 3 (*bam3*)	AT4G17090	Kaladp0086s0015.1	Mesophyll	Mesophyll	CAM
	β-amylase 4 (*bam4*)	AT5G55700	Kaladp0086s0015.1	Mesophyll	No match	No match
	β-amylase 5 (*bam5*)	AT4G15210	Kaladp0031s0061.1	Mesophyll	Mesophyll	C_3
	β-amylase 6 (*bam6*)	AT2G32290	Kaladp0031s0061.1	Mesophyll	No match	No match
	β-amylase 7 (*bam7*)	AT2G45880	Kaladp0019s0060.1	Mesophyll	No match	No match
	β-amylase 8 (*bam8*)	AT5G45300	Kaladp0172s0023.1	Mesophyll	Epidermis	CAM
	β-amylase 9 (*bam9*)	AT5G18670	Kaladp0062s0212.1	Mesophyll	Epidermis	CAM
	Disproportionating enzyme 1 (*dpe1*)	AT5G64860	Kaladp0095s0103.1	Mesophyll	Mesophyll	CAM
	Disproportionating enzyme 2 (*dpe2*)	AT2G40840	Kaladp0067s0137.1	Mesophyll	Mesophyll	CAM

Category	Gene	*A. thaliana* gene code	*K. fedtschenkoi* gene code	Reported expression site in C_3 plants	RNAseq-based expression site in *K. fedtschenkoi*	RNAseq-based expression C3/CAM in *K. fedtschenkoi*
	Glucan water dikinase 1 (*gwd1/sex1*)	AT1G10760	Kaladp0087s0025.1	Mesophyll	Mesophyll	CAM
	Glucan water dikinase 2 (*gwd2*)	AT4G24450	Kaladp0087s0025.1	Mesophyll	No match	No match
	Glucan water dikinase 3 (*gwd3/pwd*)	AT5G26570	Kaladp0046s0175.1	Mesophyll	Mesophyll	CAM
	Limit dextrinase 1 (*lda1*)	AT5G04360	Kaladp0011s0563.1	Mesophyll	Mesophyll	CAM
	Like Sex Four 1 (*lsf*1)	AT3G01510	Kaladp0058s0346.1	Mesophyll	Epidermis	C_3/CAM
	Like Sex Four 2 (*lsf2*)	AT3G10940	Kaladp0037s0206.1	Mesophyll	Mesophyll	C_3/CAM
	alpha glucan phosphorylase 1 (*phs1*)	AT3G29320	Kaladp0024s0136.1	Mesophyll	Mesophyll	CAM
	alpha glucan phosphorylase 2 (*phs2*)	AT3G46970	Kaladp0053s0423.1	Mesophyll	Mesophyll	CAM
	Starch excess 4 (*sex4*)	AT3G52180	Kaladp0011s0575.1	Mesophyll	Mesophyll	CAM
Starch synthesis	Phosphoglucomutase (*pgm*)	AT5G51820	Kaladp0008s0557.1	Mesophyll	Mesophyll	CAM
	ADP-glucose pyrophosphorylase small subunit 1 (*agpase1*)	AT5G48300	Kaladp0048s0369.1	Mesophyll	Mesophyll	CAM
	Phosphoglucose isomerase (*pgi*)	AT4G24620	Kaladp0095s0394.1	Mesophyll	Mesophyll	CAM
	Granule-bound starch synthase 1 (*gbss*)	AT1G32900	Kaladp0067s0211.1	Mesophyll	Mesophyll	CAM
	Soluble starch synthase 1 (*ss1*)	AT5G24300	Kaladp0055s0317.1	Mesophyll	Mesophyll	CAM
	Soluble starch synthase 2 (ss2)	AT3G01180	Kaladp0011s0184.1	Mesophyll	Mesophyll	CAM
	Soluble starch synthase 3 (ss3)	AT1G11720	Kaladp0068s0243.1	Mesophyll	Mesophyll	CAM
	Soluble starch synthase 4 (ss4)	AT4G18240	Kaladp0021s0076.1	Mesophyll	Mesophyll	CAM
	Starch branching enzyme 1 (*be1*)	AT3G20440	Kaladp0051s0045.1	Mesophyll	Mesophyll	C_3
	Starch branching enzyme 2 (*be2*)	AT5G03650	Kaladp0011s0279.1	Mesophyll	Mesophyll	CAM
	Starch branching enzyme 3 (be*3*)	AT2G36390	Kaladp0108s0006.1	Mesophyll	Mesophyll	C_3/CAM
	Isoamylase 1 (*isa1*)	AT2G39930	Kaladp0085s0031.1	Mesophyll	Mesophyll	C_3/CAM
	Isoamylase 2 (isa*2, dbe1*)	AT1G03310	Kaladp0088s0032.1	Mesophyll	Mesophyll	CAM
	Isoamylase 3 (*isa3*)	AT4G09020	Kaladp0088s0032.1	Mesophyll/Guard cells	Mesophyll	CAM
Sugar transporters	Glucose transporter (*glct*)	AT5G16150	Kaladp0026s0086.1	Mesophyll	Mesophyll	C_3
	Glucose6-phosphate transporter 1 (*gpt1*)	AT5G54800	Kaladp0079s0125.1	Mesophyll	Mesophyll	CAM
	Glucose6-phosphate transporter 2	AT1G61800	Kaladp0073s0108.1	Mesophyll	Mesophyll	CAM

Category	Gene	*A. thaliana* gene code	*K. fedtschenkoi* gene code	Reported expression site in C_3 plants	RNAseq-based expression site in *K. fedtschenkoi*	RNAseq-based expression C3/CAM in *K. fedtschenkoi*
	(*gpt2*)					
	Sugar transporter 1 (*stp1*)	AT1G11260	Kaladp0010s0086.1	Guard cells	Epidermis	CAM
	Maltose exporter 1 (*mex1*)	AT5G17520	Kaladp0058s0359.1	Mesophyll	Mesophyll	C_3
	Triose phosphate translocator (*tpt*)	AT5G46110.4	Kaladp0010s0052.1	Mesophyll	Mesophyll	CAM
Sugar metabolism	Sucrose synthase1 (*susy1*)	AT5G20830	Kaladp0496s0010.1	Mesophyll	Mesophyll	CAM
	Sucrose synthase3 (*susy3*)	AT4G02280	Kaladp0045s0291.1	Guard cells	Epidermis	CAM
	Sucrose synthase 6 (*susy6*)	AT1G73370	Kaladp0053s0464.1	Mesophyll	Mesophyll	C_3
	Hexokinase 1 (*hxk1*)	AT4G29130	Kaladp0022s0170.1	Mesophyll	Mesophyll	CAM
	Invertase (*inv*)	AT5G22510	Kaladp0550s0020.1	Mesophyll	Mesophyll/Epidermis	CAM
	Sedoheptulose-1-7 bisphosphatase (*sbpase*)	AT3G55800	Kaladp0024s0355.2	Mesophyll	Mesophyll	CAM

Table 3. 2. Genes selected to be silenced and or evaluated in the mesophyll and guard cell-enriched epidermis of wild type and the selected RNAi lines of *K. fedtschenkoi* at dawn and dusk. Annotation, gene ID based on the genome published on Phytozome and *Arabidopsis thaliana* orthologues are provided. Besides, coefficient of determination (R^2) and efficiency obtained after the optimisation of the designed primers for the genes are presented.

Gene name	Annotation	*K. fedtschenkoi* gene code	*A. thaliana* gene code	Forward Primer	Reverse Primer	Tm	R^2	Efficiency
pgm	Phosphoglucomutase	Kaladp0008s0557.1	AT5G51820.1	ACAGGAAGAGAGAAGCCCAC	TCACCATGCAAAACTGGCAC	60	0.98219	1.15
phs1	alpha glucan phosphorylase 1	Kaladp0024s0136.1	AT3G29320.1	AATTCTCTGGGCTCCTTCGC	ACTCGACGCAACTGAGTCTG	60	0.99696	0.96
bam9	β-amylase 9	Kaladp0062s0212.1	AT5G18670.1	AAAGGTCCATCCCAGGCAAG	TTACAACACAGCAGGCAGGG	60	0.99118	0.96
glct	Glucose transporter	Kaladp0026s0086.1	AT5G16150.1	GAGTGGGCTTCTACTTCGGG	CATACCGAGGGAGGCAAGTC	60	0.9925	1.07
abcb14	ATP-binding cassette transporter	Kaladp0095s0673.1	AT1G28010	AGCTGTCTTGTTCTCCACCAC	ATGGCCGCCATCACTATCTC	60	0.98659	1.13
amy3	α-amylase 3	Kaladp0014s0003.1	AT1G69830.1	AGCCTCCAGCCATCATAACC	TGATCACTCACAGGCCTTCG	60	0.98437	0.91
bam1	β-amylase 1	Kaladp0067s0309.1	AT3G23920.1	TGCTTTGCCTCGCTATGATG	TTTCTCTCGCTTCCCCACTG	60	0.97192	0.93
bam3	β-amylase 3	Kaladp0086s0015.1	AT4G17090.1	CCAGCATGCAAACTGTTCTCC	TCCCCAGCAAGTTCTGTTCC	60	0.99029	0.80
dpe1	Disproportionating enzyme	Kaladp0095s0103.1	AT5G64860	ACATCCTCGGTGATTACGCC	GGAAGATGGAAGGCTGGACC	60	0.98841	0.91
gpt1	Glucose6-phosphate transporter 1	Kaladp0079s0125.1	AT5G54800.1	GTACCAGGTGCCAGTGGTAG	CAACACGCTGCACTTACGTC	60	0.98706	0.90
gpt2	Glucose6-phosphate transporter 2	Kaladp0073s0108.1	AT1G61800.1	GTCTGGTAGAGGTCACAAGCC	CGGGTAGGCTCACAGTGAAC	60	0.99709	1.00
mex1	Maltose exporter 1	Kaladp0058s0359.1	AT5G17520	TATCCATGAGCCGCAGTGTC	GGCAGCAACAACCGGTTTAG	60	0.9887	0.95
sbpase	Sedoheptulose-1-7 bisphosphatase	Kaladp0024s0355.2	AT3G55800.1	TACACTGGCGGAATGGTTCC	TGTTGGGGACGTCACATTTG	60	0.99367	0.97
stp1	Sugar transporter 1	Kaladp0010s0086.1	AT1G11260.1	TCATCCACAAAGCTTCACACAAC	GGTAAAGGCGGAAAAGCTTCG	60	0.99051	0.95
susy1	Sucrose synthase1	Kaladp0496s0010.1	AT5G20830.1	TTCATGCCAATTTACAGCGG	TGAAATCAGTGTGGTTCATGGC	60	0.97682	0.96
susy3	Sucrose synthase3	Kaladp0045s0291.1	AT4G02280.1	TGTTCCCCTTTCCGCTGATG	GCTCTTCCAAAACCAGAAGACC	60	0.96555	0.88
tpt	Triose phosphate translocator	Kaladp0010s0052.1	AT5G46110.4	TGTTTCAGTTTCGCTGCTGC	CGCCATCATCACCAACACAC	60	0.98164	0.91
tedi	thioesterase/thiol ester dehydrase-isomerase	Kaladp0068s0118.1	AT2G30720.1	TGTTGTTCCTGCCACAGAAG	TAGAGGGTGAAGGTCCCAGA	60	0.98314	1.02

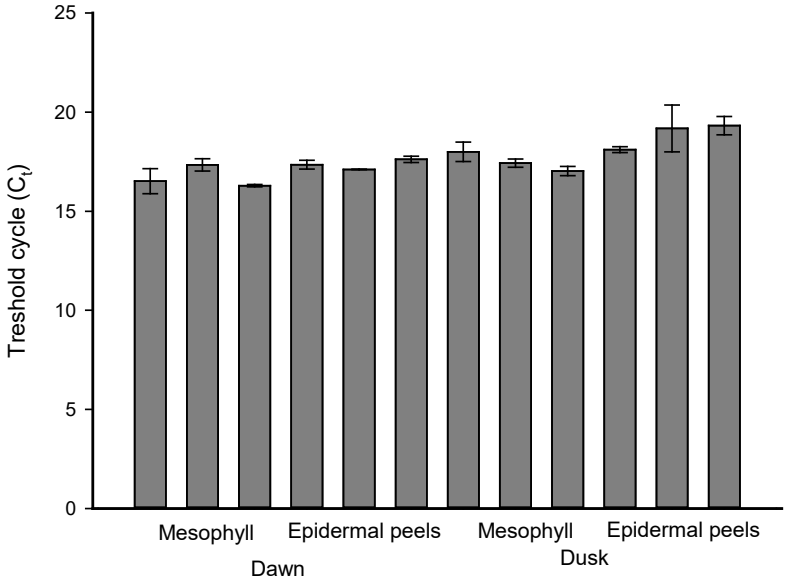

Figure 3. 12. Threshold cycle values (C_t) of the control gene *K. fedtschenkoi* thioesterase/thiol ester dehydrase-isomerase (*tedi*). The Ct values, calculated for wild type samples show similar amplification between the mesophyll and epidermal peels and between dawn and dusk using real time q-PCR.

3.4. Discussion

Kalanchoë fedtschenkoi has become an important model for genetic function in CAM research. The availability of genomic resources such as its genome sequence, transcriptomic data generated from RNAseq and protocols for its stable transformation, provide insights about gene function in different tissues and growth conditions as well as the variation in their expression over a diel period (Yang *et al.*, 2017).

The quantification of starch in *K. fedtschenkoi* guard cells showed a contrasting pattern of diel turnover compared with *Arabidopsis*. In this case, the young leaves of *K. fedtschenkoi* showed a C_3-like metabolism characterised by the degradation of starch by the action of light at the start of the photoperiod, while in CAM performing leaves starch content increased during the day and followed a slight diminution during the first hours of the night period. Males and Griffiths (2017) summarised the different internal and external factors implicated in the stomatal responses of C_3 and CAM plants. Whilst blue light and the circadian oscillator are the main diel regulators of C_3 stomata, changes in the intercellular CO_2 concentration (C_i) are proposed to be responsible for the inverted behaviour of CAM stomata. At night, CAM stomata are thought to open in response to reduced C_i caused by the consumption of CO_2 (as HCO^{3-}) by PEPC and the accumulation of malate (Borland *et al.*, 2016). In contrast, high C_i

occurs during the day (Phase III) and it is caused by the decarboxylation of the malate accumulated overnight which is thought to trigger stomatal closure (Males and Griffiths, 2017). The results in this chapter suggest day/night shift in starch turnover in CAM guard cells compared with C_3. RNAseq data from K. *fedtschenkoi* was queried to explore if this re-programming of starch metabolism in CAM guard cells is caused by a reprogramming in the expression of genes related to starch metabolism in both mesophyll and guard cell tissues.

3.4.1. Identification of genes to be further evaluated using Real Time qPCR

Based on the importance of the genes identified, three RNAi lines were selected to be biochemical and genetically characterised and these will be considered in the following chapters. These lines have curtailed expression of genes involved in starch synthesis (phosphoglucomutase 1) and starch degradation (plastidic α-glucan phosphorylase 1 and β-amylase 9).

In addition, 17 genes were chosen to be evaluated in wild type and RNAi lines. The selection was restricted to genes with differential expression patterns between mesophyll and guard cell-enriched epidermis and between C_3 and CAM leaves of *K. fedtschenkoi*, taking into account that the objective of this project is to elucidate if CAM stomatal properties are principally dictated by the mesophyll or guard cell metabolism. In this case, the genes selected are involved in starch synthesis (phosphoglucomutase - *pgm*) and degradation (β-amylases 1, 3, 9 - *bam1*, *bam3, bam9;* α-amylase 3 - *amy3;* disproportionating enzyme1 - *dpe1;* α-glucan phosphorylase1 - *phs1*), sugars transport (sugars transporter 1 - *stp1;* maltose exporter 1 - *mex1;* triose phosphate translocator - *tpt;* glucose transporter - *glct;* glucose 6-phosphate 1 and 2 - *gpt1, gpt2*), sugars metabolism (sedoheptulose-1-7 bisphosphatase - *sbpase;* sucrose synthases 1 and 3 - *susy1, susy3*), and malate transport (ATP-binding cassette transporter - *abcb14*).

3.4.2. CAM-related starch metabolism genes

Starch turnover plays an important role in plant photosynthesis and its deficiency affects both plant development and stomatal regulation (Daloso *et al.*, 2017). The highest abundance in the mesophyll and in CAM leaves of genes implicated in starch synthesis pathway, agrees with the fact that diurnal transitory accumulation of carbohydrates in mesophyll cells and their following degradation sustains the nocturnal CO_2 uptake in CAM plants (Borland *et al.*, 2016). From these genes, phosphoglucomutase (*pgm*) catalyses the interconversion of glucose

6-phosphate to glucose 1-phosphate for starch biosynthesis (Caspar *et al.*, 1985) and its absence generates a starch deficiency in plants. Lasceve *et al.* (1997) demonstrated that *pgm* deficient mutants of *Arabidopsis thaliana* were characterised by growth retardation, changes in net CO_2 uptake patterns and modifications in stomatal behaviour.

Cushman *et al.* (2008a) also studied the impact of PGM deficiency in the common ice plant *Mesembryanthemum crystallinum*, a facultative species where CAM is induced by reduced water availability or by high salinity. Under stressed salinity conditions, the starch deficient *pgm* mutants were unable to accumulate organic acids during the night as a consequence of substrate limitation, whilst nocturnal stomatal conductance and transpiration were also reduced. The importance of carbohydrate turnover to sustain CAM activity has been addressed by Borland *et al.* (2016), which proposed that transitory starch regulates plant growth and development as an energy reserve, source of soluble sugars and substrates for carbon fixation in CAM plants. The use of a phosphoglucomutase deficient line of *K. fedtschenkoi* (*rPGM1a*) for biochemical and genomic characterisation will also allow the elucidation of the starchless phenotype effect on stomatal regulation of constitutive CAM plants (Chapter 4).

Starch degradation is an important source of phosphoenolpyruvate (PEP), the main substrate for carbon fixation, which, combined with ambient CO_2 in form of HCO_3^-, produces oxaloacetate and further malate that is accumulated in vacuoles to be decarboxylated during the day-time. The high transcript abundances of α-glucan phosphorylase (*phs1*), β-amylases 1, 3, 9 (*bam1*, *bam3*, *bam9*) and α-amylase 3 (*amy3*) in CAM performing leaves supports the study of Cushman *et al.* (2008b) in *M. crystallinum* where CAM induced plants exhibited increased transcript abundances (up to 9-fold higher) of genes involved in starch degradation comparing with C_3 mode, stating the importance of starch turnover as a requirement for CAM.

Starch degradation can follow hydrolytic or phosphorolytic pathways, with some differences between C_3 and CAM plants. While nocturnal starch degradation in C_3 mesophyll follows the hydrolytic route producing maltose and glucose, via α- and β-amylases, CAM uses the phosphorolytic pathway by the action of α-glucan phosphorylase (PHS1), producing glucose 1-phosphate, which is converted either to glucose 6-phosphate, or to triose phosphate (TP) (Weise *et al.*, 2011). Higher transcript abundance of α-glucan phosphorylase (*phs1*) and disproportionating enzyme 1 (*dpe1*) in CAM performing leaves reflects the importance of phosphorolytic pathway for starch degradation. This suggests that further study of the RNAi line *rPHS1* would be valuable in determining if silencing of the phosphorolytic pathway

activates the expression of other enzymes related to starch degradation and how a deficiency of PHS1 affects CAM stomatal behaviour (Chapter 5).

The enzymes responsible for starch degradation in C_3 stomata, α-amylase 3 (AMY3) and β-amylase 1 (BAM1), are highly expressed in guard cells compared with mesophyll in *A. thaliana* (Horrer *et al.*, 2016). The expression of *amy3* and *bam1* in *K. fedtschenkoi* showed an opposite pattern reported for C_3, with transcripts for both genes being more abundant in the mesophyll. These expression differences, together with the large deposits of starch observed in guard cells over the 24 h period, could lead to the hypothesis that starch metabolism in CAM plants is more important in mesophyll to support CAM activity, while in stomata starch presence can have different roles other than serving as a precursor in the synthesis of osmolytes for stomatal opening.

Interestingly, β-amylase 9 (*bam9*) transcripts were highly expressed in guard cell-enriched epidermis compared to mesophyll. Moreover, *bam9* transcripts were negligible in C_3-like leaves but incremented at the beginning of the night period in CAM performing leaves. According to Fulton *et al.* (2008) BAM9 is a catalytically inactive enzyme and works mainly in a regulatory way, by the interaction with other enzymes facilitating the degradation of starch. In this context, the differential expression pattern observed for *bam9* between epidermis and mesophyll tissues and for α-amylase 3 (*amy3*) and β-amylase 1 (*bam1*) compared with that reported for *Arabidopsis*, could suggest a reprogramming of starch metabolism in the mesophyll and guard cells of CAM plants that could be further examined by the characterisation of *bam9* deficient lines (*rBAM9*) in *K. fedtschenkoi* (Chapter 5).

3.4.3. CAM-related sugar metabolism genes

Over the last 20 years, the starch – sucrose hypothesis has been implicated in playing a central role in stomatal opening in C_3 plants. This hypothesis proposes that during the first hours of the day, potassium is the main osmolyte responsible for stomatal opening but around midday the concentration of K^+ decreases, being replaced by sucrose, which maintains stomata open during the afternoon period (Talbott and Zeiger, 1996). Likewise, the decline in the amount of sucrose in guard cells at the end of the light period is correlated with stomatal closing (Talbott and Zeiger, 1993).

Recently, Daloso *et al.* (2016a) have proposed a non-osmoregulatory role of sucrose in guard cells, considering that its degradation generates substrates for respiration and organic acid biosynthesis that increase stomatal conductance. Experiments performed in *Nicotiana*

tabacum overexpressing the enzyme sucrose synthase 3 (SUSY3) showed that guard cells exhibited a decrease in sucrose: fructose ratio and an increase in stomatal aperture, suggesting that degradation of sucrose triggers stomatal opening. Sucrose degradation could work thus by providing substrate for the synthesis of counter ions for K^+ or by the production of ATP through the tricarboxylic acid (TCA) cycle (Daloso *et al.*, 2016b).

Based on the importance of sucrose synthases in stomatal behaviour in C_3 plants, the expressions of *susy1* and *susy3* were compared between mesophyll and guard cells-enriched epidermis of *K. fedtschenkoi*, resulting in a differential transcript abundance in both tissues with *susy1* more abundant in mesophyll and *susy3* in epidermis. This is consistent with Bieniawska *et al.* (2007) in *A. thaliana*, where *susy1* was highly expressed in mature leaves, vasculature and siliques, while *susy3* was specifically expressed in stomatal guard cells, suggesting that guard cells have a unique metabolic machinery or its regulation differs compared with mesophyll. Further evaluation of *susy1* and *susy3* in both wild type and RNAi lines of *K. fedtschenkoi* that are compromised in starch metabolism would help to elucidate if changes in starch metabolism have any implications on sucrose metabolism and stomatal regulation.

The sucrolytic activity of SUSY in the conversion of sucrose into fructose and UDP-glucose (UDPG), leads to increased levels of hexoses (Baroja-Fernández *et al.*, 2009). These degradation products of sucrose are also important in guard cell metabolism, and hexose transport can also regulate stomatal behaviour. Stadler *et al.* (2003) identified a sugar transporter protein 1 (STP1) located in the plasma membrane of guard cells involved in the import of monosaccharides to supply organic carbon in the production of energy or to have an osmoregulation function on stomatal opening. Microarray analysis from guard cells in *A. thaliana* determined the transcript abundance of genes responsive to sucrose and its implication in stomatal regulation. In relation to sugar transporters in guard cells, the abundance of sugar transporter protein 1 and 4 (*stp1* and *stp4*) were 8 to 16-fold higher than sucrose transporters (*suc*), accompanied by an increase in *susy3* expression (Bates *et al.*, 2012). This leads to the conclusion that sucrose is converted to monosaccharides by invertases before entering the guard cells and these sugars are metabolised by glycolysis or participate in the synthesis of starch (Bates *et al.*, 2012).

The expression of *stp1* in *K. fedtschenkoi* followed the same pattern observed in *Arabidopsis* by Stadler *et al.* (2003). In this case, the transcript abundance was also higher in guard cell-enriched epidermis, with a negligible abundance during the first hours of the day, followed by an increase of expression around midday and a significant increment after dusk.

According to Buttner (2007), the expression peak of sugar transporter protein (*stp1*) at midday is correlated with the maximum sucrose content in guard cells during the day and thus suggesting a possible role in osmoregulation. The higher expression of *stp1* at the start of the night could be linked to the import of monosaccharides involved in guard cell metabolism and starch synthesis. Despite seeing a similar diel expression pattern for *stp1* in *K. fedtschenkoi,* it is possible that *stp1* function differs in CAM plants compared to that proposed for *Arabidopsis*. In the case of *K. fedtschenkoi,* the higher peak in *stp1* abundance at the start of the night could imply hexose import to guard cells for an osmoregulatory function, thus connecting mesophyll metabolism and stomatal opening. However, it is also important to remember that transcript abundance does not necessarily correlate with protein abundance or activity and hexose import to the guard cells could be subject to post-translational regulation.

3.4.4. Genes related with the export of starch degradation products from the chloroplast

Several studies suggest that the main products from nocturnal starch breakdown in the chloroplasts within mesophyll are maltose and glucose. In CAM it has been reported that, besides glucose, the principal product of starch degradation in the mesophyll is glucose 1-phosphate that can be converted either to glucose 6-phosphate or to triose phosphate (Streb and Zeeman, 2012). Subsequently, these products are exported to the cytosol to undergo metabolic reactions that lead to the synthesis of sucrose, substrates for growth, development and cellular respiration (Fettke *et al.*, 2009).

Different transporters located in the chloroplast membrane, such as maltose exporter (MEX), glucose transporter (GLCT), glucose 6-phosphate transporter (GPT) and triose phosphate translocator (TPT), are responsible for exporting the products of starch degradation to the cytosol. Observing the expression between tissues in the RNAseq data for *K. fedtschenkoi*, the transcripts were more abundant in the mesophyll than in guard cell-enriched epidermis. In addition, the expression of triose phosphate translocator (*tpt*), glucose 6-phosphate transporters 1 and 2 (*gpt1* and *gpt2*) were higher in CAM leaves, while glucose transporter (*glct*) and maltose exporter (*mex*) were more abundant in C_3. This reflects the importance of starch metabolism in the mesophyll for CAM and the predominance of the phosphorolytic degradation pathway in CAM plants. Similar results were reported by Häusler *et al.* (2000) in the facultative CAM species *M. crystallinum*, where the expression of *phs1* and *gpt* increased after CAM induction, while the expression of *glct* remained unchangeable. Similarly, Neuhaus and Schulte (1996) identified the products from starch degradation in both C_3 and CAM mode, noting that in the C_3 mode maltose was the most predominant export

product from chloroplasts (50.4%), followed by 3-phosphoglyceric acid - PGA (21.9%), glucose - Glc (11%), dihydroxyacetone phosphate – DHAP (10%) and Glc6P (6.7%). On the other hand, after CAM was induced in *M. crystallinum* maltose was not produced and the main degradation product from starch breakdown was Glc6P (65.4 %) followed by 15.7% of Glc, 10.5% of PGA and 8.4% of DHAP.

Glc6P is important in the carbohydrate partitioning in CAM plants. During the day-time Glc6P is imported to the chloroplast to participate in the synthesis of starch, while in the night period it is a precursor in the supply of phosphoenolpyruvate (PEP), the main substrate for nocturnal carboxylation in CAM plants (Borland *et al.*, 2016). Apart from being a direct starch degradation product, Glc6P can also be synthesised in the cytosol by the action of hexokinases that add a phosphate group to glucose molecules exported from the chloroplast via the glucose transporter (Weber *et al.*, 2000).

3.4.5. CAM-related malate transporter genes

Malate is an important intermediate in the tricarboxylic acid cycle (TCA), involved in the production of energy and reducing power to sustain plant metabolic pathways (Fernie and Martinoia, 2009). In CAM plants, malate is accumulated in the vacuoles as the main product of the nocturnal carbon assimilation, mediated by PEPC (Borland *et al.*, 2016). Malate is also an essential modulator of stomatal behaviour, being the main counter ion for K^+ during its opening. This carboxylic acid is synthesised in the cytosol of both guard cells and mesophyll and then is transported to guard cells vacuole generating changes in stomatal turgor pressure (Santelia and Lawson, 2016).

The transport of malate across membranes can be passive through anion channels or active by transporters requiring ATP. Aluminium-activated malate transporters (ALMT) export inorganic and organic anions in response to aluminium toxicity and are located in different sites of the plant (Sasaki *et al.*, 2010). In *Arabidopsis*, three ALMT not activated by aluminium have been identified in the guard cells with roles in stomatal regulation (Eisenach and De Angeli, 2017). ALMT6 and ALMT9 are located in the tonoplast and are responsible for the transport of chloride and malate into the vacuole, while ALMT12 is located in the plasma membrane and triggers the stomata closure by the release of malate, chloride, sulphate and nitrate to the apoplast (Meyer *et al.*, 2010). Regarding malate active transport, Lee *et al.* (2008) reported that the ATP-binding cassette transporter ABCB14, located in guard cells plasma membrane, mediates malate uptake from the apoplast. Experiments with *abcb14*

deficient mutants showed an impaired stomatal opening, suggesting that the influx of apoplastic malate into guard cells increases turgor pressure and generates the opening of stomata. In addition, the rapid stomatal closure of *abcb14* mutants under high CO_2 concentrations suggest that this transporter coordinates the response of stomata to changes in internal CO_2 concentration and that malate is a pivotal metabolite regulating this response (Lee *et al.*, 2008).

Males and Griffiths (2017) suggested that diel changes in internal CO_2 concentration (C_i) as a result of starch degradation and malate carboxylation/decarboxylation that occurs in CAM mesophyll impact stomatal behaviour. This hypothesis agrees with Mott *et al.* (2008) which proposes that the signal for controlling stomatal aperture in response to C_i is generated by mesophyll cells. The findings from RNAseq data from C_3 and CAM leaves, together with the higher expression of ATP-binding cassette transporter (*abcb14*) in guard cell-enriched epidermis of *K. fedtschenkoi*, lead to hypothesise that apoplastic malate is originated by mesophyll photosynthesis and its transport to guard cells regulates stomatal behaviour. Based on that, the expression of *abcb14* in wild type and RNAi lines will help to elucidate the connection between the malate derived by CAM carboxylation and nocturnal stomatal opening. Furthermore, the differences in timing abundance of *abcb14* between CAM and C_3 performing leaves, together with the nocturnal accumulation of malate reported for CAM plants, could suggest that malate transport plays an important role in the CAM inverted stomatal rhythm.

3.5. Conclusions

- This is the first report that starch degradation in guard cells of a CAM plant differs from that in C_3 plants, evidenced by guard cell starch content over 24 hours, which rather than being degraded at the start of the day as in *Arabidopsis*, showed an increment over the first part of the day.

- The substantial differences in guard cells starch turnover and the expression of some genes implicated in starch metabolism, between C_3 and CAM suggests that a re-programming in guard cell starch metabolism in CAM plants is responsible for their inverted stomata behaviour.

- The selection of *K. fedtschenkoi* RNAi lines *rPGM1a*, *rPHS1* and *rBAM9*, and the evaluation of genes therein that are implicated in carbohydrate metabolism and which have been highlighted by the bioinformatics interrogation described in this chapter constitutes a preliminary approach for the understanding of starch metabolism and its implications for stomatal regulation in CAM plants.

Chapter 4. Investigating the effect of starch deficiency on stomatal behaviour in *Kalanchoë fedtschenkoi*

4.1. Introduction

Photosynthesis in higher plants is characterised by the accumulation of sugars, an important source for energy production and synthesis of starch, a polysaccharide formed by α-1, 4-linked and α-1, 6-linked glucose polymers that make up amylose and amylopectin molecules, respectively. Starch is located in the plastids and is generally the most important storage carbohydrate responsible for different metabolic processes such as respiration, growth, development and energy production (Stitt and Zeeman, 2012). Starch can be considered to be either transitory or storage. Transitory starch is located in the photosynthetic tissues and is accumulated over the light period and degraded at night to provide carbohydrates for growth and development, while storage starch is accumulated mainly in roots, seeds and tubers, acting as a long-term energy source (Tetlow *et al.*, 2004).

Starch turnover sustains plant metabolism; in many species with CAM (crassulacean acid metabolism), the degradation of starch in the leaf mesophyll supports nocturnal CO_2 uptake through the provision of PEP (phosphoenolpyruvate) whilst the stomata are open (Borland *et al.*, 2014). This enables the synthesis of malate (a four-carbon molecule), which is decarboxylated during the day generating a high internal CO_2 concentration that maintains stomatal closure during the light period, a unique CAM characteristic. The day-time closure of stomata in CAM ensures a massive reduction of water loss and makes these plants very efficient in arid habitats (Haider *et al.*, 2012). In plants with C_3 photosynthesis that fix ambient CO_2 during the day through Rubisco to generate the three-carbon molecule, 3-phosphoglycerate, mesophyll starch is also degraded during the night producing maltose, glucose and glucose-1-phosphate that act as substrates for ATP generation and growth (Streb and Zeeman, 2012). These degradation processes will be widely covered and discussed in the next chapter. The current chapter focuses on starch synthesis and its implications for stomatal regulation in CAM plants.

The synthesis of starch occurs within the chloroplasts of the photosynthetic tissues during the light period and is directly related to Calvin cycle activity. One of its products, fructose 6-phosphate (Fru6P), is converted to glucose 6-phosphate (Glc6P) by the action of the enzyme phosphoglucoisomerase (PGI) and subsequently transformed into glucose 1-phosphate

(Glc1P) by the enzyme phosphoglucomutase (PGM) (Stitt and Zeeman, 2012). Finally, ADP Glucose pyrophosphorylase (AGPase) produces ADPGlc from Glc1P, an irreversible step that liberates inorganic pyrophosphate (PPi), and which is the precursor of the starch granule formation catalysed by starch synthases (SSs), branching enzymes (BEs) and debranching enzymes (DBEs), involved in the synthesis of amylose and amylopectin (Streb and Zeeman, 2012). It has been proposed that mutations affecting the activity of these enzymes reduce the synthesis of starch, which in turn has a direct impact on plant growth and carbon partitioning between sink and source organs (Fernie *et al.*, 2001).

In CAM plants, a mutation in phosphoglucomutase has previously been shown to affect metabolism and growth (Cushman *et al.*, 2008a). In the facultative CAM halophyte *Mesembryanthemum crystallinum*, *pgm* mutants showed negligible starch content, an elevated content of soluble sugars and low levels of malic acid accumulated overnight compared with wild type. This indicates that starch has an important function providing substrates, as PEP for nocturnal carboxylation (Cushman *et al.*, 2008a). Likewise, the study of Haider *et al.* (2012) on the same *pgm* mutant reported a curtailment in nocturnal net CO_2 uptake and nocturnal stomatal opening which suggests that the starch-deficient phenotype also affects stomatal conductance.

The importance of starch in stomatal behaviour has been studied in the C_3 model, *Arabidopsis thaliana.* Lasceve *et al.* (1997) reported that stomatal opening under blue light is reduced in *pgm* mutants and suggested that stomatal conductance in C_3 plants is regulated by light quality and intensity. Similarly, Santelia and Lawson (2016) proposed that blue light stimulates both H^+-ATPase and starch degradation in the guard cells of C_3 plants which resulted in stomatal opening. These studies have established that starch degradation in C_3 guard cells is triggered by the effect of blue light and is pivotal for the opening of stomata. Guard cell starch degradation is believed to produce malate that acts as a counter ion for K^+ influx during the first hours of the day, which subsequently becomes the principal osmolyte to maintain stomatal opening in C_3 plants.

Because the relationship between stomatal physiology in CAM plants and starch metabolism is currently not known, the following hypotheses have been formulated to address the effect of a starchless phenotype on CAM activity and stomatal conductance:

Hypothesis 1: Starch is important for providing substrate for nocturnal CAM activity and stomatal opening.

Hypothesis 2: Low starch content in *pgm* RNAi lines generates low levels of malate and sucrose, important osmolytes to maintain the turgor pressure of guard cells.

Hypothesis 3: During the day (Phase III of CAM), stomatal conductance is higher in *pgm* compared to wild type due to the low internal CO_2 concentration caused by a reduction of malate decarboxylation.

Hypothesis 4: CAM stomata are insensitive to light and their opening is regulated by factors other than starch degradation such as the response to a low internal carbon concentration and acid accumulation.

4.2. Sampling and methods

For the experiments reported in this chapter, the RNAi line *rPGM1a* that lacks the enzyme phosphoglucomutase was used. Following the growth and sampling conditions mentioned in Section 2.1 (Chapter 2), the harvesting of samples from the RNAi line together with wild type was performed over a 24 hour day/night cycle. For mesophyll tissue, samples were collected at 8:30 (lights turned on), 12:30, 16:30, 20:30 (lights turned off), 00:30, 4:30 and 7:30; and for epidermal tissue the sampling was performed at 8:30 (lights turned on), 10:30, 14:30, 18:30, 19:30 (lights turned off), 21:30, 1:30, 5:30. Sections 2.2 – 2.5 (Chapter 2) described the biochemical assays performed to determine the effect of the starch deficiency on stomatal anatomy, content of starch, soluble sugars and malate, as well as on physiological factors such as net CO_2 uptake, stomatal conductance and transpiration.

Comparisons of stomatal pore aperture, pore length, stomatal index (Equation 4. 1) and density per mm^2 between wild type and *rPGM1a* were obtained by making stomatal impressions from both surfaces of the leaf over the 24 hours period. Clear nail varnish was painted over an approximate area of two cm^2 near the middle of the leaf but avoiding the mid rib. After 10 minutes when the nail varnish was dry, a piece of sellotape was pressed on the painted area and quickly peeled off, to ensure having the stomatal imprint attached. This was then stuck onto a microscope slide and observed under the 20 X stage lens on the microscope bright field (Leica DMRB fluorescence microscope), 10 views per peel for each surface were recorded averaging the measures obtained. All the images were analysed using the software ImageJ (Schneider *et al.*, 2012), (Appendix B gives more details of these measurements). Finally, based on pore length and stomatal density, the maximum theoretical stomatal conductance (g_{max}) was estimated using Equation 4. 2 reported by Lawson *et al.* (2018).

$$Stomatal\ index\ (\%) = \frac{Stomata\ cells}{Stomata + Epidermal\ cells} \times 100$$

Equation 4. 1. Calculation of stomatal index (%) on epidermal tissue of wild type and *rPGM1a* lines of *K. fedtschenkoi* over a 24 h period.

$$g_{max} = \frac{\frac{Dw}{v} SD.pa_{max}}{pd + \frac{\pi}{2}\sqrt{\frac{pa_{max}}{\pi}}}$$

Equation 4. 2. Maximum theoretical stomatal conductance (g_{max}).Dw is diffusivity of water vapour in air at 25 °C (0.0000249 $m^2\ s^{-1}$), v is molar volume of air (0.0245 $m^3\ mol^{-1}$), SD is stomatal density (stomata m^{-2}), pa_{max} is maximum stomatal pore area (m^2) calculated as an ellipse, pd is stomatal pore depth (m) considered to be equivalent to the width of a turgid guard cell. $\frac{\pi}{2}\sqrt{\frac{pa_{max}}{\pi}}$ is the 'end correction' that takes into account the influence of diffusion shells from outside the end of stomatal pore (Lawson *et al.*, 2018).

To establish a link between blue light and starch metabolism in determining stomatal response, changes in light quality were applied to both wild type and *rPGM1a* plants. Responses in net CO_2 uptake and stomatal conductance to changes in light quality were monitored during the night (Phase I). After five hours of darkness, the leaf was irradiated with red light (600 µmol $m^{-2}\ s^{-1}$), red plus blue (RED: 600 µmol $m^{-2}\ s^{-1}$: BLUE 10%) and blue light only (10 µmol $m^{-2}\ s^{-1}$), with each treatment imposed for one hour. A control treatment consisted of the measurement of both parameters under conditions of 12 h light/12 h darkness under a 24 hour cycle.

To determine the PGM isoform that had been silenced in the RNAi line, mesophyll tissue of both *rPGM1a* and wild type was collected at the end of the light period. Protein isolation and Native PAGE were conducted based on the methods described in Sections 2.6 and 2.7 (Chapter 2). To identify the subcellular localisation of the silenced PGM isoform, the sequences annotated for this protein in *K. fedtschenkoi* were analysed using the bioinformatics tool TargetP, which is based on N-terminal motifs and predicts chloroplastic (cTPs), mitochondrial (mTPs), secretory (SPs) and other transit peptides (Emanuelsson *et al.*, 2007), therefore confirming with UniProtKB/Swiss-Prot annotated proteins database (Boutet *et al.*, 2016). Additionally, using Geneious software, version 11.0. 3 (Kearse *et al.*, 2012), an UPGMA clustering analysis was performed with reported *K. fedtschenkoi* (Kaladp0008s0557.1, Kaladp0057s0141.1, Kaladp0059s0263.1, Kaladp0064s0039.1,

Kaladp0064s0144.1, Kaladp0101s0022.1) and annotated *Arabidopsis thaliana* (AT1G23190.1, AT5G1820.1, AT1G70730.3) PGM sequences to determine homology among isoforms.

Based on the particular interest of genes encoding enzymes involved in starch, sugars and malate metabolism and their implication in stomatal regulation, real time qPCR was used to confirm the *pgm* silencing and determine the transcript abundance of the genes ATP-binding cassette malate transporter (*abcb14*), sucrose synthases 1 and 3 (*susy1* and, *susy3*) and sugar transporter (*stp1*). These measurements were made to determine differences in abundance and day/night timing of maximal gene expression in guard cell-enriched epidermis and mesophyll cells between *rPGM1a* and wild type plants, as described in Sections 2.9 and 2.10 (Chapter2).

4.3. Results

4.3.1. Determination of starch in mesophyll and stomatal guard cells

The *rPGM1a* genotype lacked starch in both mesophyll and guard cells, compared with wild type plants (Figure 4. 1 and Figure 4. 2). In wild type, starch accumulated in the mesophyll during the light period and was then degraded at night to support carbohydrates production and phosphoenolpyruvate (PEP), an essential substrate that is carboxylated to produce malate and support CAM activity. The content of starch in wild type guard cells, represented as starch granule area (μm^2), was constant during the day, with a slight diminution at the beginning of the night period and a further increment during the middle of the night (Figure 4. 3).

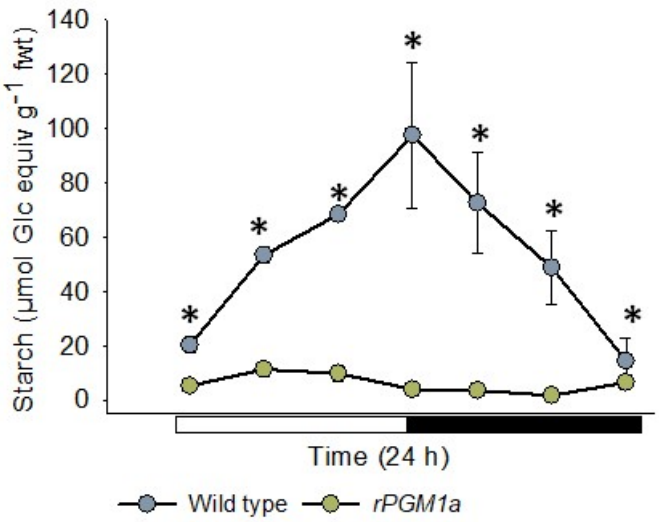

Figure 4. 1. Starch content (µmol Glc equiv g^{-1} fwt) in mesophyll of wild type (blue filling) and *rPGM1a* (green filling) plants of *K. fedtschenkoi*, during 24 hours (black bar indicates night period). Significant differences ($p \leq 0.05$) between genotypes are represented by asterisks. Leaf pair 6 was used for this analysis and the error bars indicate the standard error of three biological replicates. Plant growth conditions were set at 400 µmol CO_2 mol^{-1} air, 25°C/19°C (day/night) and a diurnal photosynthetic photon flux density – PPFD - of 250 µmol $m^{-2}s^{-1}$ at plant height.

Figure 4. 2. Starch deposits in stomatal guard cells of wild type (a) and *rPGM1a* (b) plants of *K. fedtschenkoi*. The tissue corresponds to epidermal peels of leaf pair 6. The scale bar represents 20 µm. Plant growth conditions were set at 400 µmol CO_2 mol^{-1} air, 25°C/19°C (day/night) and a diurnal photosynthetic photon flux density – PPFD - of 250 µmol $m^{-2}s^{-1}$ at plant height.

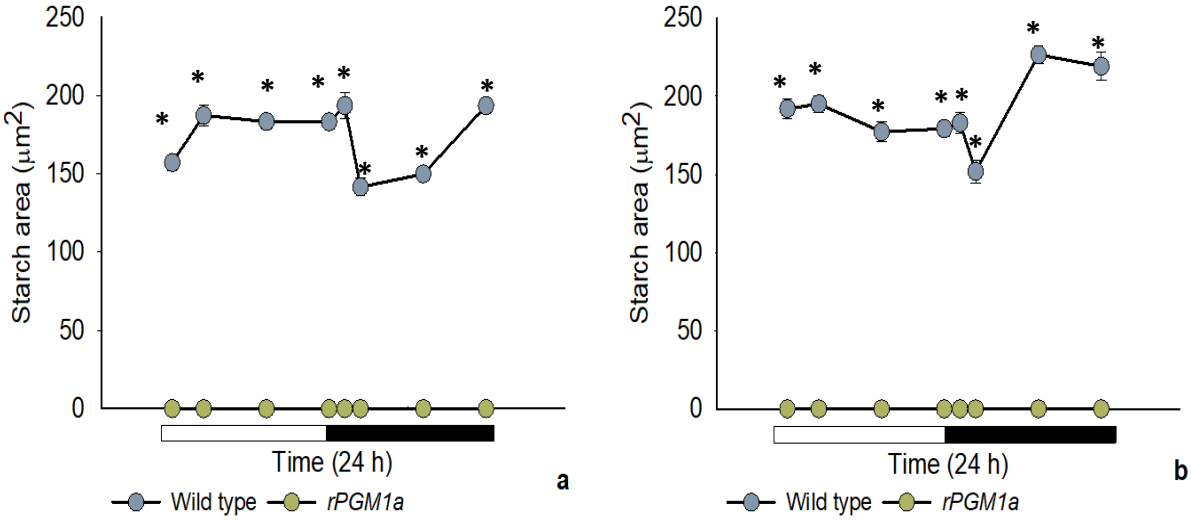

Figure 4. 3. Starch granule area (μm^2) in guard cells (a – upper epidermal surface, b – lower epidermal surface) of wild type (blue filling) and *rPGM1a* (green filling) plants of *K. fedtschenkoi*, during 24 hours (black bar indicates night period). Significant differences ($p \leq 0.05$) between genotypes are represented by asterisks. Leaf pair 6 was used for this analysis and the error bars indicate the standard error of 60 replicates (3 biological replicates, each with 20 views per replicate). Plant growth conditions were set at 400 µmol CO_2 mol^{-1} air, 25°C/19°C (day/night) and a diurnal photosynthetic photon flux density – PPFD - of 250 µmol $m^{-2}s^{-1}$ at plant height.

4.3.2. Anatomical characterisation of stomata

Stomatal impressions were taken from lower and upper epidermal surfaces from wild type and *rPGM1a* during 24 hours in order to determine the differences in pore aperture, pore length, stomatal density and stomatal index. Observations in wild type and *rPGM1a* showed that pore aperture, pore length, stomatal density and index between adaxial and abaxial surfaces were not statistically different ($p \leq 0.05$) suggesting that anatomical characteristics of stomata in both surfaces exhibit a similar pattern.

Differences between genotypes were observed for pore aperture, pore length and stomatal density. The pore aperture on the *rPGM1a* remained nearly unchanged during the 24 hours, been higher than the wild type on the day-time period but lower on the night ($p \leq 0.05$). The pattern observed in wild type corresponds with the inverted stomatal rhythm on CAM plants, characterised by the nocturnal aperture and its closure during the light period (Figure 4. 4, Table 4. 1). The starchless phenotype affected stomatal density, which was significantly lower ($p \leq 0.05$) in *rPGM1A* compared with wild type (28.638 ±1.613 and 37.164 ±1.225 stomata mm^{-2}, respectively), but did not affect the stomatal index, which was 18.361% ±0.605 for *rPGMA1a* and 17.646% ±0.501 for wild type. On the other hand, the higher pore length and

lower stomatal density observed in *rPGM1a* lines affected the maximum theoretical stomatal conductance (g_{max}) over 24 hours which was significantly higher ($p \leq 0.05$) compared with wild type (451.383 ±9.384 and 355.823 ± 15.429 mmol m^{-2} s^{-1}, respectively).

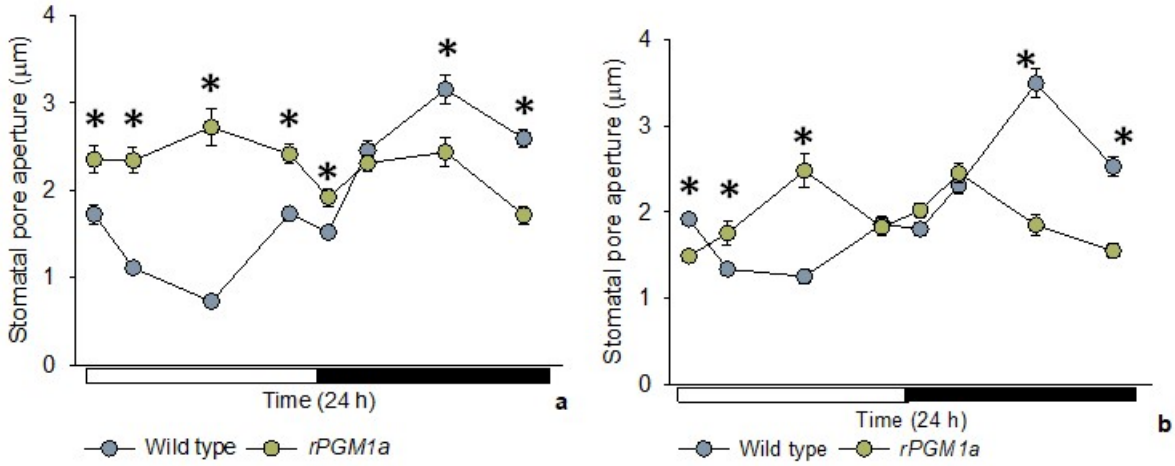

Figure 4. 4. Stomatal pore aperture (µm) measured in the guard cells (a – upper epidermal surface, b – lower epidermal surface) of wild type (blue filling) and *rPGM1a* (green filling) plants of *K. fedtschenkoi*, during 24 hours (black bar indicates night period). Significant differences ($p \leq 0.05$) between genotypes are represented by asterisks. Leaf pair 6 was used for this analysis and the error bars indicate the standard error of 60 replicates (3 biological replicates, each with 20 views per replicate). Plant growth conditions were set at 400 µmol CO_2 mol^{-1} air, 25°C/19°C (day/night) and a diurnal photosynthetic photon flux density – PPFD - of 250 µmol $m^{-2}s^{-1}$ at plant height.

Table 4. 1. Stomatal pore length and aperture (µm) measured in the guard cell-enriched epidermis of wild type and *rPGM1a* plants of *K. fedtschenkoi*, during 24 hours. Leaf pair 6 was used for this analysis and data indicate the average and the standard error of 3 biological replicates. Plant growth conditions were set at 400 µmol CO_2 mol^{-1} air, 25°C/19°C (day/night) and a diurnal photosynthetic photon flux density – PPFD - of 250 µmol $m^{-2}s^{-1}$ at plant height.

	Pore length (µm)		**Pore aperture (µm)**	
Time	WT	*rPGM1a*	WT	*rPGM1a*
8:30	15.919 (±0.207)	22.947 (±0.232)	1.820 (±0.097)	1.920 (±0.431)
10:30	15.687 (±0.340)	23.465 (±0.626)	1.222 (±0.112)	2.046 (±0.295)
14:30	18.403 (±0.278)	23.273 (±1.233)	0.988 (±0.263)	2.599 (±0.122)
18:30	17.487 (±0.516)	22.451 (±0.402)	1.793 (±0.063)	2.118 (±0.294)
20:30	16.016 (±0.084)	24.234 (±0.154)	1.658 (±0.141)	1.96 (±0.048)
22:30	17.284 (±0.590)	22.206 (±0.348)	2.381 (±0.072)	2.379 (±0.070)
2:30	17.313 (±0.068)	23.418 (±0.027)	3.321 (±0.169)	2.14 (±0.293)
6:30	17.781 (±0.447)	23.528 (±0.482)	2.558 (±0.032)	1.630 (±0.083)

4.3.3. Soluble sugars content in mesophyll and guard cell-enriched epidermis

The content of soluble sugars was significantly different ($p \leq 0.05$) between both genotypes. The concentration of sugars in *rPGM1a* increased during the day, being about seven times higher than wild type for fructose and glucose and double for sucrose (Figure 4. 5 and Figure 4. 6).

Sucrose was present in lower amounts compared with the other sugars detected, in both genotypes. In wild type, sucrose was accumulated at night, possibly as a product of the degradation of starch. In *rPGM1a* plants, sucrose content was higher in the epidermal peels than in the mesophyll, suggesting a potentially important role in the regulation of stomatal movement (Figure 4. 7). Sedoheptulose, a seven carbon monosaccharide, was also detected in both genotypes with a high content in wild type, especially in the mesophyll over 24 h and in the guard cell-enriched epidermis during the end of the light period (Figure 4. 8).

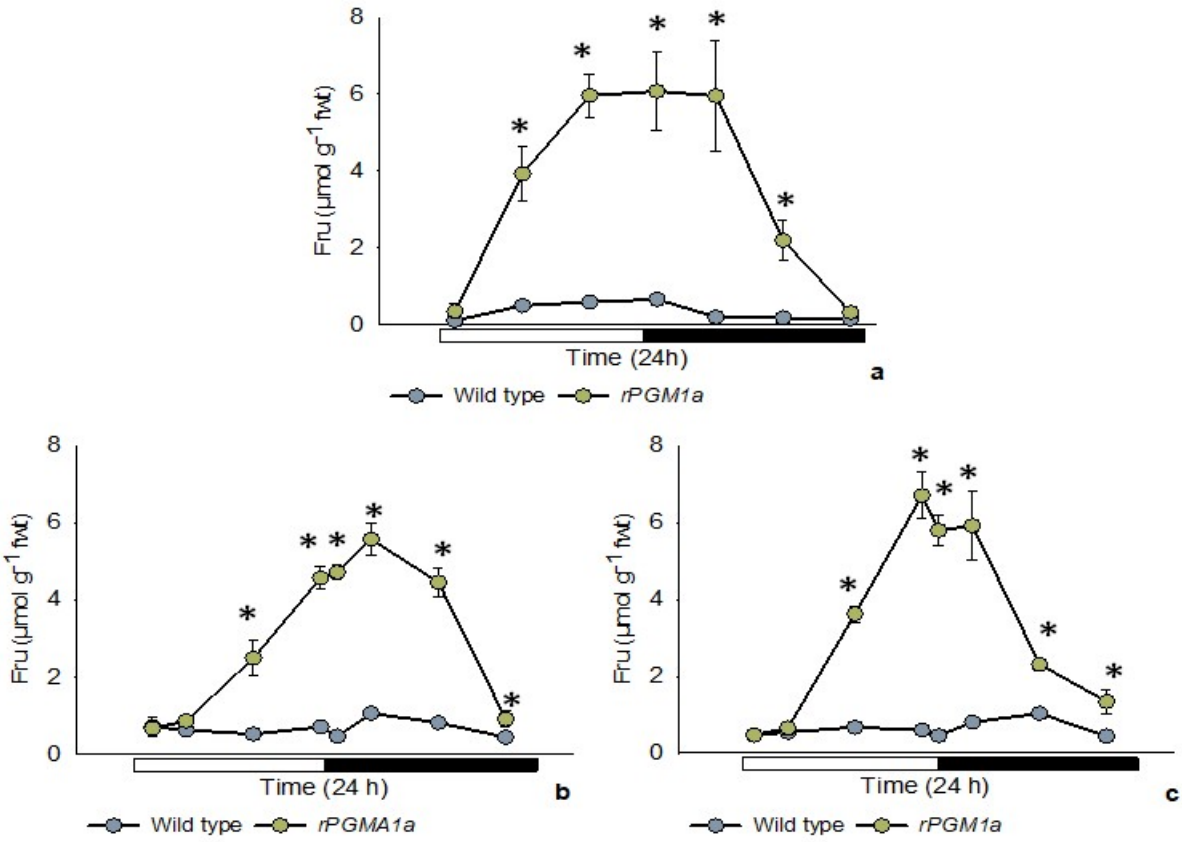

Figure 4. 5. Fructose content (µmol g^{-1} fwt) in mesophyll (a) and guard cell-enriched epidermis (b – upper surface, c – lower surface) of wild type (blue filling) and *rPGM1a* (green filling) plants of *K. fedtschenkoi*, during 24 hours (black bar indicates night period. Significant differences ($p \leq 0.05$) between genotypes are represented by asterisks. Leaf pair 6 was used for this analysis and the error bars indicate the standard error of six replicates (3 biological replicates, each with 2 technical replicates). Plant growth conditions were set at 400 µmol CO_2 mol^{-1} air, 25°C/19°C (day/night) and a diurnal photosynthetic photon flux density – PPFD - of 250 µmol $m^{-2}s^{-1}$ at plant height.

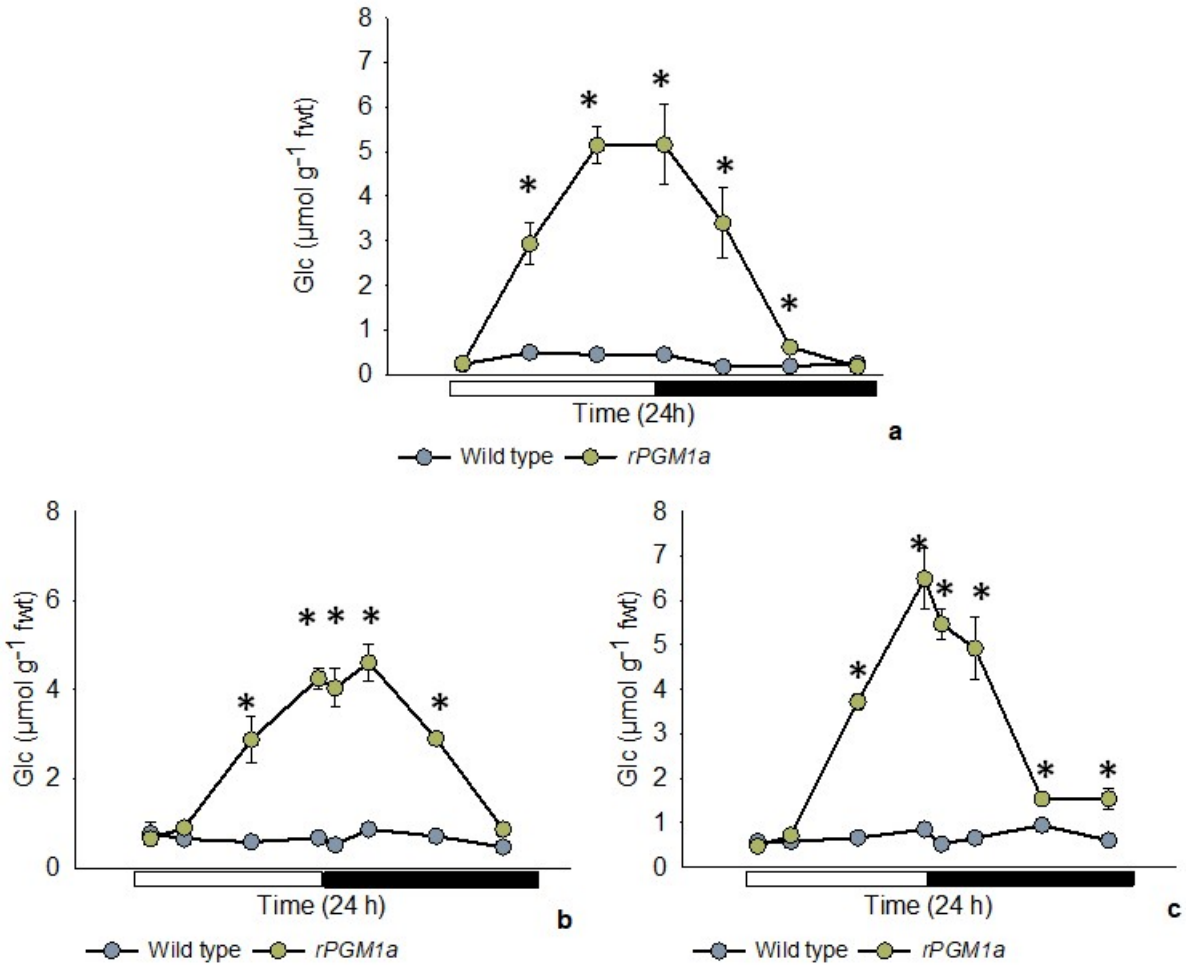

Figure 4. 6. Glucose content (µmol g^{-1} fwt) in mesophyll (a) and guard cell-enriched epidermis (b – upper surface, c – lower surface) of wild type (blue filling) and *rPGM1a* (green filling) plants of *K. fedtschenkoi*, during 24 hours (black bar indicates night period). Significant differences ($p \leq 0.05$) between genotypes are represented by asterisks. Leaf pair 6 was used for this analysis and the error bars indicate the standard error of six replicates (3 biological replicates, each with 2 technical replicates). Plant growth conditions were set at 400 µmol CO_2 mol^{-1} air, 25°C/19°C (day/night) and a diurnal photosynthetic photon flux density – PPFD - of 250 µmol $m^{-2}s^{-1}$ at plant height.

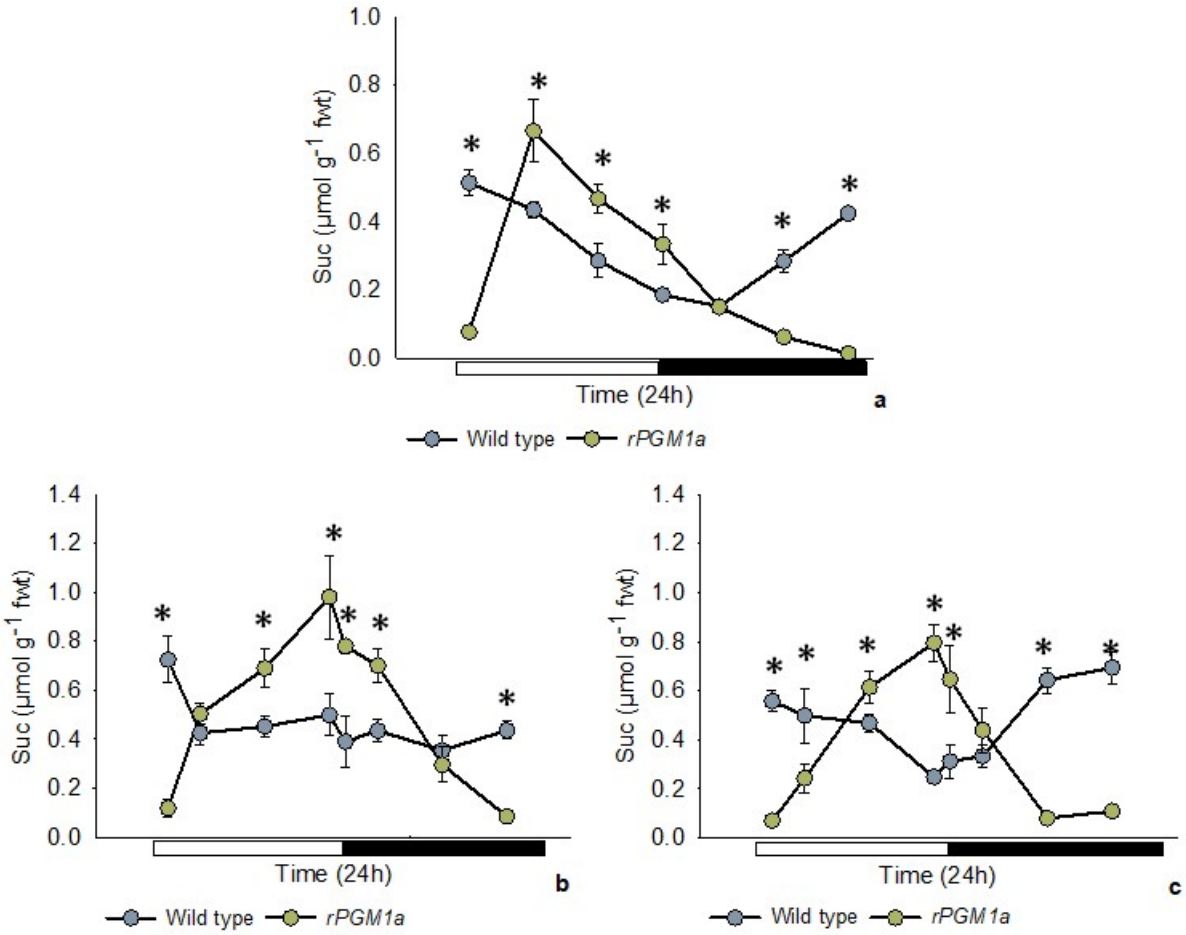

Figure 4. 7. Sucrose content (µmol g^{-1} fwt) in mesophyll (a) and guard cell-enriched epidermis (b – upper surface, c – lower surface) of wild type (blue filling) and *rPGM1a* (green filling) plants of *K. fedtschenkoi*, during 24 hours (black bar indicates night period). Significant differences ($p \leq 0.05$) between genotypes are represented by asterisks. Leaf pair 6 was used for this analysis and the error bars indicate the standard error of six replicates (3 biological replicates, each with 2 technical replicates). Plant growth conditions were set at 400 µmol CO_2 mol^{-1} air, 25°C/19°C (day/night) and a diurnal photosynthetic photon flux density – PPFD - of 250 µmol $m^{-2}s^{-1}$ at plant height.

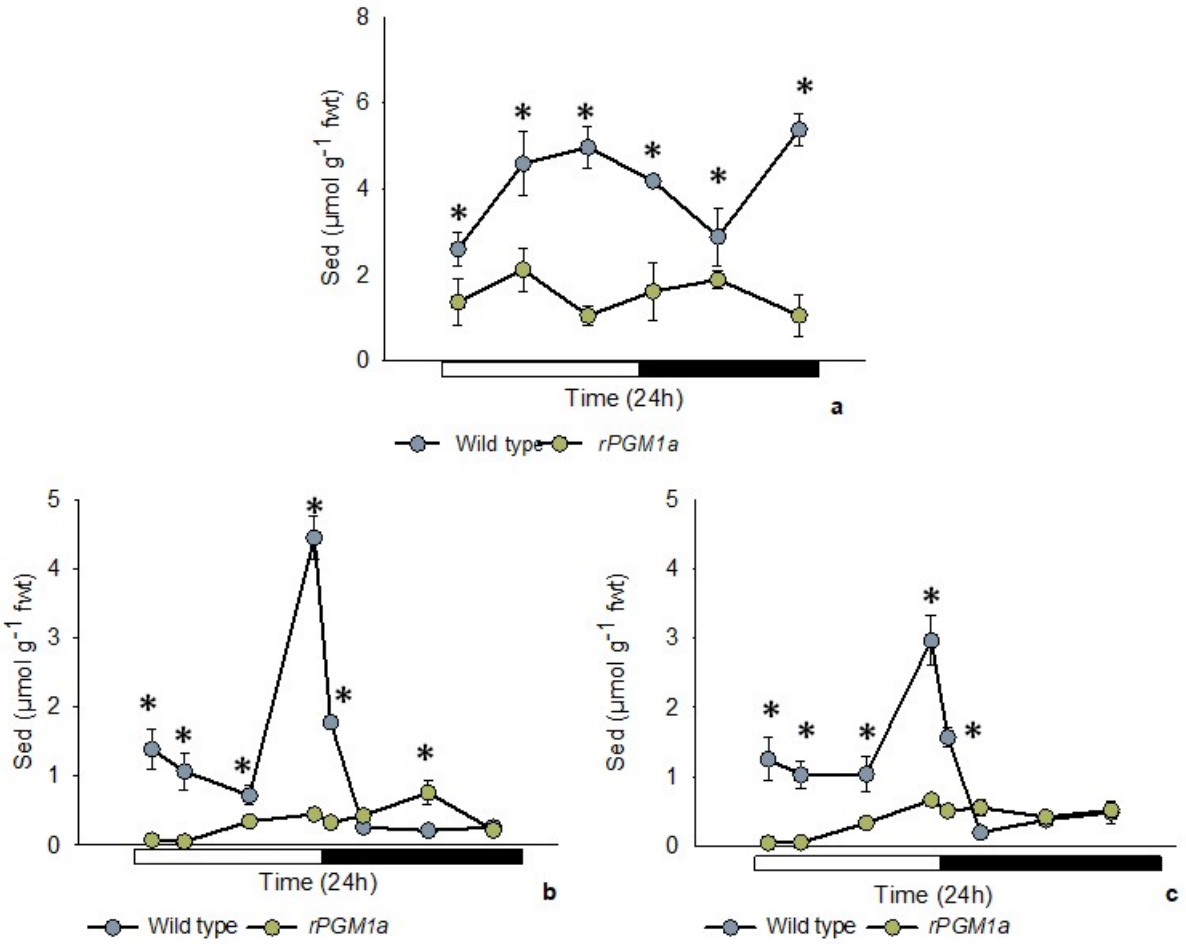

Figure 4. 8. Sedoheptulose content (µmol g^{-1} fwt) in mesophyll (a) and guard cell-enriched epidermis (b – upper surface, c – lower surface) of wild type (blue filling) and *rPGM1a* (green filling) plants of *K. fedtschenkoi*, during 24 hours (black bar indicates night period). Significant differences ($p \leq 0.05$) between genotypes are represented by asterisks. Leaf pair 6 was used for this analysis and the error bars indicate the standard error of six replicates (3 biological replicates, each with 2 technical replicates). Plant growth conditions were set at 400 µmol CO_2 mol^{-1} air, 25°C/19°C (day/night) and a diurnal photosynthetic photon flux density – PPFD - of 250 µmol $m^{-2}s^{-1}$ at plant height.

4.3.4. Quantification of malate in mesophyll and guard cell-enriched epidermis

Malate content in both genotypes represented the typical CAM turnover of this organic acid with a diurnal degradation due to its decarboxylation and a nocturnal synthesis in the mesophyll, as a product of PEP carboxylation. The nocturnal accumulation of malate in guard cells could represent its role as an osmolyte responsible for stomatal opening (Figure 4. 9).

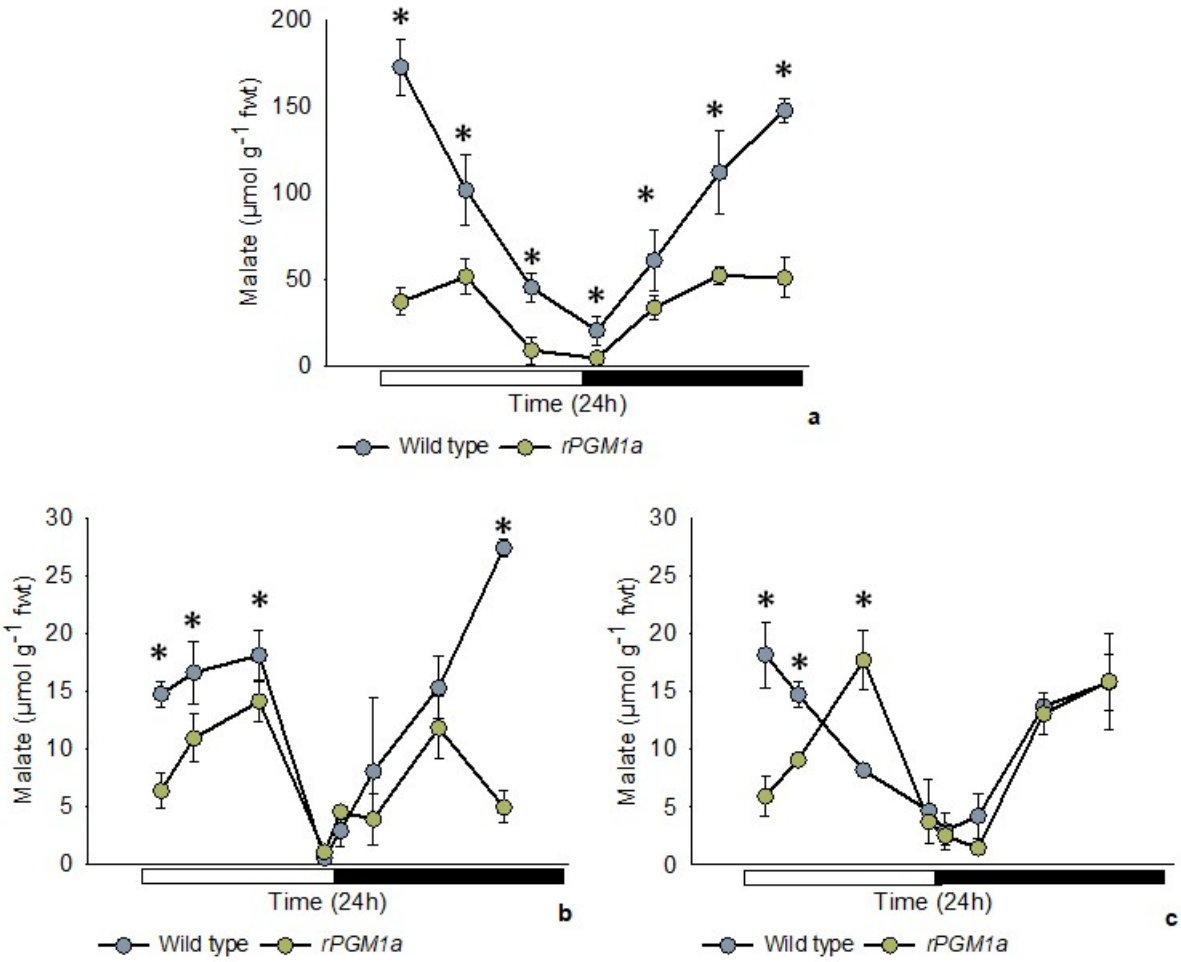

Figure 4. 9. Malate content (µmol g^{-1} fwt) in mesophyll (a) and guard cell-enriched epidermis (b – upper surface, c – lower surface) of wild type (blue filling) and *rPGM1a* (green filling) plants of *K. fedtschenkoi*, during 24 hours (black bar indicates night period). Significant differences ($p \leq 0.05$) between genotypes are represented by asterisks. Leaf pair 6 was used for this analysis and the error bars indicate the standard error of six replicates (3 biological replicates, each with 2 technical replicates). Plant growth conditions were set at 400 µmol CO_2 mol^{-1} air, 25°C/19°C (day/night) and a diurnal photosynthetic photon flux density – PPFD - of 250 µmol $m^{-2}s^{-1}$ at plant height.

Stoichiometry analysis and Pearson correlations were performed to determine the malate turnover from starch or soluble sugars, taking into account the starchless phenotype of *rPGM1a* and the lack of significant starch degradation in wild type guard cells. Starch is measured as glucose equivalents and each mole of glucose produces two moles of PEP via glycolysis and each mole of PEP is carboxylated to produce one mole of malate.

The calculations suggested that nocturnal malate formation in mesophyll was derived from starch breakdown in the same tissue ($r= -0.964$ $P\leq 0.01$), but this does not occur in guard cells ($r= -0.271$ and $r= -2.049$ for lower and upper epidermis, respectively). In the case of *rPGM1a*, the higher accumulation of soluble sugars are probably responsible for nocturnal PEP

formation by glycolysis, as a compensation for starch absence, observed in the significantly correlated turnover of malate with glucose in mesophyll ($r = -0.820$ $P \leq 0.05$) and fructose in guard cell-enriched epidermis ($r = -0.733$ $P \leq 0.05$). These data suggest that malate synthesis in *rPGM1a* is due to the higher accumulation of sugars in this line; however, the amount of malate overall is lower than in wild type, showing the importance of starch turnover in CAM activity.

4.3.5. Identification of phosphoglucomutase (PGM) isoforms using Native PAGE

The alternative gene splicing leads to the synthesis of several proteins isoforms, contributing to the proteome diversity. In some cases, the different isoforms have distinct biological roles and can be identified in multiple cell locations (Stastna and Van Eyk, 2012). The use of Native PAGE allows the identification of the protein isoforms based on protein size, shape and charge, given by the amino acid composition and post-translational modifications (Arndt *et al.*, 2012).

The PGM protein isoforms in both wild type and *rPGM1a* were identified using Native PAGE and compared with *A. thaliana* wild type. Three isoforms of PGM were observed in wild type plants and two in the starch deficient lines, lacking the middle band (Figure 4. 10). UPGMA clustering analysis shows the phylogenetic relationship among PGM isoforms in both species, suggesting that Kaladp0059s0263.1 and Kaladp0057s0141.1 gene sequences code for both PGM2 and PGM3 due to close similarity with *Arabidopsis* sequences for these isoforms. Likewise, PGM1 can be coded by Kaladp0008s0557.1, which is also the gene sequence selected to confirm the gene silencing by real time qPCR (Section 4.3.7).

Based on these results and the subcellular localisation prediction, it is expected that the silenced isoform corresponded to PGM1 and it is located in the chloroplast; while PGM2 and PGM3 are located in the cytosol. Kaladp0101s0022.1, Kaladp0064s0144.1 and Kaladp0064s0039.1 are also reported to code for PGM in *Kalanchoë*, however UniProtKB/Swiss-Prot database annotated these sequences as phosphoglucosamine mutase and 5-amino-6-uracil phosphatase, which is consistent with the lower similarity of these with the other PGM sequences, observed by the UPGMA clustering analysis (Figure 4. 11 and Table 4. 2).

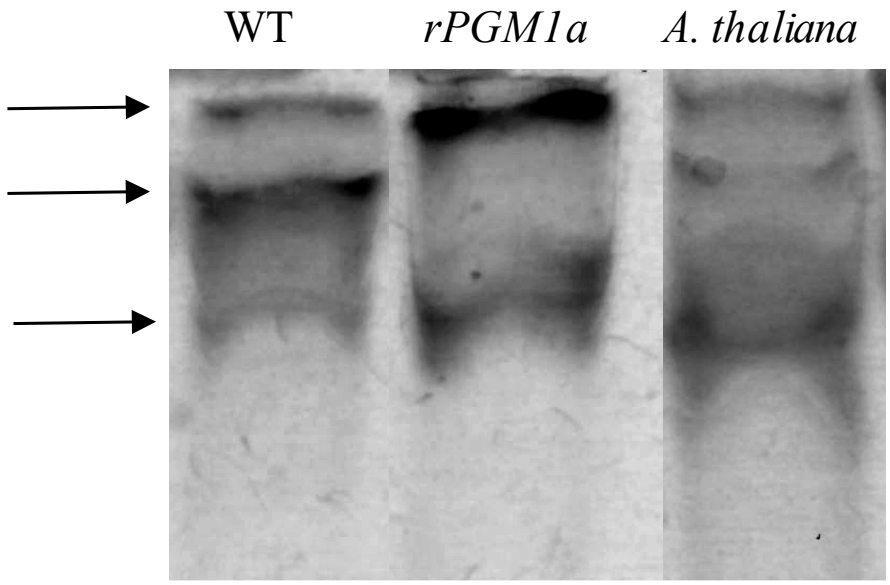

Figure 4. 10. PGM isoforms separation by Native PAGE. Whole leaf samples of *K. fedtschenkoi* wild type (WT) and *rPGM1a* lines were compared against wild type *A. thaliana* ecotype Columbia. Three isoforms (indicated with arrows) are observed in *A. thaliana* and *K. fedtschenkoi* wild type, while only two are present in *rPGM1a* starch deficient RNAi line. Plant growth conditions were set at 400 µmol CO_2 mol^{-1} air, 25°C/19°C (day/night) and a diurnal photosynthetic photon flux density – PPFD - of 250 µmol $m^{-2}s^{-1}$ at plant height.

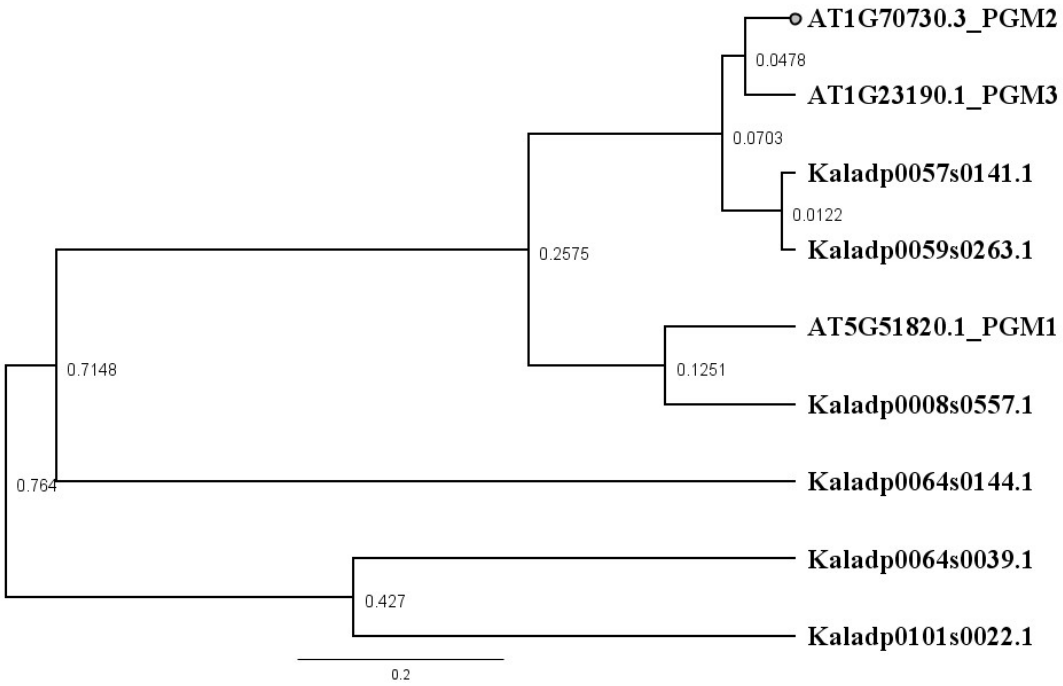

Figure 4. 11. UPGMA clustering tree for *K. fedtschenkoi* and *A. thaliana* phosphoglucomutase (PGM) isoform sequences. The overall similarities among sequences are denoted in each node by their pairwise distance value. Plant growth conditions were set at 400 µmol CO_2 mol^{-1} air, 25°C/19°C (day/night) and a diurnal photosynthetic photon flux density – PPFD - of 250 µmol $m^{-2}s^{-1}$ at plant height.

Table 4. 2. TargetP prediction of subcellular localisation of PGM isoforms reported for both *A. thaliana* and *K. fedtschenkoi*. Chloroplast transit peptide (cTP), mitochondrial targeting peptide (mTP), signal peptide (SP) and other (-) location are identified based on the final predicted score and the reliability class (RC) where 1 is the strongest prediction. UniProtKB/Swiss-Prot database annotation is also presented.

Name	Length	cTP	mTP	SP	Other	Localisation	RC	UniProtKB/Swiss-Prot annotation
AT5G51820.1_PGM1	623	0.361	0.247	0.014	0.032	Chloroplast	5	Phosphoglucomutase, chloroplastic
AT1G70730.3_PGM2	662	0.494	0.082	0.009	0.351	Chloroplast	5	Probable phosphoglucomutase, cytoplasmic 2
AT1G23190.1_PGM3	583	0.059	0.313	0.077	0.919	-	2	Probable phosphoglucomutase, cytoplasmic 1
Kaladp0008s0557.1	632	0.95	0.1	0.003	0.022	Chloroplast	1	Phosphoglucomutase, chloroplastic
Kaladp0101s0022.1	615	0.592	0.112	0.008	0.106	Chloroplast	3	Phosphoglucosamine mutase
Kaladp0059s0263.1	582	0.014	0.611	0.068	0.863	-	4	Probable phosphoglucomutase, cytoplasmic 2
Kaladp0057s0141.1	582	0.037	0.59	0.03	0.806	Chloroplast	4	Probable phosphoglucomutase, cytoplasmic 2
Kaladp0064s0144.1	352	0.504	0.856	0.005	0.017	Mitochondria	4	5-amino-6-(5-phospho-D-ribitylamino)uracil phosphatase, chloroplastic
Kaladp0064s0039.1	619	0.768	0.289	0.004	0.069	Chloroplast	3	Phosphoglucosamine mutase

4.3.6. Effect of starch deficiency on leaf gas exchange

Gas exchange analysis showed that starch absence generated a lower net CO_2 uptake during the night, but stomatal conductance was not affected, suggesting that the lower CAM activity of the *rPGM1a* is due to a deficiency in PEP carboxylation, probably by a lack of substrates and not due to a reduced stomatal opening. In addition, during the day period, *rPGM1a* line was not able to close the stomata like wild type, inferring that the higher accumulation of sugars in the *rPGM1a* guard cells during this period potentially increased stomatal turgor pressure, and thus prevented stomatal closure (Figure 4. 12).

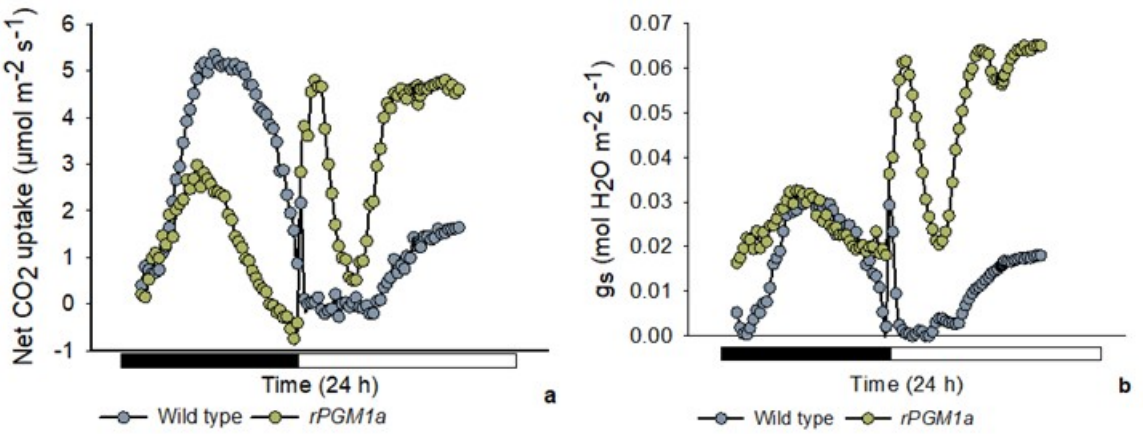

Figure 4. 12. Net CO_2 uptake (a) and stomatal conductance (b) of wild type (blue filling) and *rPGM1a* (green filling) plants of *K. fedtschenkoi*, during 24 hours (black bar indicates night period). Leaf pair 6 was used for this analysis. Plant growth conditions were set at 400 µmol CO_2 mol^{-1} air, 25°C/19°C (day/night) and a diurnal photosynthetic photon flux density – PPFD - of 250 µmol $m^{-2}s^{-1}$ at plant height.

Based on the inability of *rPGM1a* to fully close their stomata during the day it was hypothesised that a lack of substrates for nocturnal carboxylation and consequently a lower internal CO_2 concentration during day-time decarboxylation was responsible for this behaviour. Therefore, it is expected that provision of higher internal CO_2 concentration will trigger the complete closure of stomata in this RNAi line. For this reason, wild type and *rPGM1a* plants were exposed to lower (50 µmol CO_2 mol^{-1} air) and elevated (1600 µmol CO_2 mol^{-1} air) CO_2 concentrations at mid-day (Phase III) and towards the end of the photoperiod (Phase IV) in order to determine if starch deficiency impacted the stomatal response.

Data indicated that in phase III when wild type stomata are closed, the changes in CO_2 concentration do not have any effect on stomatal conductance in wild type. However, in the *rPGM1a* plants, lowering the CO_2 concentration resulted in a sustained increase in stomatal conductance (stomatal opening), which was followed by a stomatal closure when plants were exposed to elevated CO_2. Despite the high CO_2 internal concentration generated by this exposure, stomata were unable to maintain closed under elevated CO_2 and after a period, stomata re-opened (Figure 4. 13).

During phase IV (late afternoon), wild type and *rPGM1a* plants opened their stomata as a response to the reduction in internal CO_2 concentration (malate decarboxylation had ceased). Plants were again subjected to changes in external CO_2 concentration and stomatal of wild type and particularly *rPGM1a* plants opened up in response to low CO_2. After exposure to the high concentration (1600 µmol CO_2 mol^{-1} air) of CO_2, both genotypes reduced their stomata

conductance. However, in *rPGM1a* the inability to maintain the stomata closed was again observed (Figure 4. 14).

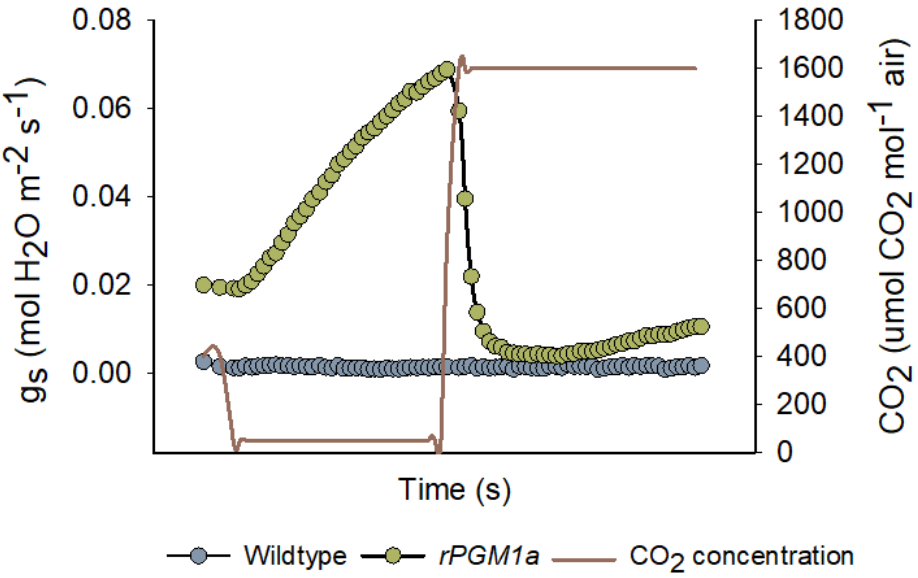

Figure 4. 13. Stomatal conductance of wild type (blue filling) and *rPGM1a* (green filling) plants of *K. fedtschenkoi*, during exposure to different ambient CO_2 concentrations (brown) during a 24 hour period of CAM phase III. Leaf pair 6 was used for this analysis. Plant growth conditions were set at 400 µmol CO_2 mol^{-1} air, 25°C/19°C (day/night) and a diurnal photosynthetic photon flux density – PPFD - of 250 µmol $m^{-2}s^{-1}$ at plant height.

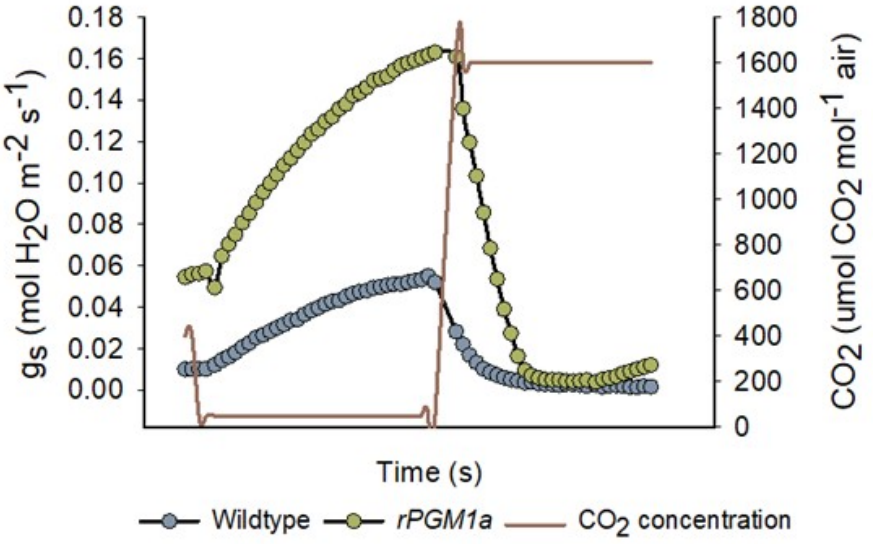

Figure 4. 14. Stomatal conductance of wild type (blue filling) and *rPGM1a* (green filling) plants of *K. fedtschenkoi*, during the exposure of different ambient CO_2 concentrations (brown) during a 24 hour period of CAM phase IV. Leaf pair 6 was used for this analysis. Plant growth conditions were set at 400 µmol CO_2 mol^{-1} air, 25°C/19°C (day/night) and a diurnal photosynthetic photon flux density – PPFD - of 250 µmol $m^{-2}s^{-1}$ at plant height.

It was also hypothesized that curtailing nocturnal CO_2 uptake will lead to a reduction in the amount of malate available for decarboxylation during the day, thus reducing day-time internal [CO_2] and preventing complete stomatal closure. To test this hypothesis, wild type and *rPGM1a* plants were exposed to CO_2 free air treatment during night period (0 µmol CO_2 mol^{-1} air) to determine the effect on net CO_2 uptake and stomatal behaviour during the day-time. A control treatment consisted of the measurement of both parameters under conditions of 400 µmol CO_2 mol^{-1} air in a 24 hour cycle.

The data indicated that after the free CO_2 night period, both genotypes fixed CO_2 during the first hours of the day, followed by a reduction in net CO_2 uptake and stomatal closure in wild type. The data also indicates that curtailing nocturnal malate accumulation delays, but does not prevent, day-time closure of stomata in wild type (Figure 4. 15). On the other hand, *rPGM1a* plants were unable to maintain their stomata closed and after a period, net CO_2 uptake increased again over the latter part of the photoperiod (Figure 4. 16). Both experiments suggested that factors other than changes in internal CO_2 concentration regulate diurnal stomatal behaviour in CAM plants and that the presence of starch has important implications for daytime stomatal regulation.

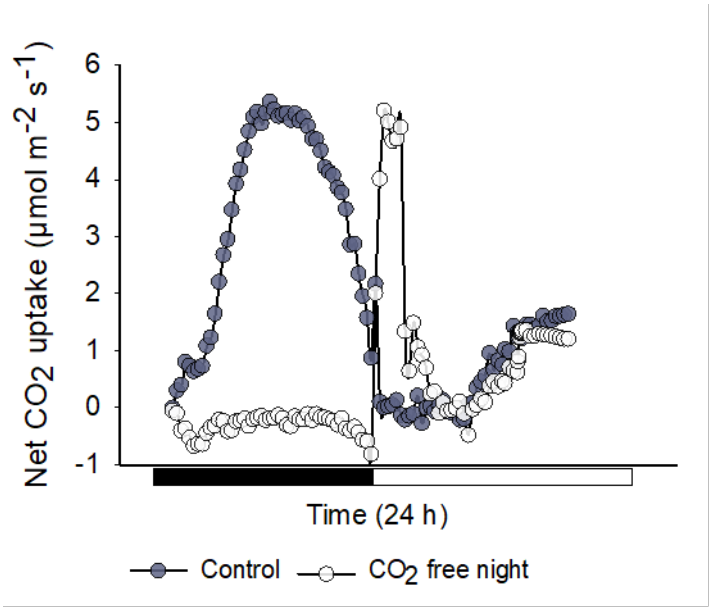

Figure 4. 15. Net CO_2 uptake of wild type plants of *K. fedtschenkoi*, during exposure to 400 µmol CO_2 mol^{-1} (blue filling) and free air treatment (white filling) during 24 hour period of CAM phase I (black bar indicates night period). Leaf pair 6 was used for this analysis. Plant growth conditions were set at 400 µmol CO_2 mol^{-1} air, 25°C/19°C (day/night) and a diurnal photosynthetic photon flux density – PPFD - of 250 µmol $m^{-2}s^{-1}$ at plant height.

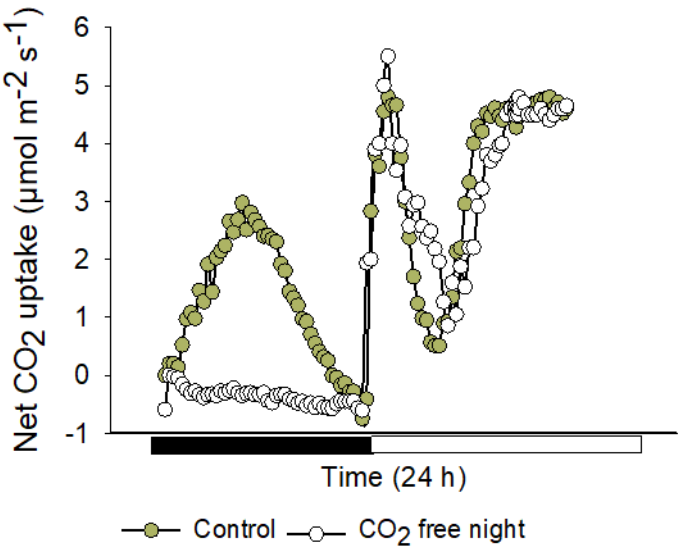

Figure 4. 16. Net CO_2 uptake of *rPGM1a* plants of *K. fedtschenkoi*, during exposure to 400 µmol CO_2 mol^{-1} (green filling) and free air treatment (white filling) during 24 hour period of CAM phase I (black bar indicates night period). Leaf pair 6 was used for this analysis. Plant growth conditions were set at 400 µmol CO_2 mol^{-1} air, 25°C/19°C (day/night) and a diurnal photosynthetic photon flux density – PPFD - of 250 µmol $m^{-2}s^{-1}$ at plant height.

Data generated from the imposition of different light qualities on both genotypes indicated that in wild type, stomatal conductance under red/blue light was greater than that measured under darkness and under red or blue light applied individually ($p \leq 0.05$). In contrast, stomatal conductance in *rPGM1a* plants increased after the imposition of red light, however, the addition of blue light did not enhance stomatal conductance as occurred in wild type, suggesting that starch is required for the blue light stomatal response (Figure 4.17 and Table 4.3).

In terms of net CO_2 uptake, this increased slightly under red/blue light in wild type compared with the other treatments, but the response was less marked than shifts in stomatal response. Likewise, there were negligible changes in net CO_2 uptake in *rPGM1a* under red and red/blue light and no increment under blue light ($p \leq 0.05$), suggesting substrate limitation for carboxylation (Figure 4.18 and Table 4.3).

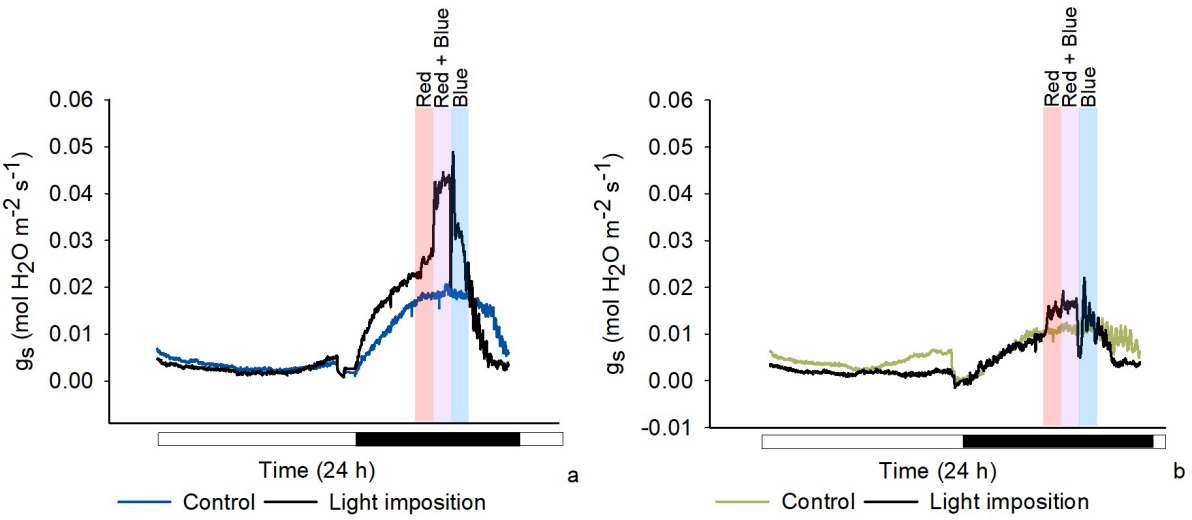

Figure 4.17. Stomatal conductance of wild type (a) and *rPGM1a* (b) plants of *K. fedtschenkoi*, during the exposure of three different light qualities: red (600 µmol m^{-2} s^{-1}), red/blue (600 µmol m^{-2} s^{-1}: blue 10%) and blue (100 µmol m^{-2} s^{-1}). Each treatment were imposed by one hour, after five hours of darkness (black bar indicates dark period). A control treatment (blue filling for wild type and green filling for *rPGM1a*) consisted of the measurement of conductance under normal conditions of light/darkness under a 24 hour cycle. Leaf pair 6 was used for this analysis. Plant growth conditions were set at 400 µmol CO_2 mol^{-1} air, 25°C/19°C (day/night) and a diurnal photosynthetic photon flux density – PPFD - of 250 µmol $m^{-2}s^{-1}$ at plant height.

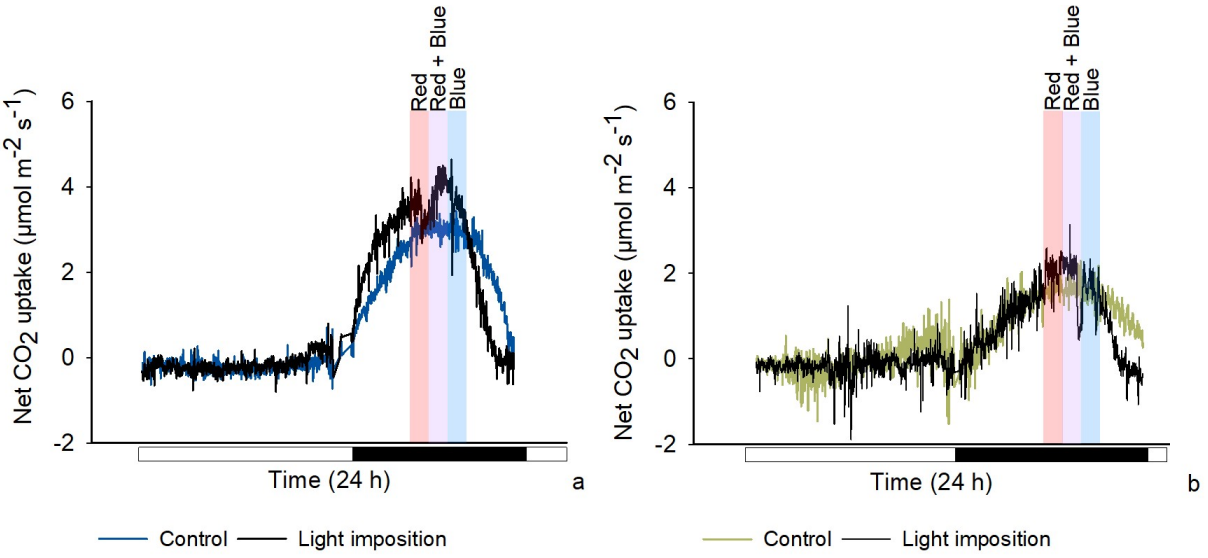

Figure 4.18. Net CO_2 uptake of wild type (a) and *rPGM1a* (b) plants of *K. fedtschenkoi*, during the exposure of three different light qualities: red (600 µmol m^{-2} s^{-1}), red/blue (600 µmol m^{-2} s^{-1}: blue 10%) and blue (100 µmol m^{-2} s^{-1}). Each treatment was imposed by one hour, after five hours of darkness (black bar indicates dark period). A control treatment (blue filling for wild type and green filling for *rPGM1a*) consisted of the measurement of conductance under normal conditions of light/darkness under a 24 hour cycle. Leaf pair 6 was used for this analysis. Plant growth conditions were set at 400 µmol CO_2 mol^{-1} air, 25°C/19°C (day/night) and a diurnal photosynthetic photon flux density – PPFD - of 250 µmol $m^{-2}s^{-1}$ at plant height.

Table 4.3. Comparisons of net CO_2 uptake and stomatal conductance in wild type and *rPGM1a* subject to each light treatment (dark, red, red/blue and blue light) for one hour. Δ represents the difference in the averaged net CO_2 uptake and stomatal conductance against dark and the previous light treatment, respectively.

					Δ against dark treatment				**Δ against previous treatment**			
Light treatment	**Average net CO_2 uptake**		**Average Stomatal conductance**		**Net CO_2 uptake**		**Stomatal conductance**		**Net CO_2 uptake**		**Stomatal conductance**	
	WT	***rPGM1a***	**WT**	***rPGM1a***	**WT**	***rPGM1a***	**WT**	***rPGM1a***	**WT**	***rPGM1a***	**WT**	***rPGM1a***
Dark	3.568	1.455	0.022	0.009	0	0	0	0	0	0	0	0
Red (600 µmol m^{-2} s^{-1})	3.259	1.944	0.026	0.014	-0.309	0.489	0.004	0.005	-0.309	0.489	0.004	0.005
Red/Blue (600 µmol m^{-2} s^{-1}: Blue 10%)	4.041	2.202	0.041	0.016	0.473	0.747	0.018	0.007	0.782	0.258	0.015	0.002
Blue (100 µmol m^{-2} s^{-1})	3.401	1.490	0.003	0.012	-0.167	0.035	-0.019	0.003	-0.640	-0.712	-0.037	-0.004

4.3.7. Transcript abundance of genes related to stomatal regulation

A down-regulation of the transcript abundance of *pgm* gene in both mesophyll and guard cell-enriched epidermis at dawn and dusk confirmed the gene silencing in the *rPGM1a* line. In wild type, *pgm* expression was significantly higher in the mesophyll compared to epidermis with a slight increment in transcript abundance at the beginning of the day, which can be associated with the time of the day when the synthesis of starch begins (Figure 4.19).

The *abcb14* malate importer was highly expressed in the epidermal peels of the wild type at the beginning of the night, the time when malate content starts to increase within the mesophyll as a response of the CO_2 fixation by the enzyme phosphoenolpyruvate carboxylase (PEPC). If transcript abundance is matched by activity, this suggests that the malate produced in mesophyll could be transported to the guard cells to support the nocturnal opening of stomata in wild type plants. On the other hand, the transcript abundance of *abcb14* was higher in the epidermal peels of *rPGM1a* at the beginning of the light period. If activity follows transcript abundance, this suggests a possible role for this transporter in the influx of malate into the guard cells of the RNAi lines and which might serve to increase guard cell osmotic pressure and curtail complete stomatal closure during the light period in *rPGM1a* (Figure 4.20).

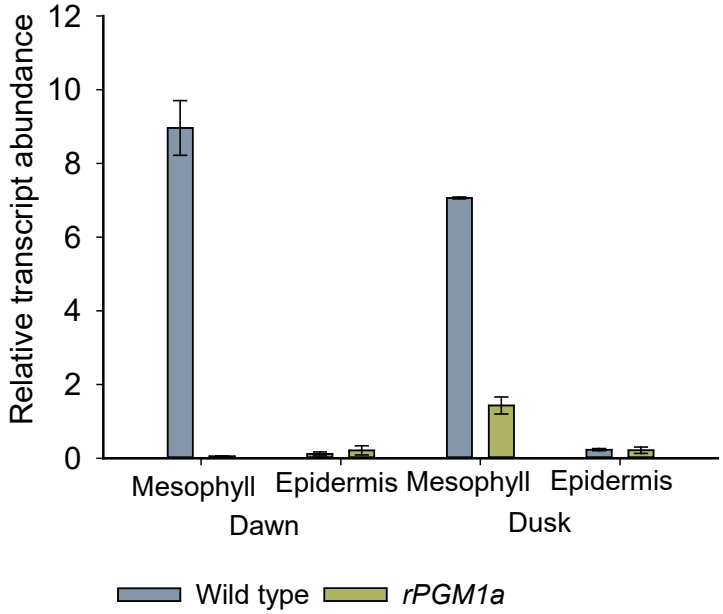

Figure 4.19**.** Relative transcript abundance of *pgm* gene in wild type (blue) and *rPGM1a* (green) in mesophyll and guard cell-enriched epidermis at dawn and dusk. Leaf pair 6 was used for this analysis. The error bars represent the standard error of six replicates (3 biological replicates, each with 2 technical replicates). Plant growth conditions were set at 400 µmol CO_2 mol^{-1} air, 25°C/19°C (day/night) and a diurnal photosynthetic photon flux density – PPFD - of 250 µmol $m^{-2}s^{-1}$ at plant height.

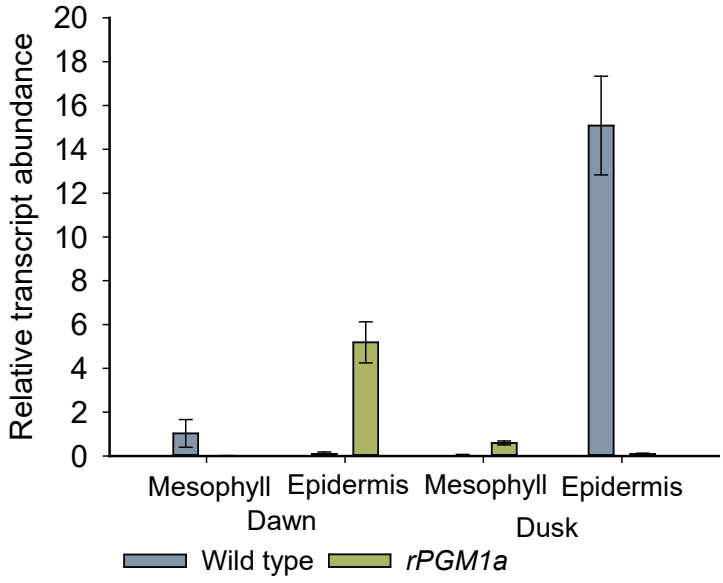

Figure 4.20. Relative transcript abundance of *abcb14* gene in wild type (blue) and *rPGM1a* (green) in mesophyll and guard cell-enriched epidermis at dawn and dusk. Leaf pair 6 was used for this analysis. The error bars represent the standard error of six replicates (3 biological replicates, each with 2 technical replicates). Plant growth conditions were set at 400 µmol CO_2 mol^{-1} air, 25°C/19°C (day/night) and a diurnal photosynthetic photon flux density – PPFD - of 250 µmol $m^{-2}s^{-1}$ at plant height.

The enzymes sucrose synthase 1 (SUSY1) and sucrose synthase 3 (SUSY3) are involved in both synthesis and degradation of sucrose. The expression of *susy1* was higher than *susy3* and was restricted to the beginning of the day. Transcript abundance for *susy1* was different between genotypes, in wild type was higher in the mesophyll, while in *rPGM1a* was highly abundant in the guard cell enriched epidermis (Figure 4.21a). In contrast, *susy3* was expressed at both dawn and dusk, with a similar expression compared with *susy1* in *rPGMA1a* at the beginning of the day, but being higher in the epidermis in wild type at dusk (Figure 4.21b).

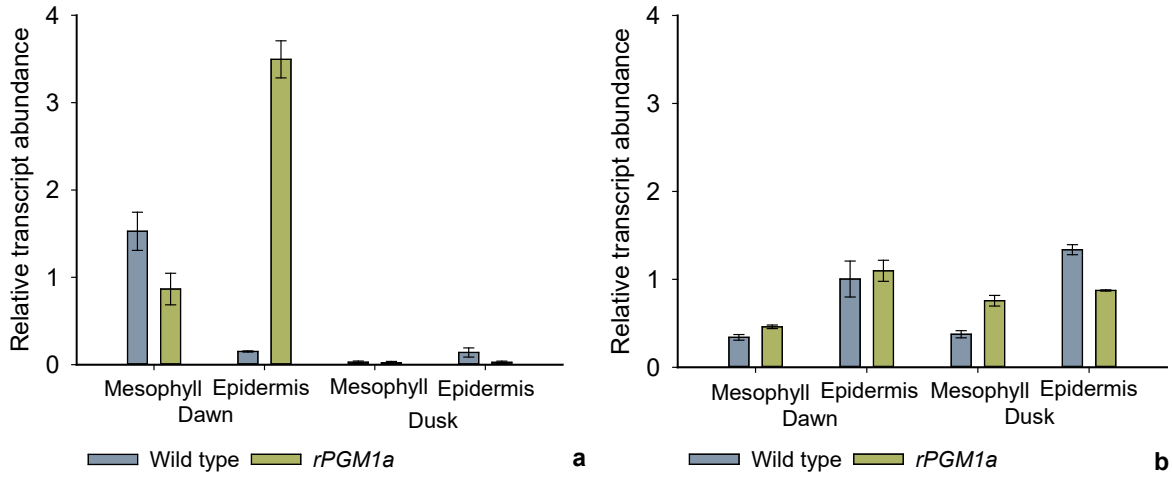

Figure 4.21. Relative transcript abundance of *susy1* (a) and *susy3* (b) genes in wild type (blue) and *rPGM1a* (green) in mesophyll and guard cell-enriched epidermis at dawn and dusk. Leaf pair 6 was used for this analysis. The error bars represent the standard error of six replicates (3 biological replicates, each with 2 technical replicates). Plant growth conditions were set at 400 µmol CO_2 mol^{-1} air, 25°C/19°C (day/night) and a diurnal photosynthetic photon flux density – PPFD - of 250 µmol $m^{-2}s^{-1}$ at plant height.

Given the higher diurnal accumulation of sugars in the *rPGM1a* and the higher expression of *susy1* at dawn in the epidermis, the transcript abundance of the sugar transporter *stp1* was also evaluated in both genotypes. Figure 4.22 revealed an increase of the transcript abundance at dawn in the guard cell enriched epidermis of the *rPGM1a* RNAi line, while in wild type *stp1* expression occurred in both tissues in lower abundance. These results suggest that lack of starch in *rPGM1a* affects the amount and transport of sugars, potentially affecting day-time stomatal conductance as observed previously.

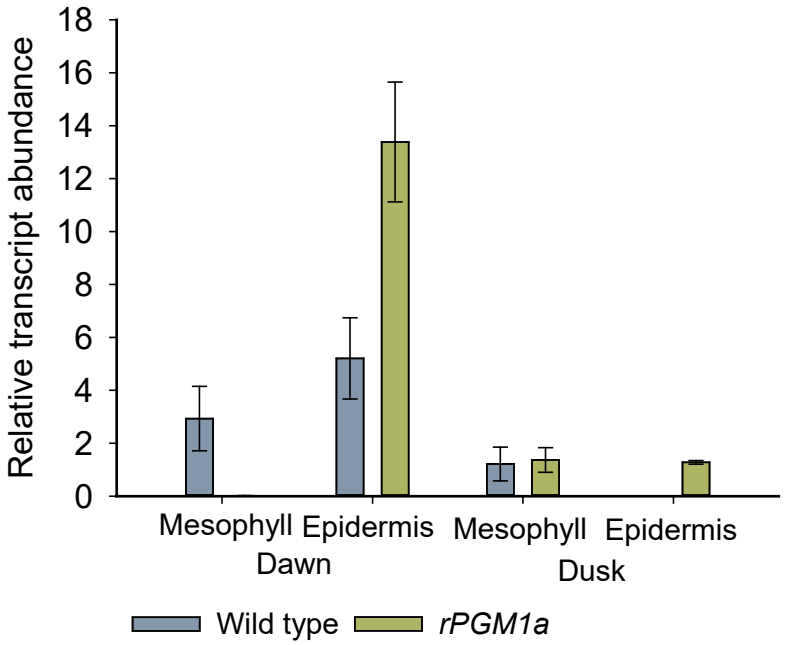

Figure 4.22. Relative transcript abundance of *stp1* gene in wild type (blue) and *rPGM1a* (green) in mesophyll and guard cell-enriched epidermis at dawn and dusk. Leaf pair 6 was used for this analysis. The error bars represent the standard error of six replicates (3 biological replicates, each with 2 technical replicates). Plant growth conditions were set at 400 µmol CO_2 mol^{-1} air, 25°C/19°C (day/night) and a diurnal photosynthetic photon flux density – PPFD - of 250 µmol $m^{-2}s^{-1}$ at plant height.

4.4. Discussion

4.4.1. A PGM-deficient line of Kalanchoë fedtschenkoi lacks starch in mesophyll and guard cells and is compromised in CAM activity

Transitory starch in higher plants acts as both source and sink and its turnover is essential to maintain metabolic processes such as respiration and growth. Likewise, the assimilates synthesised during the day by photosynthesis are destined for the production of starch (MacNeill *et al.*, 2017).

The enzyme phosphoglucomutase (PGM) catalyses the reversible interconversion of Glc6P and Glc1P in the starch synthesis pathway. Davies *et al.* (2003) and Cushman *et al.* (2008a) identified two isoforms in wheat (*Triticum aestivum*) and ice plant (*Mesembryanthemum crystallinum)*, respectively, located one in the cytosol and the other in the chloroplast. Egli *et al.* (2010), described one isoform in chloroplast and two in the cytosol in *Arabidopsis thaliana,* denoted as PGM1, PGM2 and PGM3 due to Native PAGE electrophoresis mobility, PGM1 having the highest mobility and PGM3 the lowest (Fettke *et al.*, 2008). In this study, three isoforms for PGM were observed in wild type plants of *K. fedtschenkoi* and two in the

rPGM1A line. Subcellular localisation and homology analysis with *A. thaliana* suggested that the isoform silenced in *rPGM1a* corresponds to PGM1, which is located in the chloroplast. In contrast to *A. thaliana*, the PGM1 isoform in *K. fedtschenkoi* did not present the highest mobility on the Native PAGE. This suggests that CAM evolution from C_3 could be accompanied by translational and posttranslational modifications that influence the isoelectric point, the charge and pH of proteins which influences their mobility during electrophoresis (Arndt *et al.*, 2012).

Previous investigations have concluded that starch is synthesised during the daytime and degraded under the night period in the mesophyll cells, which is consistent with the results obtained for the wild type plants studied here whilst the *rPGM1a* plants showed negligible starch content in mesophyll cells as well as in guard cells. In CAM plants, nocturnal degradation of starch supports the synthesis of PEP, which together with atmospheric or respiratory CO_2, and by the action of the enzyme PEPC forms oxaloacetate which is subsequently converted to malate (Borland *et al.*, 2016). Thus, starch deficiency would be expected to curtail nocturnal carboxylation via substrate limitation. This was confirmed by gas exchange analysis, which revealed a curtailed CAM activity in the *rPGM1a* as demonstrated by a diminution in dark net CO_2 uptake as well as nocturnal malate accumulation. At night, CAM stomata are thought to open in response to reduced C_i caused by the consumption of CO_2 (as HCO^{3-}) by PEPC and the accumulation of malate (Borland *et al.*, 2016). Thus, it was also possible that the reduced nocturnal net CO_2 uptake noted in the *rPGM1a* plants was a consequence of lower stomatal conductance in the starch deficient plants. However, measurements of nocturnal stomatal conductance were not significantly different between wild type and *rPGM1a* indicating that starch breakdown is not essential for nocturnal stomatal opening.

Stomatal size and density are important traits that influence metabolic features such as stomatal conductance, net CO_2 uptake, photosynthetic rate and water use efficiency (Hetherington and Woodward, 2003). Measurements conducted in both genotypes of *Kalanchoë* showed an increase in pore aperture and length, and a diminution in stomatal density in the *rPGM1a*. A negative correlation between stomatal density and size seems to hold for many C_3 species, where plants with lower stomatal densities show a greater mean stomatal size, and smaller stomata are found in leaves with higher stomatal densities (Doheny-Adams *et al.*, 2012; Lawson and Blatt, 2014). Such relationship is attributed to spatial limits in the placing of stomata on the leaf surface that constrains the maximum size and density of stomata (Beaulieu *et al.*, 2008; Franks *et al.*, 2009). Using these measurements

of stomatal size and density, the maximum theoretical stomatal conductance was calculated and found to be significantly higher in *rPGM1a* compared with wild type, implying that starch deficiency conferred an anatomical predisposition towards potentially higher stomatal conductance.

4.4.2. Starch deficiency curtails day-time stomatal closure

Whilst measured nocturnal stomatal conductance were comparable between the two *Kalanchoë* genotypes, day-time stomatal conductance was significantly higher in the *rPGM1a* plants compared to wild type which showed the CAM-typical day-time closure of stomata. As discussed by Males and Griffiths (2017), the substantial changes in internal CO_2 concentration (C_i) which accompany the production and breakdown of malate, are believed to be the key drivers for CAM stomatal movement. Thus, high C_i occurs during the day (Phase III) from the decarboxylation of the malate accumulated overnight which is thought to trigger day-time stomatal closure (Males and Griffiths, 2017).

The reduced level of malate decarboxylation in the *rPGM1a* lines was hypothesised to curtail generation of high C_i during the day, which prevented stomatal closure during phase III. To test this hypothesis, both genotypes were exposed to CO_2-free air overnight to abolish nocturnal malate accumulation with the prediction that both genotypes would increase stomatal conductance the following day. The data showed that whilst wild type plants increased stomatal conductance for the first few hours of the photoperiod after a night in CO_2-free air, they still showed complete stomatal closure during phase III. The *rPGM1a* plants showed little change in day-time stomatal conductance after a night in CO_2-free air. Together the data indicate that C_i is not the only factor influencing the day-time behaviour of CAM stomata.

To better understand how starch deficiency impacted stomatal responses to C_i, both genotypes were also subjected to reduced (50 µmol CO_2 mol^{-1} air) and elevated (1600 µmol CO_2 mol^{-1} air) concentrations of CO_2 during phase III and phase IV. The results obtained showed that in phase III, wild type was not affected by changes on ambient [CO_2] and stomata remained closed. During phase IV stomatal conductance of wild type increased when the applied [CO_2] was reduced to 50 µmol CO_2 mol^{-1} air and decreased when CO_2 concentration was increased to 1600 µmol CO_2 mol^{-1} air, thus consistent with the hypothesis that C_i is a key factor influencing day-time stomatal conductance. In the *rPGM1a,* when CO_2 concentration

was high (1600 μmol CO_2 mol^{-1} air), stomata closed but then started to reopen so the plant was unable to maintain stomatal closure under elevated CO_2 concentration.

The data of both experiments modifying [CO_2], indicates that other factors, in addition to fluctuations in internal CO_2 concentration, are responsible for the diurnal stomatal closure in CAM plants and suggests that starch biosynthesis is essential for the closure response. It has been reported that starch acts as a sink for sugars produced via the Calvin cycle and the disruption of starch synthesis increases the content of sucrose, which, together with its degradation products, fructose and glucose have been reported to be involved in stomatal osmoregulation (Lawson *et al.*, 2014; Azoulay-Shemer *et al.*, 2015). Likewise, the presence of sucrose within guard cells could be involved in the production of malate, an important osmolyte that promotes the opening of stomata. Similarly, during the closure of stomata, the malate exported from guard cells is accumulated in the apoplast and transported to the chloroplasts where is reconverted to starch. The inability of the *rPGM1a* line to convert osmolytes such as malate and sucrose into insoluble starch granules in the guard cells could explain the incomplete day-time stomatal closure. The higher quantities of soluble sugars observed in guard-cell enriched epidermal peels of *rPGM1a* and the data from gas exchange analysis agree with the hypothesis that soluble sugars increase guard cells turgor pressure and curtail complete closure of stomata during the day.

4.4.3. PGM-deficient phenotype affects the expression of genes involved in sugars metabolism

In previous works it has been shown that sucrose accumulation in guard cells is a regulator of the osmotic pressure for stomatal opening (Lawson *et al.*, 2014), but recent studies on C_3 plants propose that the function of sucrose is mainly energetic (Daloso *et al.*, 2016a). Apoplastic sucrose may enter the guard cells or be degraded into fructose and glucose, which can be imported to guard cells via hexose transporters (Misra *et al.*, 2015; Daloso *et al.*, 2016b). Sucrose synthases (SUSY) are important enzymes implicated in sugar metabolism and catalyse the reversible conversion of sucrose and UDP into fructose and UDP-glucose. Six different SUSY isoforms have been reported and it is thought that each one has different patterns of expression and specific functions in the plant (Bieniawska *et al.*, 2007). Based on the differential expression in *A. thaliana* of sucrose synthases 1 and 3 (*susy1* and *susy3*) in the mesophyll and guard cells, respectively (Bieniawska *et al.*, 2007; Bates *et al.*, 2012), their relative transcript abundances were determined by RT-qPCR in both *Kalanchoë* genotypes in order to elucidate the impact of starch and sugars metabolism on CAM stomata. In wild type,

the expression of both *susy1* and *susy3* genes was consistent with previous reports where *susy3* was more abundant in guard cells (Bates *et al.*, 2012).

No temporal differences in the expression of *susy3* were found in the guard cell enriched epidermis of wild type. This can be explained by the double function of this enzyme, involved in both synthesis and degradation of sucrose. According to Baroja-Fernández *et al.* (2009) sucrose synthases play an essential role in the synthesis of starch as a carbohydrate sink, which is also important during the closure of stomata, reducing the osmotic pressure created by the accumulation of sugars and osmolytes (Daloso *et al.*, 2017). In this case, and based on the absence of starch degradation in guard cells during the light period observed in wild type (Chapter 3), it can be proposed that *susy3* provides substrate for diurnal starch synthesis in guard cells that enable the closure of stomata.

Similarly, Daloso *et al.* (2016b) suggested the involvement of *susy3* in sucrose degradation to supply carbon skeletons for organic acid production, as malate, which acts as a counter ion for K^+ during stomatal opening. In line with this idea, the transcript abundance of the guard cells ATP-binding cassette malate transporter (*abcb14*) was higher in wild type epidermal peels at dusk. If transcript abundance is related to transporter activity then *abcb14* could enhance malate import to guard cells at start of the night, thereby increasing guard cell osmotic pressure and causing the opening of stomata (Lawson *et al.*, 2014). This accumulation of malate in the mesophyll and its transport to guard cells may be an important point that connects CAM photosynthesis in the mesophyll with stomatal behaviour and it is proposed to be a key regulator of stomatal movement in CAM.

Noteworthy, the abundance of sucrose synthase 1 (*susy1*) in wild type was higher in mesophyll at dawn and could be related to the provision of substrate for synthesis of starch, as reported by Baroja-Fernández *et al.* (2009) who proposed that sucrose synthases are involved in the synthesis of polysaccharides, and their functions are key for determining the levels of hexoses and starch. Additionally, Déjardin *et al.* (1999) reported that *Arabidopsis* leaves exposed to abiotic stress presented higher concentration of sugars (glucose and sucrose) and osmoticum, as polyethylene glycol (PEG) and sorbitol, that enhanced the expression of *susy1*, suggesting that gene activity is controlled by changes in the osmotic pressure and sugars levels. Following this idea, the increased expression of *susy1* in guard cell enriched peels of *rPGM1a* at dawn could be associated with the higher abundance of sugars in this tissue and a higher conversion rate of sucrose into glucose and fructose. In addition, a higher expression of the sugar transporter *stp1*, which imports hexoses into the guard cells, was noted in the *rPGM1a* plants at dawn. These patterns of elevated expression at dawn are consistent with the

higher hexose contents noted in the epidermis of *rPGM1a* during the day compared to wild type. A higher sugar content in *rPGM1a* guard cells during the day might be expected to curtail stomatal closure as reported here.

4.4.4. The deficiency of starch affects stomatal response to light

Light is one of the main factors regulating the opening of stomata. In C_3 plants, blue light activates the plasma membrane H^+-ATPase via photoreceptors, driving the export of H^+ and the influx of K^+ and its counter ions Cl^-, malate and nitrate. This in turn leads to the uptake of water, an increment in guard cells turgor pressure and stomatal opening (Inoue and Kinoshita, 2017). Concomitantly, in C_3 plants, transitory starch in guard cells chloroplasts is degraded during the first hours of the day by the action of blue light that activates the enzymes β-amylase 1 (BAM1) and α-amylase 3 (AMY3), producing malate that acts as an osmolyte triggering the opening of stomata (Horrer *et al.*, 2016).

Light responses of CAM stomata are relatively unstudied and different explanations about its effects have been proposed. The nocturnal opening of stomata in CAM plants suggests a reprogramming of metabolism that enable the inverted stomatal rhythm and make them insensitive to light. To test this hypothesis, responses in net CO_2 uptake and stomatal conductance to light imposed at night were determined in both genotypes. Additionally, the requirement of starch presence to open stomata in response to blue light was tested.

Stomatal conductance in wild type under Red/Blue light was greater than that under darkness, or under blue or red light when administered individually. This suggests a synergistic effect of both red and blue light in the stomatal response. This finding is consistent with the study on *Arabidopsis thaliana* performed by Suetsugu *et al.* (2014), who reported that the presence of weak blue light does not induce stomatal opening by itself, but together with red light greatly enhances the response. The synergistic effects of red and blue light on stomatal conductance have been observed in different species. Red light induces either mesophyll photosynthesis as a response to a decrease in C_i or the translocation of NADH and ATP in the guard cell chloroplasts. This, together with blue light, activates the guard cells membrane H^+-ATPase, increasing the H^+ pumping into the vacuole and the synthesis of malate that prompt the opening of stomata (Shimazaki *et al.*, 2007).

In this context, it can be evidenced that CAM stomata respond to light and, in principle, photoreceptors responsible are similar to those in C_3 plants, as also suggested by the stomatal opening that can occur during phases II and IV of CAM. Similarly, Ceusters *et al.* (2014)

proposed that light intensity (photosynthetic photon flux density, PPFD) determines the magnitude and duration of the four phases of CAM and proposed that a possible C_3 to CAM divergence may exist in light signalling pathways mediated by blue and red light photoreceptors. In addition, they confirmed the absence of stomatal opening under red light and suggested that blue light induces early morning (phase II) stomatal opening.

With regard to net CO_2 uptake in wild type, its increment under Red/Blue light treatment was less pronounced compared to stomatal conductance. Males and Griffiths (2017) proposed that during phase I mesophyll factors are more significant to nocturnal CO_2 assimilation than stomatal conductance. Based on this, it is possible to hypothesise that CAM stomata respond to light but this does not have a direct effect on the amount of CO_2 fixed, suggesting that internal levels of CO_2 are the main factor that regulate stomata. A possible cause of the negligible increment on net CO_2 uptake is the limitation of substrates such as PEP or enzyme limitation. Thus, despite the amount of ambient CO_2 that enters the cell, its carboxylation will not increase and the levels of malate production will remain unchangeable. In the same way, it is possible that the plant coordinates/optimises stomatal opening and the loss of water, which allows the influx of the exact amount of CO_2 needed to fix it in form of malate with the lowest transpiration affecting its fitness. Administering light at night seems to uncouple this optimisation. Unfortunately, there is no firm evidence to support this hypothesis so further investigations are required.

With regard to starch deficient lines, the imposition of red light increased the stomatal conductance but the addition of blue light did not enhance this response. According to Lasceve *et al.* (1997), in *Arabidopsis thaliana* the opening of stomata by the action of red light is independent of the presence of starch and it is related with the mesophyll photosynthesis and the accumulation of osmolytes. However, starch is required for the response to blue light, suggesting that starch degradation products provide counter ions for potassium that increase guard cells turgor pressure. This suggestion is acceptable for C_3 plants, where the action of blue light on starch degradation is well studied. However, in CAM, these mechanisms differ, as has been described above and it is necessary to resolve the relationship between blue light perception and starch presence. Based on the importance of starch for providing substrates for nocturnal carboxylation, noted by the reduced rates of net CO_2 uptake in the *rPGM1a*, and its direct implication in the stomatal regulation of CAM plants, it can be suggested that enzymes involved in guard cell carbohydrate metabolism are involved in the response of the plant to blue light.

4.5. Conclusions

- The results obtained showed that starch in the mesophyll is not required for night-time opening of stomata, evidenced by similar nocturnal stomatal conductance between wild type and *rPGM1a*, but is required in providing substrates for nocturnal CAM activity.

- An additional role for starch synthesis is to act as a sink for sugars, promoting diurnal stomatal closure, demonstrated by the higher accumulation of soluble sugars in the *rPGM1a* during the day, as well as the transcript abundance of genes involved in the synthesis and degradation of sucrose and the transport of hexoses into guard cells.

- Based on the conclusion that starch presence is not required for nocturnal stomatal opening, the further evaluation of lines with curtailed starch degradation will constitute a complement in the understanding of the role of starch in CAM activity and stomatal behaviour.

Chapter 5. Exploring CAM activity and stomatal regulation in RNAi lines of *Kalanchoë fedtschenkoi* compromised in the expression of α-glucan phosphorylase 1 and β-amylase 9

5.1. Introduction

In plants, starch is synthesised during the day as a key product of carbon assimilation that is driven by Rubisco and the Calvin cycle. In the following night, a series of reactions catalyse the degradation of this transitory starch in the chloroplast to provide carbons for the synthesis of sucrose and sustain energy production, plant growth and development (Smith *et al.*, 2005). Starch degradation in the mesophyll tissue potentially follows two routes, the hydrolytic and the phosphorolytic pathways. The hydrolytic pathway is predominant in plants with C_3 photosynthesis and the combined action of β-amylases (BAM) and disproportionating enzyme 1 (DPE1) produces maltose and glucose as the main starch degradation products (Smith *et al.*, 2005). In contrast, the phosphorolytic route of starch breakdown is less relevant for export of sugars from the C_3 chloroplast, and its main function is supplying carbons for internal chloroplast metabolism through the pentose phosphate pathway (Weise *et al.*, 2006).

In plants with crassulacean acid metabolism, it has been proposed that the degradation of starch in the mesophyll occurs mainly by the phosphorolytic pathway, catalysed by the action of plastidic α-glucan phosphorylase 1 (PHS1) which ultimately produces Glc6P for export to the cytosol where it can be converted to phosphoenolpyruvate (PEP) (Borland *et al.*, 2016). PEP production is essential for sustaining nocturnal CO_2 uptake so starch degradation is a key limiting factor for CAM. As well as PHS1, DPE1 is also implicated in starch breakdown in CAM plants, serving to produce glucose and maltopentaose through the hydrolytic pathway, which may subsequently be metabolised by BAM and PHS1, to serve as substrates for sucrose synthesis and biomass production (Borland *et al.*, 2016).

Starch degradation in the guard cells is also important for plant performance having been shown to be important for stomatal opening in C_3 plants (Horrer *et al.*, 2016). Previous work in this thesis (Chapter 3) showed that in the constitutive CAM species *K. fedtschenkoi* starch degradation in the guard cells followed a different pattern and diel timing compared to the reports in C_3 plants and is thought not be driven by the effect of blue light. In mature CAM leaves of *K. fedtschenkoi*, starch content in guard cells showed a gradual increase over the day and followed a slight diminution at the beginning of the night. In contrast, the young leaves of

K. fedtschenkoi presented a C_3-like metabolism following a significant degradation of starch during the first half hour of the day and an increase in starch content at the beginning of the night. In trying to understand which genes/proteins might be responsible for guard cell starch degradation in *K. fedtschenkoi*, diel changes in transcript abundance of several genes implicated in starch degradation were compared using RNAseq data collected for the epidermal peel and mesophyll of *K. fedtschenkoi* (see Chapter 3). In *Arabidopsis*, *amy3* and *bam1* expression is elevated in guard cells, being the main enzymes involved in diurnal starch degradation to support stomatal opening (Horrer *et al.*, 2016). In contrast, *K. fedtschenkoi* RNAseq data showed that both *amy3* and *bam1* transcripts were more abundant in the mesophyll, while *bam9* was higher in the epidermis and in the mature leaves (CAM), indicating a possible CAM-related role for this enzyme (see Chapter 3). In the case of *Arabidopsis*, Chandler *et al.* (2001) found that *bam9* expression was mostly in developing floral buds and flowers, while in leaves, stems and roots was barely detected. Additionally, BAM9 has been reported as an inactive catalytic enzyme with a regulatory role in the degradation of starch in the mesophyll of C_3 plants (Steidle, 2010).

Based on the contrasting patterns of guard cell starch turnover and transcript abundances of genes implicated in starch degradation in *K. fedtschenkoi* compared to *A. thaliana* as well as the suggested importance of the phosphorolytic pathway in CAM in terms of energetic cost effectiveness (Shameer *et al.*, 2018), a possible re-routing of starch degradation in guard cells of constitutive CAM species is suggested to allow the inverted stomatal rhythm. Given the reported importance of guard cell starch in C_3 stomatal opening, this chapter aims to determine the implications of genetically perturbing the route of starch degradation on CAM activity and stomatal behaviour. To approach this objective, biochemical and molecular characterisation of RNAi lines deficient in α-glucan phosphorylase 1 (PHS1) and β-amylase 9 (BAM9) were conducted in order to test the following hypotheses:

Hypothesis 1: Starch degradation occurs via the phosphorolytic route catalysed by PHS1 in both mesophyll and guard cells.

Hypothesis 2: BAM9 regulates the expression of enzymes involved in starch degradation in both mesophyll and guard cells.

5.2. Sampling and Methods

The RNAi lines *rPHS1*and *rBAM9* deficient for plastidic α-glucan phosphorylase 1 and β-amylase 9, respectively, were used for the experiments reported in this chapter. The RNAi

lines were previously selected by Dr Johan Ceusters from three independent transformation events, based on altered leaf acidity, starch content and net CO_2 uptake. Following the growth and sampling conditions described in Section 2.1 (Chapter 2), the harvesting of samples from the RNAi lines together with wild type was performed over a 24 hour day/night cycle at 8:30 (lights turned on), 12:30, 16:30, 20:30 (lights turned off), 00:30 and 5:30. Sections 2.2 – 2.5 (Chapter 2) describe the biochemical assays performed to determine starch, soluble sugars and malate content in all lines, as well as physiological factors such as net CO_2 uptake, stomatal conductance and transpiration.

Real time qPCR was used to measure transcript abundance of the target genes in the *phs1* and *bam9* RNAi lines. In addition, real time qPCR was performed to determine the transcript abundance of the enzymes β-amylases 1, 3 and 9 (*bam1*, *bam3, bam9*), α-amylase 3 (*amy3*), disproportionating enzyme 1 (*dpe1*) and sucrose synthases 1 and 3 (*susy1*, *susy3*). Similarly, the expression of the sugars transporter 1 (*stp1*), glucose 6-phosphate transporters 1 and 2 (*gpt1*, *gpt2),* maltose exporter 1 (*mex1)*, glucose transporter (*glct*), triose phosphate translocator (*tpt)* and the ATP-binding cassette malate transporter (*abcb14*) were evaluated. These measurements were made to determine differences in abundance and day/night timing of maximal gene expression between guard cell-enriched epidermis and mesophyll in the various RNAi lines and wild type plants, as described in Sections 2.9 and 2.10 (Chapter2).

To determine the isoforms of degrading starch enzymes knocked down in the *phs1* and *bam9* RNAi lines, whole leaves of *rPHS1*, *rBAM9* and wild type were collected at the end of the light period. The protein isolation and the Native PAGE were conducted based on the methods described in Sections 2.6 and 2.7 (Chapter 2). To identify the subcellular localisation of the β-amylase (BAM) isoforms that were targeted by RNAi, the sequences annotated for this protein in *K. fedtschenkoi* were analysed using the bioinformatics tool TargetP, which is based on N-terminal motifs and predicts chloroplast (cTPs), mitochondria (mTPs), secretory (SPs) and other transit peptides (Emanuelsson *et al.*, 2007). Therefore UniProtKB/Swiss-Prot database was used to confirm the annotated proteins (Boutet *et al.*, 2016).

Finally, using Geneious software, version 11.0. 3 (Kearse *et al.*, 2012), an UPGMA clustering analysis was performed with reported *K. fedtschenkoi* (Kaladp0067s0309.1, Kaladp1295s0027.1, Kaladp0086s0015.1,.1, Kaladp0031s0061.1, Kaladp0019s0060.1, Kaladp0172s0023.1, Kaladp0062s0212.1, Kaladp0076s0255.1, Kaladp0076s0256.1) and annotated *Arabidopsis thaliana* (AT3G23920, AT4G00490, AT4G17090, AT5G55700, AT4G15210, AT2G32290, AT2G45880, AT5G45300, AT5G18670) BAM sequences to determine homology among isoforms.

5.3. Results

5.3.1. Confirmation of phs1 and bam9 silencing

The silencing of the genes α-glucan phosphorylase1 (*phs1*) and β-amylase 9 (*bam9*) was confirmed in the *rPHS1* and *rBAM9* lines, respectively, evidenced by a down regulation of the transcripts at dawn and dusk in both sampled tissues (Figure 5. 1 and Figure 5. 2). In the case of wild type, the abundance of the *phs1* transcript was higher in the mesophyll at the beginning of the day, while at dusk the abundance was similar between both tissues. The expression of the *phs1* was also affected by the *bam9* silencing; in this case, the *rBAM9* line showed a down regulation of the transcript in both tissues at dusk, while at dawn the expression was higher in the guard cell-enriched epidermis compared to wild type (Figure 5. 1). For *bam9* gene, the transcript abundance in wild type differed between tissues at both times, being higher in the guard-cell enriched epidermis at dawn and higher in the mesophyll at the beginning of the night. Regarding *bam9* expression in the *rPHS1* line, a decrease in the transcript abundance for both tissues at dawn and dusk was observed (Figure 5. 2). These results could suggest that the silencing of genes implicated in starch degradation affects the whole metabolic pathway.

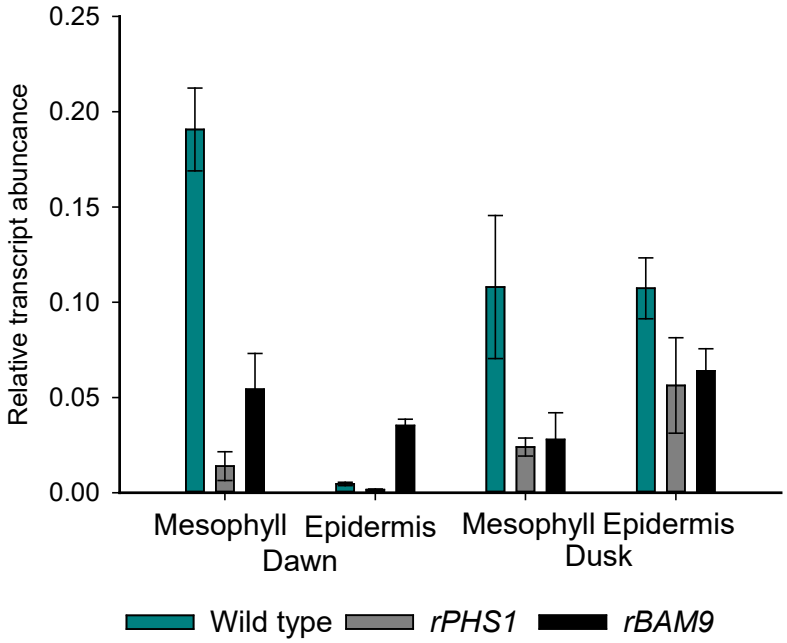

Figure 5. 1. Relative transcript abundance of *phs1* gene in wild type (green), *rPHS1* (grey) and *rBAM9* (black) in mesophyll and guard cell-enriched epidermis at dawn and dusk. Leaf pair 6 was used for this analysis. The error bars represent the standard error of six replicates (3 biological replicates, each with 2 technical replicates). Plant growth conditions were set at 400 µmol CO_2 mol^{-1} air, 25°C/19°C (day/night) and a diurnal photosynthetic photon flux density – PPFD - of 250 µmol $m^{-2}s^{-1}$ at plant height.

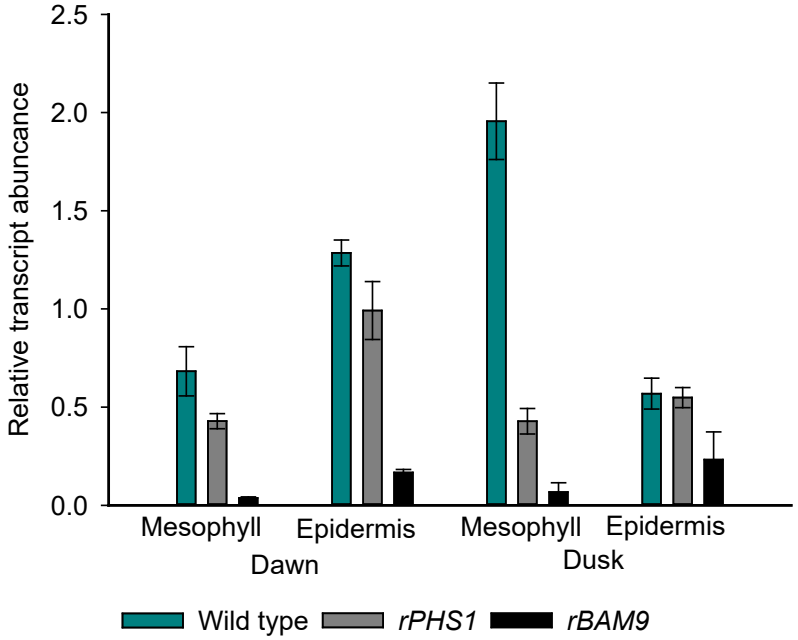

Figure 5. 2. Relative transcript abundance of *bam9* gene in wild type (green), *rPHS1* (grey) and *rBAM9* (black) in mesophyll and guard cell-enriched epidermis at dawn and dusk. Leaf pair 6 was used for this analysis. The error bars represent the standard error of six replicates (3 biological replicates, each with 2 technical replicates). Plant growth conditions were set at 400 µmol CO_2 mol^{-1} air, 25°C/19°C (day/night) and a diurnal photosynthetic photon flux density – PPFD - of 250 µmol $m^{-2}s^{-1}$ at plant height.

5.3.2. Determination of starch in mesophyll and stomatal guard cells

Differences in starch content in both mesophyll and stomatal guard cells were observed for both RNAi lines. The *rPHS1* line showed a higher amount of starch in both tissues compared with wild type. In the case of *rBAM9*, starch content differed between tissues, being lower in the mesophyll and higher in guard cells over the 24 h cycle compared to wild type (Figure 5. 3 to Figure 5. 5). Diel turnover of starch mesophyll occurred in both the RNAi lines and wild type, showing an increase during the light period and a diminution at night, conversely in stomata guard cells of the wild type and the RNAi lines starch did not follow a diel pattern of turnover and remained relatively constant during the day/night period (Figure 5. 4).

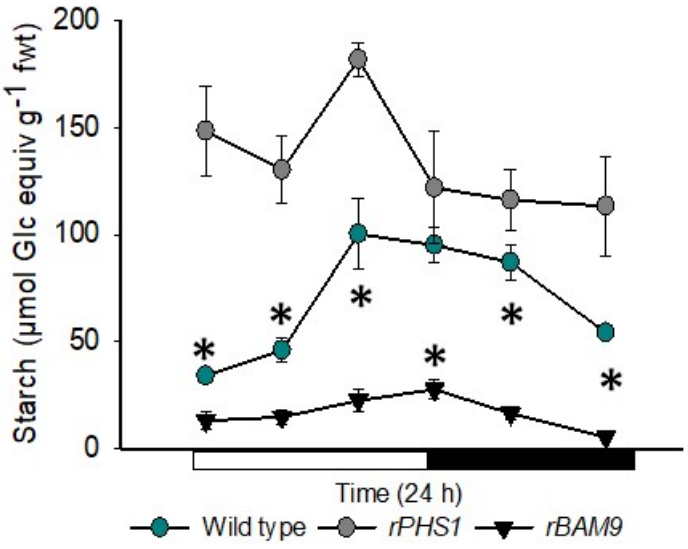

Figure 5. 3. Starch content (µmol Glc equiv g^{-1} fwt) in mesophyll of wild type (green filling), *rPHS1* (grey filling) and *rBAM9* (black filling) plants of *K. fedtschenkoi*, during 24 hours (black bar indicates night period). Significant differences ($p \leq 0.05$) between wild type and both RNAi lines are represented by asterisks. Leaf pair 6 was used for this analysis and the error bars indicate the standard error of six replicates (3 biological replicates, each with 2 technical replicates). Plant growth conditions were set at 400 µmol CO_2 mol^{-1} air, 25°C/19°C (day/night) and a diurnal photosynthetic photon flux density – PPFD - of 250 µmol $m^{-2}s^{-1}$ at plant height.

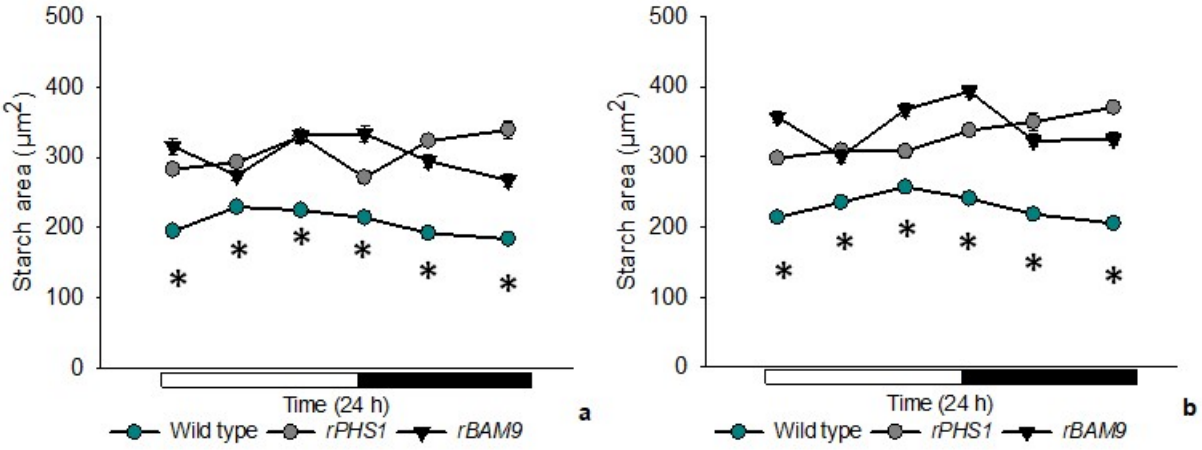

Figure 5. 4. Starch granule area (μm^2) in guard cells of wild type (green filling), *rPHS1* (grey filling) and *rBAM9* (black filling) plants of *K. fedtschenkoi*, during 24 hours (black bar indicates night period). Upper (a) and lower (b) epidermal surfaces were measured independently. Significant differences ($p \leq 0.05$) between wild type and both RNAi lines are represented by asterisks. Leaf pair 6 was used for this analysis and the error bars indicate the standard error of 60 replicates (3 biological replicates, each with 20 views per replicate). Plant growth conditions were set at 400 µmol CO_2 mol^{-1} air, 25°C/19°C (day/night) and a diurnal photosynthetic photon flux density – PPFD - of 250 µmol $m^{-2}s^{-1}$ at plant height.

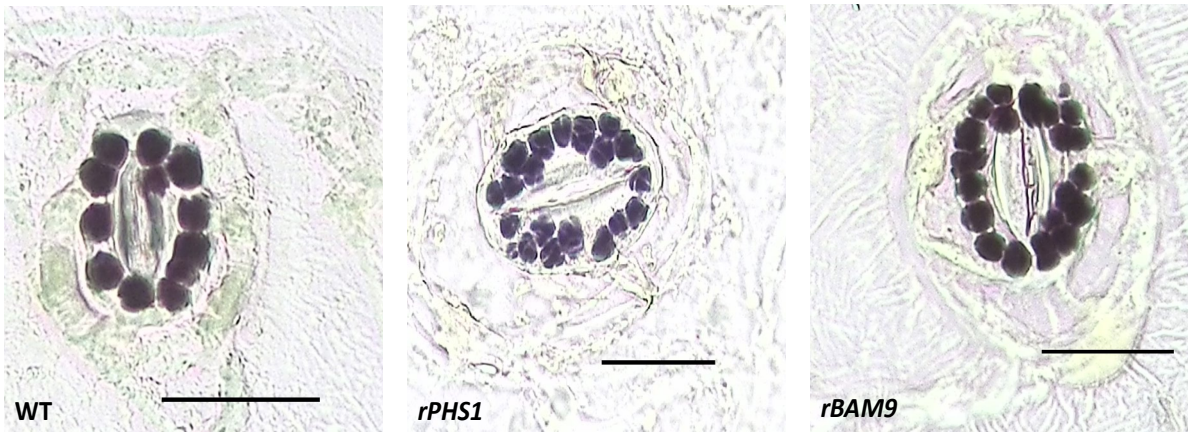

Figure 5. 5. Starch deposits in stomatal guard cells of wild type, *rPHS1* and *rBAM9* plants of *K. fedtschenkoi*. The tissue corresponded to epidermal peels of leaf pair 6. The scale bar represents 20 µm. Plant growth conditions were set at 400 µmol CO_2 mol^{-1} air, 25°C/19°C (day/night) and a diurnal photosynthetic photon flux density – PPFD - of 250 µmol $m^{-2}s^{-1}$ at plant height.

5.3.3. Determination of soluble sugars in mesophyll and guard cell-enriched epidermis

The content of soluble sugars differed significantly ($p \leq 0.05$) between wild type and the RNA lines. The content of fructose and glucose in wild type mesophyll increased at the beginning of the day, maintaining a constant concentration over the latter part of the day and being degraded during the first hour of the night. In contrast, higher accumulation of fructose and glucose in the mesophyll was observed for *rPHS1* and *rBAM9* during the 24 h period, compared with wild type. In the *rPHS1* line, fructose was degraded during the light period, and was subsequently accumulated at the end of the night. The opposite pattern was observed for *rBAM9*, where the highest fructose content was reached at the end of the day and decreased during the night (Figure 5. 6). The content of glucose in both *rPHS1* and *rBAM9* mesophyll increased during the first hours of the light period, followed by nocturnal degradation and a further accumulation at the end of the night in the *rPHS1* line (Figure 5. 7).

In the guard cell-enriched epidermis, a diurnal accumulation of fructose was evidenced in the RNAi lines, with no differences in the content during the night period between wild type and *rBAM9* and a decrease in *rPHS1* (Figure 5. 8). Changes in the glucose content were also evidenced for *rPHS1* characterised by an increment during the day and a decrease at night, compared to wild type. Conversely, glucose levels in *rBAM9* during the day did not differ but during the night period were more abundant than in wild type (Figure 5. 9).

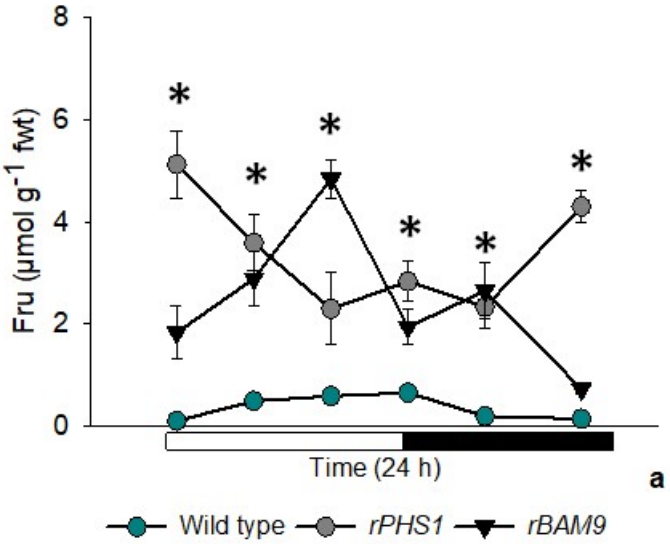

Figure 5. 6. Fructose content (µmol g^{-1} fwt) in mesophyll of wild type (green filling), *rPHS1* (grey filling) and *rBAM9* (black filling) plants of *K. fedtschenkoi*, during 24 hours (black bar indicates night period). Significant differences ($p \leq 0.05$) between wild type and both RNAi lines are represented by asterisks. Leaf pair 6 was used for this analysis and the error bars indicate the standard error of six replicates (3 biological replicates, each with 2 technical replicates). Plant growth conditions were set at 400 µmol CO_2 mol^{-1} air, 25°C/19°C (day/night) and a diurnal photosynthetic photon flux density – PPFD - of 250 µmol $m^{-2}s^{-1}$ at plant height.

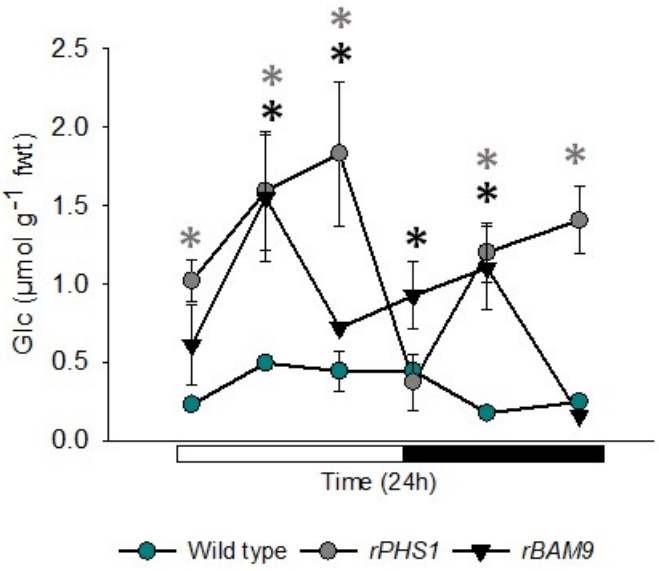

Figure 5. 7. Glucose content (µmol g^{-1} fwt) in mesophyll of wild type (green filling), *rPHS1* (grey filling) and *rBAM9* (black filling) plants of *K. fedtschenkoi*, during 24 hours (black bar indicates night period). Grey asterisks indicate significant differences ($p \leq 0.05$) between wild type and *rPHS1*, while black asterisks differences between wild type and *rBAM9*. Leaf pair 6 was used for this analysis and the error bars indicate the standard error of six replicates (3 biological replicates, each with 2 technical replicates). Plant growth conditions were set at 400 µmol CO_2 mol^{-1} air, 25°C/19°C (day/night) and a diurnal photosynthetic photon flux density – PPFD - of 250 µmol $m^{-2}s^{-1}$ at plant height.

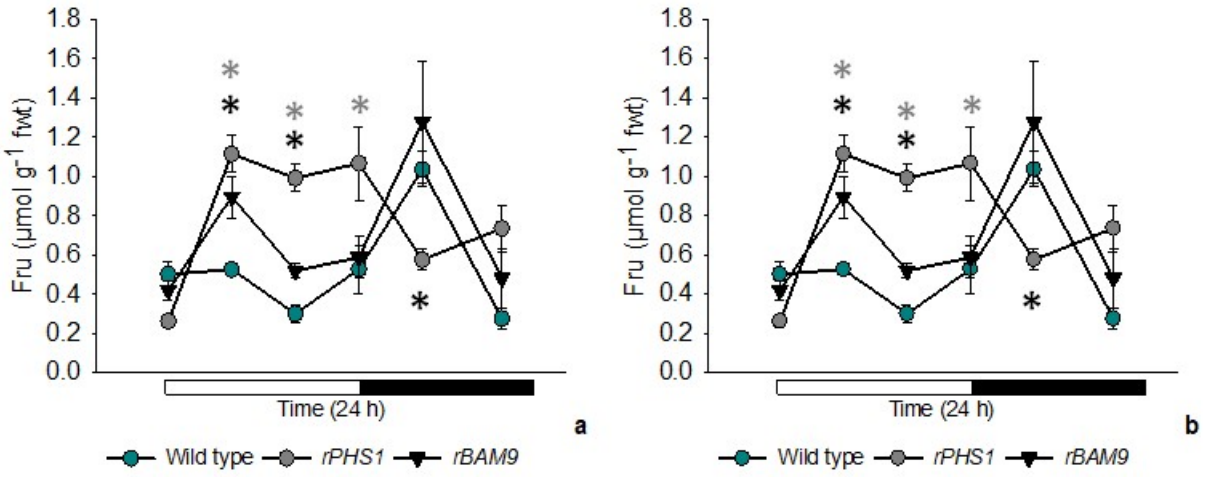

Figure 5. 8. Fructose content (µmol g^{-1} fwt) in guard cell-enriched epidermis of wild type (green filling), *rPHS1* (grey filling) and *rBAM9* (black filling) plants of *K. fedtschenkoi*, during 24 hours (black bar indicates night period). Upper (a) and lower (b) epidermal surfaces were measured independently. Grey asterisks indicate significant differences ($p \leq 0.05$) between wild type and *rPHS1*, while black asterisks differences between wild type and *rBAM9*. Leaf pair 6 was used for this analysis and the error bars represent the standard error of six replicates (3 biological replicates, each with 2 technical replicates). Plant growth conditions were set at 400 µmol CO_2 mol^{-1} air, 25°C/19°C (day/night) and a diurnal photosynthetic photon flux density – PPFD - of 250 µmol $m^{-2}s^{-1}$ at plant height.

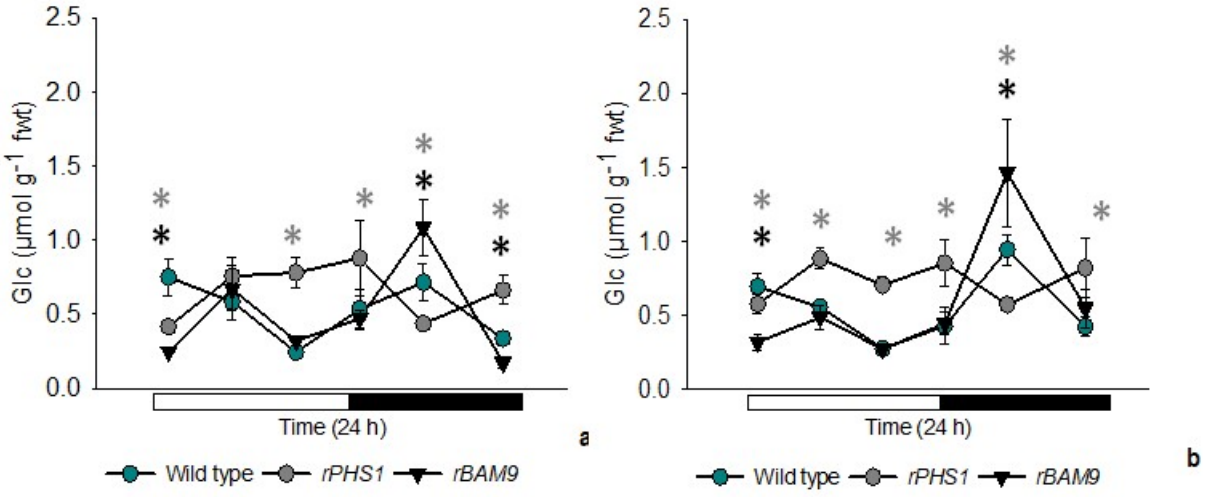

Figure 5. 9. Glucose content (µmol g^{-1} fwt) in guard cell-enriched epidermis of wild type (green filling), *rPHS1* (grey filling) and *rBAM9* (black filling) plants of *K. fedtschenkoi*, during 24 hours (black bar indicates night period). Upper (a) and lower (b) epidermal surfaces were measured independently. Grey asterisks indicate significant differences ($p \leq 0.05$) between wild type and *rPHS1*, while black asterisks differences between wild type and *rBAM9*. Leaf pair 6 was used for this analysis and the error bars represent the standard error of six replicates (3 biological replicates, each with 2 technical replicates). Plant growth conditions were set at 400 µmol CO_2 mol^{-1} air, 25°C/19°C (day/night) and a diurnal photosynthetic photon flux density – PPFD - of 250 µmol $m^{-2}s^{-1}$ at plant height.

Compared to the other sugars quantified, sucrose was less abundant in both wild type and RNAi lines. In the mesophyll of wild type, sucrose was degraded during the light period, possibly as precursor in the synthesis of starch. In *rPHS1* and *rBAM9* plants, sucrose content was lower than in wild type for the first hours of the day but remained similar to wild type during the following hours of the light period. Likewise, sucrose content in wild type and *rPHS1* was significantly different at the end of the night (Figure 5. 10). Regarding sucrose content in the epidermis tissue, the RNAi lines differed from wild type. A lower sucrose content at the end of the day and beginning of the night was detected in *rBAM9* plants (Figure 5. 11).

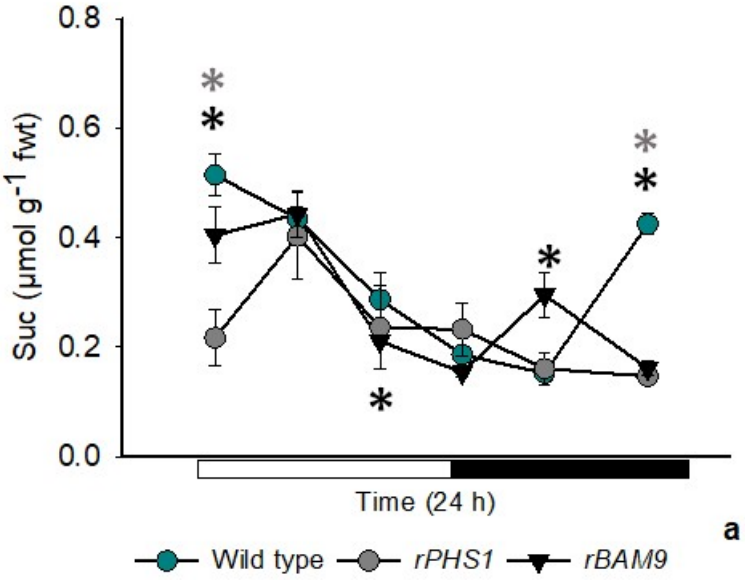

Figure 5. 10. Sucrose content (µmol g^{-1} fwt) in mesophyll of wild type (green filling), *rPHS1* (grey filling) and *rBAM9* (black filling) plants of *K. fedtschenkoi*, during 24 hours (black bar indicates night period). Grey asterisks indicate significant differences ($p \leq 0.05$) between wild type and *rPHS1*, while black asterisks differences between wild type and *rBAM9.* Leaf pair 6 was used for this analysis and the error bars indicate the standard error of six replicates (3 biological replicates, each with 2 technical replicates). Plant growth conditions were set at 400 µmol CO_2 mol^{-1} air, 25°C/19°C (day/night) and a diurnal photosynthetic photon flux density – PPFD - of 250 µmol $m^{-2}s^{-1}$ at plant height.

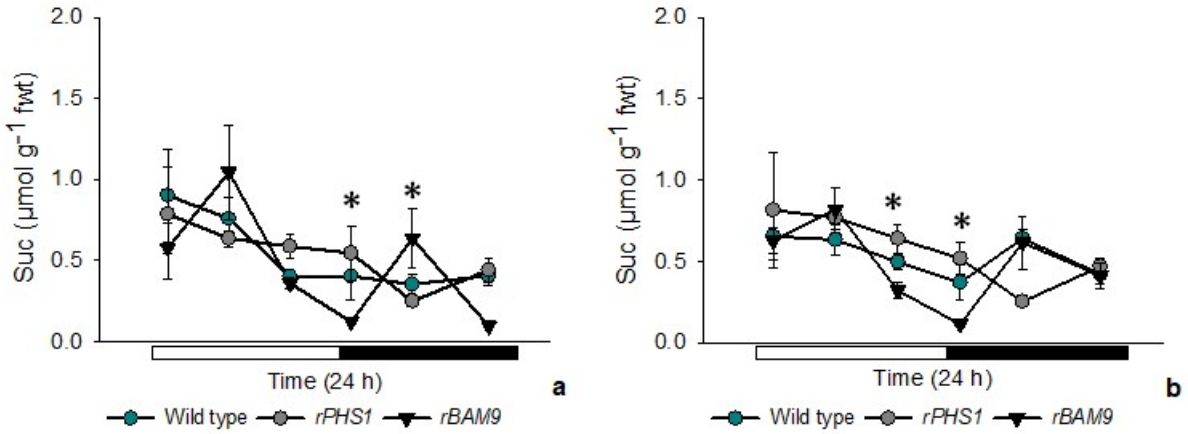

Figure 5. 11. Sucrose content (µmol g^{-1} fwt) in guard cell-enriched epidermis of wild type (green filling), *rPHS1* (grey filling) and *rBAM9* (black filling) plants of *K. fedtschenkoi*, during 24 hours (black bar indicates night period). Upper (a) and lower (b) epidermal surfaces were measured independently. Asterisks indicate significant differences ($p \leq 0.05$) between wild type and *rBAM9*, no significant differences were found between wild type and *rPHS1*. Leaf pair 6 was used for this analysis and the error bars represent the standard error of six replicates (3 biological replicates, each with 2 technical replicates). Plant growth conditions were set at 400 µmol CO_2 mol^{-1} air, 25°C/19°C (day/night) and a diurnal photosynthetic photon flux density – PPFD - of 250 µmol $m^{-2}s^{-1}$ at plant height.

Sedoheptulose, a seven-carbon monosaccharide, presented a higher content in wild type plants, in both mesophyll and guard cell-enriched epidermis at the end of the night. Interestingly, sedoheptulose content *rBAM9* mesophyll was similar to wild type during light period, while in *rPHS1* was lower over the 24 h diel cycle compared to wild type (Figure 5. 12 and Figure 5. 13). Finally, a particularly striking finding was the higher amount of maltose in both mesophyll and guard cell-enriched epidermis of *rPHS1* line, compared with wild type, evidencing the effect of the silencing of the main enzyme implicated in the degradation of starch by the phosphorolytic pathway. In *rBAM9,* small quantities of maltose were detected in the mesophyll at the end of the night (Figure 5. 14 and Figure 5. 15).

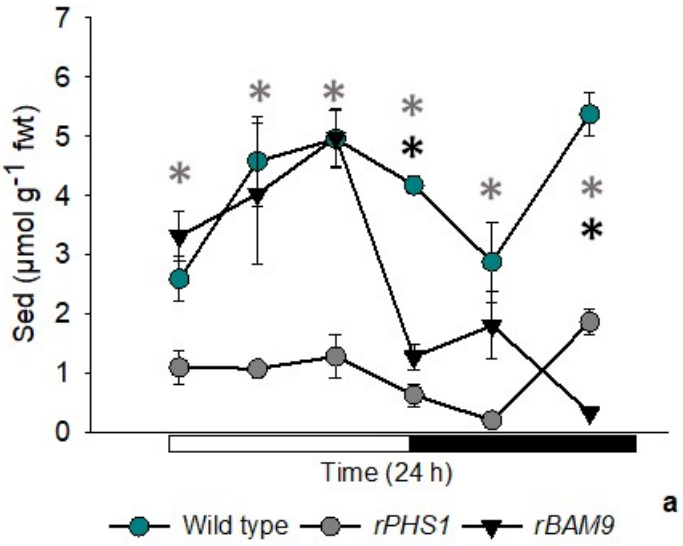

Figure 5. 12. Sedoheptulose content (µmol g^{-1} fwt) in mesophyll of wild type (green filling), *rPHS1* (grey filling) and *rBAM9* (black filling) plants of *K. fedtschenkoi*, during 24 hours (black bar indicates night period). Grey asterisks indicate significant differences ($p \leq 0.05$) between wild type and *rPHS1*, while black asterisks differences between wild type and *rBAM9*. Leaf pair 6 was used for this analysis and the error bars indicate the standard error of six replicates (3 biological replicates, each with 2 technical replicates). Plant growth conditions were set at 400 µmol CO_2 mol^{-1} air, 25°C/19°C (day/night) and a diurnal photosynthetic photon flux density – PPFD - of 250 µmol $m^{-2}s^{-1}$ at plant height.

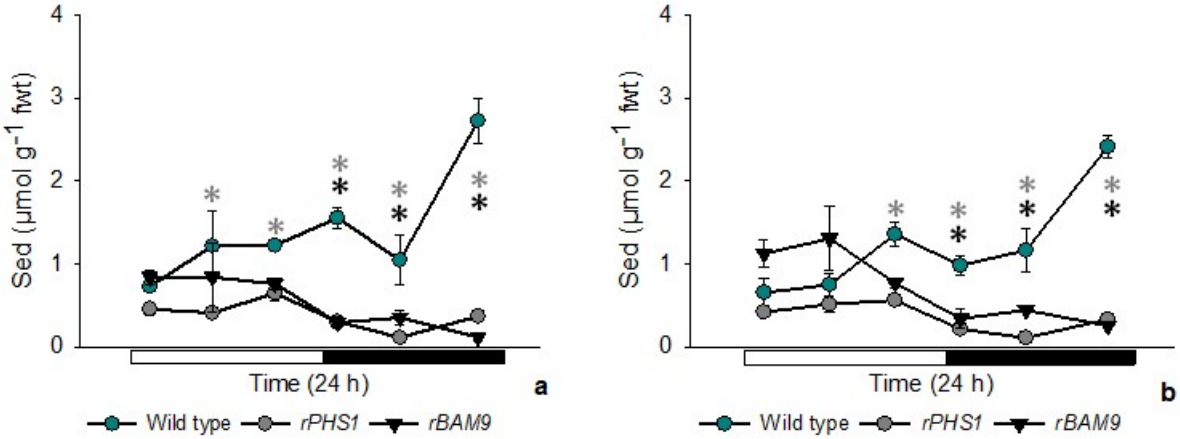

Figure 5. 13. Sedoheptulose content (µmol g^{-1} fwt) in guard cell-enriched epidermis of wild type (green filling), *rPHS1* (grey filling) and *rBAM9* (black filling) plants of *K. fedtschenkoi*, during 24 hours (black bar indicates night period). Upper (a) and lower (b) epidermal surfaces were measured independently. Grey asterisks indicate significant differences ($p \leq 0.05$) between wild type and *rPHS1*, while black asterisks differences between wild type and *rBAM9*. Leaf pair 6 was used for this analysis and the bars indicate the standard error of six replicates (3 biological replicates, each with 2 technical replicates). Plant growth conditions were set at 400 µmol CO_2 mol^{-1} air, 25°C/19°C (day/night) and a diurnal photosynthetic photon flux density – PPFD - of 250 µmol $m^{-2}s^{-1}$ at plant height.

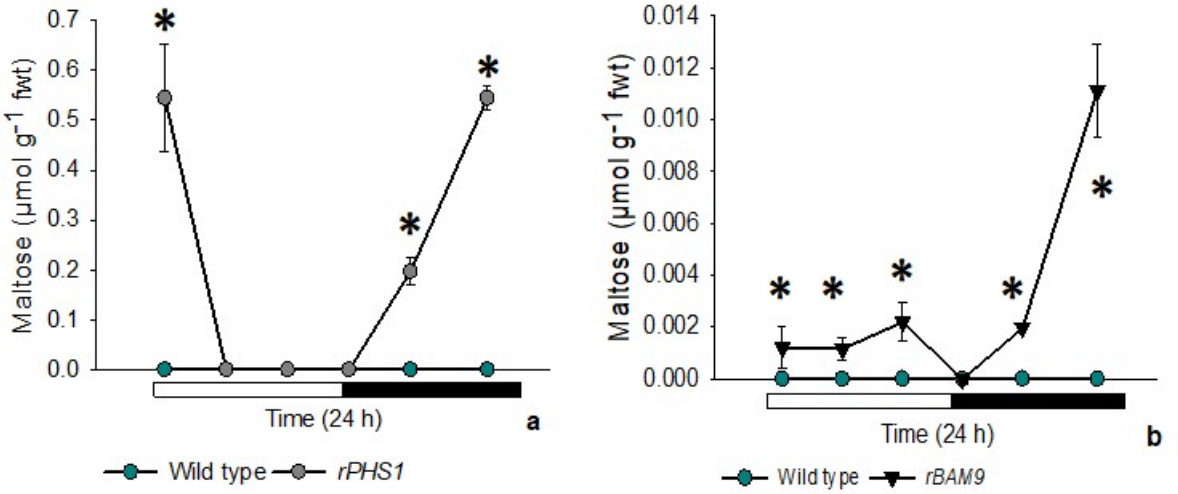

Figure 5. 14. Maltose content (µmol g^{-1} fwt) in mesophyll (a and b) of wild type (green filling), *rPHS1* (grey filling) and *rBAM9* (black filling) plants of *K. fedtschenkoi*, during 24 hours (black bar indicates night period). Significant differences ($p \leq 0.05$) between wild type and both RNAi lines are represented by asterisks. Leaf pair 6 was used for this analysis and the bars indicate the standard error of six replicates (3 biological replicates, each with 2 technical replicates). Plant growth conditions were set at 400 µmol CO_2 mol^{-1} air, 25°C/19°C (day/night) and a diurnal photosynthetic photon flux density – PPFD - of 250 µmol $m^{-2}s^{-1}$ at plant height.

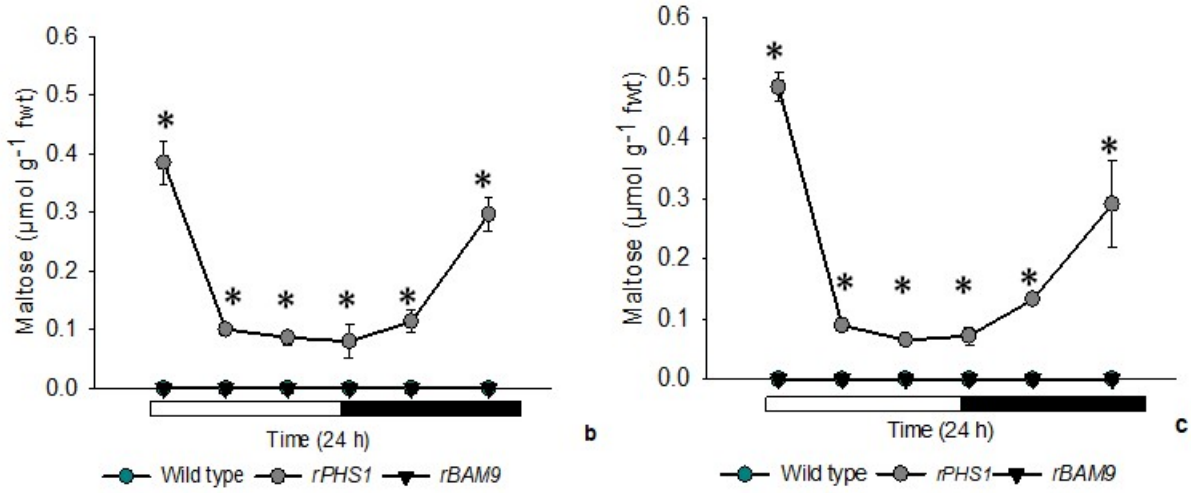

Figure 5. 15. Maltose content (µmol g^{-1} fwt) in guard cell-enriched epidermis of wild type (green filling), *rPHS1* (grey filling) and *rBAM9* (black filling) plants of *K. fedtschenkoi*, during 24 hours (black bar indicates night period). Upper (a) and lower (b) epidermal surfaces were measured independently. Asterisks indicate significant differences ($p \leq 0.05$) between wild type and *rPHS1*, no significant differences were found between wild type and *rBAM9.* Leaf pair 6 was used for this analysis and the bars indicate the standard error of six replicates (3 biological replicates, each with 2 technical replicates). Plant growth conditions were set at 400 µmol CO_2 mol^{-1} air, 25°C/19°C (day/night) and a diurnal photosynthetic photon flux density – PPFD - of 250 µmol $m^{-2}s^{-1}$ at plant height.

5.3.4. Determination of malate in mesophyll and guard cell-enriched epidermis

Malate content in the RNAi and wild type plants followed the typical turnover of this organic acid in CAM plants, with a diurnal degradation due to its decarboxylation and a nocturnal accumulation as a product of PEP carboxylation. Compared with wild type, *rPHS1* and *rBAM9* accumulated less malate over the 24 h period, with a significant reduction ($p \leq 0.05$) during the night-time (Figure 5. 16). In contrast to what occurred in mesophyll, *rPHS1* and *rBAM9* accumulated more malate in the guard cell-enriched epidermis during the dark period, suggesting a possible role as an osmolyte responsible for stomatal opening (Figure 5. 17).

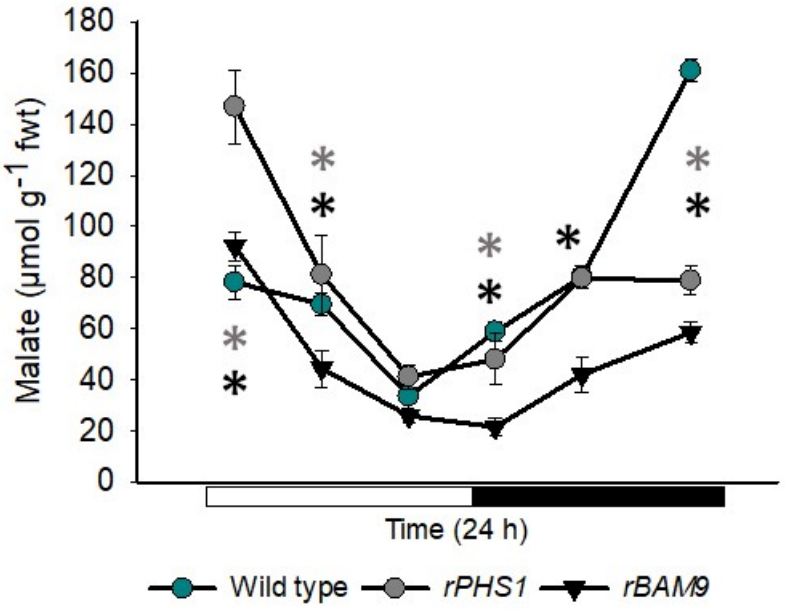

Figure 5. 16. Malate content (µmol g^{-1} fwt) in mesophyll of wild type (green filling), *rPHS1* (grey filling) and *rBAM9* (black filling) plants of *K. fedtschenkoi*, during 24 hours (black bar indicates night period). Grey asterisks indicate significant differences ($p \leq 0.05$) between wild type and *rPHS1*, while black asterisks differences between wild type and *rBAM9.* Leaf pair 6 was used for this analysis and the bars indicate the standard error of six replicates (3 biological replicates, each with 2 technical replicates). Plant growth conditions were set at 400 µmol CO_2 mol^{-1} air, 25°C/19°C (day/night) and a diurnal photosynthetic photon flux density – PPFD - of 250 µmol $m^{-2}s^{-1}$ at plant height.

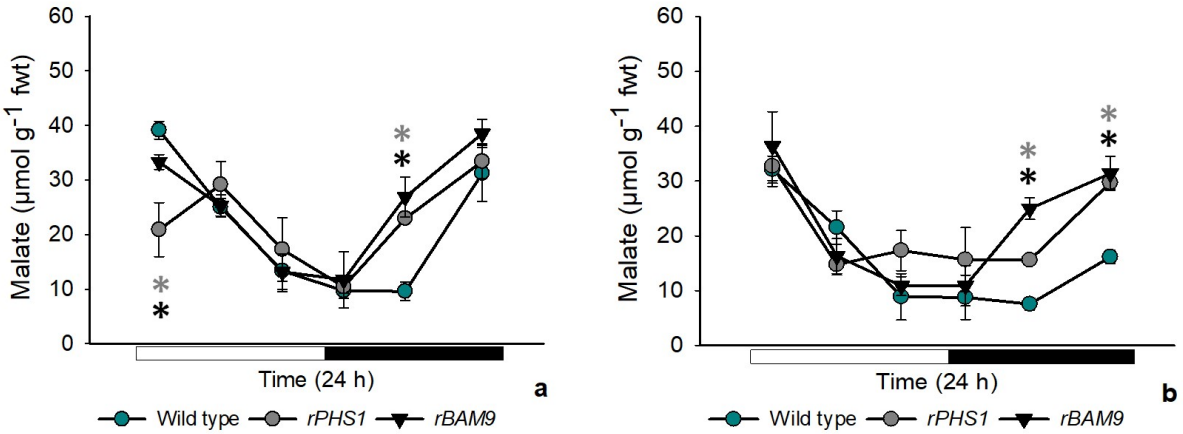

Figure 5. 17. Malate content (µmol g^{-1} fwt) in guard cell-enriched epidermis of wild type (green filling), *rPHS1* (grey filling) and *rBAM9* (black filling) plants of *K. fedtschenkoi*, during 24 hours (black bar indicates night period). Upper (a) and lower (b) epidermal surfaces were measured independently. Grey asterisks indicate significant differences ($p \leq 0.05$) between wild type and *rPHS1*, while black asterisks differences between wild type and *rBAM9*. Leaf pair 6 was used for this analysis and the bars indicate the standard error of 60 replicates (3 biological replicates, each with 20 views per replicate). Plant growth conditions were set at 400 µmol CO_2 mol^{-1} air, 25°C/19°C (day/night) and a diurnal photosynthetic photon flux density – PPFD - of 250 µmol $m^{-2}s^{-1}$ at plant height.

5.3.5. Identification of amylases and α-glucan phosphorylases isoforms using Native PAGE

In order to determine the PHS isoform silenced in the *rPHS1* line, Native PAGE was conducted in wild type, *rPHS1* and *rBAM9* lines. Figure 5. 18, corresponding to glycogen Native PAGE, shows the absence of both bands on the *rPHS1* line. Opposite to the findings of Ceusters *et al.* (submitted), both plastidic and cytosolic isoforms were absent in *rPHS1* lines, probably as an effect of the *phs1* silencing or as lower protein content imperceptible in the Native gel. On the other hand, both bands were present in *K. fedtschenkoi* wild type and *rBAM9*, which leads to hypothesise that *bam9* deficiency is not affecting the expression of PHS enzyme. Compared with *Arabidopsis* the location of the second band differed in *K. fedtschenkoi*, probably due to changes in protein electrophysical characteristics between C_3 and CAM.

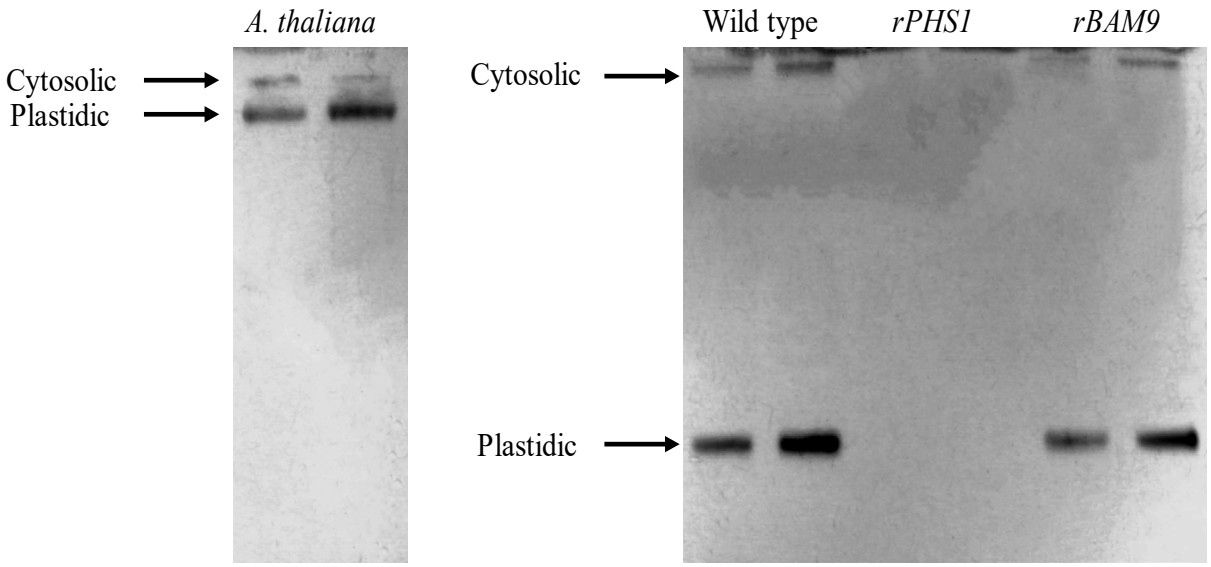

Figure 5. 18. PHS isoforms separation by Native PAGE. Whole leaf samples of *K. fedtschenkoi* wild type, *rPHS1* and *rBAM9* lines were compared against wild type *A. thaliana* ecotype Columbia. Two isoforms (indicated with arrows) are observed in *A. thaliana* and *K. fedtschenkoi* wild type and *rBAM9* line. In the case of the *rPHS1* deficient line, both isoforms are absent. All the samples were loaded in the same gel, but for isoforms differentiation purposes, the photograph was edited and divided in two parts. Plant growth conditions were set at 400 µmol CO_2 mol^{-1} air, 25°C/19°C (day/night) and a diurnal photosynthetic photon flux density – PPFD - of 250 µmol $m^{-2}s^{-1}$ at plant height.

Amylopectin containing Native PAGE was used to identify if there were any other changes in starch degrading enzymes in the *rPHS1* and *rBAM9* lines. The specific starch degrading enzymes were identified based on the description of Zeeman *et al.* (1998) in *A. thaliana*, who reported that in amylopectin-based gels, α-amylases produce clear colourless bands, β-amylases produce brown bands and debranching enzymes, pale blue bands. Prominent α-amylases were observed in *K. fedtschenkoi*, compared with *A. thaliana*, as well as differences in the distribution of the coloured bands that represent different starch degrading enzymes. Compared to wild type, the *rPHS1* lines showed an increased intensity of bands that correspond to debranching enzymes and β-amylases. In the case of *rBAM9*, an extra band corresponding to α-amylase was observed, as well as the inversion of the position of the β-amylases and D-enzymes on the Native gel (Figure 5. 19).

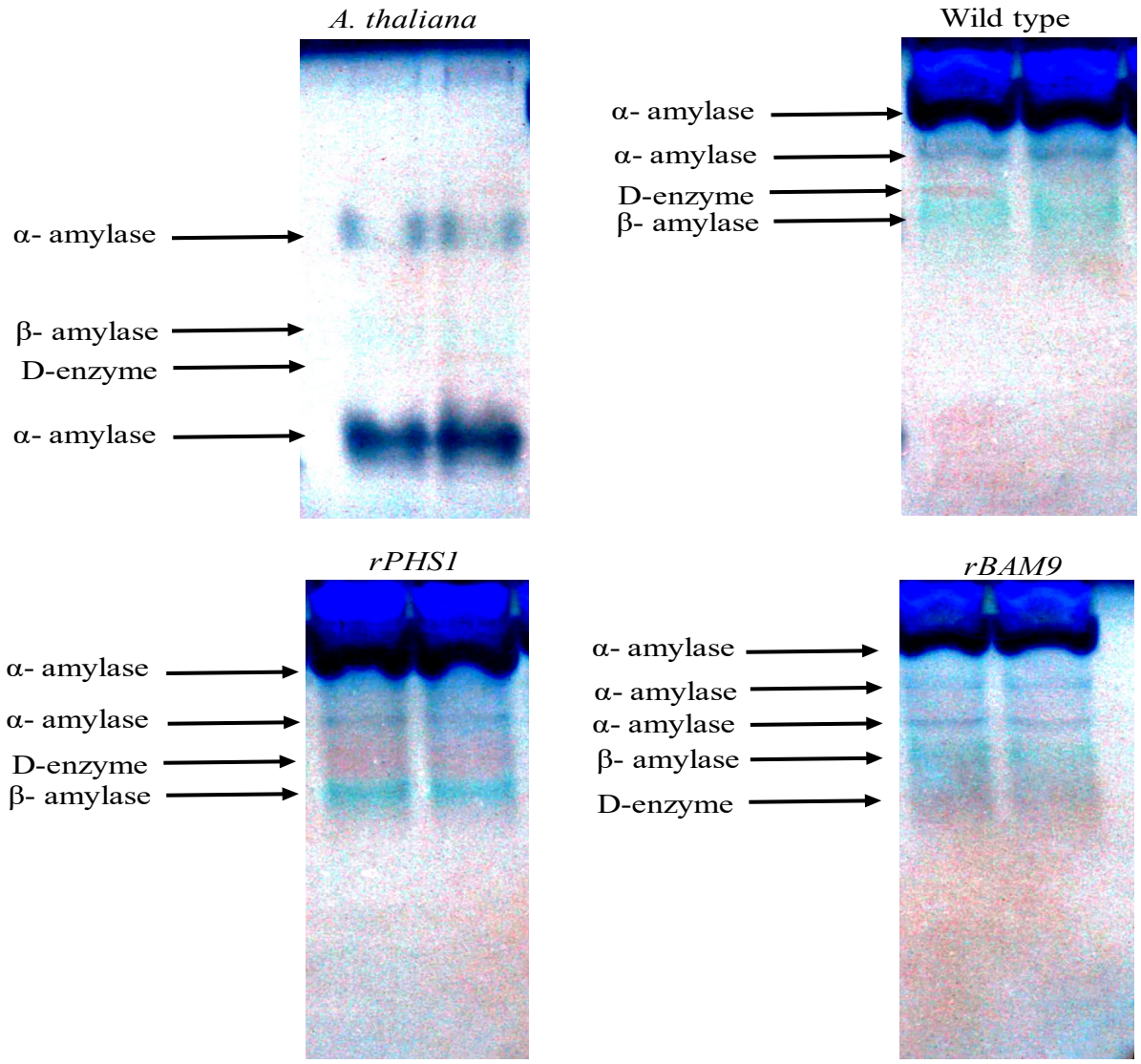

Figure 5. 19. Native PAGE of starch degrading enzymes. Whole leaf samples of *K. fedtschenkoi* wild type, *rPHS1* and *rBAM9* lines were compared against wild type *A. thaliana* ecotype Columbia. α-amylases are represented by dark blue bands, β-amylases by light blue and disproportionating enzymes (D-enzymes) are represented by pink bands. The colours of the photo are inverted in order to enhance its contrast. All the samples were loaded in the same gel, but for isoforms differentiation purposes the photograph was edited and divided in four parts. Plant growth conditions were set at 400 µmol CO_2 mol^{-1} air, 25°C/19°C (day/night) and a diurnal photosynthetic photon flux density – PPFD - of 250 µmol $m^{-2}s^{-1}$ at plant height.

5.3.6. Subcellular localisation of β-amylases and homology with Arabidopsis thaliana

The UPGMA clustering analysis shows the phylogenetic relationships among BAM isoforms in both *K. fedtschenkoi* and *A. thaliana* (Figure 5. 20). Noteworthy, *A. thaliana* BAM4 and BAM6 were homologous to *Kalanchoë* sequences reported as BAM3 and BAM5 in the published genome (DOE-JGI, http://phytozome.jgi.doe.gov/), but UniProtKB/Swiss-Prot database annotated them as β-amylase 3 and β-amylase, respectively, indicating the

probable lack of BAM4 and BAM6 isoforms in *Kalanchoë* or inaccurate annotations on the genome. In order to confirm this, further studies need to be performed. Whilst Kaladp0062s0212, Kaladp0076s0255 and Kaladp0076s0256 are all reported to code for BAM9 in *Kalanchoë*, Kaladp0062s0212 presented the highest similarity to *Arabidopsis* BAM9, evidenced by the clustering analysis. Thus, this gene sequence was used to design primers and confirm the impact on *bam9* transcript abundance in the *rBAM9* line using real time qPCR (Section 5.3.1).

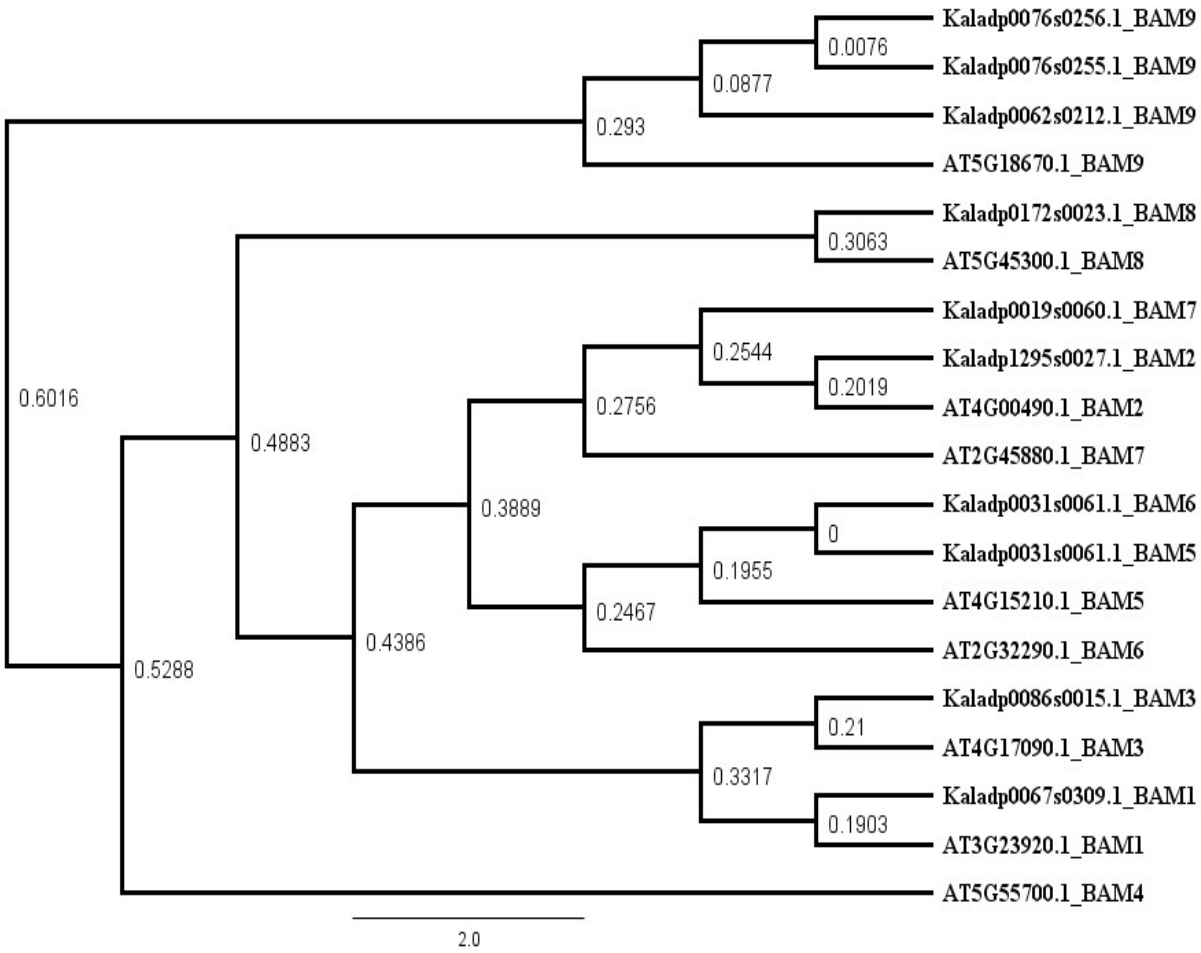

Figure 5. 20. UPGMA clustering tree for *K. fedtschenkoi* and *A. thaliana* β-amylases (BAM) protein isoform sequences. The overall similarities among sequences are denoted in each node by their pairwise distance value.

Similarities between the sequences of *K. fedtschenkoi* and *A. thaliana* β-amylases were determined through a multiple alignment. For this study purposes, Figure 5. 21 focused on the fraction of the conserved domain where changes in amino acids affect the substrate binding and catalytic activity of BAM9, based on the reports of Fulton *et al.* (2008). In this case, a

five amino acid deletion in *K. fedtschenkoi* BAM9 occurs in the flexible loop of the protein, followed by a substitution of Threonine by Proline in the 342 residue of the inner loop and the change of the catalytic Glutamic acid by Glutamine in the position 380. Finally, based on the subcellular localisation prediction, most of *Kalanchoë* sequences are located in the chloroplast similar to *Arabidopsis*, while the sequences annotated as BAM5, BAM6 and BAM7 for *Kalanchoë* are neither located in the chloroplast nor in the mitochondria (Table 5. 1).

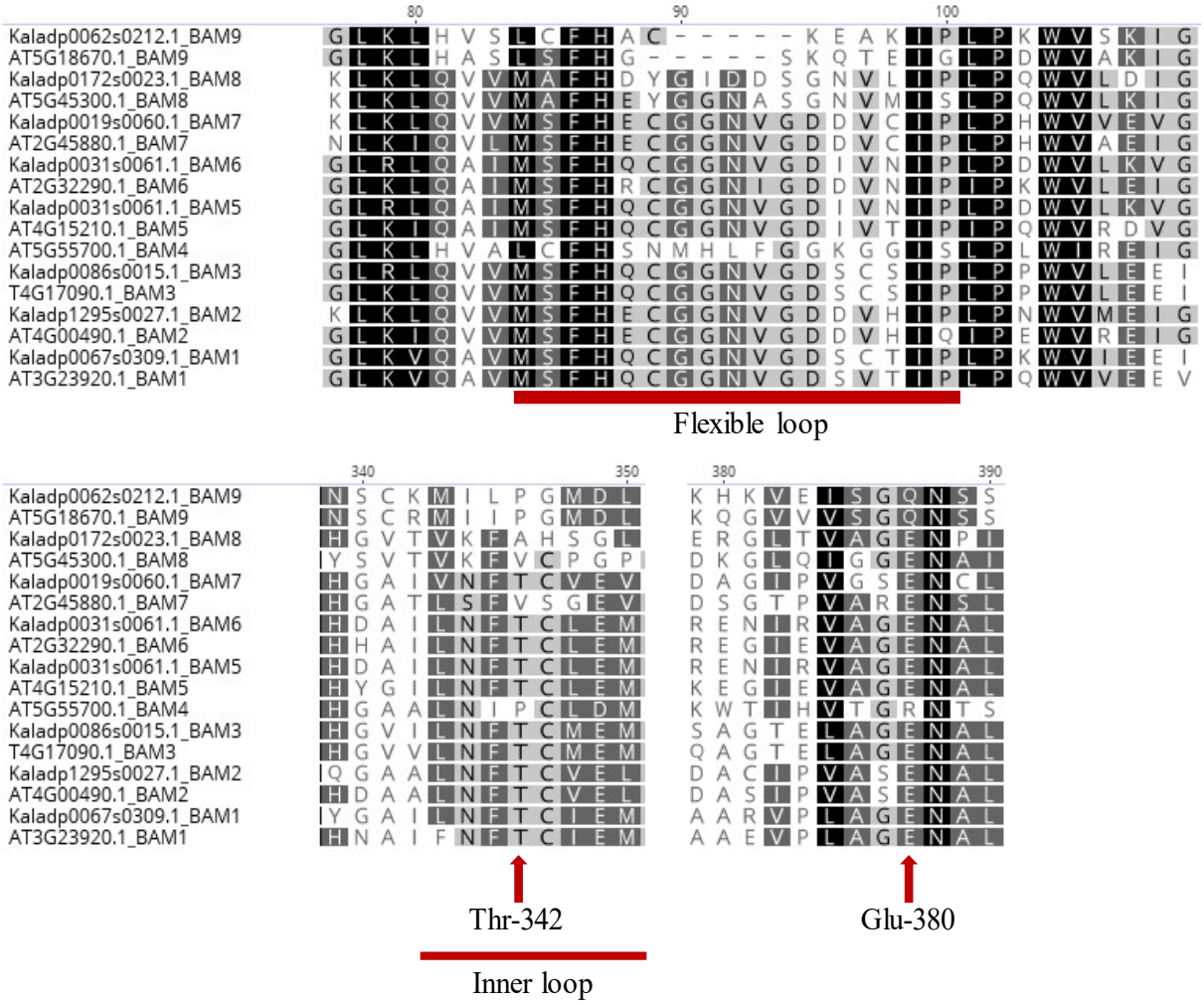

Figure 5. 21. Multiple alignment of a fraction of the conserved domain involved in the catalytic activity of β-amylases (BAM). The isoform sequences correspond to *K. fedtschenkoi* and *A. thaliana*. Residues deletion in the flexible loop, Thr-342 and Glu-380 substitutions in BAM9 of both species are highlighted.

Table 5. 1. TargetP prediction of subcellular localisation of BAM isoforms reported for both *A. thaliana* and *K. fedtschenkoi*. Chloroplast transit peptide (cTP), mitochondrial targeting peptide (mTP), signal peptide (SP) and other (-) location are identified based on the final predicted score and the reliability class (RC) where 1 is the strongest prediction. UniProtKB/Swiss-Prot database annotation is also presented.

Name	Length	cTP	mTP	SP	Other	Localisation	RC	UniProtKB/Swiss-Prot annotation
Kaladp0067s0309_BAM1	528	0.723	0.078	0.009	0.424	Chloroplast	4	Beta-amylase 1, chloroplastic
Kaladp1295s0027_BAM2	540	0.956	0.052	0.013	0.054	Chloroplast	1	Beta-amylase 2, chloroplastic
Kaladp0086s0015_BAM3	549	0.538	0.099	0.043	0.234	Chloroplast	4	Beta-amylase 3, chloroplastic
Kaladp0086s0015_BAM4	549	0.538	0.099	0.043	0.234	Chloroplast	4	Beta-amylase 3, chloroplastic
Kaladp0031s0061_BAM5	564	0.22	0.302	0.094	0.482	-	5	Beta-amylase
Kaladp0031s0061_BAM6	564	0.22	0.302	0.094	0.482	-	5	Beta-amylase
Kaladp0019s006_BAM7	686	0.026	0.121	0.072	0.942	-	1	Beta-amylase 7
Kaladp0172s0023_BAM8	651	0.504	0.081	0.02	0.455	Chloroplast	5	Beta-amylase 8
Kaladp0062s0212_BAM9	537	0.624	0.086	0.036	0.24	Chloroplast	4	Inactive Beta-amylase 9
Kaladp0076s0255_BAM9	533	0.67	0.054	0.022	0.381	Chloroplast	4	Inactive Beta-amylase 9
Kaladp0076s0256_BAM9	533	0.657	0.054	0.022	0.384	Chloroplast	4	Inactive Beta-amylase 9
At3g23920_BAM1	2519	0.695	0.032	0.032	0.241	Chloroplast	3	Beta-amylase 1, chloroplastic
At4g00490_BAM2	2031	0.214	0.094	0.09	0.209	Chloroplast	5	Beta-amylase 2, chloroplastic
At4g17090_BAM3	2441	0.032	0.016	0.404	0.141	Chloroplast	4	Beta-amylase 3, chloroplastic
At5g55700_BAM4	1997	0.286	0.222	0.01	0.373	-	5	Inactive beta-amylase 4, chloroplastic
At4g15210_BAM5	3193	0.4	0.043	0.082	0.098	Chloroplast	4	Beta-amylase 5
At2g32290_BAM6	2487	0.517	0.052	0.085	0.268	Chloroplast	4	Beta-amylase 6
At2g45880_BAM7	3272	0.459	0.105	0.053	0.164	Chloroplast	4	Beta-amylase 7
At5g45300_BAM8	3277	0.018	0.026	0.626	0.12	SP	3	Beta-amylase 8
At5g18670_BAM9	1989	0.157	0.017	0.802	0.016	Chloroplast	2	Inactive Beta-amylase 9

5.3.7. Effect of phs1 and bam9 deficiencies in leaf gas exchange

Gas exchange analysis showed that the curtailed ability of *rPHS1* and *rBAM9* to degrade starch resulted in lower net CO_2 uptake during the night in comparison to wild type (Figure 5. 22a, Figure 5. 23a). Interestingly, maximal nocturnal values for stomatal conductance were less affected in the RNAi lines compared to wild type, suggesting that a lower CAM activity in the RNAi lines was probably due to a lack of substrates (i.e. PEP originated from starch degradation) rather than because of a reduced stomatal conductance. In addition, during the light period stomatal conductance in *rPHS1* and *rBAM9* was higher than wild type. It can be hypothesised that the higher accumulation of glucose, fructose and malate in the guard cells of

these RNAi lines observed during the day, potentially increased stomatal turgor pressure and curtailed stomatal closure (Figure 5. 22b, Figure 5. 23b).

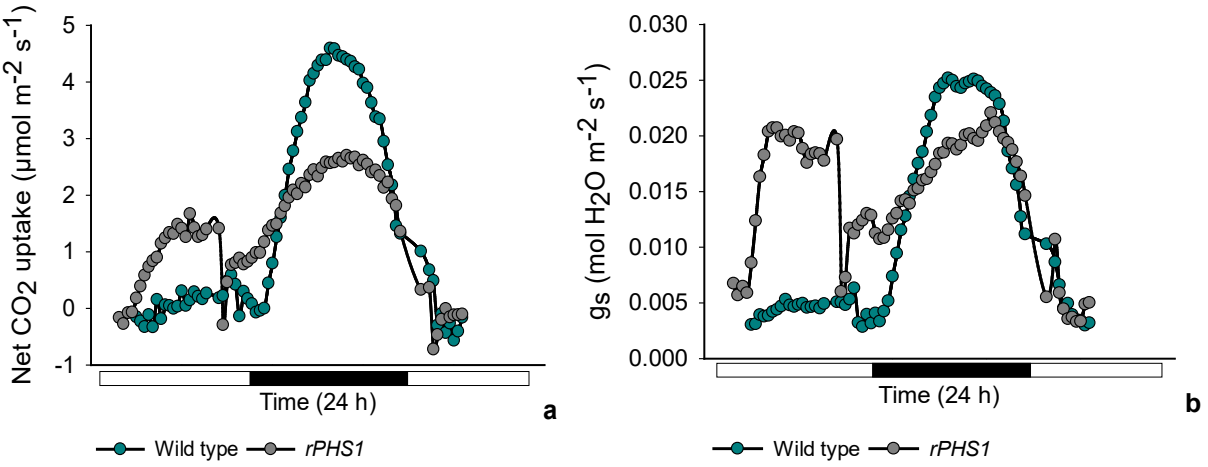

Figure 5. 22. Net CO_2 uptake (a) and stomatal conductance (b) of wild type (green filling) and *rPHS1* (grey filling) plants of *K. fedtschenkoi*, during 24 hours (black bar indicates night period). Leaf pair 6 was used for this analysis and the data correspond to three biological replicates. Plant growth conditions were set at 400 µmol CO_2 mol^{-1} air, 25°C/19°C (day/night) and a diurnal photosynthetic photon flux density – PPFD - of 250 µmol $m^{-2}s^{-1}$ at plant height.

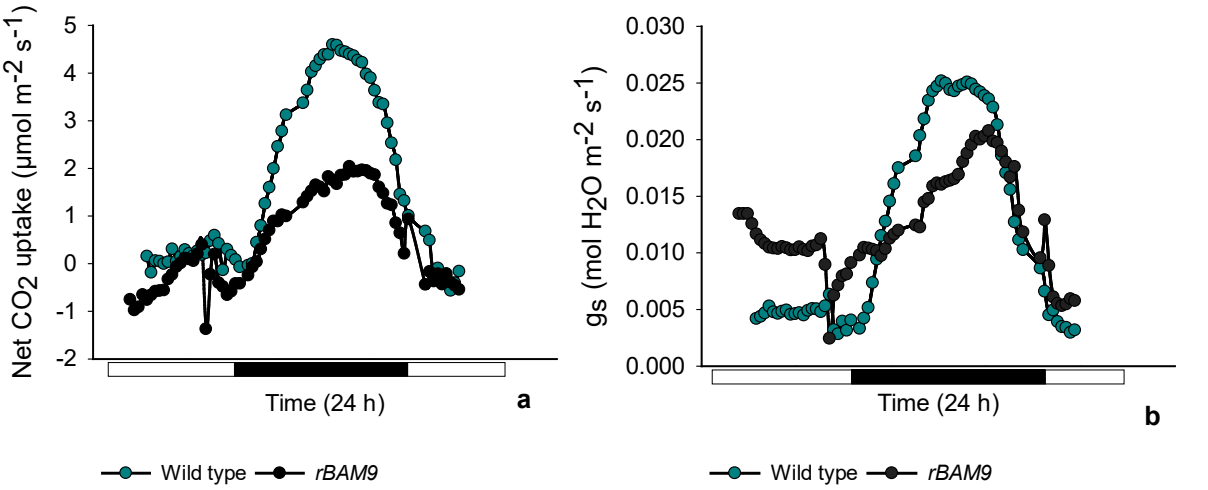

Figure 5. 23. Net CO_2 uptake (a) and stomatal conductance (b) of wild type (green filling) and *rBAM9* (black filling) plants of *K. fedtschenkoi*, during 24 hours (black bar indicates night period). Leaf pair 6 was used for this analysis and the data corresponds to three biological replicates. Plant growth conditions were set at 400 µmol CO_2 mol^{-1} air, 25°C/19°C (day/night) and a diurnal photosynthetic photon flux density – PPFD - of 250 µmol $m^{-2}s^{-1}$ at plant height.

Additionally, measurements of net CO_2 uptake and transpiration over 24 h, obtained by integrating the areas under the curves of both parameters, indicated a significantly reduced instantaneous water use efficiency (WUEi) in the RNAi lines over the 24 h day/night cycle, compared with wild type. This was linked to the lower CO_2 uptake during the night-time and the reduced stomatal closure during the day in the RNAi lines (Table 5. 2).

Table 5. 2. Instantaneous water use efficiency (WUEi) for wild type, *rPHS1* and *rBAM9* plants of *K. fedtschenkoi*, during 24 hours. WUEi was calculated by the ratio of integrated net CO_2 uptake to integrated net water loss over entire 24 h cycle. Leaf pair 6 was used for this analysis and the data corresponds to the mean and the standard error of three biological replicates.

	Instantaneous water use efficiency (mmol CO_2: mol H_2O)		
	Night	Day	24 h
Wild type	12.706 (± 0.429)	7.057 (±2.818)	8.708 (± 0.871)
rPHS1	8.195 (± 2.003)	4.661 (±1.023)	4.390 (± 1.360)
rBAM9	7.773 (± 3.093)	2.894 (±1.304)	3.386 (± 1.927)

5.3.8. Transcript abundance of genes related to starch metabolism and stomatal regulation

The enzymes β-amylases 1 and 3 (BAM1 and BAM3), α-amylase 3 (AMY3) and disproportionating enzyme 1 (DPE1) are involved in the hydrolytic degradation of starch. The expression of their transcripts differed among genotypes, time periods and tissues. The *bam1* transcript was mainly expressed at the beginning of the light period with high abundance in the mesophyll of the *rPHS1* and in the guard cell-enriched epidermis of the wild type. In the case of *rBAM9*, the transcript was less abundant at dawn but increased at dusk in the mesophyll (Figure 5. 24). Different to what occurred for *bam1*, the expression of *bam3* predominated at dusk, being similar between tissues of both wild type and *rPHS1,* but more abundant in the RNAi line compared to wild type. For *rBAM9*, the expression of *bam3* was higher in the guard cell-enriched epidermis, but in less abundance than wild type (Figure 5. 25).

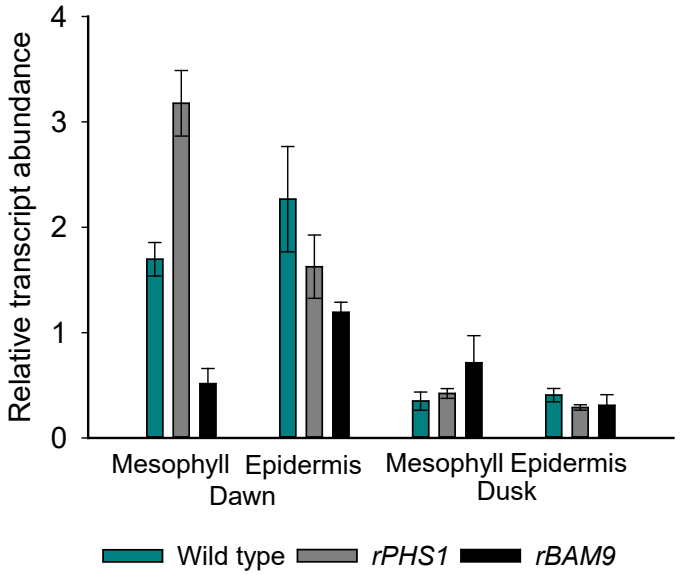

Figure 5. 24. Relative transcript abundance of *bam1* gene in wild type (green), *rPHS1* (grey) and *rBAM9* (black) in mesophyll and guard cell-enriched epidermis at dawn and dusk. Leaf pair 6 was used for this analysis. The error bars represent the standard error of six replicates (3 biological replicates, each with 2 technical replicates). Plant growth conditions were set at 400 µmol CO_2 mol^{-1} air, 25°C/19°C (day/night) and a diurnal photosynthetic photon flux density – PPFD - of 250 µmol $m^{-2}s^{-1}$ at plant height.

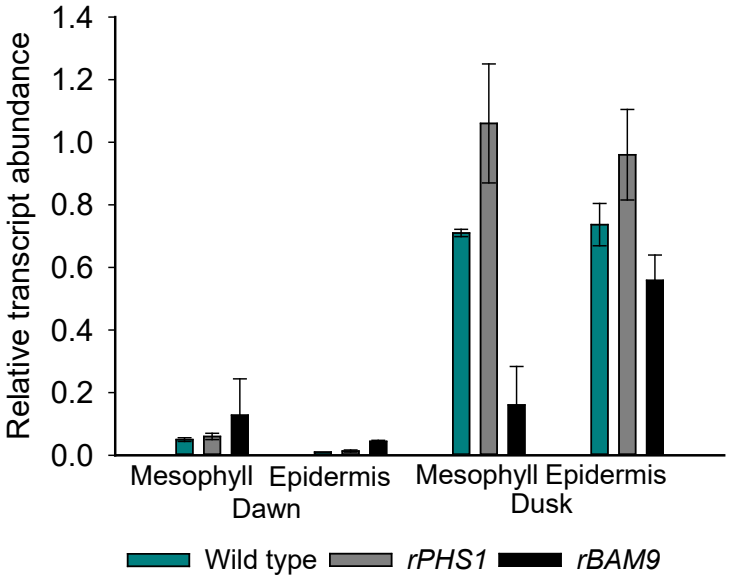

Figure 5. 25. Relative transcript abundance of *bam3* gene in wild type (green), *rPHS1* (grey) and *rBAM9* (black) in mesophyll and guard cell-enriched epidermis at dawn and dusk. Leaf pair 6 was used for this analysis. The error bars represent the standard error of six replicates (3 biological replicates, each with 2 technical replicates). Plant growth conditions were set at 400 µmol CO_2 mol^{-1} air, 25°C/19°C (day/night) and a diurnal photosynthetic photon flux density – PPFD - of 250 µmol $m^{-2}s^{-1}$ at plant height.

Regarding α-amylase 3 (*amy3*) and disproportionating enzyme 1 (*dpe1*), similar abundance patterns were found between both transcripts, characterised by a higher expression in the mesophyll than in the guard cell-enriched epidermis. Comparing to wild type, the RNAi line *rPHS1* presented an increased abundance for both genes at dawn and dusk in the mesophyll. In the case of *rBAM9,* the expression of *amy3* was higher in the guard cell-enriched epidermis at the beginning of the day and lower in the mesophyll during both times. In contrast, the expression of *dpe1* in *rBAM9* mesophyll was higher at dawn and down regulated at dusk compared to wild type (Figure 5. 26 and Figure 5. 27).

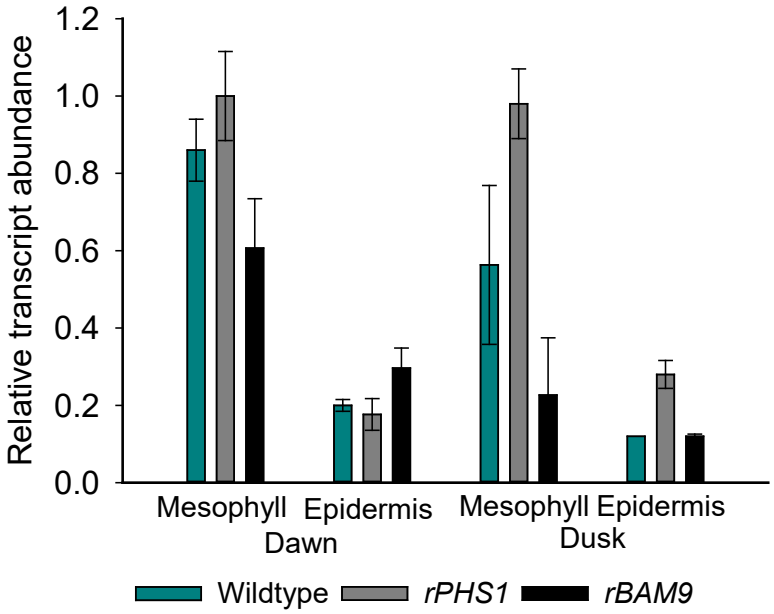

Figure 5. 26. Relative transcript abundance of *amy3* gene in wild type (green), *rPHS1* (grey) and *rBAM9* (black) in mesophyll and guard cell-enriched epidermis at dawn and dusk. Leaf pair 6 was used for this analysis. The error bars represent the standard error of six replicates (3 biological replicates, each with 2 technical replicates). Plant growth conditions were set at 400 µmol CO_2 mol^{-1} air, 25°C/19°C (day/night) and a diurnal photosynthetic photon flux density – PPFD - of 250 µmol $m^{-2}s^{-1}$ at plant height.

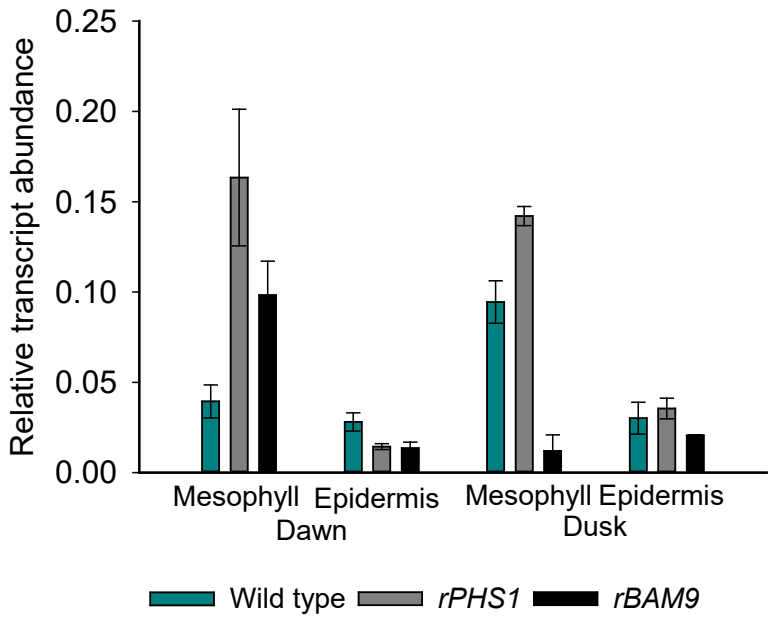

Figure 5. 27. Relative transcript abundance of *dpe1* gene in wild type (green), *rPHS1* (grey) and *rBAM9* (black) in mesophyll and guard cell-enriched epidermis at dawn and dusk. Leaf pair 6 was used for this analysis. The error bars represent the standard error of six replicates (3 biological replicates, each with 2 technical replicates). Plant growth conditions were set at 400 µmol CO_2 mol^{-1} air, 25°C/19°C (day/night) and a diurnal photosynthetic photon flux density – PPFD - of 250 µmol $m^{-2}s^{-1}$ at plant height.

Different transporters located in the plasma membrane of chloroplasts conduct the export of products derived from starch degradation. The transcript abundances of the plastidic glucose transporter (*glct*), maltose exporter 1 (*mex1*), triose phosphate translocator (*tpt*), glucose 6-phosphate transporters 1 and 2 (*gpt1* and *gpt2*) were also evaluated in both wild type and RNAi lines.

Transcript abundance for *glct* differed among genotypes. No differences in the transcript abundance in the mesophyll were detected among wild type and the RNAi lines at dawn. Additionally, *glct* expression in *rPHS1* was highly abundant at dusk in both tissues, while in *rBAM9*, the transcript was predominantly higher in the guard cell-enriched epidermis during both times and lower in the mesophyll at dusk, compared to wild type (Figure 5. 28).

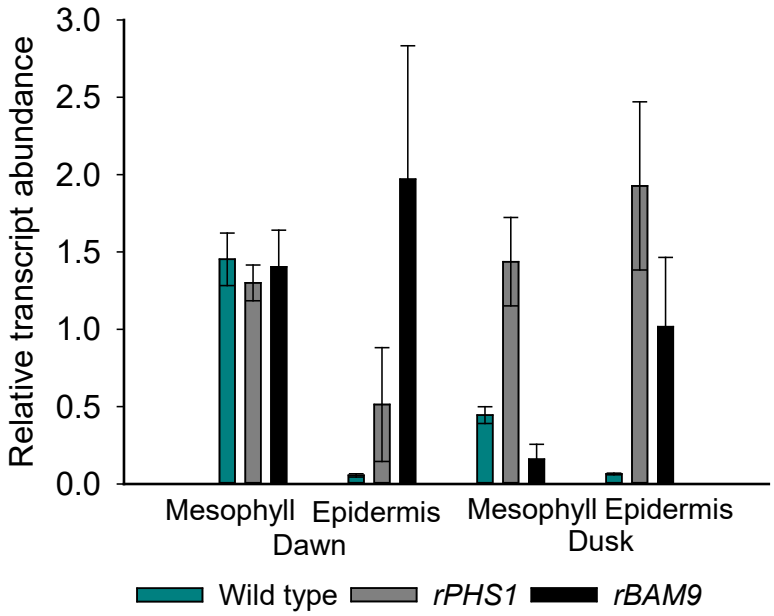

Figure 5. 28. Relative transcript abundance of *glct* gene in wild type (green), *rPHS1* (grey) and *rBAM9* (black) in mesophyll and guard cell-enriched epidermis at dawn and dusk. Leaf pair 6 was used for this analysis. The error bars represent the standard error of six replicates (3 biological replicates, each with 2 technical replicates). Plant growth conditions were set at 400 µmol CO_2 mol^{-1} air, 25°C/19°C (day/night) and a diurnal photosynthetic photon flux density – PPFD - of 250 µmol $m^{-2}s^{-1}$ at plant height.

The maltose exporter 1 (*mex1*) transcript was significantly higher in *rPHS1* and *rBAM9* lines. In the case of *rPHS1,* a higher abundance in the guard cell-enriched epidermis was evidenced at both times, accompanied by a maximum expression at the beginning of the night period in the mesophyll and a negligible expression in this same tissue at dawn. The expression of *mex1* in *rBAM9* was significantly higher than in wild type in both tissues and time periods (Figure 5. 29).

In wild type plants, the expression of the triose phosphate translocator (*tpt*) was restricted to the mesophyll at the beginning of the day. Noteworthy, comparing to the abundance pattern in wild type, the deficiencies in *phs1* and *bam9* curtailed the expression of this gene at dawn in the mesophyll, and increased it in the guard cell-enriched epidermis of *rPHS1* at the beginning of the night (Figure 5. 30).

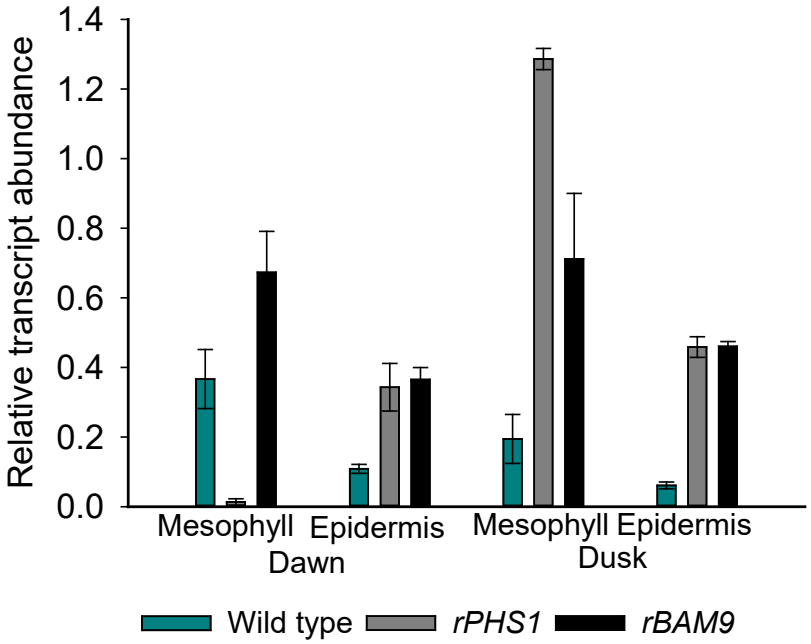

Figure 5. 29. Relative transcript abundance of *mex1* gene in wild type (green), *rPHS1* (grey) and *rBAM9* (black) in mesophyll and guard cell-enriched epidermis at dawn and dusk. Leaf pair 6 was used for this analysis. The error bars represent the standard error of six replicates (3 biological replicates, each with 2 technical replicates). Plant growth conditions were set at 400 µmol CO_2 mol^{-1} air, 25°C/19°C (day/night) and a diurnal photosynthetic photon flux density – PPFD - of 250 µmol $m^{-2}s^{-1}$ at plant height.

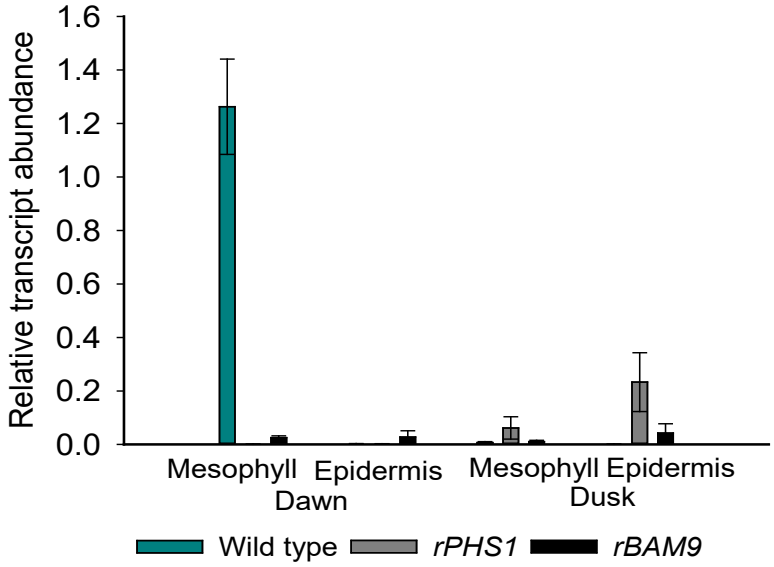

Figure 5. 30. Relative transcript abundance of *tpt* gene in wild type (green), *rPHS1* (grey) and *rBAM9* (black) in mesophyll and guard cell-enriched epidermis at dawn and dusk. Leaf pair 6 was used for this analysis. The error bars represent the standard error of six replicates (3 biological replicates, each with 2 technical replicates). Plant growth conditions were set at 400 µmol CO_2 mol^{-1} air, 25°C/19°C (day/night) and a diurnal photosynthetic photon flux density – PPFD - of 250 µmol $m^{-2}s^{-1}$ at plant height.

The glucose 6-phosphate transporters 1 and 2 (*gpt1* and *gpt2*) are implicated in both the export and import of Glc6P, respectively. The transcript abundance of both genes differed among the genotypes. Compared to wild type, the expression of *gpt1* at dawn and dusk was higher in both mesophyll and guard cell-enriched epidermis of *rBAM9*, while in *rPHS1* was more abundant in the epidermis (Figure 5. 31). Regarding *gpt2*, the expression in wild type was restricted to the beginning of the day, mainly in the mesophyll. Noteworthy, the deficiency of *bam9* generated an increment on the expression of *gpt2* in both mesophyll and guard cell-enriched epidermis, while *phs1* silencing did not affect the expression of this transporter (Figure 5. 32).

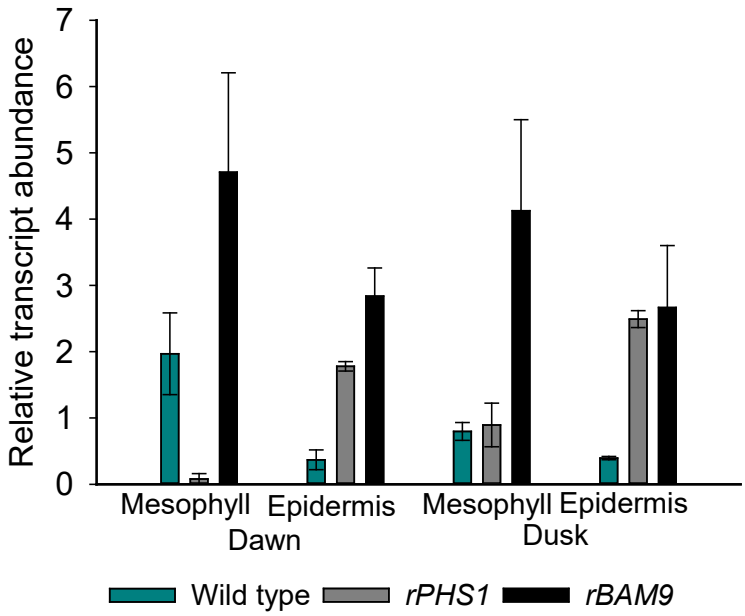

Figure 5. 31. Relative transcript abundance of *gpt1* gene in wild type (green), *rPHS1* (grey) and *rBAM9* (black) in mesophyll and guard cell-enriched epidermis at dawn and dusk. Leaf pair 6 was used for this analysis. The error bars represent the standard error of six replicates (3 biological replicates, each with 2 technical replicates). Plant growth conditions were set at 400 µmol CO_2 mol^{-1} air, 25°C/19°C (day/night) and a diurnal photosynthetic photon flux density – PPFD - of 250 µmol $m^{-2}s^{-1}$ at plant height.

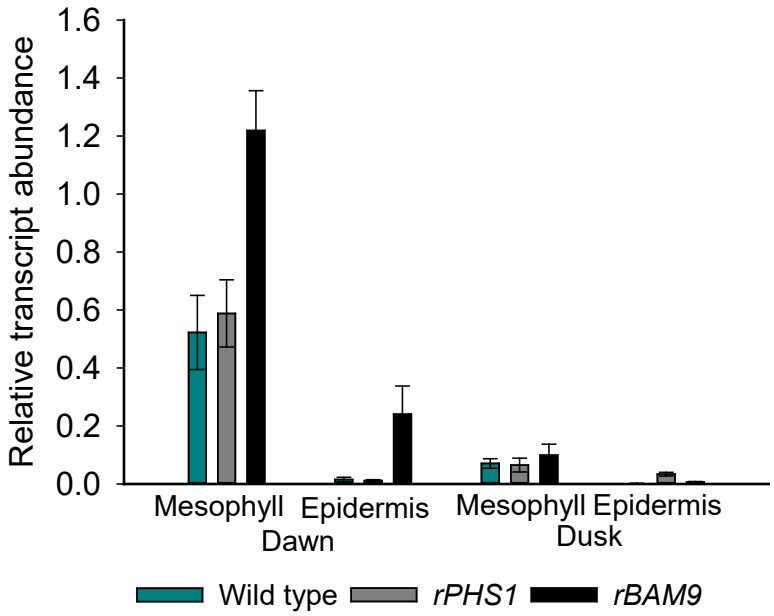

Figure 5. 32. Relative transcript abundance of *gpt2* gene in wild type (green), *rPHS1* (grey) and *rBAM9* (black) in mesophyll and guard cell-enriched epidermis at dawn and dusk. Leaf pair 6 was used for this analysis. The error bars represent the standard error of six replicates (3 biological replicates, each with 2 technical replicates). Plant growth conditions were set at 400 µmol CO_2 mol^{-1} air, 25°C/19°C (day/night) and a diurnal photosynthetic photon flux density – PPFD - of 250 µmol $m^{-2}s^{-1}$ at plant height.

The enzymes sucrose synthases 1 and 3 (SUSY1 and SUSY3) are involved in the metabolism of sucrose. Based on the importance of sugars in stomatal regulation the transcript abundance of these genes was also evaluated. The expression of *susy1* was restricted to the beginning of the day in both wild type and RNAi lines. In wild type, *susy1* was more abundant in the mesophyll than in the guard cell-enriched epidermis, different to the RNAi lines, where a higher expression of *susy1* was observed in the epidermis of *rBAM9* and in both tissues of *rPHS1* (Figure 5. 33). Different to *susy1*, *susy3* was expressed at both dawn and dusk in wild type and RNAi lines, but in both *rPHS1* and *rBAM9,* the expression of *susy3* increased in the mesophyll and guard cell-enriched epidermis during both periods (Figure 5. 34).

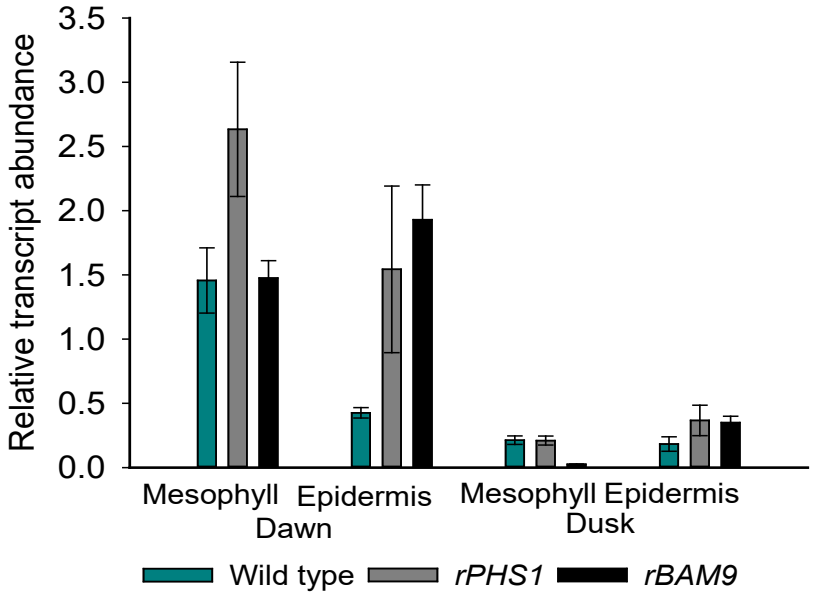

Figure 5. 33. Relative transcript abundance of *susy1* gene in wild type (green), *rPHS1* (grey) and *rBAM9* (black) in mesophyll and guard cell-enriched epidermis at dawn and dusk. Leaf pair 6 was used for this analysis. The error bars represent the standard error of six replicates (3 biological replicates, each with 2 technical replicates). Plant growth conditions were set at 400 µmol CO_2 mol^{-1} air, 25°C/19°C (day/night) and a diurnal photosynthetic photon flux density – PPFD - of 250 µmol $m^{-2}s^{-1}$ at plant height.

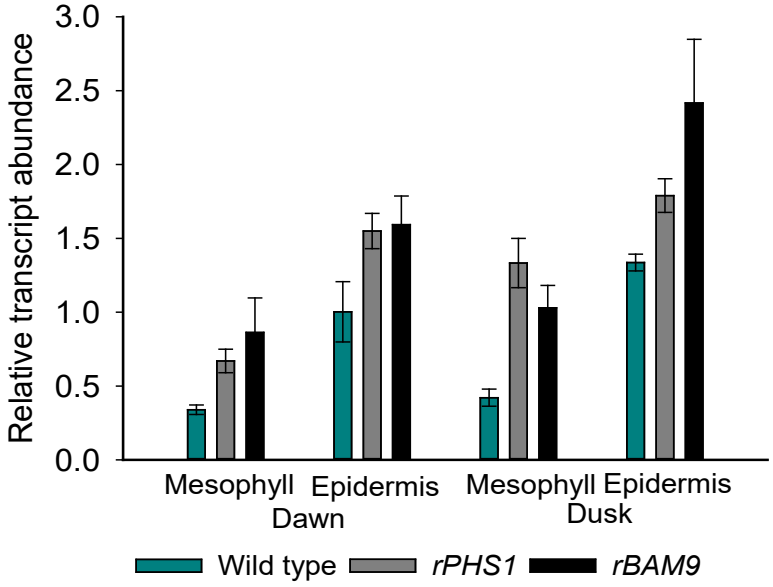

Figure 5. 34. Relative transcript abundance of *susy3* gene in wild type (green), *rPHS1* (grey) and *rBAM9* (black) in mesophyll and guard cell-enriched epidermis at dawn and dusk. Leaf pair 6 was used for this analysis. The error bars represent the standard error of six replicates (3 biological replicates, each with 2 technical replicates). Plant growth conditions were set at 400 µmol CO_2 mol^{-1} air, 25°C/19°C (day/night) and a diurnal photosynthetic photon flux density – PPFD - of 250 µmol $m^{-2}s^{-1}$ at plant height.

Given the importance of osmolytes influx in guard cells turgor pressure, the transcript abundances of the sugar transporter 1 (*stp1*) and the ATP-binding cassette malate transporter (*abcb14*) were evaluated. In wild type, *stp1* expression was significantly higher in the guard cell-enriched epidermis at dawn, while in *rPHS1* and *rBAM9* the transcript was overexpressed at the beginning of the night in both tissues (Figure 5. 35). On the other side, *abcb14* expression was specific to guard cell-enriched epidermis and in both wild type and RNAi lines, with temporal differences among genotypes. In wild type, was expressed exclusively at the beginning of the night, while in both *rPHS1* and *rBAM9* was highly expressed at dawn and significantly down regulated for *rPHS1* at dusk (Figure 5. 36).

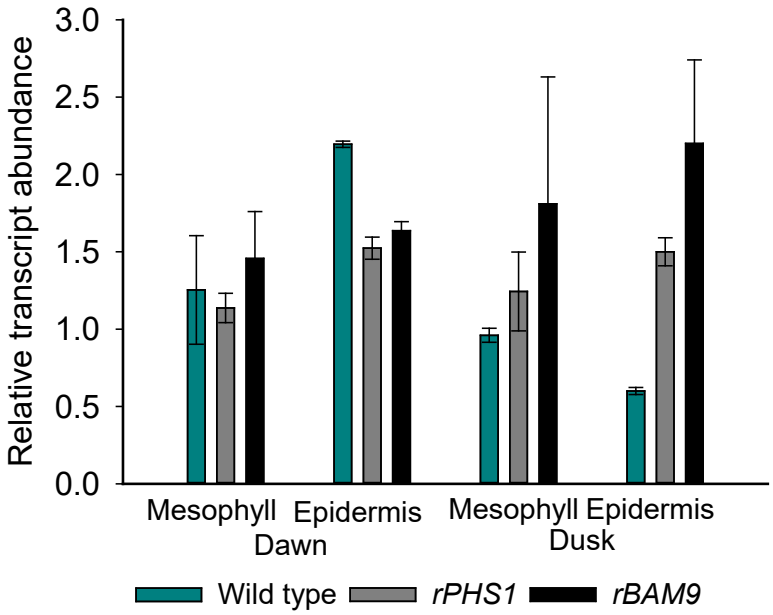

Figure 5. 35. Relative transcript abundance of *stp1* gene in wild type (green), *rPHS1* (grey) and *rBAM9* (black) in mesophyll and guard cell-enriched epidermis at dawn and dusk. Leaf pair 6 was used for this analysis. The error bars represent the standard error of six replicates (3 biological replicates, each with 2 technical replicates). Plant growth conditions were set at 400 µmol CO_2 mol^{-1} air, 25°C/19°C (day/night) and a diurnal photosynthetic photon flux density – PPFD - of 250 µmol $m^{-2}s^{-1}$ at plant height.

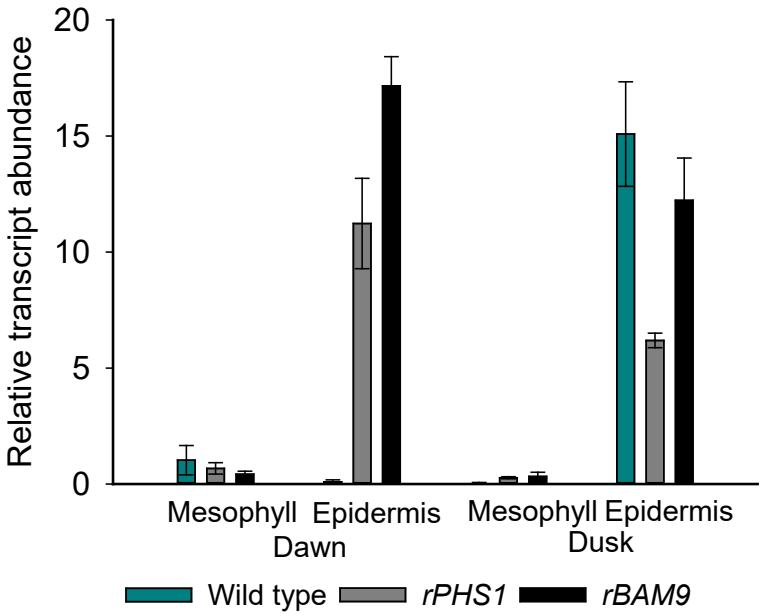

Figure 5. 36. Relative transcript abundance of *abcb14* gene in wild type (green), *rPHS1* (grey) and *rBAM9* (black) in mesophyll and guard cell-enriched epidermis at dawn and dusk. Leaf pair 6 was used for this analysis. The error bars represent the standard error of six replicates (3 biological replicates, each with 2 technical replicates). Plant growth conditions were set at 400 µmol CO_2 mol^{-1} air, 25°C/19°C (day/night) and a diurnal photosynthetic photon flux density – PPFD - of 250 µmol $m^{-2}s^{-1}$ at plant height.

5.4. Discussion

5.5.1. A PHS1-deficient line of Kalanchoë fedtschenkoi is compromised in starch degradation, CAM activity and stomatal regulation

Starch phosphorylase or α-glucan phosphorylase (PHS) is the main enzyme responsible for the phosphorolytic degradation of starch. PHS is responsible for the phosphorolytic cleavage of α-1, 4-glucosidic bonds releasing inorganic phosphate (P_i) and glucose 1-phosphate (Glc1P), which is converted to glucose 6-phosphate (Glc6P) (Zeeman *et al.*, 2004b). Two isoforms of PHS have been identified in different plant species, located in the chloroplast (L-form or PHS1) and cytosol (H-form or PHS2), respectively. The main difference between both isoforms resides in the presence of an extra 80 amino acids domain in PHS1 that increases the affinity to malto-oligosaccharides and amylose molecules, different to PHS2 which possesses a higher affinity to large branched glucans such as glycogen (Satoh *et al.*, 2008). These main differences are evidenced by the higher mobility of the plastidial isoform in Native PAGE, compared to the cytosolic one (Zeeman *et al.*, 2004b).

Based on the protein separations using Native PAGE containing glycogen, two isoforms of PHS were evident in wild type *K. fedtschenkoi* similar to published reports in C_3 plants (Malinova *et al.*, 2014). However, differences between *K. fedtschenkoi* and *A. thaliana* were observed in terms of band separation, reflecting possible changes in protein size, protein charge, amino acids composition and post-translational modifications. The glycogen Native PAGE revealed the absence of both PHS isoforms in the *rPHS1* line, opposite to Ceusters *et al.* (submitted) who detected a prominent abundance of PHS2 in the *K. fedtschenkoi KfPHS1* deficient lines. These main differences could be related with sampling time or changes in transcript abundance that affect the protein concentration, taking into account that the RNAseq interrogation, the homology against *A. thaliana* genome (Chapter 3) and the confirmation of the gene silencing using Real time qPCR concluded that the PHS plastidial isoform was silenced.

The silencing of *phs1* affected starch degradation in *K. fedtschenkoi*, causing the accumulation of starch during the 24 h diel cycle in both mesophyll and guard cells of *rPHS1* lines, compared with wild type. This was accompanied by the accumulation of maltose and glucose in both mesophyll and guard cell-enriched epidermis, as well as a higher transcript abundance of genes implicated in the hydrolytic degradation of starch such as maltose and glucose transporters (*mex1* and *glct*), β-amylases 1 and 3 (*bam1* and *bam3*), α-amylase 3 (*amy3*) and disproportionating enzyme 1 (*dpe1*). Similarly, the Native PAGE containing amylopectin revealed an increased intensity of bands corresponding to β-amylases and disproportionating enzymes in the *rPHS1* compared to wild type. Finally, the expression of genes implicated in the transport of triose phosphate and Glc6P, which are produced by the phosphorolytic degradation of starch, differed between *rPHS1* and wild type. The triose phosphate translocator (*tpt*) and the glucose 6-phosphate transporter 1 (*gpt1*) were highly expressed in wild type mesophyll at the beginning of the day, while in the *rPHS1* line, *tpt* and *gpt1* were more abundant in the guard cell-enriched epidermis at dusk. Conversely, the expression of glucose 6-phosphate transporter 2 (*gpt2*) was not affected by the *phs1* deficiency.

The obtained data lead to hypothesise that *phs1* deficiency causes a re-routing of starch degradation from the phosphorolytic to the hydrolytic pathway generating a C_3-like metabolism and a decrease in CAM activity. This idea is supported by the studies of Neuhaus and Schulte (1996) and Häusler *et al.* (2000) in the halophyte facultative CAM species *M. crystallinum* where sugar content and transcript levels differed between C_3 and CAM-induced plants. The induction of CAM by salinity stress resulted in the phosphorolytic degradation of

starch with an increased activity of chloroplastic α-glucan phosphorylase 1 (PHS1) and α-amylases (AMY) enzymes, and a higher expression of glucose 6-phosphate transporter 1 (*gpt1*) (Häusler *et al.*, 2000); furthermore, the main degradation product was Glc6P and in less amount glucose, dihydroxyacetone phosphate (DHAP) and 3-phosphoglyceric acid (3-PGA) (Neuhaus and Schulte, 1996). On the other hand, C_3-performing *M. crystallinum* degraded starch by a hydrolytic pathway producing mostly maltose and glucose, and in which the enzymatic activity of both PHS1 and AMY were low and the transcript abundance of *gpt* was negligible (Neuhaus and Schulte, 1996; Häusler *et al.*, 2000).

Reports in C_3 plants have suggested that PHS and AMY are not essential in mesophyll starch turnover, while β-amylases and disproportionating enzymes are required for the hydrolytic degradation of starch, generating substrates for the synthesis of sucrose (Thalmann and Santelia, 2017). According to Zeeman *et al.* (2004b), *Arabidopsis* lines deficient in *phs* gene have similar amounts of starch and sugars content than wild type, suggesting that in C_3 plants, PHS main function is to provide hexose phosphates for specific processes inside the chloroplast, regulating the levels of Calvin cycle intermediates and providing substrates for the oxidative pentose phosphate pathway, especially under conditions of stress to control the levels of reactive oxygen species (Smith *et al.*, 2005). Furthermore reports in C_3 indicate that products of the phosphorolytic pathway can be metabolised within the chloroplast or converted to 3-PGA and triose phosphate to be exported to the cytosol via *tpt*, taking into account that *gpt1* is generally not expressed in the chloroplasts of photosynthetic tissue (Zeeman *et al.*, 2004a; Andriotis *et al.*, 2010).

Changes in the content of soluble sugars and malate in both mesophyll and guard cell-enriched epidermis of the *rPHS1* line could be associated with differences in the expression of the plastidial transporters glucose 6-phosphate transporter (*gpt1*) and triose phosphate translocator (*tpt*), affecting nocturnal CO_2 uptake and stomatal conductance. Glc6P and triose phosphates, exported by *gpt1* and *tpt*, respectively, serve as precursors for the nocturnal synthesis of phosphoenolpyruvate (PEP) and thus malate production (Borland *et al.*, 2016). The decrease in malate content during the night period in the mesophyll and the reduced net CO_2 uptake observed in *rPHS1*, suggest the importance of the products derived from the phosphorolytic starch degradation for CAM activity by providing substrates for the nocturnal CO_2 fixation. On the other hand, the similar transcript abundance of *gpt2* between *rPHS1* and wild type suggest that the silencing of *phs1* did not affect the import of Glc6P to the chloroplast for the diurnal synthesis of starch.

Gas exchange data showed that stomatal conductance was affected by the α-glucan phosphorylase 1 (*phs1*) silencing. Whilst nocturnal stomatal opening in *rPHS1* was similar to wild type, stomatal closure during the light period was curtailed. Based on the importance of malate and sugars in regulating guard cell turgor pressure (Santelia and Lawson, 2016), the relative transcript abundances of malate and sugar transporters, *abcb14* and *stp1* respectively, as well as sucrose synthases (*susy*) were determined in both *Kalanchoë* genotypes in order to elucidate the impact of malate and sugars content on the stomatal response of *rPHS1*. Taking into account that sucrose synthases are responsible for the synthesis and degradation of sucrose and that the over expression of *susy3* in C_3 plants increased stomatal conductance (Daloso *et al.*, 2016a), it can be suggested that the accumulation of soluble sugars and the abundance of *susy3* transcript in *rPHS1* allow the nocturnal stomatal opening and prevent the closure during the light period. Likewise, compared with wild type, *abcb14* and *stp1* were highly expressed in the *rPHS1* guard cell-enriched epidermis at dawn and dusk, respectively. This was accompanied by the accumulation of malate and soluble sugars over the 24 h period in the epidermis, suggesting a possible function of these transporters in the import of osmolytes into the guard cells that support the nocturnal opening of stomata and the diurnal curtailed closure in the *rPHS1*. Besides, it can be hypothesised that ABCB14 and STP1 transporters have an important function connecting mesophyll photosynthesis and guard cell metabolism in CAM plants.

The negligible understanding of the phosphorolytic pathway in C_3 guard cells and the results of Zeeman *et al.* (2004b) that showed that α-glucan phosphorylase 1 (*phs1*) deficiency in *A. thaliana* does not affect stomatal conductance, makes it difficult to predict the role of PHS1 in CAM stomata. The results obtained in this study showed that *phs1* silencing generates the production of maltose and accumulation of glucose in guard cell-enriched epidermis, with an increase in the transcript abundance of maltose exporter 1 (*mex1*) and glucose transporter (*glct*). Furthermore, the increased expression of β-amylase 3 (*bam3*) and α-amylase 3 (*amy3*) at the beginning of both periods, suggests a rerouting of starch breakdown to the hydrolytic pathway with a possible osmotic role for maltose, based on the curtailed day-time stomatal closure of *Kalanchoë rPHS1*. However further studies are needed to test this hypothesis, taking into account that starch content in guard cells of the *rPHS1* was also higher than in wild type.

Based on these findings a higher interrogation in CAM research is to elucidate the predominance of the phosphorolytic starch degradation pathway rather than the hydrolytic route. Shameer *et al.* (2018) generated a metabolic model to investigate the energetic costs of

CAM pathways compared with C_3. Regarding starch degradation, they compared the energetic costs of both pathways in CAM and C_3, concluding that the phosphorolytic route in CAM can produce 6-12% more sucrose and amino acids, and starch breakdown is 8.7 fold higher than the hydrolytic pathway which is dominated by the action of β-amylases. Likewise, in the C_3 model, which followed the phosphorolytic degradation pathway, sucrose and amino acids production were only 0.6-1.3% higher than the hydrolytic route. These proposed models could explain that despite the increase in the expression of genes implicated in hydrolytic starch degradation, as well as the accumulation of maltose and glucose in the *rPHS1*, the amount of starch in both mesophyll and guard cells was higher than that noted in wild type.

Finally, the Shameer *et al.* (2018) model indicated that when CAM performed both routes for starch degradation, ATP saving in the phosphorolytic pathway was 14-26%, while in the hydrolytic was only 4-8%, concluding that starch degradation under a phosphorolytic pathway in CAM implies a lower energetic cost for the plant. This could be due to the avoidance of the hexokinase–mediated phosphorylation of the glucose produced to be further used as a glycolysis substrate. Similarly, the synthesis of PEP from Glc6P by the phosphorolytic route, and subsequently the production of malate consumes less energy than if it is produced from maltose or glucose. In this case, the phosphorolytic route results in a net gaining of one ATP molecule at night (Weise *et al.*, 2011).

5.5.2. A BAM9-deficient line of Kalanchoë fedtschenkoi displays contrasting pattern of starch turnover in mesophyll and guard cells, affecting CAM activity and stomatal behaviour

In *Arabidopsis*, BAM9 belongs to a non-catalytically active subfamily of β-amylases together with BAM4, and has been reported to be a key regulatory factor for starch turnover in C_3 plants. The inactivity of both enzymes resides on the absence of different substrates-binding amino acids in the active site, as well as the substitution of Glu-380, one of the catalytic glutamic acid residues (Monroe and Storm, 2018). In *Arabidopsis*, BAM4 Glu-380 is replaced by an arginine, while in BAM9 it is changed to glutamine which abolishes the activity (Fulton *et al.*, 2008). In addition, two regions have been also identified as responsible for the substrate binding and activity on β-amylases, corresponding to the residues 96 to 103 that form a flexible loop and the inner loop located at residues 340-346 (Chandler *et al.*, 2001).

In the case of the BAM9 sequence in *K. fedtschenkoi*, a deletion in the flexible loop was observed, as well as a substitution of Thr-342 to Proline in the inner loop. Reports in *Arabidopsis* and soybean indicated that these changes generate the inability of substrate binding and abolish the interaction with the catalytic Glu-186 and glucose residues, respectively (Kang *et al.*, 2004; Kang *et al.*, 2005). The similarities found in *K. fedtschenkoi* protein sequences suggest a similar regulatory function of BAM9 for starch turnover in CAM plants. Interestingly, the conserved Glu-186 was not substituted in *K. fedtschenkoi* BAM9, suggesting that the catalytic activity of this isoform is not totally abolished or that Glu-186 catalytic role differs between C_3 and CAM β-amylases.

The silencing of *bam9* gene in *K. fedtschenkoi* resulted in altered starch metabolism, characterised by the accumulation in stomatal guard cells and depletion in the mesophyll over the 24 h period in the *rBAM9* line compared with wild type. The starch reduction phenotype of *bam9* mutants has been reported in *A. thaliana* by Steidle (2010), who concluded that BAM9 and BAM3 have a synergistic activity during starch degradation. In that study, *bam9* deficient lines had similar starch content to wild type leaves at the beginning of the light period, while *bam3* and *bam3,9* mutants accumulated more starch, with higher accumulation in the double mutant, concluding that BAM9 is a down regulator of BAM3 in C_3 wild type plants. If this is the case in *K. fedtschenkoi*, we might expect to see a higher expression of *bam3* gene in *rBAM9* line compared with wild type. This response was only observed in the guard cell-enriched epidermis at dawn, and despite the significant difference from wild type, this elevated expression of *bam3* does not appear to be directly linked to the starch excess phenotype observed in the epidermal guard cells. Clearly, more studies are required to generate a reliable conclusion about the synergistic action of β-amylases in *K. fedtschenkoi.*

The gene expression data collected here suggest other possible targets for *bam9* regulation in CAM plants, which could curtail starch synthesis or elevate starch turnover. The latter situation was suggested by the enhanced transcript abundance in the *rBAM9* line of *dpe1* that codes for disproportionating enzyme 1, implicated in hydrolytic starch degradation to produce glucose. The *rBAM9* plants showed an increase in the transcript abundance of *dpe1* at the beginning of the day and higher content of glucose in the mesophyll during the 24 h day/night cycle, potentially as a result of an increase in DPE1 enzyme activity. Similarly, *phs1* transcripts were downregulated in the mesophyll of *rBAM9* lines, accompanied by a slightly accumulation of maltose in this tissue at the end of the day and an increase in the transcript abundance of maltose exporter (*mex1*). Noteworthy, maltose was not detected in the guard cell-enriched epidermis of *rBAM9*, probably as a consequence of the higher expression of

phs1 in the epidermis at the beginning of the day and the similar transcript abundance to wild type at dusk, suggesting that BAM9 regulates other enzymes apart from β-amylases, in both hydrolytic and phosphorolytic degradation pathways. The contrasting starch content between guard cells and mesophyll, as well as the lower transcript abundance of *bam1* and *dpe1* in the guard cell-enriched epidermis of *bam9* RNAi line support this idea. Unfortunately, a lack of evidence about the effects of *bam9* silencing on guard cell starch content in other plant species makes it difficult to conclude if this contrasting starch phenotype between tissues is unique to CAM plants and whether or not it has functional implications for stomatal regulation.

The *bam9* deficiency in *K. fedtschenkoi* also affected CAM activity and diurnal stomatal closure. The reduced starch content in mesophyll over the 24 h day/night cycle could be responsible for the curtailed nocturnal net CO_2 uptake in the *rBAM9* and the lower malate content over the 24 h period in the mesophyll compared to wild type. These results provide further evidence for the importance of starch turnover in mesophyll by providing substrates as PEP for the nocturnal CO_2 fixation in CAM plants (Borland *et al.*, 2016).

In contrast to the depletion of starch in the mesophyll, an over accumulation of starch and malate during the 24 h period was observed in the guard cell-enriched epidermis of *rBAM9*. This phenotype could be related to the finding that day-time stomatal closure was compromised in the *rBAM9* line and the maximal nocturnal stomatal conductance was similar to that in wild type, despite the lower rates of net CO_2 uptake. Higher contents of fructose, glucose and sucrose were detected in both tissues of the *rBAM9* line, together with increased transcript abundance of *susy1* and *susy3* in the guard cell enriched epidermis. This leads to the hypothesis that *bam9* deficiency increases the sucrolytic activity of sucrose synthases, generating sugars implicated in the synthesis of PEP, as compensation for lack of starch degradation. Likewise, the increase of the ATP-binding cassette malate transporter (*abcb14*) expression at dawn and of the sugars transporter 1 (*stp1*) expression at dusk in guard cell-enriched epidermis of the *rBAM9* line could be associated with the import of malate and hexoses from the mesophyll, respectively, acting as osmolytes or ATP producers that trigger the opening of stomata and curtailing closure during the light time.

Based on the data obtained, the specific function of BAM9 in CAM plants is still unknown but the similarities found against *A. thaliana* protein sequences lead to the hypothesis that this enzyme may also work as a regulatory factor in the degradation of starch. The contrasting content of starch and malate in both mesophyll and guard cell-enriched epidermis also suggests that the route of starch turnover differs between tissues. The initial work reported

here with *K. fedtschenkoi bam9* deficient lines, together with the few reports about the function of BAM9 in C_3 plants, indicate that further studies are required to elucidate its role in the degradation of starch and thus in stomatal behaviour.

5.5. Conclusions

- The results obtained showed that *phs1* silencing up-regulates the hydrolytic pathway of starch degradation in both mesophyll and guard cell-enriched epidermis, evidenced by the accumulation of maltose and glucose and increased transcript abundance of genes implicated in the hydrolytic degradation of starch (Figure 5. 37). These results together with further proteomics approaches will contribute with the elucidation of the starch degradation pathways in *Kalanchoë fedtschenkoi.*

- Despite potentially higher hydrolytic activity, starch degradation and CAM activity was curtailed in the *rPHS1* line, indicating that CAM relies predominantly on the phosphorolytic route of starch degradation for production of PEP at night. The decreased activity of phosphorolytic starch degradation also affected stomatal conductance, which increased during the light period, compared to wild type. The obtained data suggest that the higher content of maltose and glucose in the *rPHS1* line provide substrates for guard cell osmolytes or energy production during the light period, which impedes the stomatal closure and generating a C_3-like metabolism.

- The silencing of *bam9* indicates that this enzyme is a key regulatory factor for starch turnover in *K. fedtschenkoi*, evidenced by the altered and opposing impact on starch content in mesophyll and guard cells. The accumulation of starch in guard cells and the depletion in the mesophyll suggested that this enzyme could affect both synthesis and degradation of starch and that these mechanisms differed between tissues. The similarities found in the protein sequence of BAM9 in *K. fedtschenkoi* and *Arabidopsis*, suggest a similar regulatory function of this enzyme for starch turnover in CAM and C_3 plants.

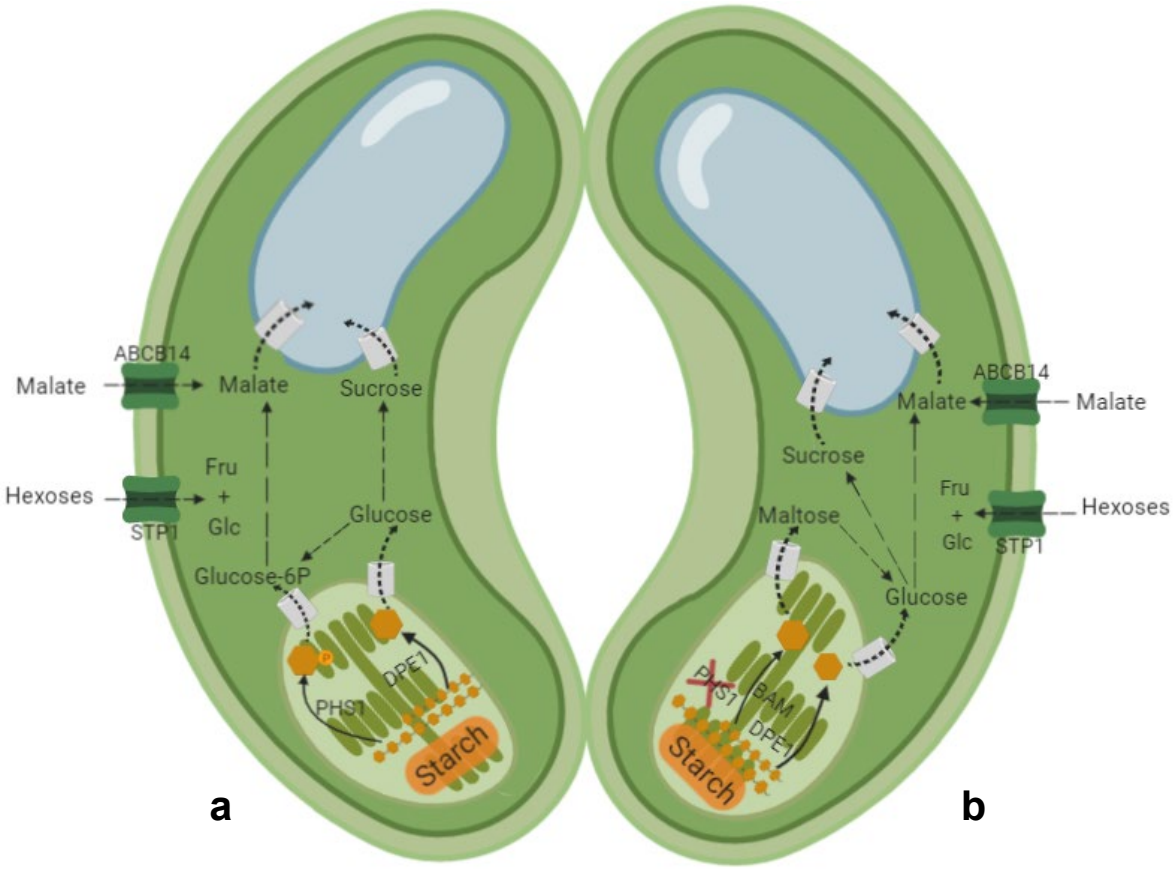

Figure 5. 37. Proposed starch degradation pathway in stomatal guard cells of wild type (a) and *rPHS1* (b) plants of *Kalanchoë fedtschenkoi*. The results obtained in this chapter proposed that starch degradation in CAM guard cells occurs via the phosphorolytic pathway (a) by the action of the enzymes α-glucan phosphorylase (PHS1) and disproportionating enzyme (DPE1) producing glucose 6-phosphate and glucose, respectively, possibly implicated in the synthesis of osmolytes that allow the opening of stomata. The silencing of the PHS1 enzyme (b) led to the activation of the hydrolytic starch degradation pathway, evidenced by the increased transcript abundance of β-amylases (BAM) and the production of maltose, as well as a higher expression of disproportionating enzyme (DPE1) gene accompanied by a higher content of glucose.

Chapter 6. Comparative proteomic analysis of the mesophyll and epidermis of *Kalanchoë fedtschenkoi*

6.1. Introduction

Crassulacean acid metabolism is defined by the temporal turnover of malate as a result of the nocturnal CO_2 fixation and subsequent diurnal decarboxylation that produces phosphoenolpyruvate (PEP) and carbohydrates. Diel regulation of key enzymatic activities by the circadian clock and regulatory metabolites are thought to be responsible for this temporal control of CAM (Borland and Taybi, 2004; Boxall *et al.*, 2005). This is evidenced by the nocturnal activation of PEPC by phosphorylation which reduces the allosteric inhibition of malate, allowing its activity and the accumulation of malate in the vacuole (Boxall *et al.*, 2017). Likewise, changes in internal CO_2 concentration, metabolite control and humidity are thought to be responsible for the unique stomatal rhythm in CAM (i.e. nocturnal opening and closure during the day) that leads to water conservation and thus an increased water use efficiency compared to C_3 and C_4 plants (Males and Griffiths, 2017). The recent transcriptomic data available for different CAM species such as *Mesembryanthemum crystallinum, Ananas comosus*, *Agave tequilana*, *Kalanchoë laxiflora* and *Kalanchoë fedtschenkoi* (Cushman *et al.*, 2008b; Zhang *et al.*, 2014; Abraham *et al.*, 2016; Boxall *et al.*, 2017; Boxall *et al.*, 2019; Heyduk *et al.*, 2019) among others, has allowed the identification of the major genetic factors that define CAM. Recently, Abraham *et al.* (2016) integrated the transcriptomics, proteomics and metabolomics of *Agave tequilana,* evidencing a rescheduling of genes and proteins responsible for nocturnal carboxylation and stomatal behaviour compared to *Arabidopsis thaliana,* as well as changes in the diel turnover of malic acid, sucrose, NADPH and $NADP^+$. These major differences demonstrate that temporal changes in gene expression and protein abundance were required during CAM evolution.

Despite the biochemical, genetic and proteomic resources that reveal the main genes, enzymes and metabolic profiles unique to CAM, knowledge about guard cell metabolism in CAM plants is still lacking. Guard cell metabolism has been studied mainly in C_3 plants where activation of plasma membrane H^+-ATPase by blue light triggers the pumping of protons outside the cell and allows the influx of potassium. Concomitantly, starch degrading products, malate and sucrose, become the main K^+ counter ions contributing to the increase of turgor pressure and opening of C_3 stomata (Santelia and Lunn, 2017). In *Arabidopsis*, guard cell starch is broken down at the start of the day, whilst starch in the mesophyll accumulates

at the start of the day. The different diel patterns of starch turnover in C_3 guard cells and mesophyll are accompanied by different enzymatic routes for starch degradation in these different cell types. The hydrolytic enzymes, BAM1 and AMY3 are the main enzymes for starch degradation in the C_3 guard cells while BAM3 is the responsible for mesophyll starch degradation (Horrer *et al.*, 2016). In contrast to reports for C_3, the data obtained from the present study showed a diel reprogramming of starch turnover in *Kalanchoë* guard cells, with an increase in starch content during the light period and a diminution in starch at the beginning of the night (Chapter 3). This nocturnal breakdown is probably catalysed by the enzyme α-glucan phosphorylase (PHS) via the phosphorolytic pathway, the main starch degradation route in CAM mesophyll, responsible for the Glc6P synthesis to sustain nocturnal CO_2 assimilation (Borland *et al.*, 2016).

The differences in starch turnover between mesophyll and guard cells in C_3 plants suggest independent control of the proteins that underpin guard cell metabolism/stomatal behaviour as well as mesophyll metabolism (Simon *et al.*, 2019). In CAM plants, it is still unknown if guard cell metabolism is dependent on mesophyll control, although Males and Griffiths (2017) suggest that the response to C_i is probably the main factor regulating stomatal behaviour, based on the correlation between the four phases of CAM and stomatal conductance over the 24 h diel cycle. In this case, malate has been proposed as the connection between both tissues, its nocturnal accumulation by CO_2 fixation and its transport from mesophyll to guard cells could contribute to stomatal opening. Likewise, the diurnal increased of C_i concentration due to malate decarboxylation could trigger stomatal closure (Males and Griffiths, 2017). However, the extent to which malate is synthesized and broken down directly by the CAM guard cells *per se* is not known.

The contrasting pattern of diel starch turnover found in guard cells of *K. fedtschenkoi* compared to *Arabidopsis* might represent a starting point to investigate if the inverted stomatal rhythm in CAM is exclusively to guard cell metabolism or due to signals that emanate from the mesophyll. The development of a proteome dataset that compares protein abundances between mesophyll and guard cell-enriched epidermis over a 24 h diel cycle will contribute to the identification of differences in protein composition and function and the interconnection of metabolism in both tissues. Specifically, this chapter aims to identify differences in abundance and temporal turnover between mesophyll and epidermis of proteins implicated in CAM carboxylation/decarboxylation and starch and sugar metabolism in wild type plants of *Kalanchoë fedtschenkoi*. The following hypotheses are proposed:

Hypothesis 1: The differential abundance of key metabolic proteins between mesophyll and guard cell-enriched epidermis provide evidence for functional independence of both tissues.

Hypothesis 2: Proteins responsible for starch and sugar metabolism show temporal re-programming of diel abundances in CAM in order to allow nocturnal CO_2 fixation and the opening of stomata.

6.2. Sampling and methods

Wild type plants of *Kalanchoë fedtschenkoi* were selected for the development of the proteome datasets. Following the growth conditions described in Section 2.1 (Chapter 2), the sampling was performed over a 24 h day/night cycle at 8:00, 12:00, 16:00, 20:00, 00:00 and 4:00 (taking into account that lights came on at 8:30 and went off at 20:30). Mesophyll and epidermis tissue were collected independently, using three biological replicates for each time point, as described in Section 2.1, In this case, the epidermis tissue of both abaxial and adaxial leaf surfaces was harvested together to ensure a higher amount of tissue required for the proteomics analyses. All samples were stored at -80^{o} C before being packaged into a dry shipper (-150^{o} C) and sent to the Oak Ridge National Laboratory, TN, USA for subsequent processing.

To confirm the absence of cross contamination from the mesophyll, the epidermis tissue was stained with Lugol's iodine solution as described in Section 2.2 (Chapter 2), in order to detect possible contamination from starch containing-chloroplasts from the mesophyll. Additionally, the presence and distribution of chloroplasts and mitochondria within cell types in the epidermis was investigated using confocal microscopy and the use of mitochondrial staining. Following the protocol of Schoor *et al.* (2015), the epidermis peels were incubated in 0.1M HEPES buffer pH 7 for 5 min, followed by mitochondrial staining with 10µg ml^{-1} of Rhodamine123 (Sigma catalogue number R8004) in the dark at room temperature for 30 min. Next, the peels were washed with two changes of 0.1M HEPES buffer pH 7 for 10 min and were transferred to microscope slides to be observed on a LEICA SP8 STED 3X microscope on an excitation λ of 511nm. The identification of chloroplasts was performed based on the auto florescence of chlorophyll at an excitation λ of 598nm.

The extraction, identification and annotation of proteins were conducted by Dr Paul Abraham in Oak Ridge National Laboratory (USA), (Abraham *et al.*, submitted). As

described in Abraham *et al.* (2012), the samples were analysed on an Exactive Plus mass spectrometer (Thermo Fischer Scientific) coupled with a with a Proxeon EASY-nLC 1200 liquid chromatography (LC) pump (Thermo Fisher Scientific).

The obtained data were aligned against the *Kalanchoë fedtschenkoi* v1.1 proteome FASTA database (DOE-JGI, http://phytozome.jgi.doe.gov/) (Yang *et al.*, 2017), filtered to remove the low abundant proteins and categorised based on a Student's t-test significance threshold requiring a p-value ≤0.05 and absolute value of log2 fold-change difference ≥ 1 between the epidermis peel and mesophyll proteomes (Abraham *et al.*, submitted). The identified proteins were clustered based on a sequence similarity of > 90% and annotated using Blast2GO (Conesa *et al.*, 2005) with a BLASTP e-value hit filter of 1×10^{-5}, an annotation cut-off value of 55 and a GO weight of 5. Finally, a student's t-test (p ≤0.05) were conducted to determine the significant differences on protein abundance between both tissues (Abraham *et al.*, submitted).

6.3. Results

Guard cell-enriched epidermis and ground leaf mesophyll of *Kalanchoë fedtschenkoi* were sampled independently in order to obtain the first differential proteome datasets in CAM that allowed the characterisation of tissue-specific proteins. Abraham *et al.* (submitted) identified 9,102 proteins that were grouped based on a sequence similarity of > 90%, taking into account the higher protein sequences redundancy as a result of genome duplication, alternative splicing and protein families. The sequences similarities led to the overall identification of 8,585 proteins, including 5,002 proteins and 2,718 protein groups per epidermis peel sample and an average of 3,583 proteins and 1,973 protein groups identified per mesophyll sample. A higher diversity of proteins was detected in the epidermis compared to the mesophyll, while 60% of proteins were shared between both tissues. Multivariate partial least squares analyses found a clear distinction between proteins identified in the epidermis and mesophyll, indicating that the epidermis and mesophyll have unique proteomes. Likewise, lugol-staining for starch in the epidermis showed starch confined to the guard cells of the epidermis and negligible contamination from mesophyll starch-containing chloroplasts (Figure 6. 1).

Fluorescent staining with rhodamine123 of the epidermis showed the presence of mitochondria and chloroplasts confined to the stomata. In the case of mitochondria, these organelles were located in both subsidiary and guard cells, while chloroplasts were located

mainly in the guard cells. In contrast, neither mitochondria nor chloroplasts were detected in the epidermal pavement cells, suggesting that most of the proteins implicated in carbon and energy metabolism found in the epidermis tissue are associated with the stomatal complex (Figure 6. 2).

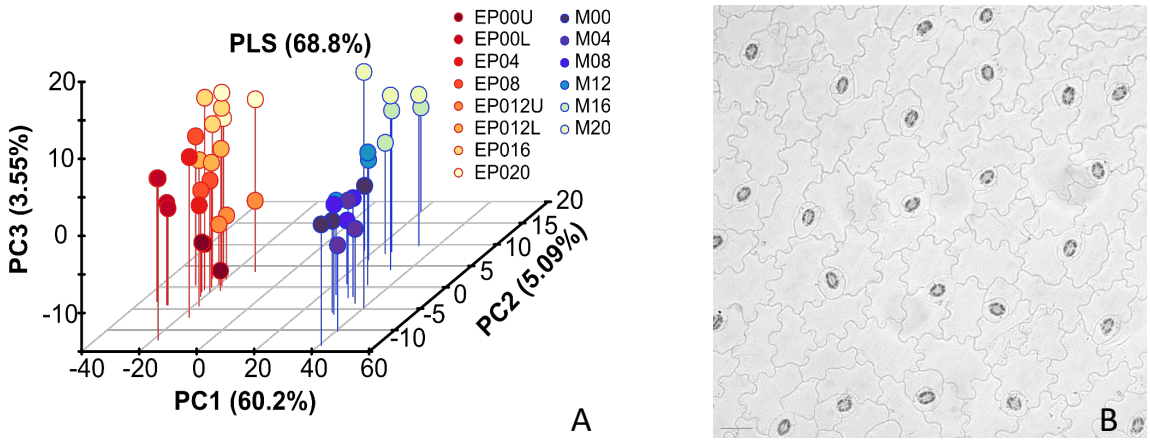

Figure 6. 1. (A) Partial least square (PLS) analysis shows the distinctive proteomes identified in both mesophyll (M) and guard cell-enriched epidermis (EP) sampled at 4 h intervals over a diel cycle. The principal components showed the grouping between biological replicates of both tissues and the separation by time of sampling. For two time points (12 and 00), upper and lower surface of the epidermis were collected separately. (B) Iodine staining of epidermis shows that starch granules are unique to the guard cells and indicate the negligible contamination from mesophyll chloroplasts. The epidermis tissue was harvested from leaf pair 6 during the first hours of the light period. The scale bar corresponded to 50 µm (Abraham *et al.*, submitted).

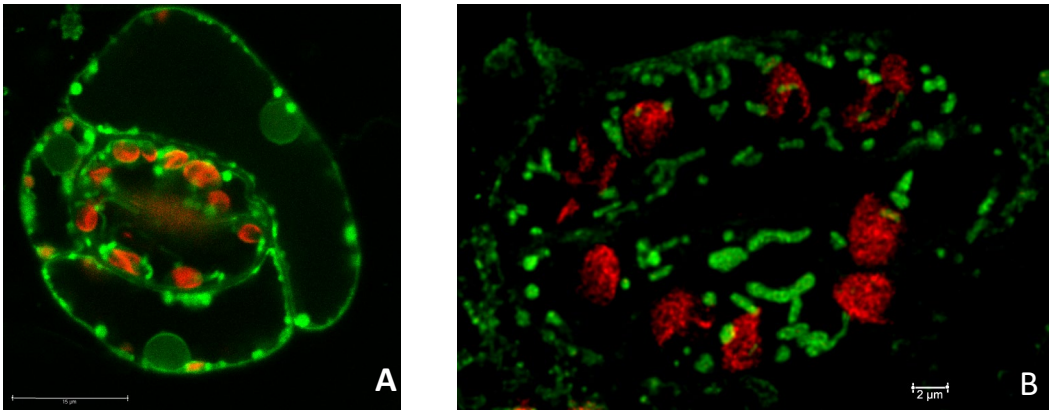

Figure 6. 2. Confocal microscopy of *K. fedtschenkoi* epidermis with Rhodamine123. Mitochondria are present in both guard cells and subsidiary cells (green colouring) while auto florescence of chlorophyll is evidence of chloroplast localisation in guard cells (red colouring). The epidermis tissue was sampled from leaf pair 6 during the first hour of the light period. The scale bars corresponded to (A) 15 µm (showing two guard cells surrounded by three subsidiary cells) and (B) 2 µm (showing two guard cells).

Across the protein dataset provided by Abraham *et al.* (submitted) from mesophyll and guard cell-enriched epidermis, proteins implicated in CAM carbon metabolism, stomatal regulation, starch synthesis and degradation, and sugar metabolism were selected to be analysed in this chapter. Overall, from the 96 proteins analysed under these categories, significant differences ($p \leq 0.05$) between mesophyll and guard cell-enriched epidermis were detected. In some cases, the same protein was found several times either in the same group or in a different group, probably as a result of multigene families that encode different isoforms (Table 6. 1).

Table 6. 1. Proteins interrogated from the proteome dataset derived from mesophyll and guard cell-enriched epidermis of *Kalanchoë fedtschenkoi* (Abraham *et al.*, submitted). Annotation, protein ID based on the genome published on Phytozome and *Arabidopsis thaliana* orthologues, the 24 h average abundance in both tissues and the significant differences ($p \leq 0.05$) based on T-test are provided.

Category	Annotation	Protein group	*K. fedtschenkoi* protein code	*A. thaliana* protein code	Epidermis abundance (24 h)	Mesophyll abundance (24 h)	T-test Epidermis vs Mesophyll
CAM carboxylation /decarboxylation	Phosphoenolpyruvate carboxylase (PEPC) cytosolic	1236	Kaladp0011s0355.1.p	AT1G53310.3	32.577 (±0.286)	32.658 (±0.62)	
	Phosphoenolpyruvate carboxylase (PEPC) cytosolic	1236	Kaladp0011s0355.2.p	AT1G53310.3	32.639 (±0.3)	32.751 (±0.62)	
	Phosphoenolpyruvate carboxylase 2 (PEPC2) cytosolic	1191	Kaladp0011s1355.1.p	AT3G14940.1	32.8 (±0.214)	32.904 (±0.466)	
	Phosphoenolpyruvate carboxylase 2 (PEPC2) cytosolic	1191	Kaladp0011s1355.4.p	AT3G14940.1	32.8 (±0.214)	32.904 (±0.466)	
	Phosphoenolpyruvate carboxylase 2 (PEPC2) cytosolic	1205	Kaladp0095s0055.1.p	AT3G14940.1	34.131 (±0.136)	34.735 (±0.284)	* M
	β-carbonic anhydrase 1 chloroplastic (BCA1)	12556	Kaladp0538s0011.1.p	AT3G01500.2	32.444 (±0.241)	32.552 (±0.205)	
	β-carbonic anhydrase 3 chloroplastic (BCA3)	24472	Kaladp0034s0051.1.p	AT1G23730.1	32.859 (±0.269)	33.459 (±0.3)	* M
	NAD+ malate dehydrogenase (NAD+ MDH) cytosolic	9253	Kaladp0101s0012.1.p	AT5G58330.1	30.558 (±0.146)	32.107 (±0.117)	* M
	NAD+ malate dehydrogenase (NAD+ MDH) cytosolic	10684	Kaladp0093s0088.1.p	AT1G04410.1	11.999 (±8.527)	19.544 (±8.884)	
	NAD+ malate dehydrogenase (NAD+ MDH) cytosolic	13020	Kaladp0095s0052.1.p	AT1G53240.1	32.703 (±0.192)	33.037 (±0.342)	
	NAD+ malate dehydrogenase (NAD+ MDH) cytosolic	13020	Kaladp0101s0211.1.p	AT1G53240.1	32.634 (±0.237)	32.915 (±0.344)	
	NAD+ malate dehydrogenase (NAD+ MDH) cytosolic	13421	Kaladp0082s0194.1.p	AT1G04410.1	34.166 (±0.132)	34.94 (±0.144)	* M
	NAD+ malate dehydrogenase (NAD+ MDH) cytosolic	13421	Kaladp1038s0012.1.p	AT1G04410.1	33.675 (±0.17)	34.475 (±0.13)	* M
	NAD+ malate dehydrogenase (NAD+ MDH) cytosolic	13421	Kaladp1038s0012.2.p	AT1G04410.1	33.675 (±0.17)	34.475 (±0.13)	* M
	NADH dehydrogenase mitochondrial	19078	Kaladp0011s0650.1.p	AT5G11770.1	25.379 (±1.454)	10.7 (±6.233)	* E
	NADH dehydrogenase mitochondrial	19078	Kaladp0102s0137.1.p	AT5G11770.1	25.379 (±1.454)	10.7 (±6.233)	* E
	NADH dehydrogenase mitochondrial	19078	Kaladp0662s0004.1.p	AT5G11770.1	25.379 (±1.454)	10.7 (±6.233)	* E
	NADH dehydrogenase mitochondrial	21326	Kaladp0517s0001.1.p	AT5G52840.1	30.573 (±0.371)	31.471 (±0.11)	* M
	NADP-dependent malic enzyme (NADP-ME) cytosolic /chloroplastic	4789	Kaladp0024s0016.2.p	AT5G25880.1	32.201 (±0.146)	30.31 (±0.223)	* E
	NADP-dependent malic enzyme (NADP-ME) cytosolic /chloroplastic	4789	Kaladp0024s0016.3.p	AT5G25880.1	32.201 (±0.146)	30.31 (±0.223)	* E
	NADP-dependent malic enzyme (NADP-ME) cytosolic /chloroplastic	4789	Kaladp0024s0016.4.p	AT5G25880.1	32.264 (±0.146)	30.375 (±0.223)	* E
	NADP-dependent malic enzyme (NADP-ME) cytosolic /chloroplastic	4789	Kaladp0102s0114.1.p	AT5G25880.1	33.077 (±0.096)	30.906 (±0.169)	* E
	NADP-dependent malic enzyme (NADP-ME) cytosolic /chloroplastic	4789	Kaladp0102s0114.2.p	AT5G25880.1	33.135 (±0.096)	30.962 (±0.17)	* E

Category	Annotation	Protein group	*K. fedtschenkoi* protein code	*A. thaliana* protein code	Epidermis abundance (24 h)	Mesophyll abundance (24 h)	T-test Epidermis vs Mesophyll
	NADP-dependent malic enzyme (NADP-ME) cytosolic /chloroplastic	9999	Kaladp0048s0189.1.p	AT3G47520.1	31.407 (±0.171)	31.780 (±0.16)	* M
	NADP-dependent malic enzyme (NADP-ME) cytosolic /chloroplastic	9999	Kaladp0048s0189.2.p	AT3G47520.1	31.407 (±0.171)	31.780 (±0.16)	* M
	NADP-dependent malic enzyme (NADP-ME) cytosolic /chloroplastic	10021	Kaladp0095s0564.1.p	AT3G47520.1	31.545 (±0.156)	31.890 (±0.152)	* M
	NADP-dependent malic enzyme (NADP-ME) cytosolic /chloroplastic	10021	Kaladp0095s0564.2.p	AT3G47520.1	31.545 (±0.156)	31.890 (±0.152)	* M
	NADP-dependent malic enzyme (NADP-ME) cytosolic /chloroplastic	10743	Kaladp0058s0569.1.p	AT3G47520.1	31.789 (±0.19)	32.726 (±0.166)	* M
Stomatal metabolism	Open Stomata 1 (OST1)	12333	Kaladp0016s0289.1.p	AT4G33950.1	27.005 (±2.158)	6 (±4.899)	* E
	Open Stomata 1 (OST1)	12333	Kaladp0016s0289.2.p	AT4G33950.2	8.824 (±3.261)	0 (±0)	* E
	Open Stomata 1 (OST1)	13033	Kaladp0808s0028.1.p	AT4G33950.1	23.503 (±4.747)	1.515 (±1.237)	* E
	Open Stomata 1 (OST1)	13227	Kaladp0049s0026.2.p	AT4G33950.2	28.857 (±0.44)	0 (±0)	* E
	Plasma membrane ATPase 1 (PMA1)	1265	Kaladp0098s0188.1.p	AT4G30190.1	30.29 (±0.123)	27.656 (±0.455)	* E
	Plasma membrane ATPase 4 (PMA4)	1265	Kaladp0001s0196.1.p	AT4G30190.1	30.16 (±0.131)	27.492 (±0.435)	* E
	Plasma membrane ATPase 4 (PMA4)	1266	Kaladp0001s0322.1.p	AT4G30190.1	30.126 (±0.131)	27.103 (±0.464)	* E
	Plasma membrane ATPase 4 (PMA4)	1266	Kaladp0037s0068.1.p	AT4G30190.1	30.15 (±0.133)	27.145 (±0.454)	* E
	Plasma membrane ATPase 8 (PMA8)	1319	Kaladp0005s0009.1.p	AT3G42640.1	30.068 (±0.139)	27.149 (±0.34)	* E
Starch synthesis	ADP glucose pyrophosphorylase small subunit (APS1)	6520	Kaladp0610s0014.1.p	AT5G48300.1	31.845 (±0.174)	32.635 (±0.19)	* M
	α-1, 4-glucan- synthase (ADP-forming)	12149	Kaladp0071s0048.1.p	AT5G15650.1	29.43 (±0.194)	27.55 (±0.309)	* E
	Phosphoglucose isomerase (PGI)	4369	Kaladp0095s0394.1.p	AT4G24620.1	29.92 (±0.176)	29.869 (±0.431)	
	Phosphoglucose isomerase (PGI)	4522	Kaladp0089s0069.1.p	AT4G24620.1	31.171 (±0.141)	32.799 (±0.142)	* M
	Phosphoglucomutase (PGM)	4475	Kaladp0101s0022.1.p	AT5G17530.3	27.327 (±0.335)	14.68 (±3.74)	* E
	Phosphoglucomutase (PGM)	4475	Kaladp0101s0022.2.p	AT5G17530.3	27.51 (±0.332)	14.84 (±3.784)	* E
	Phosphoglucomutase 1 (PGM1)	4153	Kaladp0008s0557.1.p	AT5G51820.1	30.2 (±0.219)	32.049 (±0.129)	* M
	Phosphoglucomutase 2 (PGM2)	5069	Kaladp0059s0263.1.p	AT1G70730.3	31.522 (±0.132)	30.854 (±0.143)	* E
	ADP-glucose synthase (AGPase)	6726	Kaladp0427s0014.1.p	AT5G19220.1	28.97 (±0.297)	27.68 (±1.93)	
	ADP-glucose synthase (AGPase)	16283	Kaladp0024s0618.2.p	AT4G39210.1	23.461 (±3.485)	26.47 (±2.059)	
	ADP glucose pyrophosphorylase (AGPase, APL2)	6237	Kaladp0099s0052.1.p	AT1G27680.1	18.645 (±7.905)	12.301 (±7.726)	
	ADP glucose pyrophosphorylase (AGPase, APL4)	6402	Kaladp0015s0180.1.p	AT2G21590.2	30.144 (±0.415)	30.706 (±0.293)	* M
	Starch branching enzyme 1 (SBE1)	9927	Kaladp0911s0001.1.p	AT5G03650.1	26.162 (±1.506)	19.829 (±1.44)	* E

Category	Annotation	Protein group	*K. fedtschenkoi* protein code	*A. thaliana* protein code	Epidermis abundance (24 h)	Mesophyll abundance (24 h)	T-test Epidermis vs Mesophyll
	Starch branching enzyme 2 (SBE2)	9932	Kaladp0011s0279.1.p	AT5G03650.1	24.181 (±3.325)	24.174 (±3.302)	
	Starch synthase (SSI - SSIV)	3899	Kaladp0055s0317.1.p	AT5G24300.2	25.592 (±1.55)	28.645 (±0.266)	* M
	Starch synthase 2 (SSI - SSIV)	2518	Kaladp0011s0184.1.p	AT3G01180.1	26.666 (±0.376)	27.022 (±0.374)	
	Granule-bound starch synthase I (GBSS-I)	4498	Kaladp0067s0211.1.p	AT1G32900.1	25.567 (±1.483)	29.215 (±0.29)	
Starch degradation	Phosphoglucan phosphatase amyloplastic (SEX4, DSP4)	15416	Kaladp0011s0575.1.p	AT3G52180.2	28.874 (±0.291)	29.605 (±0.133)	* M
	Glucan water dikinase 1 (GWD1, SEX1)	198	Kaladp0087s0025.1.p	AT1G10760.1	28.271 (±0.296)	27.813 (±0.56)	
	Glucan water dikinase 3 (PWD)	620	Kaladp0045s0118.1.p	AT5G26570.1	26.956 (±0.298)	27.826 (±0.245)	* M
	α-amylase 1 (AMY1)	5551	Kaladp0018s0080.1.p	AT4G25000.1	28.599 (±0.169)	27.847 (±0.205)	* E
	α-amylase 3 (AMY3)	1199	Kaladp0014s0003.1.p	AT1G69830.1	26.861 (±0.193)	27.433 (±0.275)	
	α-amylase 3 (AMY3)	1199	Kaladp0014s0003.2.p	AT1G69830.1	26.861 (±0.193)	27.433 (±0.275)	
	α-amylase 3 (AMY3)	1199	Kaladp0014s0003.3.p	AT1G69830.1	26.861 (±0.193)	27.433 (±0.275)	
	α-amylase 3 (AMY3)	1199	Kaladp0014s0003.4.p	AT1G69830.1	26.861 (±0.193)	27.433 (±0.275)	
	α-amylase 3 (AMY3)	1199	Kaladp0014s0003.5.p	AT1G69830.1	26.861 (±0.193)	27.433 (±0.275)	
	α-amylase 3 (AMY3)	1199	Kaladp0014s0003.6.p	AT1G69830.1	26.861 (±0.193)	27.433 (±0.275)	
	α-amylase 3 (AMY3)	1199	Kaladp0014s0003.7.p	AT1G69830.1	26.861 (±0.193)	27.433 (±0.275)	
	α-amylase 3 (AMY3)	1199	Kaladp0014s0003.8.p	AT1G69830.1	26.861 (±0.193)	27.433 (±0.275)	
	β-amylase 2 (BAM2)	5952	Kaladp1295s0027.2.p	AT4G00490.1	26.378 (±0.251)	0 (±0)	* E
	β-amylase 9 (BAM9)	6035	Kaladp0062s0212.1.p	AT5G18670.1	8.705 (±3.875)	14.817 (±0.151)	
	β-amylase 9 (BAM9)	6169	Kaladp0076s0255.1.p	AT5G18670.1	8.347 (±1.785)	12.245 (±1.231)	
	β-amylase 9 (BAM9)	6169	Kaladp0076s0256.1.p	AT5G18670.1	10.579 (±1.225)	10.843 (±1.236)	
	β-amylase 9 (BAM9)	19511	Kaladp1203s0004.1.p	AT5G18670.1	7.189 (±1.888)	11.033 (±2.575)	
	Disproportionating enzyme 1 (DPE1)	5063	Kaladp0095s0103.1.p	AT5G64860.1	28.822 (±0.209)	30.39 (±0.188)	* M
	Disproportionating enzyme 1 (DPE1)	5063	Kaladp0095s0103.2.p	AT5G64860.1	29.207 (±0.215)	30.801 (±0.164)	* M
	Disproportionating enzyme 2 (DPE2)	1182	Kaladp0067s0137.1.p	AT2G40840.1	27.589 (±0.281)	19.53 (±3.804)	* E
	α-glucan phosphorylase 1 (PHS1)	1186	Kaladp0024s0136.1.p	AT3G29320.1	32.026 (±0.154)	32.496 (±0.296)	* M
	α-glucan phosphorylase 2 (PHS2)	1870	Kaladp0053s0423.1.p	AT3G46970.1	27.751 (±0.238)	24.392 (±1.514)	* E
	α-glucan phosphorylase 2 (PHS2)	1870	Kaladp0053s0423.2.p	AT3G46970.1	27.906 (±0.237)	24.556 (±1.519)	* E

Category	Annotation	Protein group	*K. fedtschenkoi* protein code	*A. thaliana* protein code	Epidermis abundance (24 h)	Mesophyll abundance (24 h)	T-test Epidermis vs Mesophyll
Sugars metabolism	Hexokinase (HXK)	7204	Kaladp0022s0170.1.p	AT4G29130.1	29.569 (±0.125)	27.434 (±0.258)	* E
	Phosphofructokinase (PFK)	5325	Kaladp0060s0401.1.p	AT1G12000.1	27.776 (±0.181)	0 (±0)	* E
	Phosphofructokinase (PFK)	5417	Kaladp0040s0319.1.p	AT1G12000.1	15.924 (±4.973)	0 (±0)	* E
	Phosphofructokinase (PFK)	5417	Kaladp0040s0323.1.p	AT1G12000.1	16.751 (±4.416)	0 (±0)	* E
	Phosphofructokinase (PFK)	5417	Kaladp0068s0218.1.p	AT1G12000.1	24.299 (±2.669)	0 (±0)	* E
	Phosphofructokinase (PFK)	5417	Kaladp0068s0218.2.p	AT1G12000.1	24.302 (±2.67)	0 (±0)	* E
	Phosphofructokinase (PFK)	5417	Kaladp0068s0218.3.p	AT1G12000.1	22.691 (±3.836)	0 (±0)	* E
	Pyruvate carboxylase (PC)	15558	Kaladp0003s0030.1.p	AT3G56130.1	26.941 (±1.091)	26.831 (±0.465)	
	Pyruvate carboxylase (PC)	16326	Kaladp0064s0159.1.p	AT3G56130.1	23.215 (±2.717)	0 (±0)	* E
	Pyruvate kinase (PK)	6435	Kaladp0046s0187.1.p	AT2G36580.1	27.003 (±1.487)	4.611 (±3.765)	* E
	Pyruvate kinase (PK)	6435	Kaladp0046s0187.2.p	AT2G36580.1	27.055 (±1.49)	4.621 (±3.773)	* E
	Sedoheptulose bisphosphatase (SBPase)	10526	Kaladp0045s0221.1.p	AT3G55800.1	31.836 (±0.146)	33.75 (±0.095)	* M
	Sedoheptulose bisphosphatase (SBPase)	10526	Kaladp0024s0355.1.p	AT3G55800.1	31.167 (±0.142)	33.029 (±0.11)	* M
	Sedoheptulose bisphosphatase (SBPase)	10526	Kaladp0024s0355.2.p	AT3G55800.1	31.575 (±0.138)	33.454 (±0.117)	* M
	Sucrose-phosphatase 1 (SPP1)	9680	Kaladp0091s0029.1.p	AT2G35840.3	27.489 (±0.963)	26.729 (±1.601)	* E
	Sucrose-phosphatase 1 (SPP1)	9680	Kaladp0091s0029.2.p	AT2G35840.3	27.489 (±0.963)	26.729 (±1.601)	* E
	Sucrose-phosphatase 1 (SPP1)	9680	Kaladp0091s0029.3.p	AT2G35840.3	27.495 (±0.963)	26.736 (±1.602)	* E
	Sucrose-phosphatase 1 (SPP1)	9680	Kaladp0091s0029.4.p	AT2G35840.3	27.495 (±0.963)	26.736 (±1.602)	* E
	Transketolase (TK) chloroplastic	2733	Kaladp0096s0045.1.p	AT2G45290.1	31.623 (±0.124)	32.189 (±0.126)	* M

6.3.1. CAM-related proteins

Regarding CAM, proteins implicated in carboxylation and decarboxylation processes were identified. The first step in the nocturnal carboxylation is the conversion of ambient CO_2 to HCO_3^-, catalysed by the enzyme β-carbonic anhydrase (CA). Two carbonic anhydrases were identified, βCA1 and βCA3. βCA1 abundance increased in the middle of both time periods, with no differences between mesophyll and epidermis while βCA3 abundance was similar over the 24 h period and higher in the mesophyll. Phosphoenolpyruvate carboxylase 1 and 2 (PEPC1 and PEPC2), the main enzymes implicated in the nocturnal CO_2 fixation in CAM plants, by the carboxylation of phosphoenolpyruvate (PEP) were detected in both mesophyll and epidermis. No differences in the abundance of PEPC between mesophyll and guard cell-enriched epidermis were detected, in both tissues the diel abundance was higher in the light period and decreased at night. Three isoforms of PEPC2 were identified in two different protein groups. The isoforms encoded by Kaladp0011s1355.1.p and Kaladp0011s1355.4.p were both found in the 1191 group and no differences between mesophyll and epidermis were detected, while PEPC2 encoded by Kaladp0095s0055.1.p and found in protein group 1205 was significantly ($p \leq 0.05$) more abundant in the mesophyll (Figure 6. 3).

The cytosolic synthesis of malate from oxaloacetate during nocturnal CO_2 fixation is catalysed by NAD^+ malate dehydrogenase (NAD^+ MDH). Seven NAD^+ MDH isoforms were identified, belonging to four protein groups. Interestingly, the 24 h diel pattern between mesophyll and epidermis was similar for all the isoforms, suggesting that OAA produced via PEPC is converted to malate during the night period in both the mesophyll and epidermis. Significant differences between epidermis and mesophyll were found for the NAD^+ MDH belonging to groups 9523 (encoded by Kaladp0101s0012.1.9) and 13421 (encoded by Kaladp0082s0194.1.p, Kaladp1038s0012.1.9 and Kaladp1038s0012.2.p); in both cases, the abundances were higher in the mesophyll tissue (Figure 6. 3).

The diurnal decarboxylation of malate can be catalysed by NAD-malic enzyme (NAD-ME), NADP malic enzyme (NADP-ME) or phosphoenolpyruvate carboxykinase (PEPCK). The mitochondrial NAD-malic enzyme (NAD-ME) and the cytosolic/chloroplastic NADP-malic enzyme (NADP-ME) were identified in the *K. fedtschenkoi* protein dataset. Several isoforms of the cytosolic/chloroplastic NADP-ME were found in four protein groups (Table 6. 1), with diel changes characterised by an increased abundance in the middle of the day and a decreased abundance during the first hours of the night. Significant differences ($p \leq 0.05$) between mesophyll and epidermis were found for the isoforms identified, with a higher abundance in the epidermis of the isoforms belonging to the protein group 4789

(Kaladp0024s0016.1.p, Kaladp0024s0016.2.p, Kaladp0024s0016.3.p, Kaladp0024s0016.4.p), while the ones of the groups 999 (Kaladp0102s0114.1.p, Kaladp0102s0114.2.p), 100021 (Kaladp0095s0564.1.p, Kaladp0095s0564.2.p) and 10743 (Kaladp0058s0569.1.p) were more abundant in the mesophyll (Figure 6. 3).

6.3.2. Stomatal regulation-related proteins

Proteins responsible for stomatal regulation were significantly more abundant in the epidermis than in the mesophyll. The serine/threonine protein kinase OST1 (Open Stomata 1) was identified in three different protein groups, with differences noted in diel abundance. For the OST isoforms encoded by Kaladp0016s0289.1.p and Kaladp0016s0289.2.p (protein group 12333) a slight decrease at the end of the night and beginning of the day was evidenced, while for Kaladp0808s0028.1.p (protein group 13033) the abundance increased at the beginning of the day and at the middle of both light and dark period. Noteworthy, OST encoded by Kaldp0049s0026.2p (protein group 13227) did not present any diel changes in the epidermis (Figure 6. 4).

The plasma membrane H^+-ATPases implicated in stomatal opening as a result of light induction and membrane hyperpolarisation were identified in three different proteins groups, encoding isoforms more abundant in the epidermis compared to the mesophyll ($p \leq 0.05$). Noteworthy, diel changes in epidermis abundance were detected only at the end of the night period, while in mesophyll diel abundance changes were more pronounced during the day (Figure 6. 4).

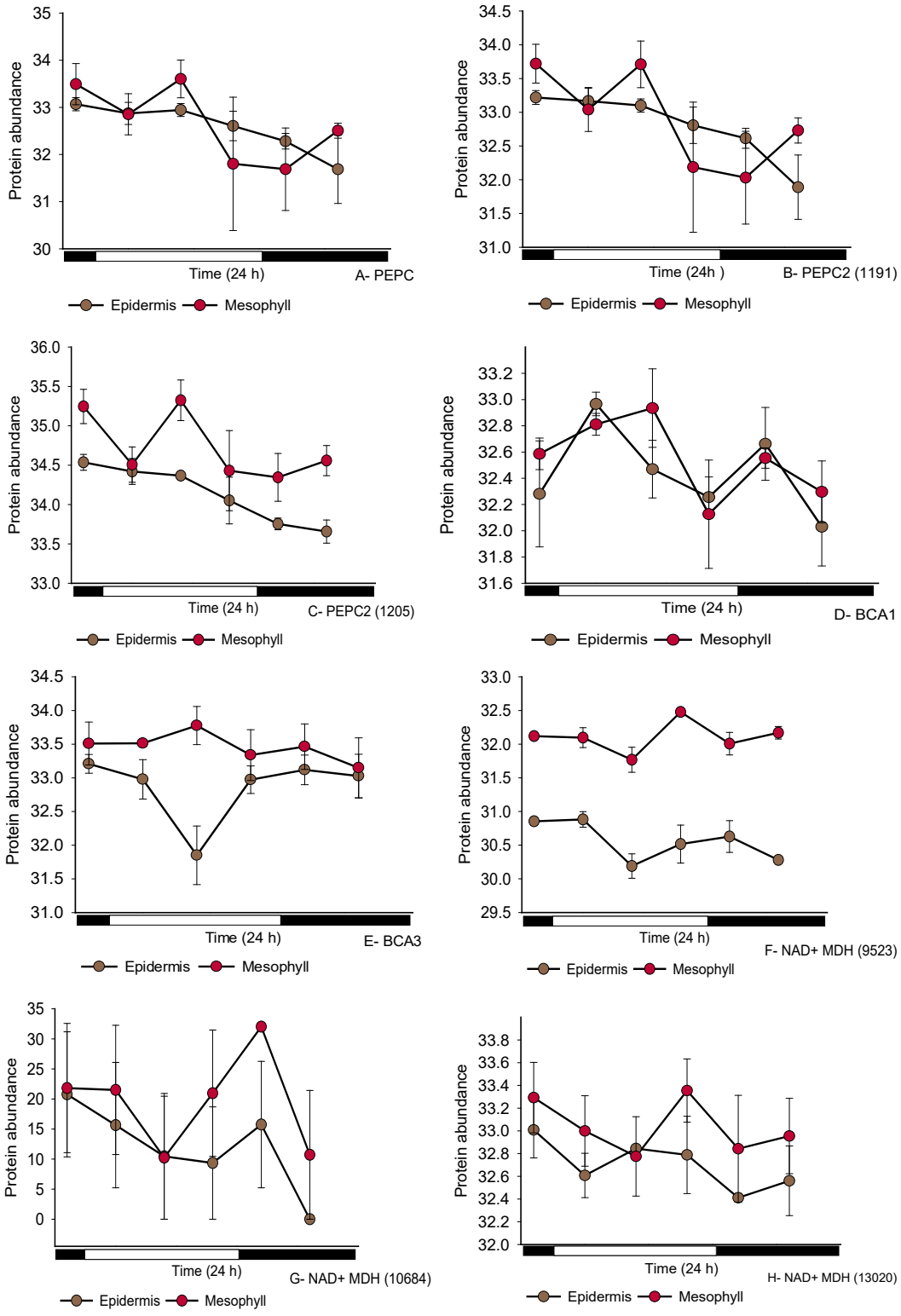

Figure 6. 3. Normalised abundance in the mesophyll (red) and guard cell-enriched epidermis (brown) of proteins implicated in the carboxylation and decarboxylation modules of CAM metabolism. The data corresponds to a 24 hour day/night cycle (black bars indicate night period). In the case of proteins found in different groups, the group is indicated in parenthesis. Leaf pair 6 was used for this analysis and the bars indicate the error of three biological replicates. Plant growth conditions were set at 400 µmol CO_2 mol^{-1} air, 25°C/19°C (day/night) and a diurnal photosynthetic photon flux density – PPFD - of 250 µmol $m^{-2}s^{-1}$ at plant height. (A) PEPC; (B, C) PEPC2; (D) βCA1; (E) βCA3; (F) NAD^+ MDH; (G, H) NAD^+ MDH;

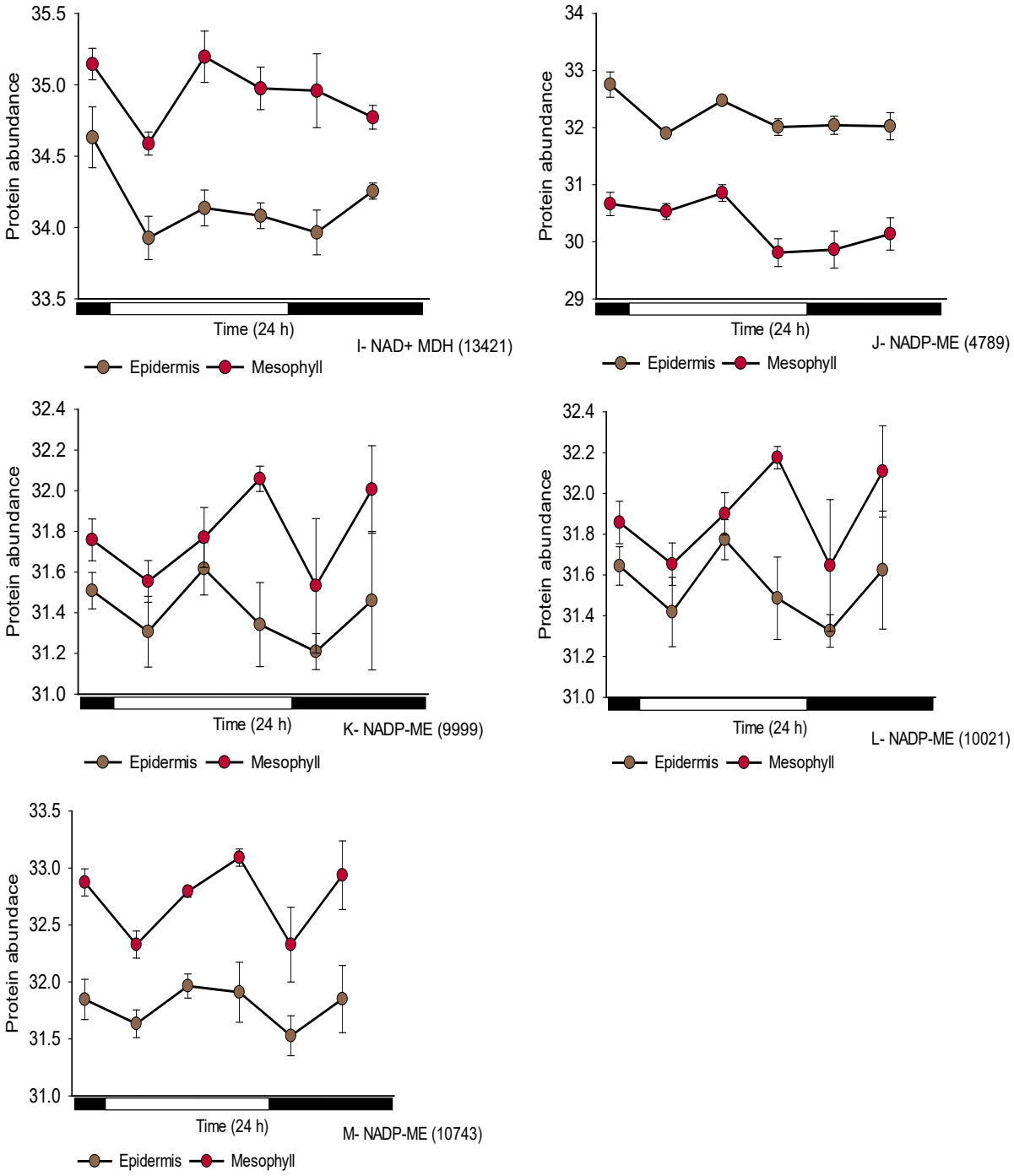

Continue Figure 6.3. (I) NAD^+ MDH; (J - M) NADP-ME;

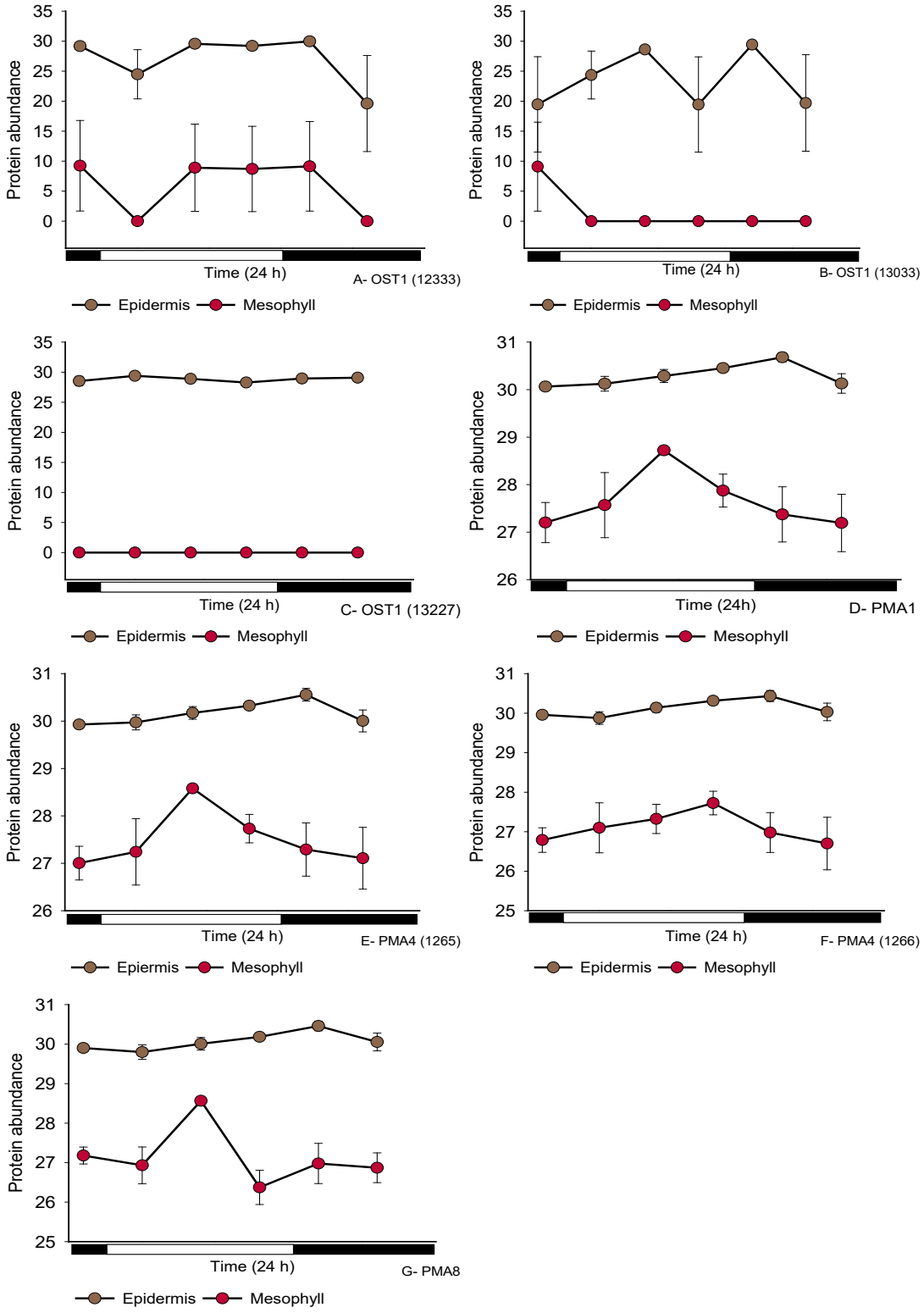

Figure 6. 4. Normalised abundance in the mesophyll (red) and guard cell-enriched epidermis (brown) of proteins implicated in the opening of stomata. In the case of proteins found in different groups, the group is indicated in parenthesis. Leaf pair 6 was used for this analysis and the bars indicate the error of three biological replicates. Plant growth conditions were set at 400 µmol CO_2 mol^{-1} air, 25°C/19°C (day/night) and a diurnal photosynthetic photon flux density – PPFD - of 250 µmol $m^{-2}s^{-1}$ at plant height. (A - C) OST1; (D) PMA1; (E - F) PMA4; (G) PMA8.

6.3.3. Starch metabolism-related proteins

Regarding starch metabolism, enzymes implicated in both synthesis and degradation were identified. Comparing protein abundance between tissues, significant differences were observed for most of the proteins implicated in starch synthesis. ADP glucose pyrophosphorylase small subunit (APS1) and α-1, 4-glucan synthase (ADP-forming) were found in higher abundance in the mesophyll and epidermis, respectively. For phosphoglucose isomerase (PGI), phosphoglucomutase (PGM), ADP glucose pyrophosphorylase (AGPase, APL), starch branching enzyme (SBE) and starch synthase (SSI – SSIV), differences between tissues were present in some of the isoforms identified. In the case of PGM, the isoforms encoded by Kaladp0101s022.1.p (PGM) and Kaladp0059s0263.1 (PGM2) were more abundant in the epidermis, while PGM1 encoded by Kaladp0008s0557.1.p was higher in the mesophyll. Interestingly, similar diel patterns between mesophyll and epidermis were found for most of the proteins. In the case of APS1, AGPase-APL4, PGM1, PGM2 and the PGI (Kaladp0089s0069.1 – group 4522), the abundance increased in the middle of the day and decreased at the end of the day, suggesting similarities in starch turnover in both tissues (Figure 6. 5).

Proteins implicated in phosphorylation and dephosphorylation of starch granules, thought to be critical for initiating starch degradation, were detected in both tissues. In the mesophyll, phosphoglucan phosphatase amyloplastic (SEX4, DSP4) and glucan water dikinase 3 (PWD), were in higher abundance compared to epidermis while glucan water dikinase 1 (GWD1, SEX1) did not differ in abundance between tissues. In relation to starch degrading enzymes, α-glucan phosphorylase (PHS) and disproportionating enzyme (DPE) were the most abundant proteins, confirming the importance of the phosphorolytic pathway in CAM species as a source of PEP for nocturnal carboxylation and glucose for plant growth. The reduced abundances of chloroplastic PHS1 and DPE1 in the epidermis compared to the mesophyll suggest the importance of mesophyll starch metabolism for predominantly sustaining CAM, while the increased abundances of the cytosolic PHS2 and DPE2 in the epidermis might suggest a different route for starch degradation in the epidermis and could be related to sugar metabolism in stomatal guard cells (Figure 6. 6).

Additionally, α-amylase 3 (AMY3) and β-amylase 1 (BAM1) have been reported as the main starch degrading enzymes in C_3 stomatal guard cells. In the proteomics dataset, BAM1 was not detected and AMY3 abundance did not differ between mesophyll and epidermis. In contrast, α-amylase 1 (AMY1) was significantly more abundant in the epidermis compared to the mesophyll, suggesting possible changes in starch degradation pathways in CAM stomata

compared to C_3 plants. No differences between mesophyll and epidermis for the reported non-catalytically active BAM9 were observed but the exclusive presence of BAM2 in the epidermis is further indication that different routes of starch degradation are found in the CAM guard cells and mesophyll (Figure 6. 6).

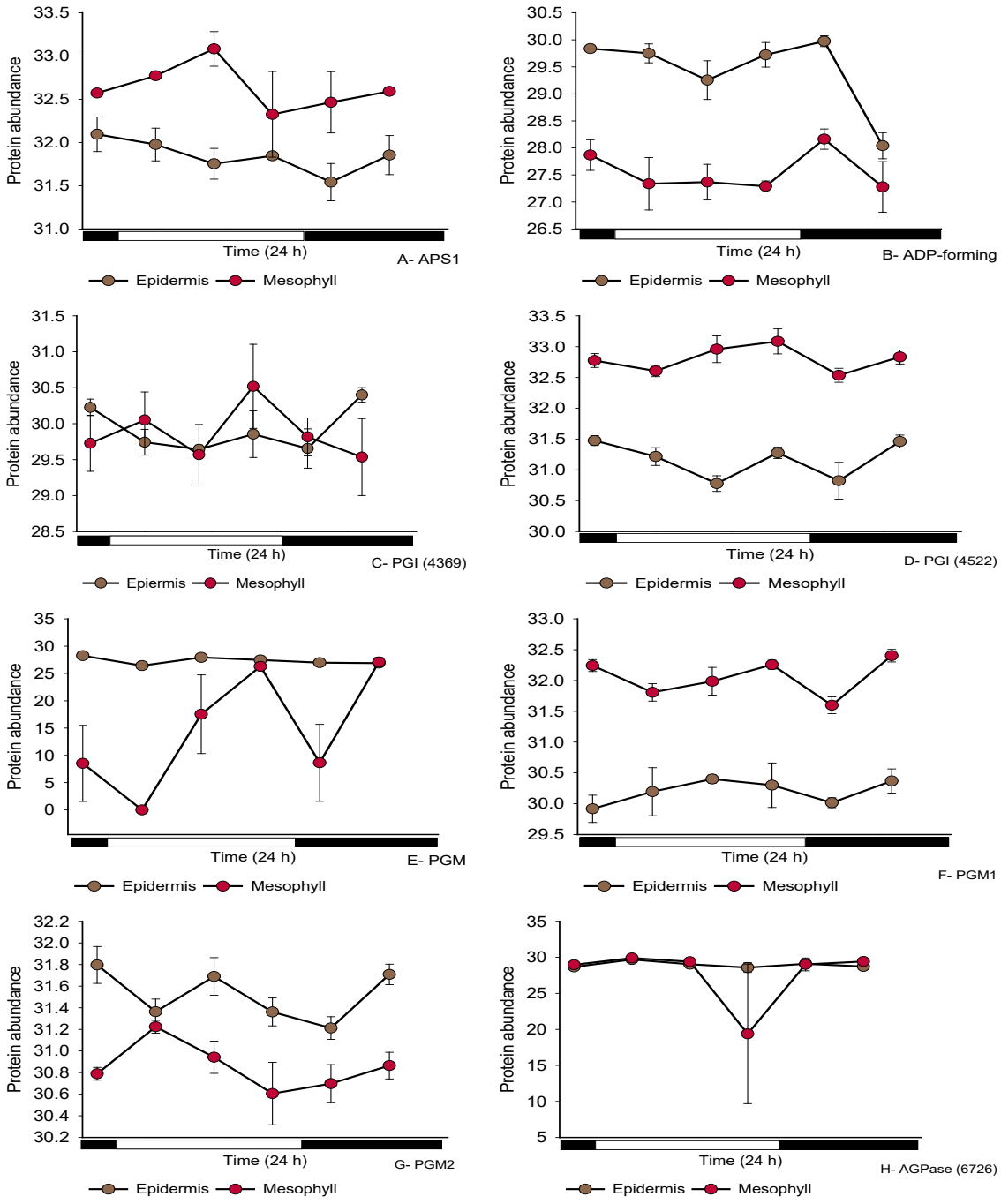

Figure 6. 5. Normalised abundance in the mesophyll (red) and guard cell-enriched epidermis (brown) of proteins implicated in starch synthesis. In the case of proteins found in different groups, the group is indicated in parenthesis. Leaf pair 6 was used for this analysis and the bars indicate the error of three biological replicates. Plant growth conditions were set at 400 µmol CO_2 mol^{-1} air, 25°C/19°C (day/night) and a diurnal photosynthetic photon flux density – PPFD - of 250 µmol $m^{-2}s^{-1}$ at plant height. (A) APS; (B) ADP-forming; (C - D) PGI; (E) PGM; (F) PGM1; (G) PGM2; (H) AGPase;

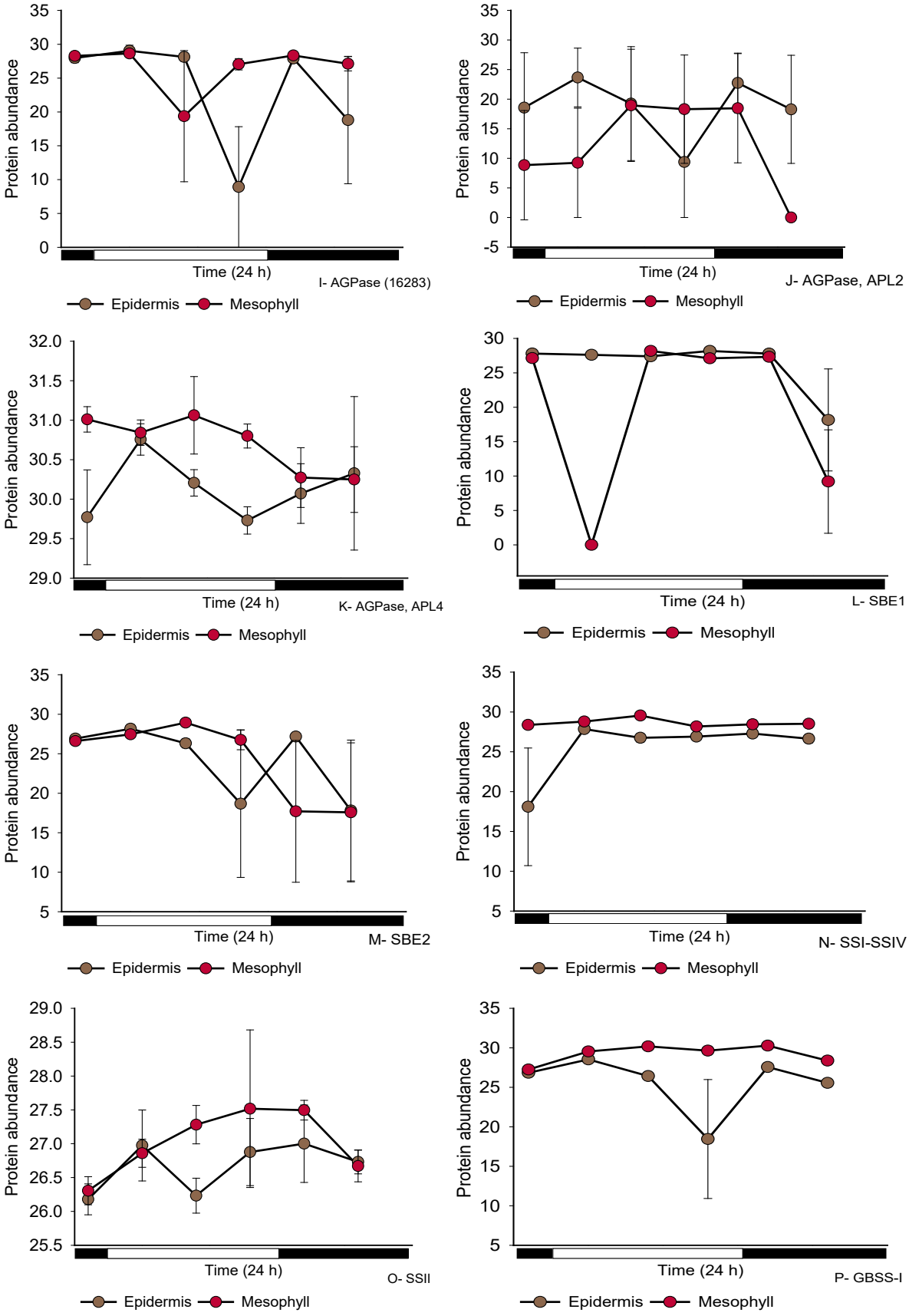

Continue Figure 6.5. (I) AGPase; (J) AGPase, APL2; (K) AGPase, APL4; (L) SBE1; (M) SBE2; (N) SSI-SSIV; (O) SSII; (P) GBSS-I.

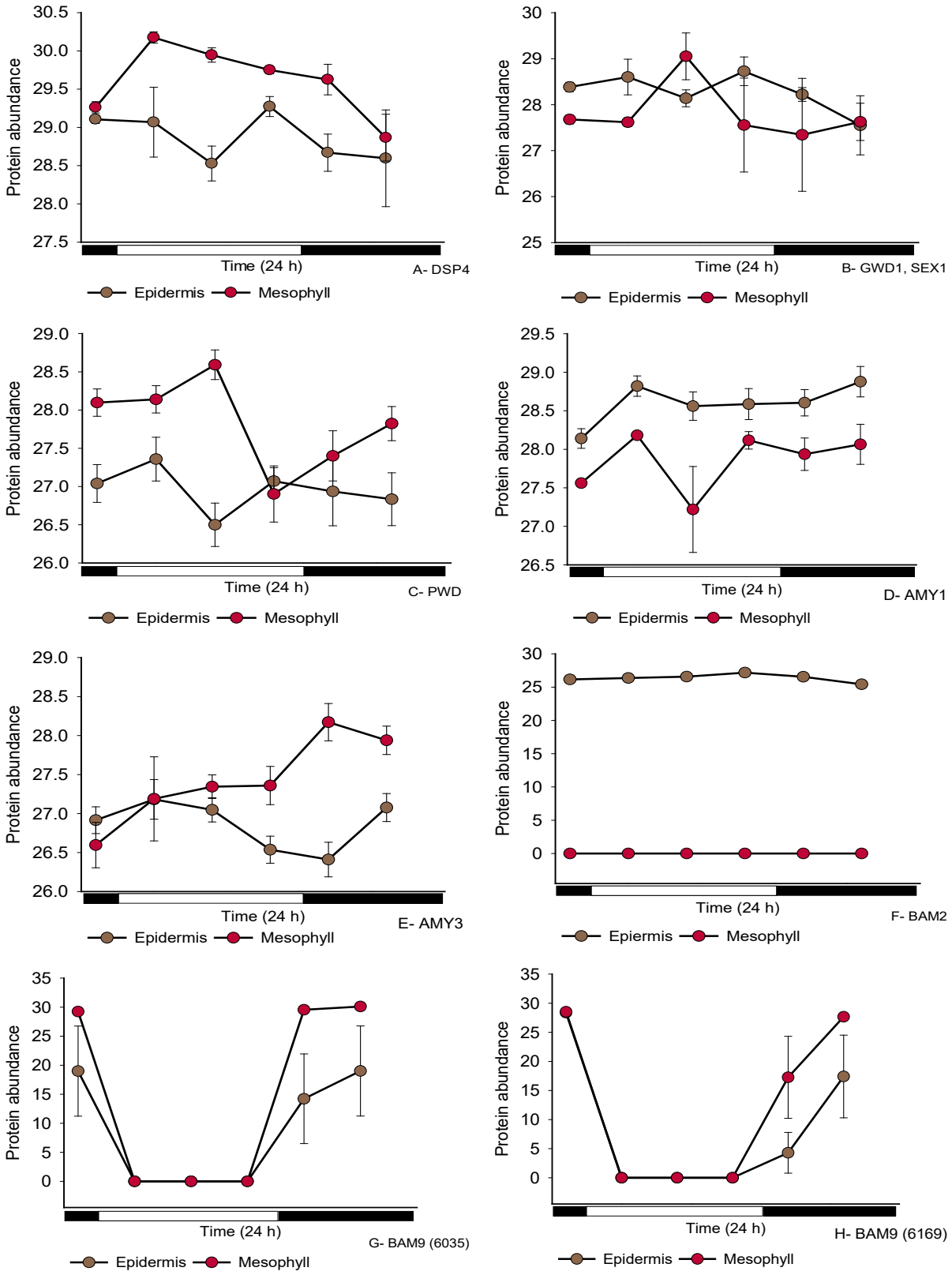

Figure 6. 6. Normalised abundance in the mesophyll (red) and guard cell-enriched epidermis (brown) of proteins implicated in starch degradation. In the case of proteins found in different groups, the group is indicated in parenthesis. Leaf pair 6 was used for this analysis and the bars indicate the error of three biological replicates. Plant growth conditions were set at 400 µmol CO_2 mol^{-1} air, 25°C/19°C (day/night) and a diurnal photosynthetic photon flux density – PPFD - of 250 µmol $m^{-2}s^{-1}$ at plant height. (A) DSP4; (B) GWD1; (C) PWD; (D) AMY1; (E) AMY3; (F) BAM2; (G – H) BAM9;

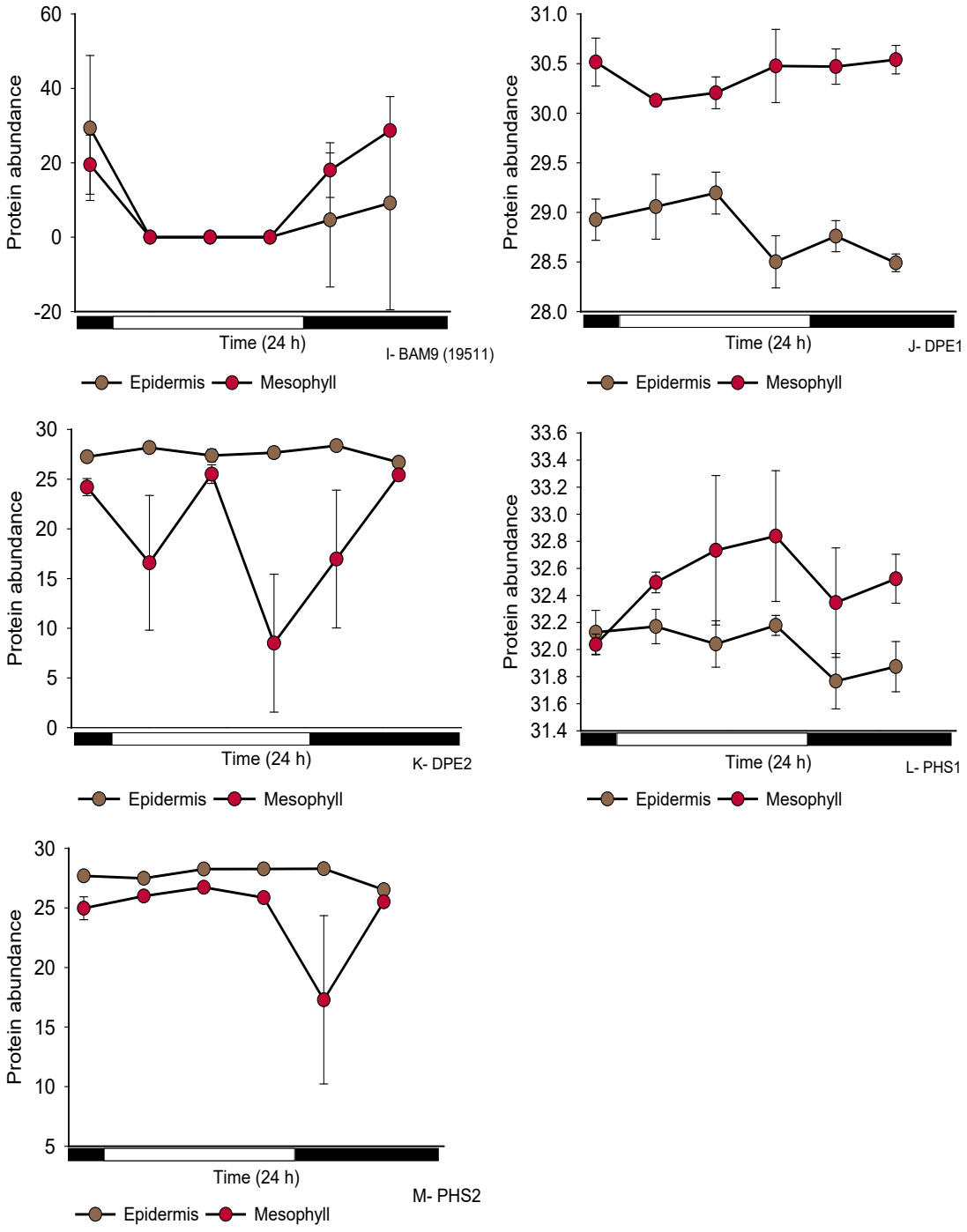

Continue Figure 6.6. (I) BAM9; (J) DPE1; (K) DPE2; (L) PHS1; (M) PHS2

6.3.4. Sugar metabolism-related proteins

Based on the importance of sugars in stomatal behaviour in terms of osmolytes and/or as potential carbon sources for the synthesis of organic acids, proteins implicated in glycolysis and gluconeogenesis were also examined. Hexokinase (HXK), phosphofructokinase (PFK) and pyruvate kinase (PK) were highly abundant in the epidermis compared to the mesophyll. Interestingly one of the isoforms of pyruvate carboxylase (PC) was only detected in the

epidermis (Kaldp0064s0159.1.p – group 16326), while the abundance of the isoform encoded by Kaldp0003s0030.1 (protein group 15558) was similar between both tissues (Figure 6. 7). For other proteins implicated in sugar metabolism, sedoheptulose bisphosphatase (SBPase) and transketolase (TKL) were more abundant in the mesophyll than in the epidermis. Noteworthy, both enzymes are implicated in the non-oxidative pentose phosphate pathway, an important route that provides glycolytic intermediates derived from ribose 5-phosophate (Figure 6. 7).

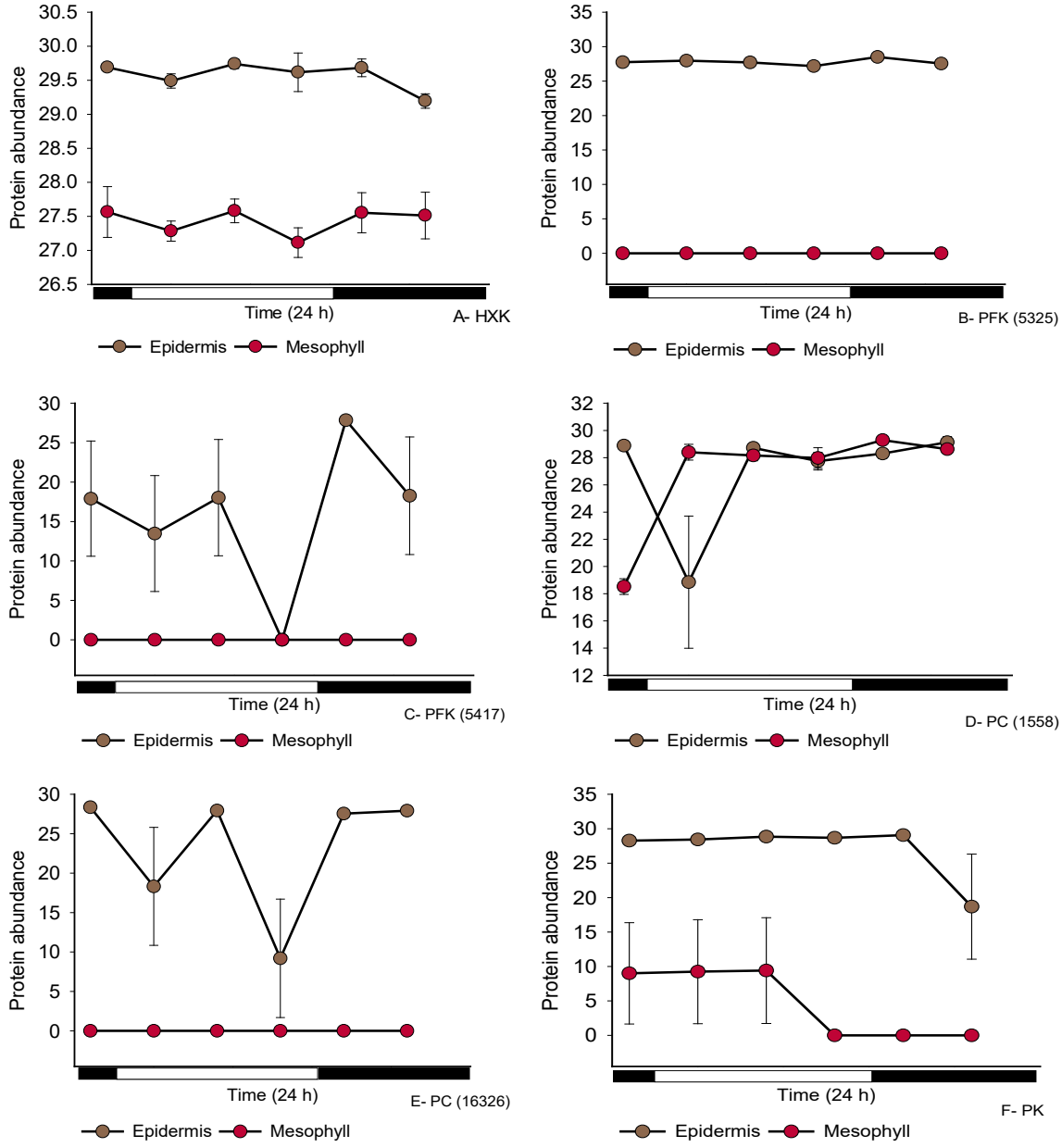

Figure 6. 7. Normalised abundance in the mesophyll (red) and guard cell-enriched epidermis (brown) of proteins implicated in sugars metabolism. In the case of proteins found in different groups, the group is indicated in parenthesis. Leaf pair 6 was used for this analysis and the bars indicate the error of three biological replicates. Plant growth conditions were set at 400 µmol CO_2 mol^{-1} air, 25°C/19°C (day/night) and a diurnal photosynthetic photon flux density – PPFD - of 250 µmol $m^{-2}s^{-1}$ at plant height. (A) HXK; (B - C) PFK; (D - E) PC; (F) PK;

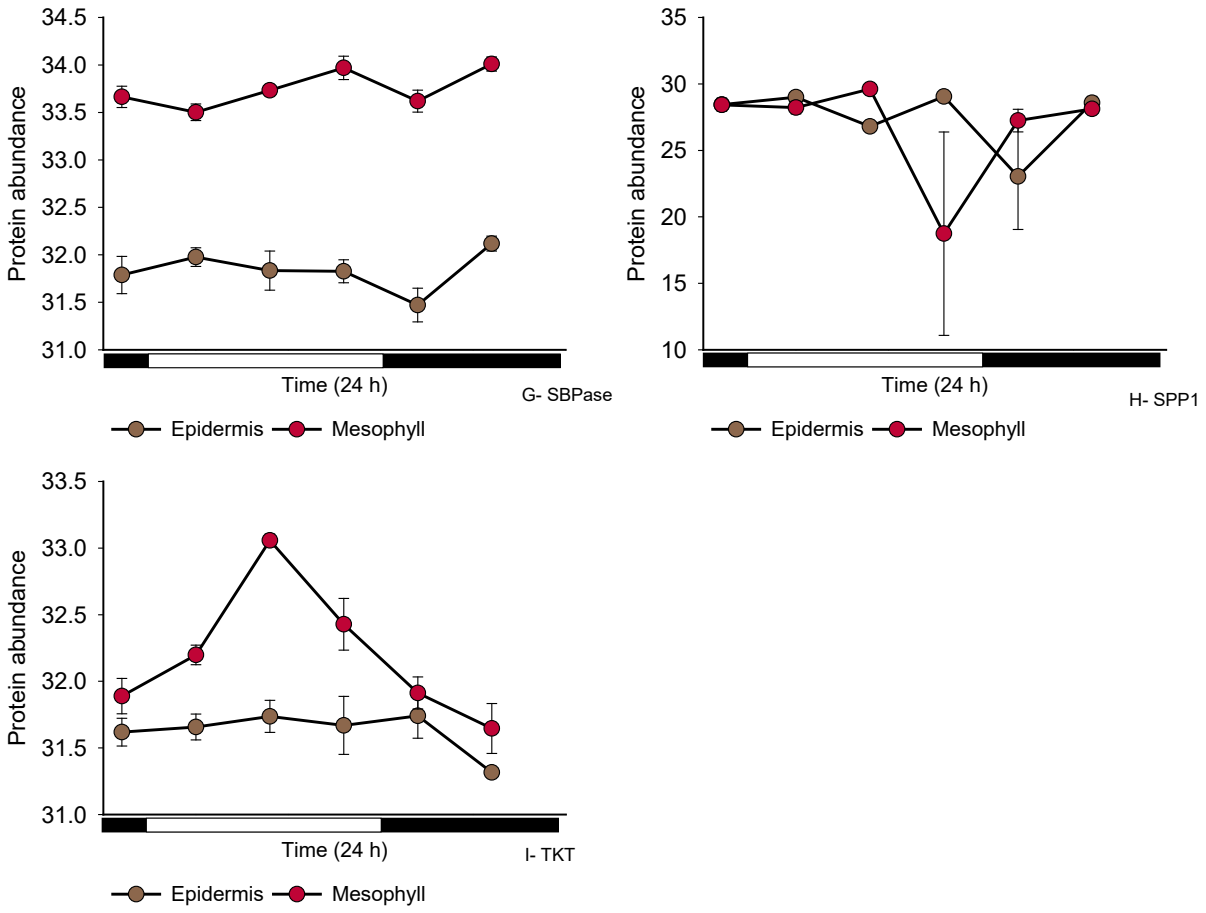

Continue Figure 6.8. (G) SBPase; (H) SPP1; (I) TKT.

6.3.5. Mitochondrial respiration-related proteins

Proteins involved in mitochondrial respiration were identified, taking into account the importance of energetics for not only CAM in the mesophyll but also for stomatal movement. NADH dehydrogenase is one of the complexes involved in ATP synthesis in the mitochondria; four isoforms of NADH dehydrogenase were detected in two protein groups. The isoforms of NADH dehydrogenase belonging to 19078 (encoded by Kaladp011s0650.1.p, Kaladp0102s0137.1.p and Kaladp0662s0004.1.p) were more abundant in the epidermis, while the isoform encoded by Kaladp0517s0001.1.p (group 21326) was higher in the mesophyll. These differences suggest independence between the mesophyll and epidermis in supplying energy to the different metabolic processes that occur in these tissues (Figure 6. 8).

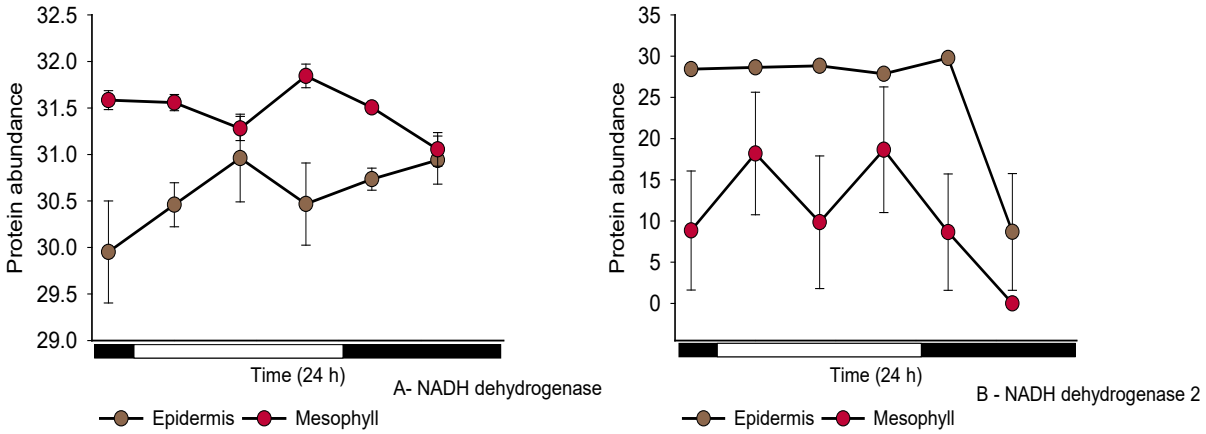

Figure 6. 8. Normalised abundance in the mesophyll (red) and guard cell-enriched epidermis (brown) of proteins implicated in mitochondrial respiration. In the case of proteins found in different groups, the group is indicated in parenthesis. Leaf pair 6 was used for this analysis and the bars indicate the error of three biological replicates. Plant growth conditions were set at 400 µmol CO_2 mol^{-1} air, 25°C/19°C (day/night) and a diurnal photosynthetic photon flux density – PPFD - of 250 µmol $m^{-2}s^{-1}$ at plant height. (A) NADH dehydrogenase; (B) NADH dehydrogenase 2.

6.4. Discussion

The unique day/night metabolism and stomatal rhythm of plants with crassulacean acid metabolism has led to the hypothesis that temporal changes in diel protein abundance occurred during the evolution of CAM. Likewise, it was hypothesised that differential protein expression between mesophyll and guard cell-enriched epidermis could indicate metabolic independence between both tissues. Abraham *et al.* (submitted) have presented the first proteome dataset comparing the protein abundance between mesophyll and epidermis in a 24 h day/night cycle in the CAM species *Kalanchoë fedtschenkoi.* This chapter used this dataset to focus on proteins implicated in CAM, stomatal regulation, starch metabolism, sugar turnover and mitochondrial respiration.

6.4.1. Carboxylation and decarboxylation-related proteins

The CAM diel cycle is defined by four phases when carboxylation and decarboxylation occur alongside the opening and closure of stomata. At night, the opening of stomata allow the uptake of ambient CO_2, which is hydrated to HCO^-_3 by the enzyme carbonic anhydrase (CA) (Borland *et al.*, 2011). The difference in abundance of the CA identified (βCA1, βCA3) in the proteome dataset shows the diversity of this protein and indicates specific roles of each isoform in the HCO^-_3 conversion in mesophyll and epidermis, this was evidenced by the

similar diel turnover between both tissues for βCA1 and the higher abundance of βCA3 in the mesophyll, respectively. Similar diel patterns were detected for phosphoenolpyruvate carboxylase (PEPC) and NAD^+ malate dehydrogenase (NAD^+ MDH) isoforms, which were highly abundant at the end of the light period. The 24 h diel pattern of protein abundances for βCA3, PEPC and NAD-MDH indicate possible circadian clock regulation of these enzymes, evidenced by an increased abundance at the end of both time periods, indicating a possible correlation with phases I, II and IV when stomata open for CO_2 uptake. Additionally, Abraham *et al.* (submitted) identified a significantly enriched βCA in epidermis of *K. fedtschenkoi*, orthologue to βCA5 in *Arabidopsis*, with a maximal expression during the night period, corresponding to the maximal period of nocturnal CO_2 assimilation. Transcriptomic analysis in pineapple showed similar results, in that case, the maximum βCA gene expression was observed during the first hours of the morning and at night suggesting a synchronisation between the expression of carboxylation enzymes and the time of maximum CO_2 uptake and stomatal conductance in CAM plants (Ming *et al.*, 2015).

Similar phosphoenolpyruvate carboxylase (PEPC) abundances found between epidermis and mesophyll agree with recent studies in C_3 that identified CO_2 fixation in guard cells via Rubisco and PEPC with an increased activity of NAD- or NADP-malate dehydrogenase as well as higher content of malate in C_3 guard cells compared to mesophyll (Daloso *et al.*, 2015; Santelia and Lawson, 2016). Additionally, Cousins *et al.* (2007) in the C_4 species, *Amaranthus edulis,* suggested that stomatal conductance depends on PEPC activity, PEP synthesis and malate content in the guard cells, this latter acting as the main osmolyte during stomatal opening. Interestingly, PEPC abundance in the C_3 monocotyledonous *Commelina communis*, was higher in the guard cells than in the mesophyll (Cotelle *et al.*, 1999) while in terms of gene expression the study of Aubry *et al.* (2016) found similar transcript abundance between mesophyll and guard cells in C_4 species. Those reports, together with the results presented in this chapter agree with Daloso *et al.* (2017) who suggested that metabolism of guard cells in C_3 plants is similar to C_4 and CAM, based on the higher activity of PEPC, NAD-MDH and ME and the increased CO_2 fixation during night period compared to the mesophyll.

Boxall *et al.* (2019) stated the importance of PEPC1 as defining CAM and controlling stomatal behaviour. The silencing of *pepc1* in *Kalanchoë laxiflora* led to the loss of nocturnal CO_2 fixation and the inability of stomatal opening at night and closure during the day-time. Likewise, phosphorylation of PEPC during the night reduces its inhibition by malate and this is associated with increased CO_2 fixation (Boxall *et al.*, 2017). In guard cells, the osmolytic

role of malate could potentially inhibit PEPC, affecting guard cell metabolism and stomatal opening. Thus, PEPC phosphorylation is important for the opening of stomata and the CO_2 fixation mediated by PEPC in the guard cells (Zhang *et al.*, 1994). In C_3 and C_4 plants, PEPC phosphorylation occurs during the day, the time when stomata are open. Noteworthy, Abraham *et al.* (submitted) identified that the PEPC isoforms in the *K. fedtschenkoi* proteome dataset were phosphorylated during the night period in both mesophyll and epidermis, indicating the importance of CO_2 carboxylation via PEPC in both tissues, as well as the circadian control of PEPC phosphorylation that allows the inverted stomatal rhythm in CAM plants (Boxall *et al.*, 2017).

During the day, malate decarboxylation and CO_2 re-fixation occur by a series of reactions in the mesophyll of CAM plants. NAD-malic enzyme (NAD-ME), NADP malic enzyme (NADP-ME) and phosphoenolpyruvate carboxykinase (PEPCK) catalyse the conversion of malate to pyruvate and CO_2 depending on the species (Honda *et al.*, 2000). Ten different isoforms of NADP-ME, clustered in four protein groups, showed an abundance peak during the day period, correlating with the maximal decarboxylation rate. A higher abundance in the epidermis was detected for the isoforms identified in the protein group 4789, indicating a role not only in mesophyll malate decarboxylation, but also in guard cell metabolism. Laporte *et al.* (2002) reported a reduced stomatal conductance in tomato plants over expressing NADP-ME, probably linked to increased malate degradation that supports stomatal closure. The higher protein abundance of NADP-ME during the day period in the epidermis proteome dataset of *K. fedtschenkoi* could suggest a similar role for this protein in the closure of stomata, however further studies are required to confirm this hypothesis.

In the mesophyll, Dever *et al.* (2015) suggested that NAD-malic enzyme (NAD-ME) is the major decarboxylase in *K. fedtschenkoi*, by investigating the RNAi-mediated silencing of light-period malate decarboxylation. In the RNAi line *rNAD-ME1*, Dever *et al.* (2015) reported an effect on key enzymes involved in both CAM carboxylation and decarboxylation, with a slight but not significant increase of NADP-ME activity, and a day-time pattern of CO_2 fixation, comparable to C_3 photosynthesis, evidencing that NAD-ME is responsible by diurnal decarboxylation. Abraham *et al.* (submitted) reported a similar protein abundance of NAD-ME between mesophyll and epidermis, with abundance peaks at the beginning and end of the day, correlating with the maximal decarboxylation rate and suggesting that malate decarboxylation is also a pivotal process in stomatal guard cells.

6.4.2. Starch turnover-related proteins and role in stomatal behaviour

Starch metabolism has been widely studied in the mesophyll of different CAM species since starch breakdown supports the production of sugars for growth as well as the synthesis of PEP, the main substrate for nocturnal carboxylation (Borland *et al.*, 2016). Unfortunately, all of the information about starch metabolism in CAM is restricted to the mesophyll. Previous work in this thesis has shown that starch metabolism in stomatal guard cells also plays a pivotal role in CAM plants. Increased protein abundance during the light period in both mesophyll and epidermis was observed for the starch synthesis enzymes ADP glucose pyrophosphorylase small subunit (APS1), ADP glucose pyrophosphorylase (AGPase, APL4), phosphoglucomutase (PGM), and phosphoglucose isomerase (PGI). Additionally, no differences in protein abundance between mesophyll and epidermis were detected for PGI isoform encoded by Kaladp0095s0394.1.p, ADP-glucose synthase (AGPase), ADP-glucose pyrophosphorylase (AGPase/APL2), starch branching enzyme 2 (SBE2), starch synthase 2 (SSII) and granule-bound starch synthase I (GBSSI). These findings are in contrast to reports in *Brassica napus* (Zhu *et al.*, 2009), where starch synthesis enzymes predominated in mesophyll. Noteworthy, the RNA sequence dataset interrogated previously in this study showed an increased transcript expression in the mesophyll of all the enzymes implicated in starch synthesis (Table 3. 2 – Chapter 3), which suggest post-transcriptional and post-translational regulation in CAM starch synthesis similar to that observed by Dodd *et al.* (2003) for starch degrading enzymes of *M. crystallinum.*

In C_3 plants, starch turnover in both guard cells and mesophyll follows an opposite pattern. During the night, starch degradation in C_3 mesophyll is catalysed by the hydrolytic enzymes β-amylases (mainly BAM3) and disproportionating enzyme 1 (DPE1), while during the day is synthesised from Calvin cycle-derived products (Stitt and Zeeman, 2012). On the other hand, starch in C_3 guard cells is synthesised during the night period and degraded during the first hours of the day, by the action of β-amylase 1 (BAM1) and α-amylase 3 (AMY3), to trigger the opening of stomata (Horrer *et al.*, 2016). Opposite to reports in C_3, the present study indicated that starch is predominantly synthesised during the day and degraded at night in both mesophyll and guard cells of CAM-performing leaves in *K. fedtschenkoi* (Chapter 3). These results, together with similar diel patterns of abundance between mesophyll and epidermis for most of the proteins implicated in starch synthesis, and the increased abundances during the light period in both tissues for ADP glucose pyrophosphorylase small subunit (APS1), phosphoglucomutase 1 and 2 (PGM), phosphoglucose isomerase (PGI - Kaladp0089s0069.1.p) and ADP glucose pyrophosphorylase (AGPase, APL4), imply a re-

programming of C_3 starch metabolism in CAM plants that is linked to the unique inverted stomatal behaviour.

These findings could also indicate modifications in the circadian control of carbohydrates metabolism in CAM to ensure the diurnal closure of stomata. It is known that the circadian clock synchronises the diel phases of CAM and a key enzyme implicated in this process is phosphoenolpyruvate carboxylase kinase (PPCK), which controls nocturnal carboxylation by the activation of phosphoenolpyruvate carboxylase (PEPC), and thereby modulating the levels of malate and carbohydrates during the 24 h diel cycle (Boxall *et al.*, 2017). Likewise, the circadian regulation of starch synthesis in the mesophyll of C_3 plants and CAM-performing leaves of *M. crystallinum* (Borland and Taybi, 2004; Azoulay-Shemer *et al.*, 2018), led to the hypothesis that differences in the diel patterns observed for *K. fedtschenkoi* proteins in the epidermis could represent changes to clock-output for regulation of guard cell metabolism.

Regarding starch degrading enzymes, the proteome dataset showed enrichment in both tissues of α-glucan phosphorylase (PHS1), the enzyme responsible for phosphorolytic degradation of starch, while β-amylases 1 and 3 (BAM1 and BAM3), the main hydrolytic enzymes in C_3 starch degradation, were not detected. These findings are consistent with Borland *et al.* (2016) and Shameer *et al.* (2018) who reported that starch degradation in CAM plants follows mainly the phosphorolytic pathway, to provide glucose 6-phosphate that is exported from the chloroplast and subsequently converted to phosphoenolpyruvate (PEP) in the cytosol for nocturnal CO_2 assimilation. On the other hand, the hydrolytic disproportionating enzyme 1 (DPE1) was also identified in the proteome. DPE1 is implicated in starch breakdown in CAM plants, producing glucose and maltopentaose, which are metabolised by BAM and PHS1, to provide Glc1P that serves as substrate for sucrose synthesis and biomass production (Borland *et al.*, 2016). The higher expression of PHS1 and DPE1 in the mesophyll compared to the epidermis indicates that starch degradation in the mesophyll primarily supports nocturnal CAM activity, while in guard cells starch degradation functions mainly to provide sugars/osmolytes for stomatal opening at night.

Apart from a role in the degradation of starch in C_3 guard cells, reports in *Arabidopsis* indicate that α-amylases (AMY) do not have a prominent function in mesophyll starch degradation (Yu *et al.*, 2005). However, lines lacking *amy1* in rice showed a starch excess phenotype, suggesting differences in the function of this enzyme depending on the species (Asatsuma *et al.*, 2005). While AMY3 has been reported predominantly in *Arabidopsis* guard cells, acting together with BAM1 (Horrer *et al.*, 2016) and AMY1 expressed in the mesophyll, the results obtained in this study indicated no differences in AMY3 abundance

between mesophyll and epidermis but an increased abundance for AMY1 in the epidermis. Differences in the protein abundances of AMY1 and AMY3 between the *K. fedtschenkoi* protein dataset and the reports for these proteins in C_3 plants, lead also to hypothesise about different roles for these enzymes in CAM plants. Following the same idea, in the facultative CAM plant *M. crystallinum* increased transcript abundance of *amy* genes was shown after CAM induction, suggesting key roles for AMYs in starch degradation, either directly and/or or enabling PHS1 access to the starch granule for further degradation (Cushman *et al.*, 2008b).

Preliminary phosphorylation and dephosphorylation of starch granules allow the initiation of starch degradation. Phosphoglucan phosphatase (SEX4, DSP4), glucan water dikinase 1 (GWD1, SEX1) and glucan water dikinase 3 (PWD), implicated in these processes were identified in both mesophyll and epidermis proteome datasets with a higher abundance in the mesophyll of both SEX4 and PWD, while GWD1 was similar between tissues. According to Smith *et al.* (2005), the combined action of GWD and PWD is required for nocturnal starch degradation in *A. thaliana* and its silencing generates an over accumulation of starch compared to wild type plants. Subsequently, the action of SEX4 removing phosphates groups, enhances the release of soluble glucans, being accessible to degrading enzymes (Stitt and Zeeman, 2012). The phosphorylation/dephosphorylation process in guard cells is less understood, however Edner *et al.* (2007) reported that GWD increases the activity of BAM1 *in vitro*, one of the main enzymes responsible for starch degradation in C_3 guard cells (Santelia and Lawson, 2016), suggesting a similar phosphorylation role in starch degradation between both tissues. In the *K. fedtschenkoi* protein data set, similar diel patterns were found for SEX4 and PWD in both tissues, with enrichment in the mesophyll, while GWD1 did not differ in abundance between mesophyll and epidermis, suggesting a possible action of this latter enzyme in the starch granule phosphorylation in CAM guard cells. Those similarities in GWD1, PWD and SEX4 turnover between tissues, together with the non-detection of BAM1 in the epidermis, supports the hypothesis that starch degradation in both mesophyll and guard cells is catalysed by PHS, following the same diel turnover and thus might have implications in the nocturnal opening of stomata.

Regarding β-amylases, only two isoforms were detected in the *K. fedtschenkoi* proteome dataset, BAM2 and BAM9. Both isoforms have been reported as non-catalytically active enzymes with a regulatory function during starch degradation (Fulton *et al.*, 2008). Recently, Monroe and Storm (2018) indicated that catalytic activity of BAM2 requires physiological levels of KCl and its active site possesses a secondary binding site, thought to increase the

catalytic activity by the interaction with other enzymes or by reaching the substrate. Interestingly, BAM2 was restricted to the epidermis with no variations in the 24 h diel pattern of abundance. On the other side, BAM9 showed a decreased abundance during the first hour of the light period and an increase at the beginning of the night, with no differences between tissues. This pattern was opposite to the RNAseq data findings and gene expression in both Chapters 3 and 5, respectively. These differences between protein and RNA for BAM9 could be due to post-transcriptional and post-translational regulation or by changes in the growth conditions, plant age or water status between the different plant batches during the sampling process. Overall, further studies are needed to elucidate the function of BAM2 and BAM9 in starch metabolism and CAM stomatal function.

6.4.3. Sugar metabolism and mitochondrial respiration in guard cells

The biochemical and molecular characterisation of RNAi lines (Chapters 4 and 5), together with the RNAseq data interrogation in Chapter 3 have shown the importance of sugar metabolism in CAM plants and stomatal regulation. This was evidenced by the impact on carbohydrate content in the RNAi lines that curtailed nocturnal CAM activity and avoided stomatal closure during the light period. The significant enrichment in the epidermis proteome of disproportionating enzyme 2 (DPE2), α-glucan phosphorylase 2 (PHS2), hexokinase (HXK) and phosphoglucomutase 2 (PGM2), as well as the presence of sucrose phosphate phosphatase (SPP), indicate the importance of sugar metabolism in guard cells. These enzymes catalyse the cytosolic processing of starch degradation products during the night period to generate either sucrose for biomass production or Glc1P that sustains glycolysis (Stitt and Zeeman, 2012).

Hite *et al.* (1993) reported an increased sucrose phosphate phosphatase (SPP) expression in *Vicia faba* guard cells, indicating a correlation between sucrose interconversion rate and stomatal movement, and suggested a potential osmolytic role for sucrose in guard cells. This idea was in line with Talbott and Zeiger (1996), who proposed the starch – sucrose hypothesis, stating that sucrose is the main osmolyte replacing potassium in the middle of the day to increase guard cell turgor pressure in C_3 plants. In addition to the osmoticum role, an energetic function of sucrose in guard cells has been proposed recently by Daloso *et al.* (2015), indicating that sucrose degradation products are substrates for respiration and organic acid synthesis based on the fact that stomatal movement has a high energetic requirement which is fulfilled by increased mitochondrial respiration.

The increased abundance in the *K. fedtschenkoi* epidermis proteome of phosphofructokinase (PFK) and pyruvate kinase (PK), agrees with the higher glycolytic activity reported for C_3 guard cells. Following this idea, Medeiros *et al.* (2018) proposed that sucrose is not accumulated in the guard cells as an osmolyte but rather has an energetic role as shown using ^{13}C-sucrose labelling in *A. thaliana* guard cells. Complete labelling of fructose and most of the glucose after sucrose degradation in the guard cells was identified in Medeiros *et al.* (2018) study, evidencing high activity of both invertase and sucrose synthase in guard cells, followed by an increased in Glc1P content which enters glycolysis. Additionally, the higher ^{13}C enrichment in glutamic acid and glutamine indicates that sucrose degradation products are also substrates for the tricarboxylic acid (TCA) cycle during the light period in C_3 guard cells, associated with the diurnal opening of stomata.

The enrichment of TCA enzymes such ATPases, H^+-ATPase, malate dehydrogenase (NAD-MDH), pyruvate carboxylase (PC) and phosphoenolpyruvate carboxylases (PEPC) in the *K. fedtschenkoi* epidermis, agrees with the idea that mitochondrial respiration provides energy for stomatal processes. Additionally, similar 24h diel pattern for hexokinase (HXK), phosphofructokinase (PFK), pyruvate kinase (PK), ATPases (PMA) and open stomata (OST) indicates temporal changes occurring in CAM stomata compared to C_3. In *Agave*, nocturnal increases in malic acid, fumaric acid and $NADP^+$ content evidenced the higher mitochondrial activity associated with the nocturnal carbon fluxes in CAM (Abraham *et al.*, 2016). Together with the higher nocturnal energetic activity in *Agave*, the differences in *K. fedtschenkoi* protein turnover in the epidermis, lead to the hypothesis that temporal changes of TCA enzymes compared to C_3 might be implicated in the inverted stomatal rhythm in CAM. Further studies are necessary to elucidate the main metabolic processes responsible of energetic production during stomatal movements in CAM plants.

6.5. Conclusions

- The aim of this chapter was to present a comparative proteome subset from the Abraham *et al.* (submitted) study, between mesophyll and guard cell-enriched epidermis of *K. fedtschenkoi* to identify differentially expressed protein isoforms between mesophyll and epidermis and thereby indicate specialisation of functions in these tissues.

- The enrichment of proteins implicated in sugar metabolism, glycolysis and mitochondrial respiration in the epidermis confirm the importance of the energetic demands for stomatal

movement. Additionally, the presence of carboxylation/decarboxylation proteins in both epidermis and mesophyll tissues indicated the importance of PEPC-mediated CO_2 fixation to support CAM activity in the mesophyll and in guard cells to drive stomatal metabolism.

- Similar 24 h patterns of abundance were observed for most of the enzymes responsible for synthesis and degradation of starch in mesophyll and epidermis, accompanied by the enrichment of PHS and DPE isoforms in both mesophyll and epidermis. These findings support the hypothesis that starch degradation in CAM guard cells is not mediated via the hydrolytic pathway, which in C_3 plants is linked to blue light signalling. These substantial differences between CAM and the reports from C_3 plants indicate a reprogramming of starch metabolism in CAM guard cells, which underpins the inverted stomatal rhythm.

Chapter 7. General Discussion

Guard cell metabolism plays a key role in stomatal regulation and has been studied mainly in *Arabidopsis thaliana.* In C_3 plants, it is widely accepted that blue light is the main factor triggering diurnal stomatal opening with a key role for starch degradation in supplying osmolytes which act as counter ions for potassium to increase guard cells turgor pressure (Santelia and Lawson, 2016). The unique inverted stomatal rhythm of plants with crassulacean acid metabolism (CAM) enhances tolerance to arid environments and increases water use efficiency (WUE) compared to species with C_3 and C_4 photosynthesis (Yang *et al.*, 2015). Understanding stomatal regulation in CAM plants could provide the genetic tools for engineering CAM into non-CAM plants and thus improve crops productivity under drought conditions (Moseley *et al.*, 2019). This thesis aimed to test the hypothesis that starch metabolism has been re-programmed in CAM plants to enable stomatal opening at night.

7.1. Role of starch turnover in CAM activity and stomatal metabolism

The interrogation of RNA sequence datasets from *Kalanchoë fedtschenkoi* which compared transcript abundance between tissues (epidermis versus mesophyll), and between ages of leaves (young C_3 versus mature CAM) showed differential expression of genes related with starch and sugars metabolism that have been reported to influence stomatal behaviour in C_3 plants. For example, from genes implicated in starch degradation, α-glucan phosphorylase (*phs1*) was predominantly expressed in mesophyll and in CAM leaves, agreeing with Borland *et al.* (2016) and Shameer *et al.* (2018) that the main starch degradation pathway in CAM plants is the phosphorolytic route with a direct action of PHS1 to sustain nocturnal CO_2 fixation. On the other hand, genes reported to be specifically expressed in *Arabidopsis* guard cells (i.e. *amy3* and *bam1*) were more abundant in the mesophyll of *K. fedtschenkoi* RNAseq dataset, while *bam9*, a gene coding for β-amylase 9 was highly expressed in guard cell-enriched epidermis compared to mesophyll at the beginning of the night period in CAM performing leaves.

The substantial differences observed in the RNAseq data suggested a re-programming in guard cell starch metabolism in CAM plants, which might be responsible for their inverted stomatal behaviour. Following this idea, measurements of guard cell starch content over 24 hours in wild type plants of *Kalanchoë fedtschenkoi* showed that rather than being degraded at

the start of the day as in C_3, starch content increased in guard cells over the first part of the day and decreased at the beginning of the night (Chapter 3). This observation of an inverse pattern of starch turnover in CAM guard cells, together with the importance of starch for night-time CAM metabolism and for C_3 stomata, led to the characterisation of RNAi lines of *Kalanchoë fedtschenkoi* with a silenced expression of plastidic phosphoglucomutase (*rPGM1A*), plastidic α-glucan phosphorylase (*rPHS1*) and β-amylase 9 (*rBAM9*), respectively. This constituted a preliminary approach for the understanding of how starch metabolism influences the behaviour of CAM.

A decrease in nocturnal malate accumulation in the mesophyll of the RNAi lines, together with gas exchange analysis confirmed that curtailed starch metabolism affects CAM activity, evidenced by a diminution in nocturnal CO_2 uptake, demonstrating that starch is required to provide substrates for nocturnal phosphoenolpyruvate carboxylase (PEPC) activity. Similar results are reported by Cushman *et al.* (2008a) in a starchless *pgm* mutant of the facultative CAM species *Mesembryanthemum crystallinum* which accumulated less titratable acids overnight as a consequence of decreased CO_2 fixation and thus CAM activity. Similarly, stoichiometric analysis of the *KfPHS1* RNAi line in *K. fedtschenkoi* indicated that the inability to degrade starch during the night period reduced the production of PEP and the accumulation of malic acid (Ceusters *et al.*, submitted).

The decreased nocturnal CO_2 fixation in the RNAi lines was accompanied by a curtailed stomatal closure during the light period. In the case of *rPGM1a*, the higher accumulation of soluble sugars during the day indicated that an additional role for starch synthesis is to act as a sink for sugars in the guard cells, promoting diurnal stomatal closure. Similarly, the silencing of phosphorolytic starch degradation in the *rPHS1* line caused a re-routing to the hydrolytic pathway with production of maltose and accumulation of glucose, fructose and sucrose in the epidermis tissue during the light period. It is possible that this could result in an increase in the turgor pressure in guard cells, thereby curtailing day-time closure. Likewise, the over-accumulation of malate during the 24 h cycle in the epidermis tissue of *rPHS1* could be associated with curtailed day-time stomatal closure, and the higher content of soluble sugars could provide carbon substrates for malate synthesis. In the case of *rBAM9* line, higher contents of fructose, glucose and sucrose were also detected in both mesophyll and guard cell-enriched epidermis.

In addition to changes in both soluble sugars content and stomatal conductance during the day, increased transcript abundances of both sugars and malate transporters (*stp1* and *abcb14,* respectively) in the epidermis tissue were found for the RNAi lines during the first hours of

the day, while in wild type these transporters were highly abundant at the beginning of the night period. If transcript abundance is related to transporter activity then *stp1* and *abcb14* could enhance sugars and malate import to guard cells, increasing guard cell osmotic pressure and causing the day-time opening of stomata in the RNAi lines (Lawson *et al.*, 2014). Changes in sugar content could also be associated with the activity of sucrose synthases (SUSY), responsible for the interconversion of sucrose into fructose and UDP-glucose (Daloso *et al.*, 2016b). The higher expression of *susy3* in the epidermis tissue of the RNAi lines led to the hypothesis that effects on starch metabolism increase the sucrolytic activity of sucrose synthases and have a direct impact on stomatal conductance, allowing nocturnal stomatal opening but preventing stomatal closure during the light period. These findings agree with evidence provided by Daloso *et al.* (2016a) for the role of *susy3* role in C_3 stomatal opening, by the provision of C substrates for energy production and synthesis of organic acids that increase guard cells turgor pressure.

The importance of sugars in guard cell metabolism has been also stated by Medeiros *et al.* (2018) who suggest the importance of sucrose as an energetic provider in stomatal movement rather than being an osmolyte. Kelly *et al.* (2013) identified that the role of hexokinase (HXK) in tomato *Solanum lycopersicum* and *Arabidopsis thaliana* is to allow the closure of stomata in response to sucrose content. They suggest that sucrose is cleaved either in the apoplast or within guard cells and the produced hexoses are sensed by HXK to stimulate stomatal closure by a feedback-inhibition mechanism that leads to a reduced expression of photosynthetic genes in mesophyll and closure of stomata. However, the increased stomatal conductance and soluble sugars content in *Kalanchoë* RNAi lines, together with similar protein abundance for hexokinase over the 24 h cycle in wild type epidermis might suggest a different role of this enzyme in CAM stomatal regulation that needs to be further studied.

The increased abundance in the *K. fedtschenkoi* epidermis proteome of hexokinase (HXK), sucrose phosphate phosphatase (SPP), phosphofructokinase (PFK) and pyruvate kinase (PK) also confirms the importance of sugars in energy production in CAM stomata. Likewise, the detection of proteins/enzymes implicated in tricarboxylic acid (TCA) cycle, the presence of mitochondria in both guard cells and subsidiary cells (Chapter 6) and their absence from the epidermal pavement cells indicate that mitochondrial respiration is exclusive to the stomatal complex and their role might thus be associated with guard cell metabolism. This agrees with earlier studies in epidermal strips of *Commelina benghalensis* (Raghavendra, 1981) which indicated that stomatal opening is driven by energy produced from phosphorylation and

photophosphorylation due to the presence of numerous mitochondria and chloroplasts and the activity of TCA enzymes in C_3 guard cells.

7.2. Other findings related to the hypotheses of this thesis

7.2.1. Effect of light on CAM stomata

Based on the relationship between light and stomatal opening in C_3 plants and the inverted stomatal rhythm of CAM plants, one of the hypotheses of this thesis was that *Kalanchoë fedtschenkoi* stomata are unresponsive to light. Light imposition at night in both wild type and *rPGM1a* line showed that CAM stomata respond to both red and blue light, and the presence of starch is essential for the blue light response. An increase in stomatal conductance was observed for wild type plants under blue and red light, showing a synergistic effect of both wavelengths and a response from CAM stomata. In contrast, net CO_2 uptake did not change under the different light treatments.

According to Shimazaki *et al.* (2007), C_3 stomata respond to both blue and red light. Blue light activates the plasma membrane H^+-ATPase, hyperpolarising the membrane potential and activating potassium uptake through K^+ channels. Red light induces photosynthesis, lowering internal CO_2 concentrations which is thought to act as a signal for stomatal opening (Shimazaki *et al.*, 2007). Suetsugu *et al.* (2014) reported that the presence of weak blue light does not induce stomatal opening by itself, but together with red light greatly enhances the response of intact leaves of several plant species. It has also been reported that blue light stimulates the formation of malate, which serves as the negative counter ion for potassium ions in guard cells; this malate formation was synergistically enhanced by red light in epidermal peels of *Vicia faba* (Suetsugu *et al.*, 2014).

Tallman *et al.* (1997) reported blue-light insensitivity of stomata for the facultative CAM plant *Mesembryanthemum crystallinum*, suggesting that the shift from diurnal to nocturnal opening in CAM plants depends on regulatory mechanisms within the guard cells and that inhibition of zeaxanthin (blue-light photoreceptor) formation inhibits blue-light stomatal opening. Assmann and Shimazaki (1999) indicated that *M. crystallinum* has stomata with a normal blue-light response and a functioning xanthophyll cycle when in C_3 mode, but loses both blue-light responsiveness and light-stimulated zeaxanthin accumulation upon conversion to CAM mode. Nonetheless, the role of zeaxanthin in response to blue light in plants has not been completely elucidated and contradictory results have been published. Srivastava and Zeiger (1995) reported in *Vicia faba* that zeaxanthin acts as a guard cells photoreceptor

mediating stomatal opening in response to blue light. Using dithiothreitol (DTT), an inhibitor of zeaxanthin synthesis, Srivastava and Zeiger (1995) found that both stomatal response and phototropism induced by blue light were inhibited, without affecting the response to red light, suggesting that zeaxanthin is involved in guard cells and coleoptiles blue light reception. On the other side, Palmer *et al.* (1996) stated the lack of correlation between the content of zeaxanthin and phototropism, indicating that neither zeaxanthin nor any carotenoids are blue light receptors in maize coleoptiles. Similarly, recent studies have indicated that zeaxanthin does not influence the stomatal opening in response to blue light. It is case of *Arabidopsis thaliana* zeaxanthin-less mutants *npq1-2,* which had similar stomatal responses to blue and red light compared to wild type evidenced by gas exchange analysis (Eckert and Kaldenhoff, 2000) as well as H^+ pumping in response to blue light in guard cells protoplasts (Ueno *et al.*, 2005), leading to the conclusion that zeaxanthin is not the principal blue light receptor.

The identification of five different isoforms of phototropins (*phot*) in the RNAseq data that compared mesophyll and epidermis transcript expression, indicate a capacity for blue light responsiveness in *K. fedtschenkoi*. From these, two isoforms (KF110080, KF102250) were highly expressed in the mesophyll, two in the epidermis (KF00375 and KF104985) and one (KF139610) was similarly expressed in both tissues. Additionally, a transcript for the blue light signalling1 (*blus1*) protein kinase (KF90085) was also identified in the epidermis with an expression peak at the end of the day period. The higher expression at the beginning of the day of *phot1* (KF00375) and at dusk of *blus1* in the epidermis could be related with the opening of stomata during phase IV as a response to light, but again assuming that transcript expression is correlated with protein abundance (Appendix C). Nevertheless, the negligible detection of these light receptors in the protein dataset makes it difficult to conclude that the expression of light receptors are correlated with CAM phases or confirm Ceusters *et al.* (2014) suggestions about blue light inducing early morning (Phase II) stomatal opening.

Following this idea, Gotoh *et al.* (2018) investigated stomatal response to light in the obligate CAM species *Kalanchoë pinnata* and *Kalanchoë daigremontiana*, by the imposition of blue, red and blue/red light during the day-time phases II, III and IV. Gotoh *et al.* (2018) identified that during phase II the combination of blue and red light increased stomatal opening and prevented complete stomatal closure at phase III. Imposing both red and blue light independently did not affect stomatal closure in phase III, confirming the synergistic effect of red and blue lights on stomatal conductance. It is noteworthy that the magnitude of stomatal response to light in *K. daigremontiana* depended on the CAM phase and thus the internal CO_2 concentration (C_i) which was evidenced by a higher response in phase IV when

stomata are open (lower C_i), and a lower response during phases II and III when C_i is higher. Additionally, the same study showed that inhibition of guard cell plasma membrane H^+-ATPase confirmed that CAM stomata possess the same signal transduction cascade that allows the opening of C_3 stomata in response to blue light. Transcriptomic analysis in the CAM species *Ananas comosus* and *K. fedtschenkoi* by Yang *et al.* (2017) showed a temporal shift, from dawn to dusk, in the expression of phototropin *2 (phot2)* compared to *Arabidopsis*, which might suggest a possible contribution of PHOT2 in the opening of stomata at dusk. The results of this thesis agree with those findings, by the identification of phototropins and BLUS1 in the RNAseq data, as well as different H^+-ATPase isoforms in the epidermis proteome. However, the correlation of the light response with the inverted stomatal rhythm and the [C_i] changes in CAM is still unknown and needs further investigation.

In contrast to the stomatal conductance response, net CO_2 uptake increased only slightly under the imposition of blue/red light, suggesting that stomata are responsive to light changes but opening is constrained by internal CO_2 concentration and the availability of substrates to be carboxylated. According to Males and Griffiths (2017) during phase I mesophyll factors are more significant to nocturnal CO_2 assimilation than stomatal conductance, suggesting the importance of starch degradation for providing substrates to be carboxylated. These authors also suggest that mesophyll metabolism influences stomatal movements.

An alternative explanation of the net CO_2 uptake response is based on a study conducted by Nobel and Hartsock (1983), who concluded that higher intensities (560 μmol m^{-2} s^{-1}) of photosynthetically active radiation (PAR) during phase III inhibit net CO_2 uptake and the organic acids accumulation during the following night-time on the constitutive CAM *Opuntia ficus-indica.* Even though the current study imposed light treatments in the middle of the night period, the radiation applied was similar to the levels used by Nobel and Hartsock (1983) and might suggest that the higher radiation applied at night can have the same effect as if it were applied continuously during the day. In order to confirm this hypothesis and construct a robust knowledge of the effect of light in the nocturnal CO_2 uptake, further studies with different light treatments on the remaining CAM phases should be conducted.

7.2.2. Identification of sedoheptulose in K. fedtschenkoi mesophyll

The soluble sugars quantification showed an abundant presence of sedoheptulose in the mesophyll of wild type *K. fedtschenkoi*, accompanied by an enrichment of the enzyme sedoheptulose-1, 7-bisphosphatase (SBPase) in both transcriptomic (Chapter 3) and proteomic

datasets (Chapter 6). Sedoheptulose is a seven-carbon monosaccharide and has been identified in different plant species such as mango (*Mangifera indica*), papaya (*Carica papaya*), carrot (*Daucus carota*), and the CAM species *Hylotelephium spectabile* and *Kalanchoë pinnata* (Ogata *et al.*, 1972; Soria *et al.*, 2009; Ceusters *et al.*, 2013). Cowan (2017) indicated that seven-carbon sugars act as carbon sinks, metal chelators and are involved in the translocation of nutrients to fulfil the demand of nutrients for growth and development.

Despite sedoheptulose being the most abundant sugar in *K. fedtschenkoi* wild type plants, knowledge about its function in CAM plants is scarcely. Ceusters *et al.* (2013) proposed that the accumulation of sedoheptulose in *Kalanchoë pinnata* and *Sedum spectabile* contributes to both carbon and phosphorous homeostasis as an alternative carbon store under elevated CO_2 concentrations, in order to avoid sucrose accumulation and depletion of Pi. Additionally, sedoheptulose could serve as a cellular antioxidant taking into account that CAM plants generally inhabit environments with high solar radiations. Ceusters *et al.* (2013) indicated that free sedoheptulose is derived from the dephosphorylation of sedoheptulose1, 7-phosphate by the action of a cytosolic sedoheptulose 1, 7-phosphate phosphatase. However, to date it has not been possible to isolate this enzyme, indicating further studies are required to identify the proteins responsible for the synthesis of free sedoheptulose.

Since the evidence regarding activity and function of sedoheptulose-1, 7 phosphate phosphatase is negligible and most of the studies have been restricted to sedoheptulose 7-phosphate, this thesis focused on identifying the transcript expression and protein abundance of sedoheptulose-1,7-bisphosphatase (SBPase) in order to understand the role of sedoheptulose in CAM. SBPase is responsible for the conversion of sedoheptulose 1-7 bisphosphate to sedoheptulose 7-phosphate during the regeneration phase of the Calvin cycle (Raines *et al.*, 1999). Sedoheptulose 7-phosphate can also be converted to sedoheptulose + ADP by the enzyme sedoheptulokinase (Kardon *et al.*, 2008). Since the sequence of this last enzyme was not found in the *Kalanchoë fedtschenkoi* genome or in the RNAseq, and no matches with orthologous genes were found, the expression of sedoheptulose 1-7 bisphosphatase (*sbpase*) was studied and showed a higher expression in the mesophyll of *Kalanchoë* wild type compared to epidermis (Appendix C).

SBPase activity has been reported to influence photosynthetic capacity, growth, and tolerance to stress in plants. In tomato Ding *et al.* (2016) reported that the overexpression of SBPase increased the levels of sucrose and starch accumulation, improving growth and biomass content, suggesting that this enzymes is involved in the regulation of carbon assimilation in tomato plants. Similarly, the overexpression of SBPase in wheat resulted in an

increase on CO_2 assimilation, total biomass and total seed weight, stating at the same time, the higher potential to improve photosynthesis in important crops (Driever *et al.*, 2017).

Additionally, Feng *et al.* (2007) stated the importance of SBPase in the tolerance of photosynthesis to high temperatures in rice. This role for SBPase is based on the high sensitivity to higher temperatures by Rubisco activase and its consequences for Rubisco activity. Rubisco activase removes inhibitory sugar phosphates from the active site of Rubisco in the chloroplast stroma and at higher temperatures the content of Rubisco activase decreases affecting the CO_2 assimilation rate by Rubisco (Yang *et al.*, 2005). Feng *et al.* (2007) identified that overexpressing SBPase increases thermo tolerance of Rubisco activase by preventing the sequestration of Rubisco activase to the thylakoid membrane from the soluble stroma fraction under high temperature stress.

It can be speculated that sedoheptulose metabolism contributes to carbohydrate accumulation in CAM plants, taking into account the importance of starch and soluble sugars in the provision of substrates for nocturnal carboxylation. Besides, the identification of sedoheptulose-1,7-bisphosphatase (SBPase) in both the RNAseq data and in the mesophyll proteome on *K. fedtschenkoi* could indicate the importance of sedoheptulose metabolism in the improvement of photosynthesis efficiency under the higher temperatures, typically encountered by CAM, particularly during day-time phase III when stomata are closed. The development of future studies is necessary to test this hypothesis.

7.3. New perspectives and further work

This thesis is the first study of starch metabolism in CAM guard cells. In contrast to what is reported in C_3 species like *Arabidopsis thaliana*, diel starch turnover in guard cells of the constitutive CAM species *Kalanchoë fedtschenkoi* was similar to that in the mesophyll, with an accumulation during the day and a decrease at the beginning of the night. This finding led to the conclusion that starch metabolism in CAM plants has been re-programmed to allow the nocturnal opening of stomata. The lack of previous investigations about starch metabolism in CAM stomata lead to propose further studies to answer all the interrogations that could not be clarified in this thesis.

7.3.1. Role of mesophyll photosynthesis in stomatal behaviour

The first point would be to elucidate the contribution of the ground leaf mesophyll to guard cell metabolism. An innovative approach is the separation of the epidermis from the mesophyll and the 'grafting' of isolated epidermis onto the mesophyll of a different line to determine the contribution of the mesophyll to guard cell metabolism and behavior. Mott *et al.* (2008) investigated stomatal responses to light and CO_2 of isolated epidermis of *Tradescantia pallida*, *Vicia faba* and *Pisum sativum* as well as the importance of the ground mesophyll in this response. When the epidermis was removed from the mesophyll, no responses to light and CO_2 were identified in the three species. However, when the epidermis was transferred back to the mesophyll, either on the same or on a different species, the response was restored in *T. pallida* and *P. sativum*. Mott *et al.* (2008) concluded that the ground mesophyll is required for stomatal response to light and CO_2, known as the "mesophyll signal". A similar experiment performed by Fujita *et al.* (2013) in isolated epidermis of *Commelina communis* placed back on the mesophyll as response to changes in CO_2 concentration, indicated that stomatal opening is dependent on mesophyll photosynthesis and the "mesophyll signal" moves from the mesophyll to the epidermis via the aqueous phase in the apoplast, however this metabolite needs to be elucidated.

In CAM it is thought that changes in the internal CO_2 concentration as result of diel malate turnover in mesophyll influences the opening and closure of stomata. Additionally, based on the widely accepted idea that malate is the main counter ion for K^+ during stomatal opening in C_3 plants, a possible connection between malate turnover in CAM mesophyll and stomatal movement is suggested with a direct role for the guard cell malate importer ABCB14. Changes in stomatal conductance and expression of the malate transporter *abcb14* support this hypothesis. In line with this idea, stomata in the various RNAi lines studied in this thesis were unable to close during the day, and this was accompanied by a higher transcript abundance of *abcb14* at dawn in the epidermis, contrary to wild type higher expression at dusk. If transcript abundance is related to transporter activity then *abcb14* could enhance malate import to guard cells, thereby increasing osmotic pressure and causing the opening of stomata (Lawson *et al.*, 2014). This accumulation of malate in the mesophyll and its transport to guard cells may be an important point that connects metabolism in the ground mesophyll to stomatal regulation in CAM photosynthesis, thus further studies in isolated epidermis could elucidate this connection.

Having RNAi lines of *Kalanchoë fedtschenkoi* as a resource for CAM research, transferring the epidermis to wild type mesophyll and vice versa will give new insights about

stomatal behaviour. For instance, placing the epidermis of the starchless *rPGM1a* line onto a wild type mesophyll and hypothesizing a total contribution of mesophyll in guard cells, it might be predicted that a completely altered stomatal response/closure during the day-time would be found in the RNAi line, similar to wild type. On the contrary, if guard cells were autonomous, the higher accumulation of sugars observed during the 24 h in the epidermis of *rPGM1a* would maintain stomatal opening during the day as observed in Chapter 4.

7.3.2. Development of new RNAi lines to understand stomatal behaviour

The development of new RNAi lines is an alternative to increase the understanding of stomatal behaviour in CAM plants. The RNAseq interrogation, the real time qPCR transcript evaluation and the development of a proteome dataset, all comparing mesophyll and guard cell-enriched epidermis constitute valuable resources for exploring the inverted stomatal rhythm in *K. fedtschenkoi*. Recently, Moseley *et al.* (2019) performed an investigation of genes related to stomatal metabolism via PaperBLAST, by the identification of annotations not related to stomata but linked to stomatal processes. Using the proteome of 13 species, including monocots and dicots species performing C_3 and CAM photosynthesis, they created a database of protein sequences linked to published studies. Using transcriptomic data, they identified orthologues between *K. fedtschenkoi* and the C_3 species *Arabidopsis thaliana* and *Solanum lycopersicum* to identify rescheduled gene expression in CAM compared with C_3. These results obtained by Moseley *et al.* (2019) have increased the information about CAM stomata and are a valuable tool for the selection of candidate genes implicated in stomatal metabolism, facilitating the development of new RNAi lines for further studies.

Based on the results obtained in this thesis and following the idea of the interconnection between mesophyll and guard cells, the development of RNAi lines with guard cell –specific silencing of key transporters would help prove if guard cells metabolism can drive the opening of stomata. The ABCB14 malate transporter and both the hexose and sucrose importers, SUC and STP1, respectively, are good candidates to test this hypothesis. Evaluating different lines with affectation in the guard cells import of sugars and organic acids, will allow the study of the contribution of guard cells metabolism in the production of sugars and organic acids to support stomatal movement, not only in CAM but also in C_3 plants. This considering the C_3 evidence of starch degradation in guard cells to provide malate and sugars as osmolytes in the opening of stomata (Horrer *et al.*, 2016) as well as the higher accumulation of sugars in the epidermis of *K. fedtschenkoi* RNAi lines and the enrichment of

proteins implicated in sugars metabolism and mitochondria respiration in the epidermis proteome.

As a complement to the study of starch metabolism in CAM stomata, the creation and further study of lines with silencing of the hydrolytic enzymes β-amylases 1 and 3 (BAM1 and BAM3), implicated in starch degradation in both guard cells and mesophyll of C_3 plants, respectively could be informative. Taking into account the predominance of the phosphorolytic degradation of starch in both mesophyll and guard cells-enriched epidermis (Chapter 5), as well as the enrichment of PHS1 in both tissues (Chapter 6), silencing the hydrolytic pathway will help to understand the contribution of this pathway in CAM and confirm if starch degradation in guard cells is performed only by the phosphorolytic route.

7.3.3. Engineering inverted stomatal behaviour into non-CAM plants

The engineering of the inverted stomatal rhythm of CAM into non-CAM species offers the potential to increase water use efficiency (WUE) of important crops for human consumption and thus the productivity under arid environments. At night, CAM stomata are thought to open in response to reduced C_i caused by the consumption of CO_2 by PEPC and the accumulation of malate. According to Niechayev *et al.* (2019) to successfully engineer the CAM stomatal rhythm into non CAM, it is required that the host species have guard cells fully responsive to changes in CO_2 concentration that allows the nocturnal stomatal opening and the diurnal closure.

A first approach in the modification of *Arabidopsis* stomatal conductance has been done by Lim *et al.* (2019) overexpressing independently genes implicated in both the carboxylation and decarboxylation modules of the facultative CAM species *Mesembryanthemum crystallinum*. Transgenic lines overexpressing the carboxylation enzymes phosphoenolpyruvate carboxylase 1 (PEPC1), NAD^+ malate dehydrogenase (NAD^+ MDH), NADP malate dehydrogenase (NADP-MDH) and phosphoenolpyruvate carboxylase kinase (PPCK1), respectively, showed increased stomatal conductance compared to the control line, as a possible response to higher organic acid accumulation, mainly malate, evidenced by titratable acidity (TA). In contrast, the lines overexpressing the decarboxylation module enzymes such as NAD-malic enzyme 1 and 2 (NAD-ME1, NAD-ME2), and NADP-malic enzyme (NADP-ME) showed decreased stomatal conductance and showed depletion in organic acids content. Additionally, the presence of carboxylation/decarboxylation proteins in both epidermis and mesophyll tissues (Chapter 6) indicated the importance of PEPC-mediated

CO_2 fixation to support CAM activity in the mesophyll and in guard cells to drive stomatal metabolism. These results together with those obtained by Lim *et al.* (2019) provide insights about the main contribution of carboxylation/decarboxylation enzymes in the unique CAM stomatal behaviour and its possible engineering into non-CAM species.

Apart from the carboxylation and decarboxylation modules, engineering starch turnover in C_3 guard cells with an increased content during the day followed by degradation at beginning of the night, as observed in this study for *K. fedtschenkoi* will confirm if the re-programming of starch metabolism in guard cells is critical for the inverted stomatal rhythm in CAM plants. In the same way, based on the different starch degradation pathways in the mesophyll that CAM and C_3 follow, a re-routing to the phosphorolytic pathway in C_3 species will contribute to understanding how this pathway affects stomatal behaviour as a possible provider of substrates in the synthesis of nocturnal amino acids that can act as osmolytes in the guard cells. To achieve this, it is also necessary to elucidate if differences in both guard cells and mesophyll starch turnover in CAM are under circadian regulation, and if this altered clock control has to be engineered into C_3 plants to allow the inverted stomatal rhythm.

7.4. Final conclusions and key findings

- This thesis aimed to test the hypothesis that starch metabolism has been re-programmed in CAM plants to enable stomatal opening at night. The biochemical and genetic characterisation of *K. fedtschenkoi* wild type plants together with the RNAi lines *rPGM1a*, *rPHS1* and *rBAM9*, constituted a preliminary approach for the understanding of starch metabolism and its implications for stomatal regulation in CAM plants.

- Measurements of guard cell starch content in wild type over 24 hours showed for first time that starch degradation in the guard cells of a CAM plant differs from that in C_3 plants, which rather than being degraded at the start of the day as in *Arabidopsis*, showed an increment over the first part of the day. It is thought that the diurnal guard cell starch synthesis promotes diurnal stomatal closure, acting as a sink for sugars, demonstrated by the higher accumulation of soluble sugars in the RNAi lines during the day, providing substrates for guard cell osmolytes or energy production during the light period, which impedes the stomatal closure and generate a C_3-like metabolism.

- The silencing of *phs1* up-regulates the hydrolytic pathway of starch degradation in both mesophyll and guard cell-enriched epidermis, evidenced by the accumulation of maltose and glucose and increased transcript abundance of genes implicated in the hydrolytic pathway. Despite potentially higher hydrolytic activity, starch degradation and CAM activity was curtailed in the *rPHS1* line, indicating that CAM relies predominantly on the phosphorolytic route of starch degradation for production of PEP at night.

- The evaluation of the *rBAM9* line silencing suggested a regulatory function for *bam9* on starch turnover in *K. fedtschenkoi*, evidenced by the opposing starch content in mesophyll and guard cells, affecting both synthesis and degradation of starch, and these mechanisms differed between tissues. The similarities found in the protein sequence of BAM9 in *K. fedtschenkoi* and *Arabidopsis*, suggest a similar regulatory function of this enzyme for starch turnover in CAM and C_3 plants.

- Similarity in the protein abundance pattern of most of the enzymes responsible for synthesis and degradation of starch between mesophyll and epidermis, together with the enrichment of PHS and DPE isoforms in both mesophyll and epidermis, confirms the importance of the phosphorolytic degradation of starch in CAM and supports the idea of a reprogramming of starch metabolism in CAM guard cells responsible for the inverted stomatal rhythm.

- The results obtained in this thesis open the possibility of new studies about the main factors driving the inverted stomatal metabolism in CAM plants and the potential engineering of CAM into C_3 species to enhance water use efficiency.

References

Abraham, P., Adams, R., Giannone, R.J., Kalluri, U., Ranjan, P., Erickson, B., Shah, M., Tuskan, G.A. and Hettich, R.L. (2012) 'Defining the Boundaries and Characterizing the Landscape of Functional Genome Expression in Vascular Tissues of Populus using Shotgun Proteomics', *Journal of Proteome Research*, 11(1), pp. 449-460.

Abraham, P., Hurtado-Castano, N., Cowan-Turner, D., Barnes, J.D., Suresh, P., Hettich, R.L., Santelia, D. and Borland, A.M. (submitted) 'Peeling back the layers of Crassulacean Acid Metabolism: Functional differentiation between *Kalanchoe fedtschenkoi* epidermis and mesophyll proteomes', *The Plant Journal*.

Abraham, P.E., Yin, H., Borland, A.M., Weighill, D., Lim, S.D., De Paoli, H.C., Engle, N., Jones, P.C., Agh, R., Weston, D.J., Wullschleger, S.D., Tschaplinski, T., Jacobson, D., Cushman, J.C., Hettich, R.L., Tuskan, G.A. and Yang, X. (2016) 'Transcript, protein and metabolite temporal dynamics in the CAM plant Agave', *Nature Plants*, 2, p. 16178.

Acharya, B.R., Jeon, B.W., Zhang, W. and Assmann, S.M. (2013) 'Open Stomata 1 (OST1) is limiting in abscisic acid responses of Arabidopsis guard cells', *New Phytologist*, 200(4), pp. 1049-1063.

Andriotis, V.M., Pike, M.J., Bunnewell, S., Hills, M.J. and Smith, A.M. (2010) 'The plastidial glucose-6-phosphate/phosphate antiporter GPT1 is essential for morphogenesis in *Arabidopsis* embryos', *The Plant Journal*, 64(1), pp. 128-39.

Antunes, W.C., Provart, N.J., Williams, T.C.R. and Loureiro, M.E. (2011) 'Changes in stomatal function and water use efficiency in potato plants with altered sucrolytic activity', *Plant, Cell & Environment*, 35(4), pp. 747-759.

Araújo, W.L., Fernie, A.R. and Nunes-Nesi, A. (2011) 'Control of stomatal aperture: A renaissance of the old guard', *Plant Signaling & Behavior*, 6(9), pp. 1305-1311.

Arndt, C., Koristka, S., Bartsch, H. and Bachmann, M. (2012) 'Native Polyacrylamide Gels', in Kurien, B.T. and Scofield, R.H. (eds.) *Protein Electrophoresis*. Humana Press, pp. 49-53.

Asatsuma, S., Sawada, C., Itoh, K., Okito, M., Kitajima, A. and Mitsui, T. (2005) 'Involvement of α-Amylase I-1 in Starch Degradation in Rice Chloroplasts', *Plant and Cell Physiology*, 46(6), pp. 858-869.

Assmann, S.M. and Shimazaki, K. (1999) 'The Multisensory Guard Cell. Stomatal Responses to Blue Light and Abscisic Acid', *Plant Physiology*, 119(3), pp. 809-16.

Aubry, S., Aresheva, O., Reyna-Llorens, I., Smith-Unna, R.D., Hibberd, J.M. and Genty, B. (2016) 'A Specific Transcriptome Signature for Guard Cells from the C4 Plant *Gynandropsis gynandra*', *Plant physiology*, 170(3), pp. 1345-1357.

Azoulay-Shemer, T., Palomares, A., Bagheri, A., Israelsson-Nordstrom, M., Engineer, C.B., Bargmann, B.O.R., Stephan, A.B. and Schroeder, J.I. (2015) 'Guard cell photosynthesis is critical for stomatal turgor production, yet does not directly mediate CO_2- and ABA-induced stomatal closing', *The Plant Journal*, 83(4), pp. 567-581.

Azoulay-Shemer, T., Schwankl, N., Rog, I., Moshelion, M. and Schroeder, J.I. (2018) 'Starch biosynthesis by AGPase, but not starch degradation by BAM1/3 and SEX1, is rate-limiting for CO2-regulated stomatal movements under short-day conditions', *FEBS Letters*, 592(16), pp. 2739-2759.

Bahaji, A., Li, J., Sánchez-López, Á.M., Baroja-Fernández, E., Muñoz, F.J., Ovecka, M., Almagro, G., Montero, M., Ezquer, I., Etxeberria, E. and Pozueta-Romero, J. (2014) 'Starch biosynthesis, its regulation and biotechnological approaches to improve crop yields', *Biotechnology Advances*, 32(1), pp. 87-106.

Baroja-Fernández, E., Muñoz, F.J., Montero, M., Etxeberria, E., Sesma, M.T., Ovecka, M., Bahaji, A., Ezquer, I., Li, J., Prat, S. and Pozueta-Romero, J. (2009) 'Enhancing sucrose synthase activity in transgenic potato (*Solanum tuberosum* L.) tubers results in increased levels of starch, ADP glucose and UDP glucose and total yield', *Plant and Cell Physiology*, 50(9), pp. 1651-1662.

Barrera Zambrano, V.A., Lawson, T., Olmos, E., Fernandez-Garcia, N. and Borland, A.M. (2014) 'Leaf anatomical traits which accommodate the facultative engagement of crassulacean acid metabolism in tropical trees of the genus *Clusia*', *Journal of Experimental Botany*, 65(13), pp. 3513-23.

Bates, G.W., Rosenthal, D.M., Sun, J., Chattopadhyay, M., Peffer, E., Yang, J., Ort, D.R. and Jones, A.M. (2012) 'A comparative study of the *Arabidopsis thaliana* guard-cell transcriptome and its modulation by sucrose', *PLoS One*, 7(11), p. e49641.

Beaulieu, J.M., Leitch, I.J., Patel, S., Pendharkar, A. and Knight, C.A. (2008) 'Genome size is a strong predictor of cell size and stomatal density in angiosperms', *New Phytologist*, 179(4), pp. 975-986.

Bertolino, L.T., Caine, R.S. and Gray, J.E. (2019) 'Impact of Stomatal Density and Morphology on Water-Use Efficiency in a Changing World', *Frontiers in Plant Science*, 10(225).

Bieniawska, Z., Paul Barratt, D.H., Garlick Andrew, P., Thole, V., Kruger Nicholas, J., Martin, C., Zrenner, R. and Smith Alison, M. (2007) 'Analysis of the sucrose synthase gene family in *Arabidopsis*', *The Plant Journal*, 49(5), pp. 810-828.

Borland, A.M., Barrera Zambrano, V.A., Ceusters, J. and Shorrock, K. (2011) 'The photosynthetic plasticity of crassulacean acid metabolism: an evolutionary innovation for sustainable productivity in a changing world', *New Phytologist*, 191, pp. 619-633.

Borland, A.M., Griffiths, H., Hartwell, J. and Smith, J.A.C. (2009) 'Exploiting the potential of plants with crassulacean acid metabolism for bioenergy production on marginal lands', *Journal of Experimental Botany*, 60(10), pp. 2879-96.

Borland, A.M., Guo, H.-B., Yang, X. and Cushman, J.C. (2016) 'Orchestration of carbohydrate processing for crassulacean acid metabolism', *Current Opinion in Plant Biology*, 31, pp. 118-124.

Borland, A.M., Hartwell, J., Weston, D.J., Schlauch, K., Tschaplinski, T.J., Tuskan, G.A., Yang, X. and Cushman, J.C. (2014) 'Engineering crassulacean acid metabolism to improve water-use efficiency', *Trends in Plant Science*, 19(5), pp. 327-338.

Borland, A.M., Leverett, A., Hurtado-Castano, N., Hu, R. and Yang, X. (2018) 'Functional Anatomical Traits of the Photosynthetic Organs of Plants with Crassulacean Acid Metabolism', in Adams Iii, W.W. and Terashima, I. (eds.) *The Leaf: A Platform for Performing Photosynthesis*. Cham: Springer International Publishing, pp. 281-305.

Borland, A.M. and Taybi, T. (2004) 'Synchronization of metabolic processes in plants with Crassulacean acid metabolism', *Journal of Experimental Botany*, 55(400), pp. 1255-1265.

Borland, A.M., Wullschleger, S.D., Weston, D.J., Hartwell, J., Tuskan, G.A., Yang, X. and Cushman, J.C. (2015) 'Climate-resilient agroforestry: physiological responses to climate change and engineering of crassulacean acid metabolism (CAM) as a mitigation strategy', *Plant Cell Environ*, 38(9), pp. 1833-49.

Boutet, E., Lieberherr, D., Tognolli, M., Schneider, M., Bansal, P., Bridge, A.J., Poux, S., Bougueleret, L. and Xenarios, I. (2016) 'UniProtKB/Swiss-Prot, the manually annotated section of the UniProt knowledge base: How to use the entry view', in Edwards, D. (ed.) *Plant Bioinformatics: Methods and Protocols*. New York, NY: Springer New York, pp. 23-54.

Boxall, S.F., Dever, L.V., Kneřová, J., Gould, P.D. and Hartwell, J. (2017) 'Phosphorylation of Phosphoenolpyruvate Carboxylase Is Essential for Maximal and Sustained Dark CO_2 Fixation and Core Circadian Clock Operation in the Obligate Crassulacean Acid Metabolism Species Kalanchoe fedtschenkoi', *The Plant Cell*, 29(10), p. 2519.

Boxall, S.F., Foster, J.M., Bohnert, H.J., Cushman, J.C., Nimmo, H.G. and Hartwell, J. (2005) 'Conservation and Divergence of Circadian Clock Operation in a Stress-Inducible Crassulacean Acid Metabolism Species Reveals Clock Compensation against Stress', *Plant Physiology*, 137, pp. 969-982.

Boxall, S.F., Kadu, N., Dever, L.V., Kneřová, J., Waller, J.L., Gould, P.J.D. and Hartwell, J. (2019) 'Silencing hosphoenolpyruvate carboxylase 1 in the obligate crassulacean acid metabolism species *Kalanchoë laxiflora* causes reversion to C_3-like metabolism and amplifies rhythmicity in a subset of core circadian clock genes', *bioRxiv*, p. 684050.

Bräutigam, A., Schlüter, U., Eisenhut, M. and Gowik, U. (2017) 'On the Evolutionary Origin of CAM Photosynthesis', *Plant physiology*, 174(2), pp. 473-477.

Buttner, M. (2007) 'The monosaccharide transporter(-like) gene family in *Arabidopsis*', *FEBS Letters*, 581(12), pp. 2318-24.

Caspar, T., Huber, S.C. and Somerville, C. (1985) 'Alterations in growth, photosynthesis, and respiration in a starchless mutant of *Arabidopsis thaliana* (L.) deficient in chloroplast phosphoglucomutase activity', *Plant Physiology*, 79(1), pp. 11-17.

Ceusters, J., Borland, A.M., Taybi, T., Frans, M., Godts, C. and De Proft, M.P. (2014) 'Light quality modulates metabolic synchronization over the diel phases of crassulacean acid metabolism', *Journal of Experimental Botany*, 65(13), pp. 3705-14.

Ceusters, J., Godts, C., Peshev, D., Vergauwen, R., Dyubankova, N., Lescrinier, E., De Proft, M.P. and Van den Ende, W. (2013) 'Sedoheptulose accumulation under CO_2 enrichment in leaves of *Kalanchoë pinnata:* a novel mechanism to enhance C and P homeostasis?', *Journal of Experimental Botany*, 64(6), pp. 1497-1507.

Ceusters, N., Ceusters, J., Hurtado-Castano, N., Barnes, J.D., Dever, L.V., Boxall, S.F., Kneřová, J., Hartwell, J. and Borland, A.M. (submitted) 'Degrading leaf starch via plastidic α-glucan phosphorylase optimises plant growth and water use efficiency over the diel phases of Crassulacean acid metabolism', *Journal of Experimental Botany*.

Chandler, J.W., Apel, K. and Melzer, S. (2001) 'A novel putative β-amylase gene and ATβ-Amy from Arabidopsis thaliana are circadian regulated', *Plant Science*, 161(5), pp. 1019-1024.

Conesa, A., Gotz, S., Garcia-Gomez, J.M., Terol, J., Talon, M. and Robles, M. (2005) 'Blast2GO: a universal tool for annotation, visualization and analysis in functional genomics research', *Bioinformatics*, 21(18), pp. 3674-6.

Cotelle, V., Pierre, J.-N. and Vavasseur, A. (1999) 'Potential strong regulation of guard cell phosphoenolpyruvate carboxylase through phosphorylation', *Journal of Experimental Botany*, 50(335), pp. 777-783.

Cousins, A.B., Baroli, I., Badger, M.R., Ivakov, A., Lea, P.J., Leegood, R.C. and von Caemmerer, S. (2007) 'The role of phosphoenolpyruvate carboxylase during C_4 photosynthetic isotope exchange and stomatal conductance', *Plant physiology*, 145(3), pp. 1006-1017.

Cowan, A.K. (2017) 'Occurrence, metabolism, transport and function of seven-carbon sugars', *Phytochemistry Reviews*, 16(1), pp. 137-157.

Cushman, J.C. (2001) 'Crassulacean Acid Metabolism. A Plastic Photosynthetic Adaptation to Arid Environments', *Plant Physiology*, 127, pp. 1439-1448.

Cushman, J.C., Agarie, S., Albion, R.L., Elliot, S.M., Taybi, T. and Borland, A.M. (2008a) 'Isolation and characterization of mutants of common ice plant deficient in crassulacean acid metabolism', *Plant Physiology*, 147, pp. 228-238.

Cushman, J.C., Davis, S.C., Yang, X. and Borland, A.M. (2015) 'Development and use of bioenergy feedstocks for semi-arid and arid lands', *Journal of Experimental Botany*, 66(14), pp. 4177-4193.

Cushman, J.C., Tillett, R.L., Wood, J.A., Branco, J.M. and Schlauch, K.A. (2008b) 'Large-scale mRNA expression profiling in the common ice plant, *Mesembryanthemum crystallinum*, performing C_3 photosynthesis and Crassulacean acid metabolism (CAM)', *Journal of Experimental Botany*, 59(7), pp. 1875-1894.

Daloso, D.M., Antunes, W.C., Pinheiro, D.P., Waquim, J.P., Araujo, W.L., Loureiro, M.E., Fernie, A.R. and Williams, T.C. (2015) 'Tobacco guard cells fix CO_2 by both Rubisco and PEPcase while sucrose acts as a substrate during light-induced stomatal opening', *Plant Cell Environ*, 38(11), pp. 2353-71.

Daloso, D.M., Dos Anjos, L. and Fernie, A.R. (2016a) 'Roles of sucrose in guard cell regulation', *New Phytologist*, 211(3), pp. 809-18.

Daloso, D.M., Medeiros, D.B., Dos Anjos, L., Yoshida, T., Araujo, W.L. and Fernie, A.R. (2017) 'Metabolism within the specialized guard cells of plants', *New Phytologist*, 216(4), pp. 1018-1033.

Daloso, D.M., Williams, T.C., Antunes, W.C., Pinheiro, D.P., Muller, C., Loureiro, M.E. and Fernie, A.R. (2016b) 'Guard cell-specific upregulation of sucrose synthase 3 reveals that the role of sucrose in stomatal function is primarily energetic', *New Phytologist*, 209(4), pp. 1470-83.

Davies, E.J., Tetlow, I.J., Bowsher, C.G. and Emes, M.J. (2003) 'Molecular and biochemical characterization of cytosolic phosphoglucomutase in wheat endosperm (*Triticum aestivum* L. cv. Axona)', *Journal of Experimental Botany*, 54(386), pp. 1351-60.

Davis, S.C., Simpson, J., Gil Vega, K.d.C., Niechayev, N.A., Tongerlo, E.v., Hurtado-Castano, N., Dever, L.V. and Búrquez, A. (2019) 'Undervalued potential of crassulacean acid metabolism for current and future agricultural production', *Journal of Experimental Botany*.

de Faria, A.P.G., Vieira, A.C.M. and Wendt, T. (2012) 'Leaf anatomy and its contribution to the systematics of Aechmea subgenus Macrochordion (de Vriese) Baker (Bromeliaceae)', *Anais da Academia Brasileira de Ciências*, 84, pp. 961-971.

Déjardin, A., Sokolov, L.N. and Kleczkowski, L.A. (1999) 'Sugar/osmoticum levels modulate differential abscisic acid-independent expression of two stress-responsive sucrose synthase genes in Arabidopsis', *The Biochemical journal*, 344 Pt 2(Pt 2), pp. 503-509.

Dever, L.V., Boxall, S.F., Knerova, J. and Hartwell, J. (2015) 'Transgenic Perturbation of the Decarboxylation Phase of Crassulacean Acid Metabolism Alters Physiology and Metabolism But Has Only a Small Effect on Growth', *Plant Physiology*, 167(1), pp. 44-59.

Ding, F., Wang, M., Zhang, S. and Ai, X. (2016) 'Changes in SBPase activity influence photosynthetic capacity, growth, and tolerance to chilling stress in transgenic tomato plants', *Scientific reports*, 6, pp. 32741-32741.

Dodd, A.N., Griffiths, H., Taybi, T., Cushman, J.C. and Borland, A.M. (2003) 'Integrating diel starch metabolism with the circadian and environmental regulation of Crassulacean acid metabolism in Mesembryanthemum crystallinum', *Planta*, 216(5), pp. 789-97.

Doheny-Adams, T., Hunt, L., Franks, P.J., Beerling, D.J. and Gray, J.E. (2012) 'Genetic manipulation of stomatal density influences stomatal size, plant growth and tolerance to restricted water supply across a growth carbon dioxide gradient', *Philosophical Transactions of the Royal Society of London B: Biological Sciences*, 367(1588), pp. 547-555.

Driever, S.M., Simkin, A.J., Alotaibi, S., Fisk, S.J., Madgwick, P.J., Sparks, C.A., Jones, H.D., Lawson, T., Parry, M.A.J. and Raines, C.A. (2017) 'Increased SBPase activity improves

photosynthesis and grain yield in wheat grown in greenhouse conditions', *Philosophical Transactions of the Royal Society B: Biological Sciences*, 372(1730).

Dubois, M., Gilles, K., Hamilton, J., Rebus, P. and Smith, F. (1956) 'Colorimetric Method for Determination of Sugars and Related Substances', *Analytical Chemistry*, 28, pp. 350-356.

Eckert, M. and Kaldenhoff, R. (2000) 'Light-induced stomatal movement of selected *Arabidopsis thaliana* mutants', *Journal of Experimental Botany*, 51(349), pp. 1435-1442.

Edner, C., Li, J., Albrecht, T., Mahlow, S., Hejazi, M., Hussain, H., Kaplan, F., Guy, C., Smith, S.M., Steup, M. and Ritte, G. (2007) 'Glucan, Water Dikinase Activity Stimulates Breakdown of Starch Granules by Plastidial β-Amylases', *Plant Physiology*, 145(1), pp. 17-28.

Egli, B., Kolling, K., Kohler, C., Zeeman, S.C. and Streb, S. (2010) 'Loss of cytosolic phosphoglucomutase compromises gametophyte development in Arabidopsis', *Plant Physiology*, 154(4), pp. 1659-71.

Eisenach, C. and De Angeli, A. (2017) 'Ion transport at the vacuole during stomatal movements', *Plant Physiology*, 174(2), pp. 520-530.

Emanuelsson, O., Brunak, S., von Heijne, G. and Nielsen, H. (2007) 'Locating proteins in the cell using TargetP, SignalP and related tools', *Nature Protocols*, 2, p. 953.

Feng, L., Wang, K., Li, Y., Tan, Y., Kong, J., Li, H., Li, Y. and Zhu, Y. (2007) 'Overexpression of SBPase enhances photosynthesis against high temperature stress in transgenic rice plants', *Plant Cell Reports*, 26(9), pp. 1635-1646.

Fernie, A.R. and Martinoia, E. (2009) 'Malate. Jack of all trades or master of a few?', *Phytochemistry*, 70(7), pp. 828-32.

Fernie, A.R., Roessner, U., Trethewey, R.N. and Willmitzer, L. (2001) 'The contribution of plastidial phosphoglucomutase to the control of starch synthesis within the potato tuber', *Planta*, 213(3), pp. 418-426.

Fettke, J., Hejazi, M., Smirnova, J., Höchel, E., Stage, M. and Steup, M. (2009) 'Eukaryotic starch degradation: integration of plastidial and cytosolic pathways', *Journal of Experimental Botany*, 60(10), pp. 2907-2922.

Fettke, J., Nunes-Nesi, A., Alpers, J., Szkop, M., Fernie, A.R. and Steup, M. (2008) 'Alterations in cytosolic glucose-phosphate metabolism affect structural features and biochemical properties of starch-related heteroglycans', *Plant Physiology*, 148(3), pp. 1614-29.

Flütsch, S., Distefano, L. and Santelia, D. (2018) 'Quantification of starch in guard cells of *Arabidopsis thaliana*', *Bio-protocol*, 8(13), p. e2920.

Franks, P.J., Drake, P.L. and Beerling, D.J. (2009) 'Plasticity in maximum stomatal conductance constrained by negative correlation between stomatal size and density: an analysis using Eucalyptus globulus', *Plant, Cell & Environment*, 32, pp. 1737-1748.

Fujita, T., Noguchi, K. and Terashima, I. (2013) 'Apoplastic mesophyll signals induce rapid stomatal responses to CO_2 in *Commelina communis*', *New Phytol*, 199(2), pp. 395-406.

Fulton, D.C., Stettler, M., Mettler, T., Vaughan, C.K., Li, J., Francisco, P., Gil, M., Reinhold, H., Eicke, S., Messerli, G., Dorken, G., Halliday, K., Smith, A.M., Smith, S.M. and Zeeman, S.C. (2008) 'β-AMYLASE4, a noncatalytic protein required for starch breakdown, acts upstream of three active β-Amylases in *Arabidopsis* chloroplasts', *The Plant Cell*, 20(4), p. 1040.

Gehrig, H., Gaußmann, O., Marx, H., Schwarzott, D. and Kluge, M. (2001) 'Molecular phylogeny of the genus *Kalanchoe* (Crassulaceae) inferred from nucleotide sequences of the ITS-1 and ITS-2 regions', *Plant Science*, 160(5), pp. 827-835.

Gotoh, E., Oiwamoto, K., Inoue, S.-i., Shimazaki, K.-i. and Doi, M. (2018) 'Stomatal response to blue light in crassulacean acid metabolism plants *Kalanchoe pinnata* and *Kalanchoe daigremontiana*', *Journal of Experimental Botany*, 70(4), pp. 1367-1374.

Haider, M.S., Barnes, J.D., Cushman, J.C. and Borland, A.M. (2012) 'A CAM- and starch-deficient mutant of the facultative CAM species *Mesembryanthemum crystallinum* reconciles

sink demands by repartitioning carbon during acclimation to salinity', *Journal of Experimental Botany*, 63(5), pp. 1985-1996.

Hartwell, J., Dever, L.V. and Boxall, S.F. (2016) 'Emerging model systems for functional genomics analysis of Crassulacean acid metabolism', *Current Opinion in Plant Biology*, 31, pp. 100-108.

Häusler, R.E., Baur, B., Scharte, J., Teichmann, T., Eicks, M., Fischer, K.L., Flugge, U.-I., Schubert, S., Weber, A. and Fischer, K. (2000) 'Plastidic metabolite transporters and their physiological functions in the inducible crassulacean acid metabolism plant *Mesembryanthemum crystallinum*', *The Plant Journal*, 24(3), pp. 285-296.

Hetherington, A.M. and Woodward, F.I. (2003) 'The role of stomata in sensing and driving environmental change', *Nature*, 424(6951), pp. 901-908.

Heyduk, K., McKain, M.R., Lalani, F. and Leebens-Mack, J. (2016) 'Evolution of a CAM anatomy predates the origins of Crassulacean acid metabolism in the Agavoideae (Asparagaceae)', *Mol Phylogenet Evol*, 105, pp. 102-113.

Heyduk, K., Ray, J.N., Ayyampalayam, S., Moledina, N., Borland, A., Harding, S.A., Tsai, C.J. and Leebens-Mack, J. (2019) 'Shared expression of Crassulacean acid metabolism (CAM) genes predates the origin of CAM in the genus Yucca', *J Exp Bot*.

Hite, D.R.C., Outlaw Jr, W.H. and Tarczynski, M.C. (1993) 'Elevated Levels of Both Sucrose-Phosphate Synthase and Sucrose Synthase in Vicia Guard Cells Indicate Cell-Specific Carbohydrate Interconversions', *Plant Physiology*, 101(4), p. 1217.

Hohorst, H.J. (1970) 'L-malate estimation with malate dehydrogenase and NAD', in Bergmeyer, H.V. (ed.) *Methods in enzymatic analysis*. Weinheim, Germany: Verlag Chemie, pp. 1544-1548.

Honda, H., Akagi, H. and Shimada, H. (2000) 'An isozyme of the NADP-malic enzyme of a CAM plant, Aloe arborescens, with variation on conservative amino acid residues', *Gene*, 243(1), pp. 85-92.

Horrer, D., Flütsch, S., Pazmino, D., Matthews, Jack S.A., Thalmann, M., Nigro, A., Leonhardt, N., Lawson, T. and Santelia, D. (2016) 'Blue light Induces a distinct starch degradation pathway in guard cells for stomatal opening', *Current Biology*, 26(3), pp. 362-370.

Hou, J., Zhang, H., Liu, J., Reid, S., Liu, T., Xu, S., Tian, Z., Sonnewald, U., Song, B. and Xie, C. (2017) 'Amylases StAmy23, StBAM1 and StBAM9 regulate cold-induced sweetening of potato tubers in distinct ways', *Journal of experimental botany*, 68(9), pp. 2317-2331.

Hubbard, K.E., Hotta, C.T., Gardner, M.J., Baek, S.J., Dalchau, N., Dontamala, S., Dodd, A.N. and Webb, A.A.R. (2007) 'Circadian Rhythms in Stomata: Physiological and Molecular Aspects', in Mancuso, S. and Shabala, S. (eds.) *Rhythms in Plants: Phenomenology, Mechanisms, and Adaptive Significance*. Verlag Berlin Heidelberg: Springer, pp. XX, 361.

Inoue, S.-i. and Kinoshita, T. (2017) 'Blue light regulation of stomatal opening and the plasma membrane $H^{(+)}$-ATPase', *Plant Physiology*, 174(2), pp. 531-538.

Kang, Y.-N., Adachi, M., Utsumi, S. and Mikami, B. (2004) 'The Roles of Glu186 and Glu380 in the Catalytic Reaction of Soybean β-Amylase', *Journal of Molecular Biology*, 339(5), pp. 1129-1140.

Kang, Y.-N., Tanabe, A., Adachi, M., Utsumi, S. and Mikami, B. (2005) 'Structural Analysis of Threonine 342 Mutants of Soybean β-Amylase: Role of a Conformational Change of the Inner Loop in the Catalytic Mechanism', *Biochemistry*, 44(13), pp. 5106-5116.

Kardon, T., Stroobant, V., Veiga-da-Cunha, M. and Schaftingen, E.V. (2008) 'Characterization of mammalian sedoheptulokinase and mechanism of formation of erythritol in sedoheptulokinase deficiency', *FEBS Lett*, 582(23-24), pp. 3330-4.

Karimi, M., Inzé, D. and Depicker, A. (2002) 'GATEWAY™ vectors for Agrobacterium-mediated plant transformation', *Trends in Plant Science*, 7(5), pp. 193-195.

Kearse, M., Moir, R., Wilson, A., Stones-Havas, S., Cheung, M., Sturrock, S., Buxton, S., Cooper, A., Markowitz, S., Duran, C., Thierer, T., Ashton, B., Meintjes, P. and Drummond, A. (2012) 'Geneious Basic: An integrated and extendable desktop software platform for the organization and analysis of sequence data', *Bioinformatics*, 28(12), pp. 1647-1649.

Kelly, G., Moshelion, M., David-Schwartz, R., Halperin, O., Wallach, R., Attia, Z., Belausov, E. and Granot, D. (2013) 'Hexokinase mediates stomatal closure', *The Plant Journal*, 75(6), pp. 977-988.

Kore-Eda, S., Nozawa, A., Okada, Y., Takashi, K., Azad, M.A.K., Ohnishi, J.-i., Nishiyama, Y. and Tozawa, Y. (2013) 'Characterization of the plastidic phosphate translocators in the inducible Crassulacean Acid Metabolism plant *Mesembryanthemum crystallinum*', *Bioscience, Biotechnology, and Biochemistry*, 77(7), pp. 1511-1516.

Laporte, M.M., Shen, B. and Tarczynski, M.C. (2002) 'Engineering for drought avoidance: expression of maize NADP-malic enzyme in tobacco results in altered stomatal function', *Journal of Experimental Botany*, 53(369), pp. 699-705.

Lasceve, G., Leymarie, J. and Vavasseur, A. (1997) 'Alterations in light-induced stomatal opening in a starch-deficient mutant of *Arabidopsis thaliana* L. deficient in chloroplast phosphoglucomutase activity', *Plant, Cell & Environment*, 20(3), pp. 350-358.

Lawson, T. and Blatt, M.R. (2014) 'Stomatal Size, Speed, and Responsiveness Impact on Photosynthesis and Water Use Efficiency', *Plant Physiology*, 164(4), pp. 1556-1570.

Lawson, T. and Morison, J.I.L. (2004) 'Stomatal function and physiology', in A.R., H. and I, P. (eds.) *The Evolution of Plant Physiology; from whole plants to ecosystem*. United States: Elsevier Academic Press, pp. 217-242.

Lawson, T., Simkin, A.J., Kelly, G. and Granot, D. (2014) 'Mesophyll photosynthesis and guard cell metabolism impacts on stomatal behaviour', *New Phytologist*, 203(4), pp. 1064-81.

Lawson, T., Terashima, I., Fujita, T. and Wang, Y. (2018) 'Coordination Between Photosynthesis and Stomatal Behavior', in Adams Iii, W.W. and Terashima, I. (eds.) *The Leaf: A Platform for Performing Photosynthesis*. Cham: Springer International Publishing, pp. 141-161.

Lee, J.S. (2010) 'Stomatal opening mechanism of CAM plants', *Journal of Plant Biology*, 53(1), pp. 19-23.

Lee, M., Choi, Y., Burla, B., Kim, Y.Y., Jeon, B., Maeshima, M., Yoo, J.Y., Martinoia, E. and Lee, Y. (2008) 'The ABC transporter AtABCB14 is a malate importer and modulates stomatal response to CO_2', *Nature Cell Biology*, 10(10), pp. 1217-23.

Li, J., Francisco, P., Zhou, W., Edner, C., Steup, M., Ritte, G., Bond, C.S. and Smith, S.M. (2009) 'Catalytically-inactive β-amylase BAM4 required for starch breakdown in Arabidopsis leaves is a starch-binding-protein', *Archives of Biochemistry and Biophysics*, 489(1), pp. 92-98.

Li, J., Zhou, W., Francisco, P., Wong, R., Zhang, D. and Smith, S.M. (2017) 'Inhibition of Arabidopsis chloroplast β-amylase BAM3 by maltotriose suggests a mechanism for the control of transitory leaf starch mobilisation', *PLOS ONE*, 12(2), p. e0172504.

Lim, S.D., Lee, S., Choi, W.-G., Yim, W.C. and Cushman, J.C. (2019) 'Laying the Foundation for Crassulacean Acid Metabolism (CAM) Biodesign: Expression of the C4 Metabolism Cycle Genes of CAM in Arabidopsis', *Frontiers in Plant Science*, 10(101).

Liu, D., Palla, K.J., Hu, R., Moseley, R.C., Mendoza, C., Chen, M., Abraham, P.E., Labbé, J.L., Kalluri, U.C., Tschaplinski, T.J., Cushman, J.C., Borland, A.M., Tuskan, G.A. and Yang, X. (2018) 'Perspectives on the basic and applied aspects of crassulacean acid metabolism (CAM) research', *Plant Science*, 274, pp. 394-401.

Livak, K.J. and Schmittgen, T.D. (2001) 'Analysis of Relative Gene Expression Data Using Real-Time Quantitative PCR and the $2^{-\Delta\Delta CT}$ Method', *Methods*, 25(4), pp. 402-408.

MacNeill, G.J., Mehrpouyan, S., Minow, M.A.A., Patterson, J.A., Tetlow, I.J. and Emes, M.J. (2017) 'Starch as a source, starch as a sink: the bifunctional role of starch in carbon allocation', *Journal of Experimental Botany*, 68(16), pp. 4433-4453.

Males, J. and Griffiths, H. (2017) 'Stomatal biology of CAM Plants', *Plant Physiology*, 174(2), p. 550.

Malinova, I., Mahlow, S., Alseekh, S., Orawetz, T., Fernie, A.R., Baumann, O., Steup, M. and Fettke, J. (2014) 'Double Knockout Mutants of Arabidopsis Grown under Normal Conditions Reveal that the Plastidial Phosphorylase Isozyme Participates in Transitory Starch Metabolism', *Plant Physiology*, 164(2), pp. 907-921.

Medeiros, D.B., Perez Souza, L., Antunes, W.C., Araújo, W.L., Daloso, D.M. and Fernie, A.R. (2018) 'Sucrose breakdown within guard cells provides substrates for glycolysis and glutamine biosynthesis during light-induced stomatal opening', *The Plant Journal*, 94(4), pp. 583-594.

Meyer, S., Mumm, P., Imes, D., Endler, A., Weder, B., Al-Rasheid, K.A., Geiger, D., Marten, I., Martinoia, E. and Hedrich, R. (2010) 'AtALMT12 represents an R-type anion channel required for stomatal movement in *Arabidopsis* guard cells', *The Plant Journal*, 63(6), pp. 1054-62.

Ming, R., VanBuren, R., Wai, C.M., Tang, H., Schatz, M.C., Bowers, J.E., Lyons, E., Wang, M.-L., Chen, J., Biggers, E., Zhang, J., Huang, L., Zhang, L., Miao, W., Zhang, J., Ye, Z., Miao, C., Lin, Z., Wang, H., Zhou, H., Yim, W.C., Priest, H.D., Zheng, C., Woodhouse, M., Edger, P.P., Guyot, R., Guo, H.-B., Guo, H., Zheng, G., Singh, R., Sharma, A., Min, X., Zheng, Y., Lee, H., Gurtowski, J., Sedlazeck, F.J., Harkess, A., McKain, M.R., Liao, Z., Fang, J., Liu, J., Zhang, X., Zhang, Q., Hu, W., Qin, Y., Wang, K., Chen, L.-Y., Shirley, N., Lin, Y.-R., Liu, L.-Y., Hernandez, A.G., Wright, C.L., Bulone, V., Tuskan, G.A., Heath, K., Zee, F., Moore, P.H., Sunkar, R., Leebens-Mack, J.H., Mockler, T., Bennetzen, J.L., Freeling, M., Sankoff, D., Paterson, A.H., Zhu, X., Yang, X., Smith, J.A.C., Cushman, J.C., Paull, R.E. and Yu, Q. (2015) 'The pineapple genome and the evolution of CAM photosynthesis', *Nat Genet*, advance online publication.

Misra, B.B., Acharya, B.R., Granot, D., Assmann, S.M. and Chen, S. (2015) 'The guard cell metabolome: functions in stomatal movement and global food security', *Frontiers in Plant Science*, 6, p. 334.

Monja-Mio, K.M., Pool, F.B., Herrera, G.H., EsquedaValle, M. and Robert, M.L. (2015) 'Development of the stomatal complex and leaf surface of *Agave angustifolia* Haw. 'Bacanora' plantlets during the in vitro to ex vitro transition process', *Scientia Horticulturae*, 189, pp. 32-40.

Monroe, J.D. and Storm, A.R. (2018) 'Review: The Arabidopsis beta-amylase (BAM) gene family: Diversity of form and function', *Plant Sci*, 276, pp. 163-170.

Moreira, N.S., Nascimento, L.B.S., Leal-Costa, M.V. and Tavares, E.S. (2012) 'Comparative anatomy of leaves of *Kalanchoe pinnata* and *K. crenata* in sun and shade conditions, as a support for their identification', *Revista Brasileira de Farmacognosia*, 22, pp. 929-936.

Moseley, R.C., Tuskan, G.A. and Yang, X. (2019) 'Comparative Genomics Analysis Provides New Insight Into Molecular Basis of Stomatal Movement in Kalanchoë fedtschenkoi', *Frontiers in Plant Science*, 10(292).

Mott, K.A., Gibson, A.C. and O'Leary, J.W. (1982) 'The adaptive significance of amphistomatic leaves', *Plant, Cell & Environment*, 5(6), pp. 455-460.

Mott, K.A., Sibbernsen, E.D. and Shope, J.C. (2008) 'The role of the mesophyll in stomatal responses to light and CO_2', *Plant, Cell & Environment*, 31(9), pp. 1299-306.

Neuhaus, H.E. and Schulte, N. (1996) 'Starch degradation in chloroplasts isolated from C3 or CAM (crassulacean acid metabolism)-induced *Mesembryanthemum crystallinum* L', *Biochemical Journal*, 318(3), pp. 945-953.

Niechayev, N.A., Pereira, P.N. and Cushman, J.C. (2019) 'Understanding trait diversity associated with crassulacean acid metabolism (CAM)', *Current Opinion in Plant Biology*, 49, pp. 74-85.

Nobel, P.S. and Hartsock, T.L. (1983) 'Relationships between photosynthetically active radiation, nocturnal acid accumulation, and CO_2 uptake for a crassulacean acid metabolism plant, *Opuntia ficus-indica*', *Plant Physiology*, 71(1), p. 71.

Ogata, J.N., Kawano, Y., Bevenue, A. and Casarett, L.J. (1972) 'The ketoheptose content of some tropical fruits', *J Agric Food Chem*, 20(1), pp. 113-5.

Palmer, J.M., Warpeha, K.M. and Briggs, W.R. (1996) 'Evidence that zeaxanthin is not the photoreceptor for phototropism in maize coleoptiles', *Plant physiology*, 110(4), pp. 1323-1328.

Pfaffl, M.W. (2006) 'Relative quantification', in Dorak, M.T. (ed.) *Real-time PCR*. Newcastle-upon-Tyne, UK: Taylor & Francis, p. 333.

Pfister, B. and Zeeman, S.C. (2016) 'Formation of starch in plant cells', *Cellular and Molecular Life Sciences*, 73(14), pp. 2781-2807.

Raghavendra, A.S. (1981) 'Energy Supply for Stomatal Opening in Epidermal Strips of *Commelina benghalensis*', *Plant Physiology*, 67(2), pp. 385-387.

Raines, C.A., Lloyd, J.C. and Dyer, T.A. (1999) 'New insights into the structure and function of sedoheptulose-1,7-bisphosphatase; an important but neglected Calvin cycle enzyme', *Journal of Experimental Botany*, 50(330), pp. 1-8.

Santelia, D. and Lawson, T. (2016) 'Rethinking guard cell metabolism', *Plant Physiology*, 172(3), p. 1371.

Santelia, D. and Lunn, J.E. (2017) 'Transitory starch metabolism in guard cells: unique features for a unique function', *Plant Physiology*.

Sasaki, T., Mori, I.C., Furuichi, T., Munemasa, S., Toyooka, K., Matsuoka, K., Murata, Y. and Yamamoto, Y. (2010) 'Closing plant stomata requires a homolog of an aluminum-activated malate transporter', *Plant and Cell Physiology*, 51(3), pp. 354-65.

Satoh, H., Shibahara, K., Tokunaga, T., Nishi, A., Tasaki, M., Hwang, S.-K., Okita, T.W., Kaneko, N., Fujita, N., Yoshida, M., Hosaka, Y., Sato, A., Utsumi, Y., Ohdan, T. and Nakamura, Y. (2008) 'Mutation of the Plastidial α-Glucan Phosphorylase Gene in Rice Affects the Synthesis and Structure of Starch in the Endosperm', *The Plant Cell*, 20(7), pp. 1833-1849.

Schneider, C.A., Rasband, W.S. and Eliceiri, K.W. (2012) 'NIH Image to ImageJ: 25 years of image analysis', *Nature Methods*, 9, p. 671.

Schoor, S., Lung, S.-C., Sigurdson, D. and Chuong, S.D.X. (2015) 'Fluorescent Staining of Living Plant Cells', in Yeung, E.C.T., Stasolla, C., Sumner, M.J. and Huang, B.Q. (eds.) *Plant Microtechniques and Protocols*. Cham: Springer International Publishing, pp. 153-165.

Shameer, S., Baghalian, K., Cheung, C.Y.M., Ratcliffe, R.G. and Sweetlove, L.J. (2018) 'Computational analysis of the productivity potential of CAM', *Nature Plants*, 4(3), pp. 165-171.

Shimazaki, K.-i., Doi, M., Assmann, S.M. and Kinoshita, T. (2007) 'Light regulation of stomatal movement', *Annual Review of Plant Biology*, 58(1), pp. 219-247.

Shrestha, R.L., Dhakal, D.D., Gautum, D.M., Paudyal, K.P. and Shrestha, S. (2012) 'Variation of Physiochemical Components of Acid Lime (<i>Citrus aurantifolia</i> Swingle) Fruits at Different Sides of the Tree in Nepal', *American Journal of Plant Sciences*, Vol.03No.12, p. 5.

Silver, D.M., Kötting, O. and Moorhead, G.B.G. (2014) 'Phosphoglucan phosphatase function sheds light on starch degradation', *Trends in Plant Science*, 19(7), pp. 471-478.

Simon, N.M.L., Comben, N.E., Hetherington, A.M. and Dodd, A.N. (2019) 'A significant role for the circadian clock in the long-term water use efficiency of Arabidopsis', *bioRxiv*, p. 583526.

Smith, A.M. (2012) 'Starch in the *Arabidopsis* plant', *Starch - Stärke*, 64(6), pp. 421-434.

Smith, A.M., Zeeman, S.C. and Smith, S.M. (2005) 'Starch degradation', *Annual Review of Plant Biology*, 56(1), pp. 73-98.

Soria, A.C., Sanz, M.L. and Villamiel, M. (2009) 'Determination of minor carbohydrates in carrot (Daucus carota L.) by GC–MS', *Food Chemistry*, 114(2), pp. 758-762.

Srivastava, A. and Zeiger, E. (1995) 'The inhibitor of zeaxanthin formation, dithiothreitol, inhibits blue-light-stimulated stomatal opening in *Vicia faba*', *Planta*, 196(3), pp. 450-457.

Stadler, R., Büttner, M., Ache, P., Hedrich, R., Ivashikina, N., Melzer, M., Shearson, S.M., Smith, S.M. and Sauer, N. (2003) 'Diurnal and Light-Regulated Expression of AtSTP1 in Guard Cells of *Arabidopsis*', *Plant Physiology*, 133(2), p. 528.

Stastna, M. and Van Eyk, J.E. (2012) 'Analysis of protein isoforms: can we do it better?', *Proteomics*, 12(19-20), pp. 2937-2948.

Steidle, E.A. (2010) *Investigation of the role of BAM9 in starch metabolism in Arabidopsis thaliana*. James Madison University [Online]. Available at: https://commons.lib.jmu.edu/master201019/384.

Stitt, M. and Zeeman, S.C. (2012) 'Starch turnover: pathways, regulation and role in growth', *Current Opinion in Plant Biology*, 15(3), pp. 282-292.

Streb, S. and Zeeman, S.C. (2012) 'Starch metabolism in *Arabidopsis*', *The Arabidopsis Book*, p. e0160.

Suetsugu, N., Takami, T., Ebisu, Y., Watanabe, H., Iiboshi, C., Doi, M. and Shimazaki, K.-i. (2014) 'Guard cell chloroplasts are essential for blue light-dependent stomatal opening in *Arabidopsis*', *PLoS ONE*, 9(9), p. e108374.

Talbott, L.D. and Zeiger, E. (1993) 'Sugar and organic acid accumulation in guard cells of *Vicia faba* in response to red and blue Light', *Plant Physiology*, 102(4), pp. 1163-1169.

Talbott, L.D. and Zeiger, E. (1996) 'Central roles for potassium and sucrose in guard-cell osmoregulation', *Plant Physiology*, 111(4), p. 1051.

Tallman, G., Zhu, J.X., Mawson, B.T., Amodeo, G., Nouhi, Z., Levy, K. and Zeiger, E. (1997) 'Induction of CAM in Mesembryanthemum crystallinum Abolishes the Stomatal Response to Blue Light and Light-Dependent Zeaxanthin Formation in Guard Cell Chloroplasts', *Plant and Cell Physiology*, 38(3), pp. 236-242.

Tetlow, I.J., Morell, M.K. and Emes, M.J. (2004) 'Recent developments in understanding the regulation of starch metabolism in higher plants', *Journal of Experimental Botany*, 55(406), pp. 2131-2145.

Thalmann, M. and Santelia, D. (2017) 'Starch as a determinant of plant fitness under abiotic stress', *New Phytologist*, 214(3), pp. 943-951.

Ueno, K., Kinoshita, T., Inoue, S.-i., Emi, T. and Shimazaki, K.-i. (2005) 'Biochemical Characterization of Plasma Membrane H+-ATPase Activation in Guard Cell Protoplasts of Arabidopsis thaliana in Response to Blue Light', *Plant and Cell Physiology*, 46(6), pp. 955-963.

Valerio, C., Costa, A., Marri, L., Issakidis-Bourguet, E., Pupillo, P., Trost, P. and Sparla, F. (2011) 'Thioredoxin-regulated beta-amylase (BAM1) triggers diurnal starch degradation in guard cells, and in mesophyll cells under osmotic stress', *J Exp Bot*, 62(2), pp. 545-55.

Wai, C.M., VanBuren, R., Zhang, J., Huang, L., Miao, W., Edger, P.P., Yim, W.C., Priest, H.D., Meyers, B.C., Mockler, T., Smith, J.A.C., Cushman, J.C. and Ming, R. (2017) 'Temporal and spatial transcriptomic and microRNA dynamics of CAM photosynthesis in pineapple', *The Plant Journal*, 92(1), pp. 19-30.

Weber, A., Servaites, J.C., Geiger, D.R., Kofler, H., Hille, D., Groner, F., Hebbeker, U. and Flugge, U.I. (2000) 'Identification, purification, and molecular cloning of a putative plastidic glucose translocator', *Plant Cell*, 12(5), pp. 787-802.

Weise, S.E., Schrader, S.M., Kleinbeck, K.R. and Sharkey, T.D. (2006) 'Carbon balance and circadian regulation of hydrolytic and phosphorolytic breakdown of transitory starch', *Plant physiology*, 141(3), pp. 879-886.

Weise, S.E., van Wijk, K.J. and Sharkey, T.D. (2011) 'The role of transitory starch in C3, CAM, and C4 metabolism and opportunities for engineering leaf starch accumulation', *Journal of Experimental Botany*, 62(9), pp. 3109-3118.

Wilmer, C. and Fricker, M. (1996) *Stomata*. London, UK: Chapman & Hall.

Winter, K. (2019) 'Ecophysiology of constitutive and facultative CAM photosynthesis', *Journal of Experimental Botany*.

Winter, K., Garcia, M. and Holtum, J.A. (2008) 'On the nature of facultative and constitutive CAM: environmental and developmental control of CAM expression during early growth of Clusia, Kalanchoe and Opuntia', *Journal of Experimental Botany*, 59(7), pp. 1829-40.

Xu, X., Dees, D., Dechesne, A., Huang, X.-F., Visser, R.G.F. and Trindade, L.M. (2017) 'Starch phosphorylation plays an important role in starch biosynthesis', *Carbohydrate Polymers*, 157, pp. 1628-1637.

Yang, X., Cushman, J.C., Borland, A.M., Edwards, E.J., Wullschleger, S.D., Tuskan, G.A., Owen, N.A., Griffiths, H., Smith, J.A.C., De Paoli, H.C., Weston, D.J., Cottingham, R., Hartwell, J., Davis, S.C., Silvera, K., Ming, R., Schlauch, K., Abraham, P., Stewart, J.R., Guo, H.-B., Albion, R., Ha, J., Lim, S.D., Wone, B.W.M., Yim, W.C., Garcia, T., Mayer, J.A., Petereit, J., Nair, S.S., Casey, E., Hettich, R.L., Ceusters, J., Ranjan, P., Palla, K.J., Yin, H., Reyes-García, C., Andrade, J.L., Freschi, L., Beltrán, J.D., Dever, L.V., Boxall, S.F.,

Waller, J., Davies, J., Bupphada, P., Kadu, N., Winter, K., Sage, R.F., Aguilar, C.N., Schmutz, J., Jenkins, J. and Holtum, J.A.M. (2015) 'A roadmap for research on crassulacean acid metabolism (CAM) to enhance sustainable food and bioenergy production in a hotter, drier world', *New Phytologist*, 207, pp. 491-504.

Yang, X., Hu, R., Yin, H., Jenkins, J., Shu, S., Tang, H., Liu, D., Weighill, D.A., Cheol Yim, W., Ha, J., Heyduk, K., Goodstein, D.M., Guo, H.-B., Moseley, R.C., Fitzek, E., Jawdy, S., Zhang, Z., Xie, M., Hartwell, J., Grimwood, J., Abraham, P.E., Mewalal, R., Beltrán, J.D., Boxall, S.F., Dever, L.V., Palla, K.J., Albion, R., Garcia, T., Mayer, J.A., Don Lim, S., Man Wai, C., Peluso, P., Van Buren, R., De Paoli, H.C., Borland, A.M., Guo, H., Chen, J.-G., Muchero, W., Yin, Y., Jacobson, D.A., Tschaplinski, T.J., Hettich, R.L., Ming, R., Winter, K., Leebens-Mack, J.H., Smith, J.A.C., Cushman, J.C., Schmutz, J. and Tuskan, G.A. (2017) 'The *Kalanchoë* genome provides insights into convergent evolution and building blocks of crassulacean acid metabolism', *Nature Communications*, 8(1), p. 1899.

Yang, X., Liang, Z. and Lu, C. (2005) 'Genetic Engineering of the Biosynthesis of Glycinebetaine Enhances Photosynthesis against High Temperature Stress in Transgenic Tobacco Plants', *Plant Physiology*, 138(4), p. 2299.

Yu, T.-S., Zeeman, S.C., Thorneycroft, D., Fulton, D.C., Dunstan, H., Lue, W.-L., Hegemann, B., Tung, S.-Y., Umemoto, T., Chapple, A., Tsai, D.-L., Wang, S.-M., Smith, A.M., Chen, J. and Smith, S.M. (2005) 'α-Amylase Is Not Required for Breakdown of Transitory Starch in Arabidopsis Leaves', *Journal of Biological Chemistry*, 280(11), pp. 9773-9779.

Zeeman, S.C., Kossmann, J. and Smith, A.M. (2010) 'Starch: Its Metabolism, Evolution, and Biotechnological Modification in Plants', *Annual Review of Plant Biology*, 61(1), pp. 209-234.

Zeeman, S.C., Northrop, F., Smith, A.M. and Rees, T.a. (1998) 'A starch-accumulating mutant of Arabidopsis thaliana deficient in a chloroplastic starch-hydrolysing enzyme', *The Plant Journal*, 15(3), pp. 357-365.

Zeeman, S.C., Smith, S.M. and Smith, A.M. (2004a) 'The breakdown of starch in leaves', *New Phytologist*, 163(2), pp. 247-261.

Zeeman, S.C., Thorneycroft, D., Schupp, N., Chapple, A., Weck, M., Dunstan, H., Haldimann, P., Bechtold, N., Smith, A.M. and Smith, S.M. (2004b) 'Plastidial alpha-glucan

phosphorylase is not required for starch degradation in Arabidopsis leaves but has a role in the tolerance of abiotic stress', *Plant Physiology*, 135(2), pp. 849-58.

Zhang, J., Liu, J. and Ming, R. (2014) 'Genomic analyses of the CAM plant pineapple', *Journal of Experimental Botany*, 65(13), pp. 3395-3404.

Zhang, L., Chen, F., Zhang, G.-Q., Zhang, Y.-Q., Niu, S., Xiong, J.-S., Lin, Z., Cheng, Z.-M. and Liu, Z.-J. (2016) 'Origin and mechanism of crassulacean acid metabolism in orchids as implied by comparative transcriptomics and genomics of the carbon fixation pathway', *The Plant Journal*, 86(2), pp. 175-185.

Zhang, S.Q., Outlaw, W.H. and Chollet, R. (1994) 'Lessened malate inhibition of guard-cell phosphoenolpyruvate carboxylase velocity during stomatal opening', *FEBS Letters*, 352(1), pp. 45-48.

Zhu, M., Dai, S., McClung, S., Yan, X. and Chen, S. (2009) 'Functional differentiation of *Brassica napus* guard cells and mesophyll cells revealed by comparative proteomics', *Mol Cell Proteomics*, 8(4), pp. 752-66.

Appendix A. Sampling optimisation

A.1. Effect of leaf age on CAM activity and carbohydrates content

Based on the ontogenetic change from C_3 to CAM of the constitutive species *Kalanchoë fedtschenkoi* with a C_3-like metabolism of the youngest leaves and an obligate CAM cycle in mature leaves (Winter *et al.*, 2008), leaves of different ages were characterised in order to select the most appropriate for the biochemical, physiological and genetic evaluations performed throughout this thesis. This preliminary characterisation helped to address the following hypothesis:

Hypothesis: The different leaf ages determine CAM activity, measured as titratable acidity, soluble sugars content and starch content in the mesophyll, as well as the starch granules area in stomatal guard cells.

A.1.1. Materials and Methods

Following the growth and sampling conditions mentioned in Section 2.1 (Chapter 2), five biological replicates per time were sampled from younger (pair 3), middle age (pair 6) and mature leaves (pair 8) of *Kalanchoë fedtschenkoi* wild type plants. Whole leaves were harvested at dawn (8:30) and dusk (20:30), exactly when the lights turned on and off, respectively.

Following the methods described in Section 2.1 (Chapter 2), a methanol extraction was performed separating both supernatant and pellet. CAM activity on supernatant extract was determined via titratable acid analysis with NaOH 0.005 mM, measuring the acidity produced by the presence of organic acids (Cushman *et al.*, 2008a; Shrestha *et al.*, 2012), using the following equation:

$$Acidity = \frac{\left(A \times B \times C / Sample\ volume\right) \times 1000}{fwt}$$

Equation A. 1. Calculation of acidity (mmol H^+ g^{-1} fwt) in leaf mesophyll. A is volume of titrate, B is concentration of titrate, C is milliequivalent factor, and fwt is the fresh weight of tissue.

The supernatant obtained from the methanol extracts was also used to determine the soluble sugars content in the leaf mesophyll by the colorimetric phenol/sulphuric acid test described in Section 2.2 (Chapter 2). The sugar content (µmol Glc g^{-1} fwt) was calculated as follows:

$$Soluble\ sugars\ content = \frac{\left(\left(\frac{A}{G}/180\right) \times DF\right)}{fwt}$$

Equation A. 2. Soluble sugars content (µmol g^{-1} fwt) in leaf mesophyll. A is absorbance, G is gradient of line calculated from calibration curve, DF is dilution factor (amount of sample used divided by total volume of water, phenol and sulphuric acid added), and fwt is the fresh weight of tissue.

For quantifying starch content in mesophyll, phenol/sulphuric acid test was performed to quantify glucose equivalents from starch degradation as described in Section 2.2 (Chapter 2). Additionally, to measure starch in guard cells the epidermis were stained with Lugol's iodine solution and starch granule area was measure as indicated in Appendix B.

The significant differences in all the biochemical measurements over time were determined as indicated in Section 2.10 (Chapter 2).

A.1.2. Key findings

Comparisons between dawn and dusk showed an accumulation of acidity overnight in the three leaf ages, representing the typical CAM behaviour, characterised by organic acids accumulation during the night (malic acid and/or citric acid) and the decarboxylation in the following light period. This turnover is also represented by the accumulation of soluble sugars and starch during the day as a product of malate decarboxylation and their depletion at night to serve as substrates for nocturnal CO_2 assimilation (Figure A. 1). In contrast, no significant differences were found in starch granule area in guard cells between dawn and dusk indicating little day/night turnover of this carbohydrate in the stomatal complex (Figure A. 2 and Figure A. 3).

Interestingly, no differences in acidity and carbohydrates turnover in the mesophyll were found among the three different pairs of leaves, which means that leaves of the ages selected present a similar CAM activity and carbohydrates content in mesophyll. However, leaf pair six was chosen for further analyses because the guard cells presented well-defined starch granules which facilitates their quantification, and the leaf area was suitable for future gas exchange analysis.

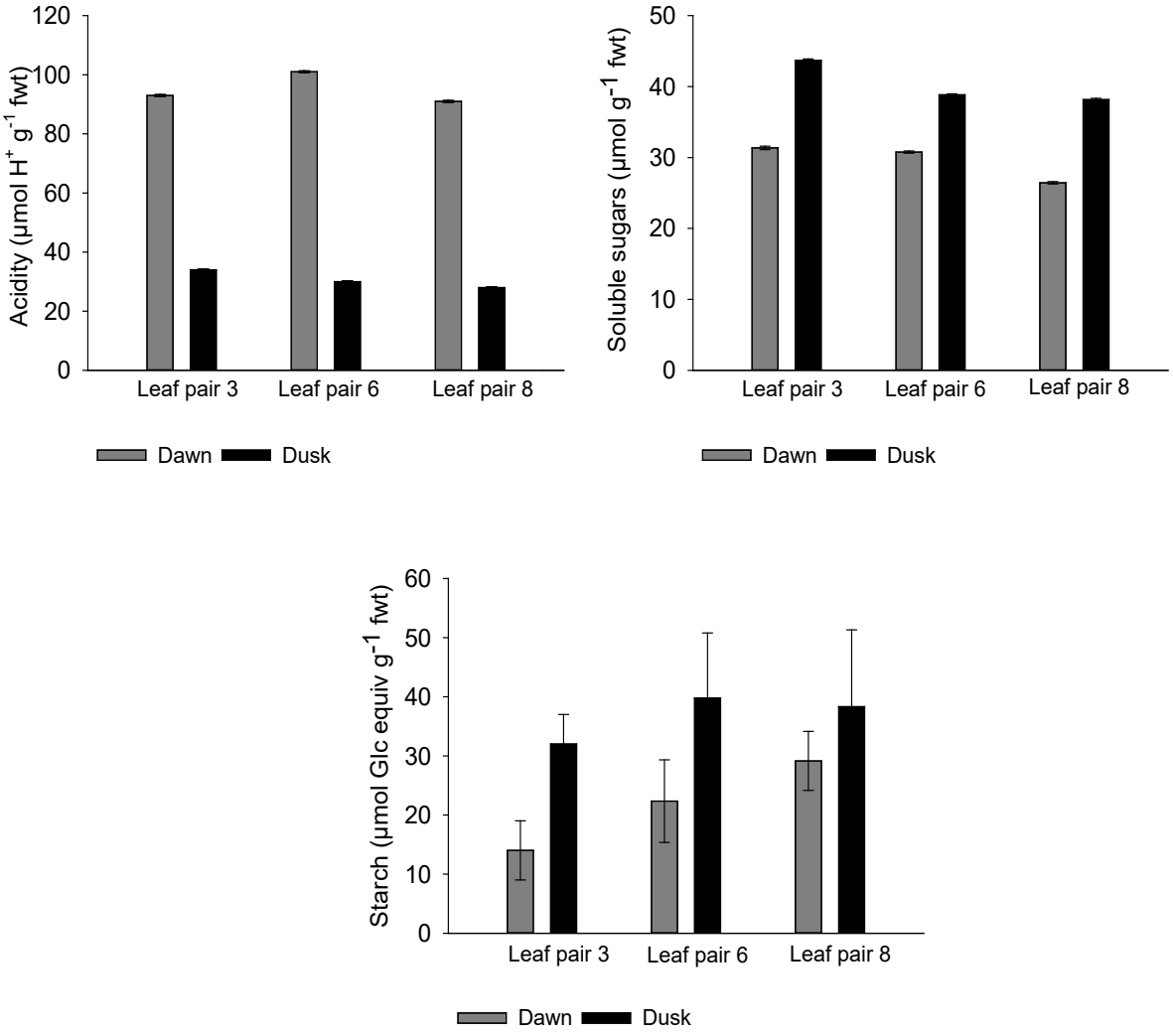

Figure A. 1. (a) Acidity (µmol H^+ g^{-1} fwt), (b) soluble sugars content (µmol g^{-1} fwt), and (c) mesophyll starch content (µmol Glc equiv g^{-1} fwt) on younger (pair 3), middle age (pair 6) and mature leaves (pair 8) of wild type plants of *K. fedtschenkoi*. The comparison was done between dawn (grey filling) and dusk (black filling). The error bars indicate the standard error of 5 biological replicates. Plant growth conditions were set at 400 µmol CO_2 mol^{-1} air, 25°C/19°C (day/night) and a diurnal photosynthetic photon flux density – PPFD - of 250 µmol $m^{-2}s^{-1}$ at plant height.

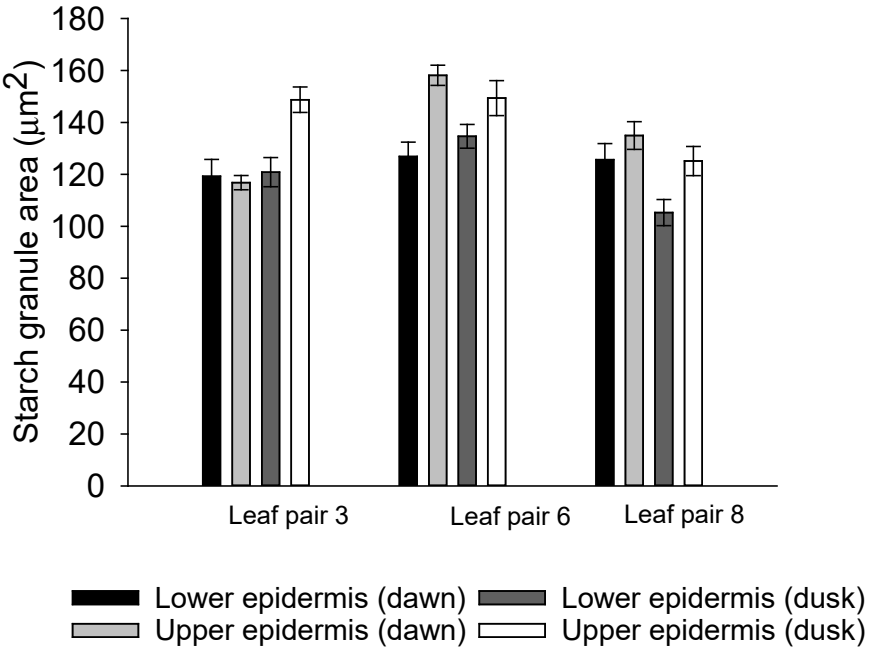

Figure A. 2. Starch granule area (μm^2) in guard cells (upper epidermal surface and lower epidermal surface) on younger (pair 3), middle age (pair 6) and mature leaves (pair 8) of *K. fedtschenkoi* wild type plants. The bars indicate the standard error of 60 replicates (3 biological replicates, each with 20 views per replicate). Plant growth conditions were set at 400 µmol CO_2 mol^{-1} air, 25°C/19°C (day/night) and a diurnal photosynthetic photon flux density – PPFD - of 250 µmol $m^{-2}s^{-1}$ at plant height.

Figure A. 3.Starch deposits in stomatal guard cells of younger - pair 3 (a), middle age - pair 6 (b) and mature – pair 8 (c) leaves of *K. fedtschenkoi* wild type plants. The scale bar represents 20 µm. Plant growth conditions were set at 400 µmol CO_2 mol^{-1} air, 25°C/19°C (day/night) and a diurnal photosynthetic photon flux density – PPFD - of 250 µmol $m^{-2}s^{-1}$ at plant height.

A.2. Identification of the best *pgm* RNAi line for further study

Independent events of transformation have generated different RNAi lines with a curtailed expression of the gene that codes for enzyme phosphoglucomutase (PGM). Consequently, the *K. fedtschenkoi* lines *rPGM1a*, *rPGM1c* and *rPGM2c* were evaluated in order to select the best line for further study. The selection criteria was based on obtaining the most contrasting *pgm* line with curtailed CAM activity and carbohydrates turnover in the mesophyll and starch content in guard cells compared with wild type plants. The following hypothesis was addressed:

Hypothesis: The independent transformation events generated *pgm* RNAi lines with differences in nocturnal acid accumulation, starch and soluble sugars content compared to wild type genotype.

A.2.1. Materials and Methods

The RNAi lines were grown and sampled in the same conditions mentioned in Section 1.2. Four replicates of leaf pair 6 were collected at dawn and dusk from wild type as well as from *rPGM1a*, *rPGM1c* and *rPGM2c* lines and from wild type using one leaf for mesophyll and one for guard cells analysis. Immediately the samples were snap frozen in liquid nitrogen and stored at - 80°C until further evaluation. Section 1.2 describes the biochemical assays performed to determine acidity, soluble sugars content in the mesophyll, as well as starch granules area in stomata guard cells.

A.2.2. Key findings

Significant differences in acidity, soluble sugars and starch turnover in mesophyll were observed between wild type and the *pgm* RNAi lines. In terms of CAM activity, measured as acidity, a significant decrease at dawn in the *pgm* lines were observed as a result of the depletion of starch content, affecting the nocturnal synthesis of organic acids, with a pronounced effect on *rPGM1a* followed by *rPGM1c* and *rPGM2c* (Figure A. 4).

On the other hand, an accumulation of soluble sugars was observed in the RNAi lines compared to wild type at dusk, with a higher content in the *rPGM1a*. This is caused by the inability of using soluble sugars as substrates during the synthesis of starch, however in the case of *rPGM2c* the lower soluble sugars content with respect to *rPGM1a* and *rPGM1c* and the accumulation of starch during the day indicates a partial silencing of the *pgm* gene in this

line (Figure A. 4). Both *rPGM1a* and *rPGM1c* lacked starch completely in the guard cells, while *rPGM2c* showed variations, with a similar content than wild type and in other cases, guard cells completely starchless or with starch in one guard cell. In the case of wild type, starch content in the guard cells did not differ significantly between dawn and dusk (Figure A. 5 and Figure A. 6).

The results indicated that *rPGM1a* is the most contrasting line compared to wild type and the best for further studies based on the lower CAM activity (acidity), higher soluble sugars content in mesophyll, minimum content of starch in mesophyll and absence in the guard cells.

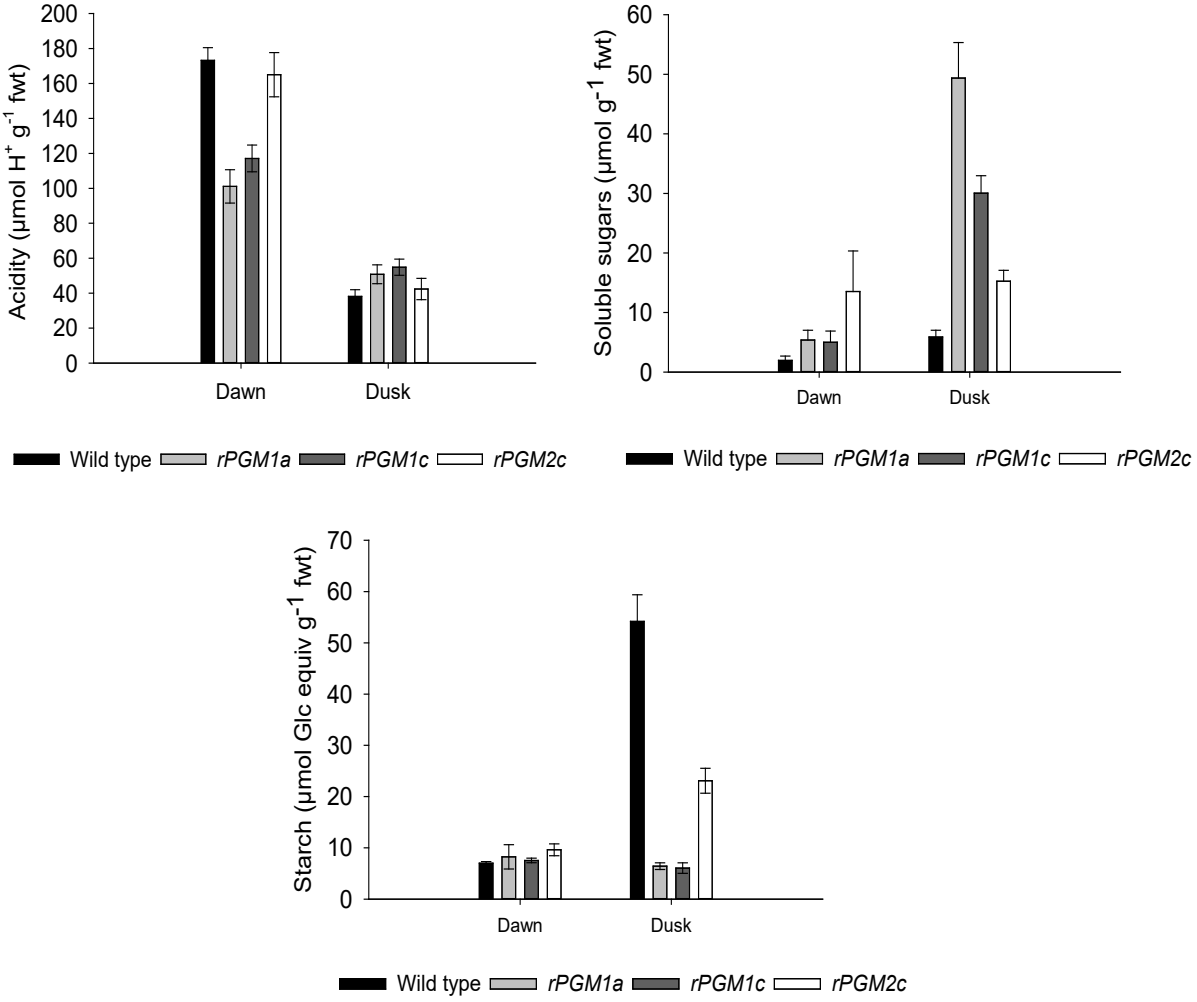

Figure A. 4. (a) Acidity (µmol H^+ g^{-1} fwt), (b) soluble sugars content (µmol g^{-1} fwt), and (c) mesophyll starch content (µmol Glc equiv g^{-1} fwt) in the mesophyll of wild type and *pgm* (*rPGM1a*, *rPGM1c*, *rPGM2c*) lines of *K. fedtschenkoi*. Leaf pair 6 was used for this analysis. The comparison was done between dawn and dusk. The error bars indicate standard error of 4 biological replicates. Plant growth conditions were set at 400 µmol CO_2 mol^{-1} air, 25°C/19°C (day/night) and a diurnal photosynthetic photon flux density – PPFD - of 250 µmol $m^{-2}s^{-1}$ at plant height.

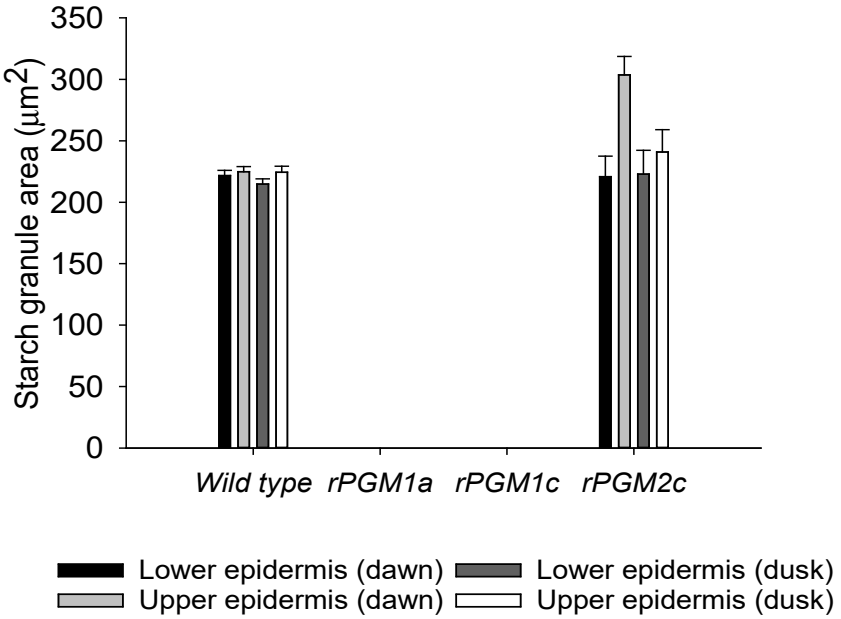

Figure A. 5. Starch granule areas (μm^2) in guard cells (upper epidermal surface and lower epidermal surface) of wild type and *pgm* (*rPGM1a*, *rPGM1c*, *rPGM2c*) lines of *K. fedtschenkoi*. Leaf pair 6 was used for this analysis and the error bars indicate the standard error of 80 replicates (4 biological replicates, each with 20 views per replicate). Plant growth conditions were set at 400 µmol CO_2 mol^{-1} air, 25°C/19°C (day/night) and a diurnal photosynthetic photon flux density – PPFD - of 250 µmol $m^{-2}s^{-1}$ at plant height.

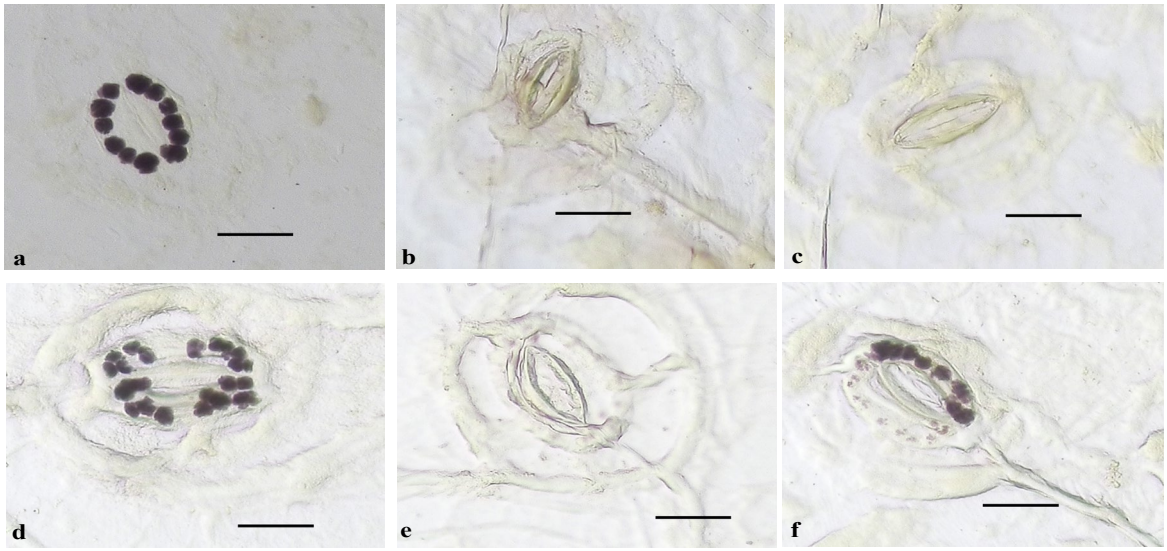

Figure A. 6.Starch deposits in guard cells of wild type (a) and *pgm* RNAi lines of *K. fedtschenkoi*. *rPGM1a* (b) and *rPGM1c* (c) lack starch in the guard cells, while *rPGM2c* (d-f) presents variations in starch content, with starch similar to wild type (d), no starch (e) and more starch in one guard cell (f). The tissue corresponds to epidermal peels of leaf pair 6. The scale bar represents 20 µm. Plant growth conditions were set at 400 µmol CO_2 mol^{-1} air, 25°C/19°C (day/night) and a diurnal photosynthetic photon flux density – PPFD - of 250 µmol $m^{-2}s^{-1}$ at plant height.

Appendix B. Measurement of stomatal anatomical characteristics using the software ImageJ

B.1. Measurement of stomatal anatomy

To measure pore aperture, pore length, stomatal index and density per mm^2; stomatal impressions, using clear nail varnish and sellotape, were taken from both surfaces, and stuck onto a microscope slide. These were observed under the 20 X stage lens on the microscope bright field (Leica DMRB fluorescence microscope) and 10 views per peel for each surface were recorded averaging the measures obtained.

For a measure of scale, a photograph of a graduation slide was taken under the 20 X stage lens. The 10 mm graduation slide or graticule is represented by 100 divisions each one equal to 100 μm. To set the scale, the photograph was opened in ImageJ software and a line was drawn along the length of a 100 μm division. Then, on the main menu was selected *analyze* - *set scale*, *known distance* 100 - *unit of length* μm, - *global* - *ok*. It is important to note that setting the measurement scale must be done at the same magnification and resolution of the photographs to analyse.

To calculate stomatal pore aperture, the photograph of stomata was opened and a horizontal line was drawn across the stomatal pore. Then on the main menu was selected *analyze* - *measure* (or Ctrl + M). In the case of stomatal length, a vertical line was drawn along the pore length and measured as previously. The file was closed to continue with the rest of replicates. All the measurements appeared in a table on a new window that can be exported to Microsoft Excel for further calculations. Finally, for stomatal density, the number of stomata within a known area was counted and 10 views per peel were recorded for each surface. Data were exported to Microsoft Excel and density per mm^2 calculated.

B.2. Measurement of guard cells starch granule area

To measure starch granule area in guard cells, the stained peels were observed by light microscopy using the 40 X stage lens, recording 20 stomata per surface per time point. The measurement scale was set up under the 40 X microscope magnification following the steps explained above. To determine the area of the starch granules, the photograph of the stomata was opened and using the paintbrush tool (located in the toolbar of ImageJ) all the perimeter

around all the starch granules in both guard cells was drawn, then on the main menu was selected *process – binary - make binary*. Automatically the image was transformed to black/white and the starch granules are now defined. Using the wand tracing tool (located in the toolbar) and holding the shift key all the granules were selected, then from the main menu *analyze - measure* (or Ctrl + M) was selected. All the measurements appeared in a table on a new window that can be exported to Microsoft Excel for further calculations. Finally, a scale bar was added using the menu *analyze – tools – scale* bar, in the dialog box was selected the width in μm, the colour and location.

Appendix C. Transcript abundance of additional genes analysed

C.1. Identification of genes related to light signalling in the RNAseq dataset of *Kalanchoë fedtschenkoi*:

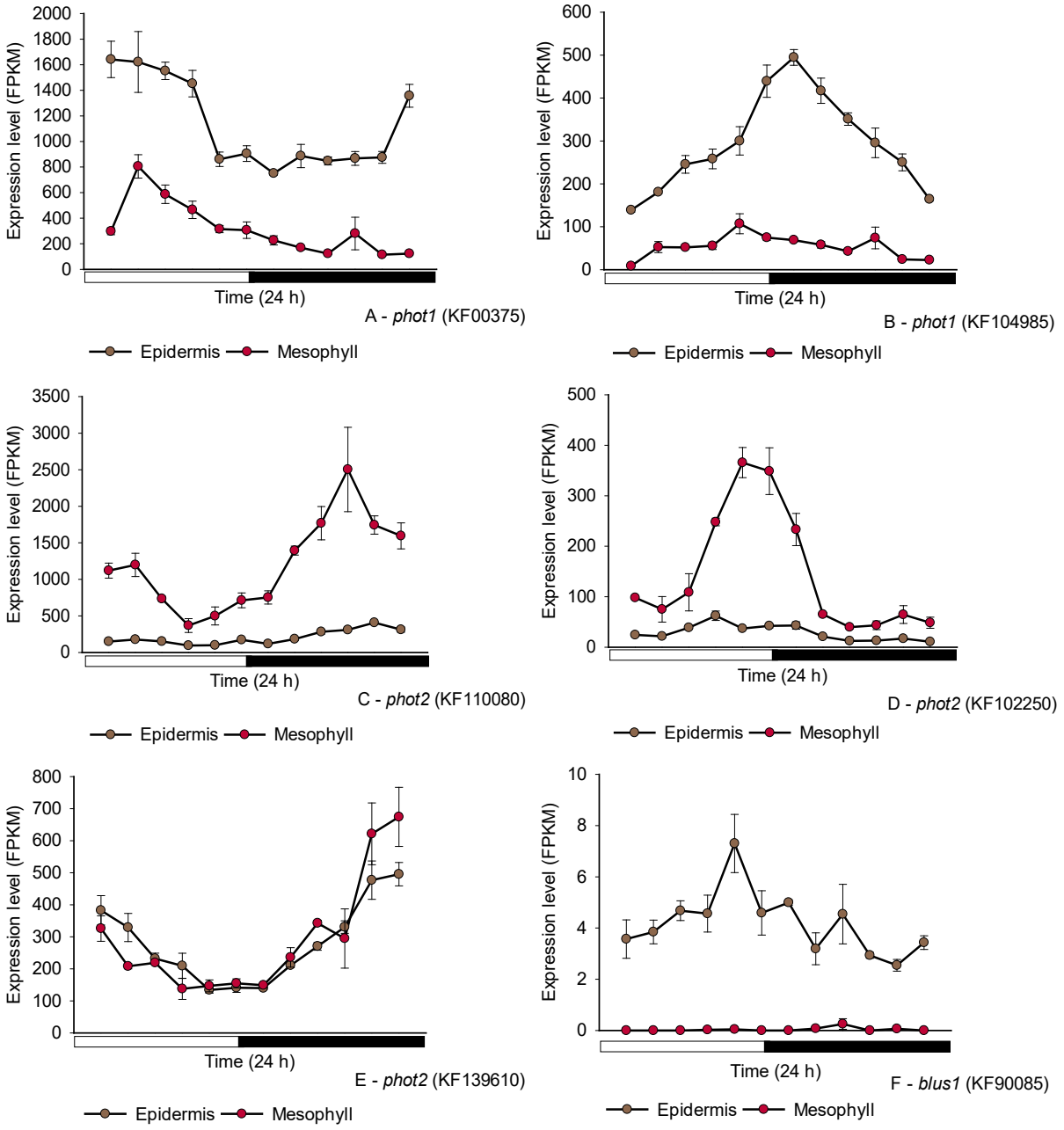

Figure C. 1. Expression level in the mesophyll (red) and guard cell-enriched epidermis (brown) of genes implicated in light signalling. The data is presented in FPKM (fragments per kilobase of exon model per million reads map) and the expression corresponds to a 24 hour day/night cycle (black bar indicates night period). (A - B) *phot1*; (C - E) *phot2*; (F) *blus1*.

C.2. Expression of genes related to sedoheptulose metabolism in *Kalanchoë fedtschenkoi*:

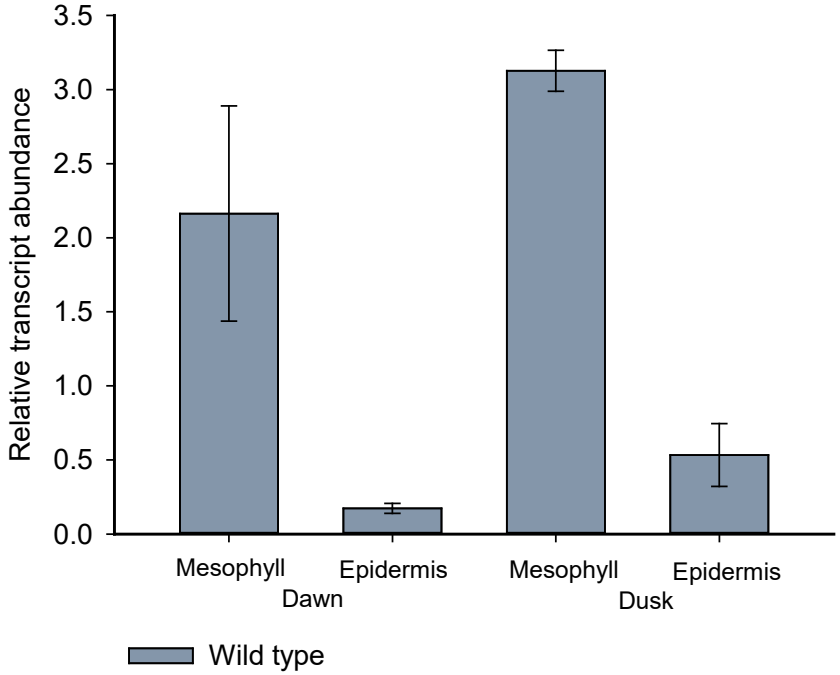

Figure C. 2. Relative transcript abundance of sedoheptulose 1, 7-bisphosphatase (*sbpase*) gene in mesophyll and guard cell-enriched epidermis of wild type plants at dawn and dusk. Leaf pair 6 was used for this analysis. The error bars represent the standard error of six replicates (3 biological replicates, each with 2 technical replicates). Plant growth conditions were set at 400 µmol CO_2 mol^{-1} air, 25°C/19°C (day/night) and a diurnal photosynthetic photon flux density – PPFD - of 250 µmol $m^{-2}s^{-1}$ at plant height.